

**University of Liverpool**

**Marine humic substances:  
distribution, cycling  
pathways, and  
biogeochemical function**

**Thesis submitted in accordance with the requirements of the University of  
Liverpool for the degree of Doctor in Philosophy by**

**Millie Goddard-Dwyer**

**June 2024**

## Declaration of Authorship

I hereby declare that the content of this thesis titled “Marine humic substances: distribution, cycling pathways, and biogeochemical function” is a product of my own work and that the material contained within this thesis has not been previously presented for the award of any other degree or qualification at any other institution.

Millie Goddard-Dwyer

## Abstract

Marine humic substances: distribution, cycling pathways, and biogeochemical function

Millie Goddard-Dwyer

Trace metal availability is an important control on the marine carbon cycle via limitation of primary production. A key factor controlling the availability of trace metals is complexation by components of the dissolved organic matter (DOM) pool called organic ligands. Organic ligands act to stabilise trace metals and are thought to mediate bioavailability to microorganisms. Within the diverse organic ligand pool, trace metal binding electroactive humic substances (eHS) are thought to play an important role due to their abundance, ubiquity, and ability to bind to a range of trace metals.

Humics are a heterogenous pool of organic matter, known to be cycled via a suite of processes including primary production, remineralisation, grazing, terrestrial, sedimentary, photo-oxidation, and hydrothermal processes. However, several key knowledge gaps exist in our understanding of humic biogeochemistry. Firstly, the distribution of eHS in the Southern Ocean, a key iron limited area, is largely unknown. Secondly, the processes that control humic cycling are poorly constrained, but could be important interaction factors with trace metal sources. As such, the impact of eHS on trace metals and carbon cycling is unknown. The overarching aim of this thesis was to advance our understanding of humic cycling in these areas and to consider the role of humic substances in trace metal and DOC cycling.

To reveal eHS distribution in the Southern Ocean and to investigate the processes involved in eHS cycling, eHS was determined in the Southwest Indian sector of the region. The Southwest Indian sector of the Southern Ocean is a predominantly iron limited, low productivity region with islands supplying iron that can stimulate phytoplankton blooms and bioavailable dissolved organic matter (DOM) production. The phytoplankton blooms associated with the islands were linked to elevated levels of eHS, potentially modulated by phytoplankton community composition and grazing. This implies a role of iron in stimulating microbial eHS production, however uncoupling between DFe and eHS also suggested a minor role of eHS in regional DFe transport. Offshore, prokaryote remineralisation was a

potential important source of eHS. Incubation experiments were performed to unravel the impact of DOM composition in controlling prokaryote eHS cycling. Higher dissolved organic carbon (DOC) supply and DOM bioavailability increased eHS production suggesting that eHS cycling is constrained by carbon availability. While lower bioavailability DOM and DOC supply promoted the removal of eHS, likely due to prokaryote carbon limitation. These results suggest that DOM bioavailability may interact with prokaryote humic cycling to influence local iron stabilisation and transport, with possible impacts on the magnitude of iron-driven phytoplankton blooms.

Finally, mass balance modelling of eHS inside a hydrothermal plume reveal that hydrothermal activity was a net eHS source due to prokaryote activity and could supply 7 % of the deep ( $\geq 2000\text{m}$ ) eHS standing stock in the 500 km downstream of the vent site, potentially impacting carbon storage. Similarities between dissolved copper and eHS profiles at plume peripheries suggest that eHS were released by oxidative dissolution of Cu-sulfide particles. Although eHS did not covary with iron, it may complex a significant portion of dissolved iron 10 km from the vent. This emphasises the complex array of interactions between eHS and trace metals in hydrothermal systems.

## **Acknowledgements**

I would like to thank my supervisors Hannah Whitby, Alessandro Tagliabue, and Claire Evans for their guidance and support throughout my PhD. Special thanks to Hannah for being my greatest advocate, a true inspiration, and for being probably the only person in the world who thinks humics are as interesting as I do. Thank you to Gemma and Pascal for always being on hand to help me with voltammetry. Big shout out to my dear friends who have got me through this by providing the most welcome distraction from work. Thanks to my parents for supporting and believing in me ever since I decided in primary school that I wanted to study the oceans when I grew up (turns out I was onto something). Lastly, but mostly, my beloved husband Tom, who makes all of this worth anything.

## Contents

<b>Chapter 1 Introduction</b> .....	1
<b>1. 1. Functioning of the oceanic carbon cycle</b> .....	1
<b>1. 2. Controls on the oceanic carbon cycle</b> .....	2
<b>1. 2. 1. Links between trace metals and carbon cycle</b> .....	4
<b>1. 2. 2. The impact of supply</b> .....	5
<b>1. 3. The impact of trace metal speciation on trace metal distribution and bioavailability to microorganisms</b> .....	6
<b>1. 3. 1. Forms of trace metal speciation</b> .....	7
<b>1. 3. 2. Mechanisms by which trace metal speciation interacts with biogeochemistry</b> .....	8
<b>1. 4. Overview of the distribution and composition of the ligand pool</b> .....	10
<b>1. 4. 1. Dynamic interactions</b> .....	10
<b>1. 4. 2. Ligand composition</b> .....	11
<b>1. 4. 2. 1. Siderophores</b> .....	12
<b>1. 4. 2. 2. Saccharides and exopolymeric substances</b> .....	13
<b>1. 4. 2. 3. Lignin</b> .....	13
<b>1. 4. 2. 4. Humic substances</b> .....	14
<b>1. 4. 2. 5. Concluding remarks on the distribution of ligands</b> .....	15
<b>1. 5. Humic substances: cycling pathways and interactions with trace metals</b> .....	15
<b>1. 5. 1. A note on the methods used to measure humic substances</b> .....	16
<b>1. 5. 2. Processes which cycle humics</b> .....	16
<b>1. 5. 2. 1. Terrestrial</b> .....	17
<b>1. 5. 2. 2. Photooxidation</b> .....	18
<b>1. 5. 2. 3. Hydrothermal activity</b> .....	18
<b>1. 5. 2. 4. Sediments</b> .....	18
<b>1. 5. 2. 5. Phytoplankton</b> .....	19
<b>1. 5. 2. 6. Zooplankton</b> .....	19
<b>1. 5. 2. 7. Prokaryote remineralisation</b> .....	20
<b>1. 6. Summary of key knowledge gaps identified</b> .....	20
<b>1. 7. Aims and objectives of this thesis</b> .....	21
<b>1. 8. References</b> .....	23
<b>Chapter 2 Methodological approaches used to quantify humics</b> .....	38
<b>2.1 Abstract</b> .....	38
<b>2.2 Background</b> .....	39

2. 3. Voltammetric measurement of humic substances .....	39
2. 3. 1. Voltammetric principles .....	39
2. 3. 2. Electrochemical vs trace metal binding .....	40
2. 3. 3. Choice of analytical trace metal and voltammetric method .....	41
2. 3. 4. Quantification of the size of the eHS peak .....	42
2. 3. 5. Quantification of eHS concentration.....	43
2. 3. 6. Composition of the eHS standard.....	44
2. 3. 6. 1. The impact of composition of the eHS standard on the eHS concentration calculation .....	45
2. 3. 7. Calculation of trace metal binding capacity.....	46
2. 3. 7. 1. Impact of the composition of the eHS standard on trace metal binding capacity calculation .....	47
2. 3. 8. Calculation of carbon content of eHS.....	49
2. 3. 8. 1. Impact of the composition of the eHS standard on the eHS Carbon concentration calculation .....	49
2. 3. 9. Non-specificity of the eHS method.....	50
2. 4. CDOM/FDOM measurement of humic substances .....	51
2. 4. 1. CDOM/FDOM analytical principles.....	51
2. 4. 2. Slope parameters: proxies of DOM, and humic, molecular composition .....	53
2. 4. 3. Humification index: a proxy for humic DOM content .....	54
2. 4. 4. Humic Coble peaks a, m, c: proxies for humic chemical composition .....	55
2. 4. 5. Humic PARAFAC peaks: proxies for humic chemical composition and origin.....	55
2. 5. Tandem CDOM/FDOM and voltammetric analysis .....	56
2. 6. References.....	58
<b>Chapter 3 Variable microbial cycling of metal binding humic substances and its interaction with iron in the Southern Ocean .....</b>	<b>64</b>
<b>3. 1. Abstract:.....</b>	<b>65</b>
<b>3. 2. Introduction.....</b>	<b>65</b>
<b>3. 3. Methods.....</b>	<b>68</b>
<b>3. 3. 1. Hydrographic setting.....</b>	<b>68</b>
<b>3. 3. 2. Sampling .....</b>	<b>69</b>
<b>3. 3. 3. Electroactive humic substances (eHS).....</b>	<b>69</b>
<b>3. 3. 3. 1. Reagents .....</b>	<b>69</b>
<b>3. 3. 3. 2. Instrumentation .....</b>	<b>69</b>
<b>3. 3. 3. 3. Validation .....</b>	<b>70</b>
<b>3. 3. 3. 4. Calculation of eHS Fe binding envelope .....</b>	<b>70</b>

3. 3. 3. 5. Calculation of eHS carbon content .....	71
3. 3. 4. Dissolved organic carbon (DOC) .....	71
3. 3. 5. Coloured/Fluorescent dissolved organic matter and PARAFAC .....	71
3. 3. 6. Prokaryote abundance .....	72
3. 3. 7. Phytoplankton pigment and community composition .....	72
3. 3. 8. Satellite derived net Primary Production .....	73
3. 3. 9. Bloom Phenology .....	73
3. 3. 10. Apparent Oxygen Utilisation .....	73
3. 3. 11. Definition of water column structures .....	73
3. 3. 12. Statistical approaches .....	74
3. 4. Results .....	74
3. 4. 1. Phytoplankton bloom characteristics .....	74
3. 4. 2. eHS distribution .....	74
3. 4. 3. DFe/eHS distribution .....	76
3. 4. 4. eHS/DOC .....	76
3. 4. 5. Influence of AOU on eHS and DFe .....	78
3. 4. 6. Links between phytoplankton pigments and phytoplankton community composition with DOC, eHS, and DFe variables.....	80
3. 4. 7. Prokaryote abundance .....	81
3. 4. 8. The relationship between CDOM/FDOM with eHS, DFe, and AOU .....	82
3. 5. Discussion.....	83
3. 5. 1. Sources and sinks of eHS across the transect.....	83
3. 5. 1. 1. Phytoplankton .....	83
3. 5. 1. 2. Zooplankton grazing .....	84
3. 5. 1. 3. Microbial remineralisation .....	84
3. 5. 1. 4. Hydrothermal activity .....	86
3. 5. 2. The potential role of eHS in DFe stabilisation .....	86
3. 5. 3. The implications of uncoupling between DOC and eHS cycling.....	88
3. 6. Conclusions .....	88
3. 7. Acknowledgements .....	89
3. 8. References.....	89
3. 9. Supplementary materials .....	102
<b>Chapter 4 Dissolved organic matter bioavailability influences Southern Ocean prokaryotic humic cycling with implications for trace metal biogeochemistry and carbon cycling .....</b>	<b>106</b>
4. 1. Abstract.....	107
4. 2. Introduction.....	108

4. 3. Methods.....	110
4. 3. 1. Site description .....	110
4. 3. 2. Experimental design .....	110
4. 3. 3. eHS analysis.....	111
4. 3. 4. CDOM and FDOM .....	112
4. 3. 5. DOC .....	113
4. 3. 6. Prokaryote abundance.....	113
4. 3. 7. Prokaryotic community composition.....	113
4. 3. 8. Statistical analyses .....	114
4. 4. Results .....	114
4. 4. 1. Initial DOM compositions.....	114
4. 4. 2. Prokaryote community .....	116
4. 4. 2. 1. Changes in prokaryote abundance over time .....	116
4. 4. 2. 2. Changes to the bacterial community composition .....	116
4. 4. 3. eHS and FDOM cycling .....	118
4. 4. 3. 1. DOM cycling between the treatments. ....	118
4. 4. 3. 2. PCA.....	120
4. 4. 3. 3. Links between prokaryote community and humic cycling.....	121
4. 5. Discussion.....	121
4. 5. 1. Role of DOM bioavailability in humic cycling and implications for Fe cycling .....	122
4. 5. 2. The role of initial DOM composition in the development of prokaryotic community composition .....	124
4. 5. 3. Links between prokaryotic abundance and bacterial community composition with humic cycling.....	125
4. 5. 4. Identifying possible chemical precursors to humics .....	126
4. 5. 5. The role of humics in regional carbon biogeochemistry.....	126
4. 6. Conclusion.....	127
4. 7. Acknowledgements .....	127
4. 8. References.....	128
4. 9. Supplementary materials .....	136
Chapter 5 First evidence for net production of hydrothermal metal-binding humic substances ..	140
5. 1. Abstract.....	141
5. 2. Introduction.....	142
5. 3. Methods.....	144
5. 3. 1. Study site and Sampling Strategy .....	144
5. 3. 2. Determination of dissolved trace metals .....	145

5. 3. 3. Electroactive humic substances (eHS).....	145
5. 3. 4. Mass Balance model.....	146
5. 3. 5. Statistics.....	149
5. 4. Results and Discussion.....	149
5. 4. 1. Hydrothermal eHS cycling through the evolution of the TAG plume.....	149
5. 4. 2. Interactions between eHS and dissolved Fe and Cu cycling.....	152
5. 4. 3. Limitations.....	154
5. 5. Conclusion.....	156
5. 6. References.....	156
5. 7. Supplementary materials.....	165
Chapter 6 Conclusions and perspectives.....	166
6. 1. Thesis findings.....	166
6. 2. Future research directions.....	168
6. 2. 1. Climate change related impacts on the eHS pool.....	168
6. 2. 2. The role of eHS in carbon cycling.....	170
6. 2. 3. The identity, chemical properties, and trace metal binding capacity of trace metal binding humics.....	170
6. 3. Closing remarks.....	172
6. 4. References.....	173
Appendix.....	175

# Chapter 1 Introduction

## 1. 1. Functioning of the oceanic carbon cycle

The global carbon cycle exerts key control on Earth's ecosystem functioning and climate. Simplistically, the carbon cycle can be understood as carbon being transformed between inorganic and organic forms. Primary production acts to transform inorganic carbon into organic carbon; in the ocean, this is primarily performed by unicellular photosynthetic autotrophs in the euphotic zone. Primary production in the ocean represents half of total global net primary production, shuttling  $\sim 48.5$  Pg inorganic carbon  $\text{y}^{-1}$  into organic carbon (Azam et al. 1983; Field et al. 1998). This carbon flux plays a key role in the earth system by supporting global marine food webs, including fisheries (Chassot et al. 2010). The fate of this organic carbon influences carbon storage, and therefore has important implications for earth system functioning (Tréguer et al. 2018).

There are three major processes by which carbon is stored in the ocean: the biological carbon pump, the microbial carbon pump, and the solubility pump. This section will mostly focus on the first two as they are driven by biological processes and therefore are relevant to this thesis, while the latter results from physiochemically driven variations in the solubility of carbon dioxide in seawater. The biological carbon pump describes the process by which particulate organic carbon (POC; operationally defined as  $>0.7 \mu\text{m}$ ) is exported from the surface ocean via sinking processes (Figure 1). When this POC is below the surface mixed layer/thermocline, it can be considered 'exported' but subsequent transfer to the deep ocean is typically required to result in longer term (order of centuries) storage. The biological carbon pump acts to store  $\sim 5$  Gt C  $\text{yr}^{-1}$  (Henson et al. 2011). Marine heterotrophic activity, in particular microbial, reduces the efficiency of this export and transfer by remineralising organic carbon into inorganic carbon throughout the water column.

However, a portion of this organic carbon is not remineralised; instead, it is transformed into a slowly cycled (refractory) pool of dissolved organic matter (DOM; typically operationally defined as  $<0.7 \mu\text{m}$ ) by the microbial carbon pump (Figure 1). Under the microbial carbon pump, "successive – and perhaps repetitive – processing of DOM" by microbial processes transforms organic carbon from the bioavailable, labile DOM to slowly cycled, refractory DOM pools (Jiao et al. 2010). The production rate of refractory DOM in the ocean is  $\sim 0.043$

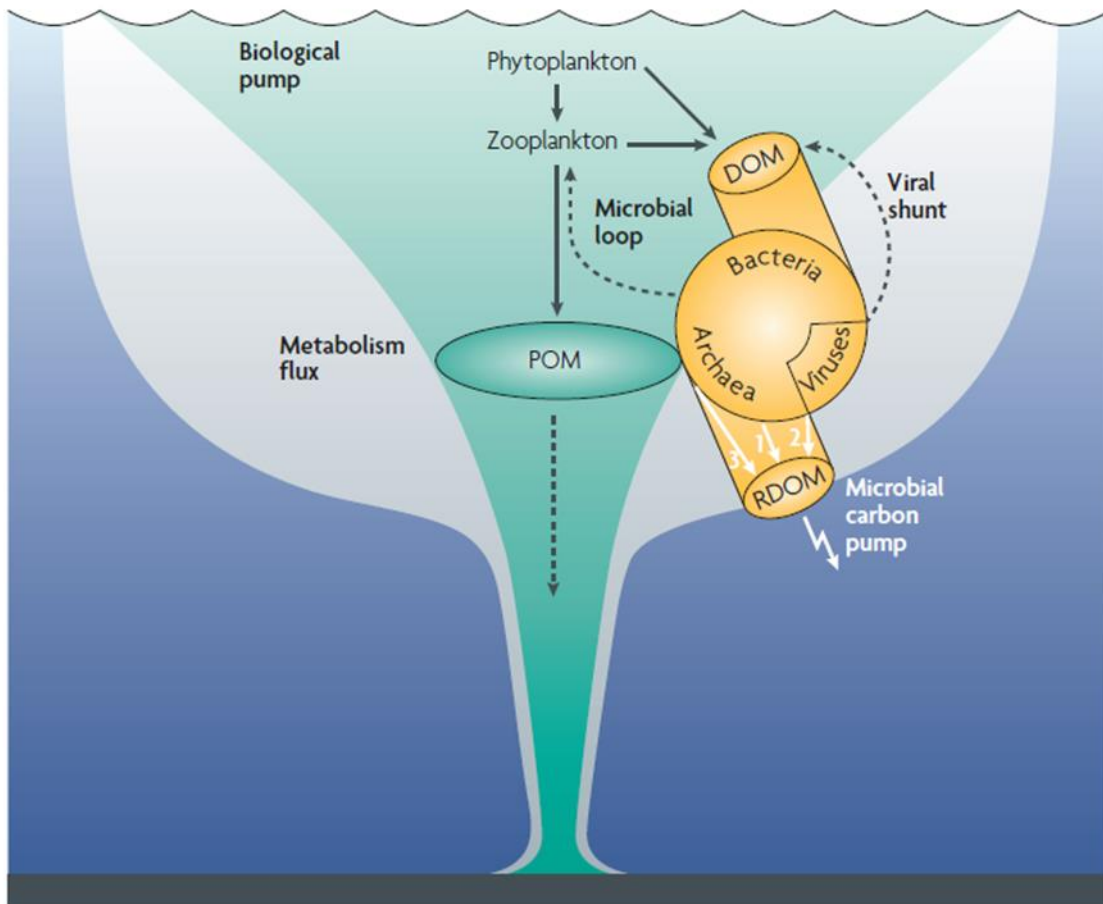


Figure 1: The biological carbon pump and the microbial carbon pump. Figure from Jiao et al. (2010).

Pg C year<sup>-1</sup> (Hansell 2013). These refractory DOM pools act as a carbon storage because they are inherently resistant to microbial remineralisation (lifetime of ~16000 years) and consequently the inventory is massive (~642 Pg C) (Hansell 2013). Carbon storage by the biological and microbial carbon pumps exert significant control on atmospheric carbon dioxide concentration, and consequently climate (Henson et al. 2011; Jiao et al. 2010).

## 1. 2. Controls on the oceanic carbon cycle

This thesis will focus on carbon cycling dynamics in terms of carbon fixation by phytoplankton, carbon cycling by heterotrophic prokaryotes, and carbon storage by the biological and microbial carbon pumps. These processes are controlled by many factors, including temperature, supply of energy, and the biogeochemistry of nutrients. All of these factors interact with ecological factors, such as microbial community composition, which in turn is strongly linked to carbon cycling and export (Guidi et al. 2016). Temperature exerts

first order control on metabolic processes via the kinetics of biochemical reactions (Gillooly et al. 2001), and therefore limits carbon fixation and carbon processing by microbes (Falkowski and Raven 2007; Rivkin and Legendre 2001).

Supply of energy also exerts key control on carbon cycling dynamics by providing energy required for carbon fixation by autotrophs. Light and reduced chemicals are major sources of energy for autotrophs. Phytoplankton, which use light as a source of energy, make the largest contribution to autotrophic carbon fixation. Rapid attenuation of light with depth means that carbon fixation by phytoplankton only occurs in the surface, euphotic ocean. In hydrothermal vent systems, plentiful supply of short-lived, reduced chemicals support carbon fixation by chemoautotrophs local to the hydrothermal vents. These autotrophic processes supply organic carbon (a source of energy) to heterotrophic microbes, the magnitude of organic carbon supplied exerts a key control on heterotrophic activity and carbon cycling (López-Urrutia and Morán 2007). Although, this is mediated by other factors such as the composition of the organic carbon pool (Giorgio and Cole 1998).

Nutrients required by microorganisms also exert strong control on carbon cycle dynamics. The macronutrients nitrogen and phosphorus are key, because they are required in large amounts for phytoplankton growth. Nitrogen is required to form proteins, DNA, and some pigments such as chlorophyll while phosphorus is required to form DNA, cell membranes, and intracellular energy sources (adenosine triphosphate, ATP). Metals are also required in trace amounts as cofactors of metalloenzymes essential for fundamental cellular processes (see references in next section). The identity of the nutrient(s) limiting a system, which can range from the cellular to ecosystem scale, depends on the interaction between their nutrient stoichiometry (ratio) and the magnitude of supply of nutrients. A system can become limited by certain nutrients if it is depleted below stoichiometric requirements, relative to the availability of other nutrients. The availability of nutrients limit carbon fixation by phytoplankton throughout much of the ocean (Moore et al. 2013) and can exert control on carbon utilisation by heterotrophic bacteria (Mills et al. 2008; Tortell et al. 1996), thereby influencing carbon storage.

Finally, physiochemical factors such as temperature, and salinity exert significant impact on the carbon cycle via mediation of the solubility pump. Carbon dioxide solubility in seawater is increased by decreasing temperature and salinity, as such downwelling cold water has the

capacity to contain, and subsequently transport, a large amount of dissolved inorganic carbon (Volk and Hoffert 1985). Further, carbon dioxide solubility is also increased by decreased inorganic carbon concentration and increased alkalinity, both of which are interconnected with pH (Stumm and Morgan 1995).

### 1. 2. 1. Links between trace metals and carbon cycle

Trace metal micronutrients have particularly complex interactions with the carbon cycle (Figure 2). Microorganisms require trace metals for fundamental cellular processes, including Fe, Mn, and Cu in photosynthesis, Fe and Mo in nitrogen fixation, Fe, Mn, and Ni for dealing with cellular oxidative stress, Cu for respiration, and Zn for protein synthesis (*reviewed by* Twining and Baines 2013). However, microbial trace metal requirement varies and reflects a combination of taxonomic biochemical demand, potential for metalloprotein substitution (e.g. Cu-plastocyanin for Fe-cytochrome C6 in photosystem II, Peers and Price 2006), potential for metal free protein substitution (e.g. flavodoxin for Fe-S ferredoxin, McKay et al. 1999), capacity for trace metal storage (e.g. pennate diatom species which store iron in the form of ferritin, Marchetti et al. 2009), and availability of certain forms of macronutrients (e.g. phytoplankton Fe requirements are greater when growing on  $\text{NO}_3^-$  versus  $\text{NH}_4^+$ , Maldonado and Price 1996).

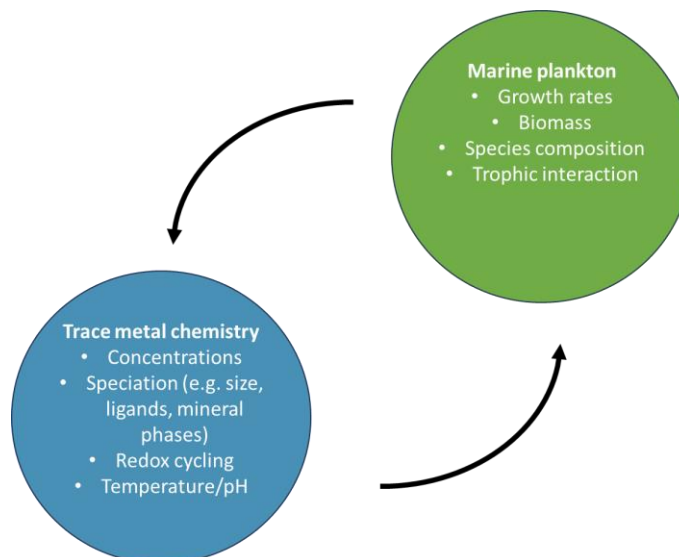


Figure 2: The interactions between marine plankton and trace metal chemistry.

Figure edited from Sunda (2012).

These strategies are utilised by different microorganisms to reduce their trace metal requirements when supply is low. Trace metals may become limiting in an environment when these strategies are exhausted, and/or trade-offs with other scarce nutrients come into play. Therefore, the impact of trace metals on carbon cycling is a function of both microbial requirements together with distribution and bioavailability. The availability of trace metals is underpinned by their supply and speciation, discussed below.

### **1. 3. Fe (and trace metal) distribution and bioavailability**

#### **1. 2. 2. The impact of supply**

All new trace metal sources originate from the Earth's crust and can enter the marine environment through different routes (Figure 3). Terrestrial trace metal sources are transported to the marine environment by riverine and/or atmospheric deposition (Hamilton et al. 2022; Krachler et al. 2005). Sedimentary trace metal sources are released by resuspension or reductive release at continental margins or bathypelagic sediments, and are particularly important in the deep ocean (Homoky et al. 2021; Zhu et al. 2021).

Hydrothermal vent systems represent another important source to the deep ocean (Tagliabue et al. 2010). The magnitude of 'new' trace metal sources has important impacts on the carbon cycle by stimulating carbon fixation, as well as subsequent food web processes, and consequently promoting carbon export (Le Moigne et al. 2016).

Distal to sources, trace metals may be depleted by microbial uptake in surface waters. Here, food web process which recycle trace metals emerge as significant supply mechanisms (Strzepek et al. 2005). Trace metal recycling processes span from the microbial scale to the largest organisms on the planet - including viruses (Poorvin et al. 2004), bacteria, protozoan grazers (Barbeau et al. 1996), krill (Schmidt et al. 2011; Tovar-Sanchez et al. 2007), seabirds (Shatova et al. 2016), and baleen whales (Ratnarajah et al. 2014; Ratnarajah et al. 2017). This can have substantial impacts: for example, biotic Fe inventories in Fe limited regions are comparable to that of Fe replete regions as a result of plasticity in Fe quotas and increased Fe recycling efficiency (Boyd et al. 2015). These recycling processes also act to replenish deep trace metal stores, for example remineralization of particulate organic matter by bacteria in the mesopelagic is a major supply of recycled Fe when the mixed layer deepens seasonally (Bressac et al. 2019). Trace metals can be transported from the deep ocean to the euphotic zone via physical processes such as upwelling (Schallenberg et al. 2018), deep

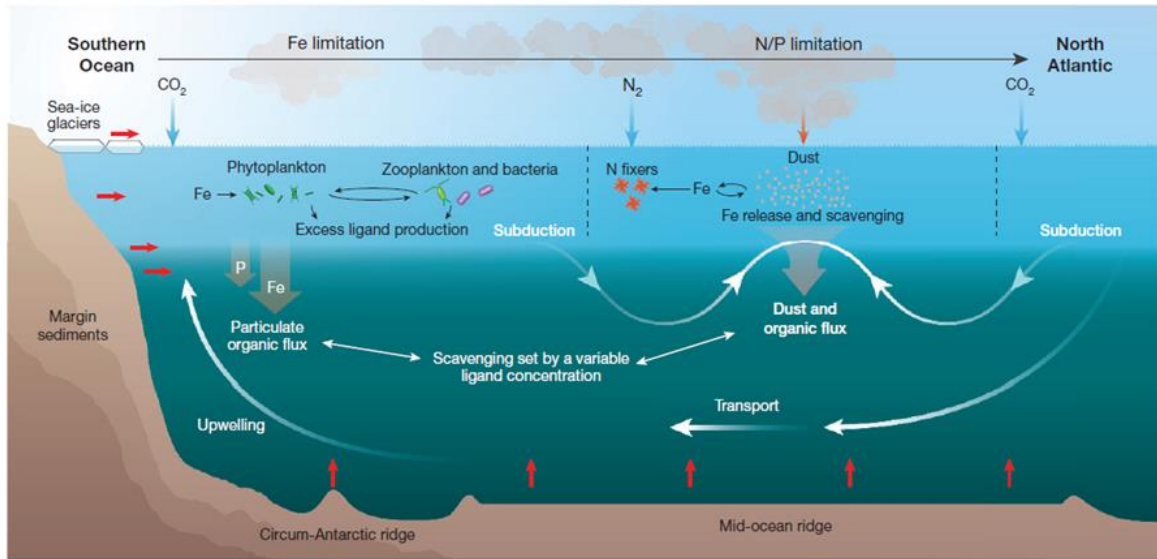


Figure 3: Schematic of the sources and processes involved in marine Fe cycling. Figure from Tagliabue et al. (2017).

winter mixing, and diapycnal mixing (Tagliabue et al. 2014), where they can be utilised by phytoplankton.

Interactions between these major sources in the ocean exerts a first order control on the overall distribution of trace metals. Vertically, trace metals are depleted in the surface ocean, due to microbial uptake and abiotic removal processes such as particle scavenging (Goldberg 1954) and authigenic precipitation (Tagliabue et al. 2023), and increase with depth due to both recycled (Boyd et al. 2010) and new sources. However, abiotic processes such as scavenging by sinking particles act to remove trace metals at depth and, in the case of Fe, can deplete deep ocean concentration (Tagliabue et al. 2019; Wagener et al. 2010). Horizontally, trace metals exhibit high spatial variability dependent on proximity to trace metal sources. For example, trace metal concentrations are greater proximal or downstream of continental landmasses. As such, trace metals are highly depleted in areas such as the Southern Ocean which are isolated from external sources. However, trace metal supply interacts with speciation to mediate distribution.

### 1. 3. The impact of trace metal speciation on trace metal distribution and bioavailability to microorganisms

Trace metal speciation has a strong impact on distribution and bioavailability to microorganisms. This section will give an overview of the chemical and physical speciation of

trace metals and discuss the mechanisms by which speciation interacts with distribution and bioavailability.

### **1. 3. 1. Forms of trace metal speciation**

The distribution and bioavailability of trace metals is complex partly because of their diverse chemical and physical forms (termed speciation) (Figure 4). Physical speciation operationally classifies the 'size' of the trace metals, which spans a continuum from free atoms and small molecules (operationally defined as soluble;  $<0.02\mu\text{m}$ ), through to larger macromolecules and colloids (operationally defined as  $0.02\ \mu\text{m} - 0.2\ \mu\text{m}$ ), and upwards to particulate (operationally defined as  $>0.2\mu\text{m} / >0.45\mu\text{m}$ ). Different trace metals have different susceptibility to forming colloids, for example Fe is highly susceptible while Pb and Cd are not (Guo et al. 2000), partly reflecting differences in chemical speciation (Santschi 2018).

Chemical speciation classifies trace metals by its chemical features and composition, and different chemical species span the physical size continuum (von der Heyden and Roychoudhury 2015). Trace metal oxidative state is the simplest level of chemical speciation. The ability of trace metals to exist in a variety of oxidative states means the atoms can easily gain or lose electrons. This feature is exploited by cells to perform cellular functions (Section 1. 2. 1.) using metalloenzymes but has significant consequences for the biogeochemical cycling of these elements. Different oxidative states may be favoured under different physiochemical conditions (including pH and oxygen concentration) and different oxidative states may have different solubility in seawater, with impacts on trace metal physical speciation. Significantly, under oxic conditions, Fe(II) is transformed to Fe(III) and Mn(II) is (not all) transformed to Mn(III) and/or Mn(IV). Fe(III), Mn(III), and Mn (IV) form oxyhydroxides, which are prone to aggregate into colloidal and particulate phases (Rose and Waite 2003). Therefore, free Fe(II) or Mn(II) are thermodynamically uncommon forms of soluble Fe or Mn in seawater. Complexation of Fe and Mn by organic ligands (defined as organic molecules which form one or more coordinate bonds with a central metal ion) is a major mechanism by which Fe and Mn remain in the soluble phase (Liu and Millero 2002); for this reason, together with the important biogeochemical role of Fe, organic complexation of Fe has been focused on by the scientific community. Organic complexation is also a biologically important speciation form for other trace metals which are comparatively less susceptible to formation of oxyhydroxides, for example, Cu (detailed in following section).

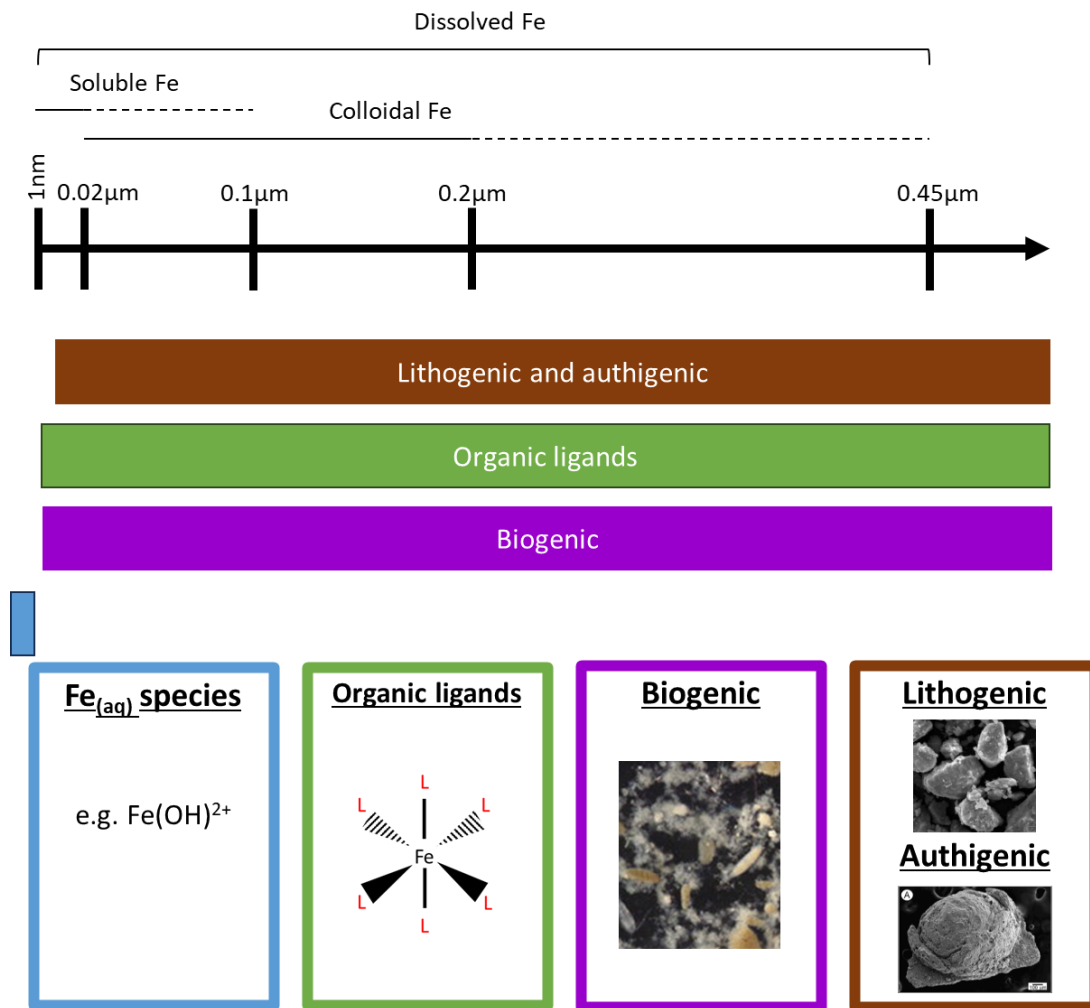


Figure 4: Schematic of the different forms physical and chemical Fe speciation. Adapted from von der Heyden and Roychoudhury (2015). Image credits: Robinson et al. (2010), García-Frank et al. (2012), and Hettiarachchi et al. (2019).

Aside from free atoms, oxyhydroxides, and organic complexation, other chemical species include lithogenic (e.g. clay, alumino-silicates), biogenic (e.g. proteins and other intra- and extra-cellular trace metals, and authigenic (colloids or particles formed in-situ).

### 1. 3. 2. Mechanisms by which trace metal speciation interacts with biogeochemistry

Trace metal speciation may influence its biogeochemistry via regulation of bioavailability and distribution. Bioavailability is defined as the relative ability for a microorganism or community to uptake a certain trace metal pool (Shaked and Lis 2012). The effect of speciation on bioavailability varies between different trace metals. For Fe, free Fe is generally the most bioavailable form to microbes (Fourquez et al. 2023; Lis et al. 2015), likely reflecting widespread utilisation of the reductive uptake of Fe(II) as an Fe acquisition

strategy (Shaked and Lis 2012). Whereas, in the case of Cu, free Cu is toxic to microbes and consequently organically complexed Cu is the preferred form (Anderson and Morel 1978; Sunda and Lewis 1978). Indeed, under experimental conditions, Fe bound to model ligands are generally highly bioavailable, with variation between different ligands (Lis et al. 2015). The composition of ligands is therefore an important control on trace metal bioavailability. However, when experiments were conducted in environmental seawater with natural Fe ligands, Fe organic ligand parameters did not relate to Fe bioavailability and some specific ligand pools were negatively associated with Fe bioavailability (Fourquez et al. 2023; Shaked et al. 2020). These apparently conflicting and surprising results highlight that the role of organic complexation in mediating trace metal bioavailability, and consequently trace metal biogeochemistry, is a major knowledge gap. Moving on to other forms of chemical speciation, biogenic forms may be bioavailable if the molecular size is small and lithogenic forms are generally considered to be low bioavailability (Boyd et al. 2010). Physical speciation also impacts Fe bioavailability: soluble forms are more bioavailable as they fit through microbial uptake channels or can be accessed by reductive release. Whereas, colloidal forms are bioavailable to some microbial groups and particulate forms are only bioavailable to specialised microbes with specific acquisition strategies, including the synthesis of specific organic ligands (Velasquez et al. 2016).

Trace metal speciation can also impact biogeochemistry via modulation of its distribution, this section will focus on Fe. In order to understand how speciation impacts Fe distribution, one must consider how ligands and colloids impact distribution individually, and then integrate this information with how ligands and colloids interact. The prevailing scientific consensus is that Fe binding organic ligands set the upper limit for dissolved Fe (DFe) concentrations by increasing the Fe solubility limit (Gledhill and van den Berg 1994; Kuma et al. 1996), via which it has been concluded that organic ligands play a vital role in mediating Fe distribution (Gledhill and Buck 2012; Hassler et al. 2017). It is also widely accepted that a major fraction of DFe is present as colloids (Wu et al. 2001) and that these colloidal phases are a key driver of variation in DFe distribution (Bergquist et al. 2007). These results were reconciled with organic complexation paradigms by the observation that some organic ligands were also part of the colloidal phase (Batchelli et al. 2010; Boye et al. 2010; Cullen et al. 2006; Wu et al. 2001). In fact, ligand associations between organic matter and trace

metals are important in mediating colloidal dynamics (Santschi 2018). As such, the partitioning of Fe between the soluble and colloidal phase is partly driven by the equilibrium partitioning of soluble versus colloidal ligands (Cullen et al. 2006). The physical partitioning of organic ligands is determined by the molecular size and organic matter composition (e.g. von der Heyden and Roychoudhury 2015), therefore different ligand pools are expected to have different impacts on colloidal dynamics. Taken together, this suggests that organic ligands play an important role in DFe distribution by increasing the solubility limit of the soluble Fe phase (Kuma et al. 1996) and by mediating Fe colloidal dynamics (Cullen et al. 2006). Therefore, understanding organic ligand distribution and cycling is clearly important to trace metal biogeochemistry via modulation of distribution and bioavailability, although the controls on this network are not well understood.

#### **1. 4. Overview of the distribution and composition of the ligand pool**

In the previous section, the distribution and composition of the ligand pool emerged as an important factor influencing wider trace metal speciation and uptake, with consequences for biogeochemistry. This section will focus on the Fe and Cu ligand pool as these are the focus of this thesis. It will introduce the different groups of ligands, their distribution, binding strengths, and highlight significant interactions with trace metals.

##### **1. 4. 1. Dynamic interactions**

One major feature which determines how different ligands interact with the trace metal pool is dynamic exchange (Figure 5). Dynamic exchange refers to the movement of different trace metals between different ligands, the rate of which depends on ligand concentration, ligand characteristics (binding strength, ligand equilibrium constants), competition between different metals for ligand binding sites (determined by the strength of the ligand for respective trace metals and trace metal concentration), dynamic exchange between different chemical forms of trace metals, and physiochemical factors such as pH, temperature, and salinity. Temperature can increase ligand metal binding due to the impacts of temperature on reaction rate, while increased salinity can reduce ligand metal binding (Fang et al. 2015). Weak organic ligands are generally outcompeted by stronger organic ligands for Fe. However, if weak organic ligands are present at high concentrations while strong ligands are present at low concentrations, it is likely that the former, weak, organic ligand pool will outcompete the latter, strong organic ligand pool (Laglera and Filella 2015).

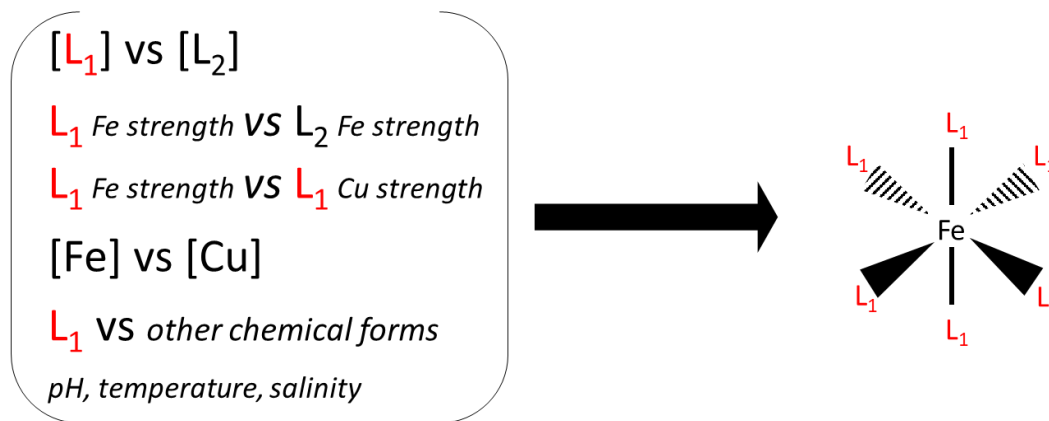


Figure 5: Conceptual framework of the impact of factors such as trace metal concentration  $[Fe]/[Cu]$ , ligand concentration  $[L]$ , and binding strength on ligand (L) dynamic exchange.

pH is also an important parameter to consider here, as ubiquitous protons are competitive cations for the ligand binding sites thereby inducing dissociation of the ligand metal complex (e.g. Tufano and Raymond, 1981). However, diffusion can also limit ligand exchange kinetics in the case of high molecular weight ligands (Laglera and Filella, 2015) and recent experimental evidence has highlighted that a simplistic description of ligand exchange (Figure 5) may not be an accurate representation of ligand exchange at environmentally relevant concentrations (Sukekava et al. 2024).

Nevertheless, ligand characteristics such as binding strength are underpinned by chemical composition. The ligand pool is a chemically heterogeneous pool. As such, distribution and composition varies according to the distribution and biogeochemistry of the diverse organic matter groups which comprise it. This presents a challenge to understanding organic ligand biogeochemistry and necessitates the need to understand the distribution of each major constituent pool.

#### 1. 4. 2. Ligand composition

Technically, trace metal complexation is a ubiquitous feature of marine DOM due to its acid base properties (Huizenga and Kester 1979), therefore to some degree it is likely that all DOM plays a role in trace metal biogeochemistry. However, the trace metal binding ligand pool is dominated by specific groups of molecules including: specific biomolecules produced by bacteria (metallophores, e.g. Fe binding siderophores (Boiteau et al. 2019; Mawji et al. 2008), Cu binding chalkophores (Balasubramanian et al. 2011)), extracellular polymeric

substances (EPS) which includes mono or poly-saccharides (Hassler et al. 2011; Norman et al. 2015), terrestrial type ligands such as lignin (Krachler et al. 2012), and terrestrial or marine humic substances (Krachler et al. 2015; Whitby et al. 2020b) (Figure 6). Each have their own chemical composition, binding properties, binding specificity, and biogeochemical cycling which can impact trace metal biogeochemistry. The next section will discuss this, and comment on the impact of these different ligand pools on trace metal biogeochemistry (via distribution and bioavailability).

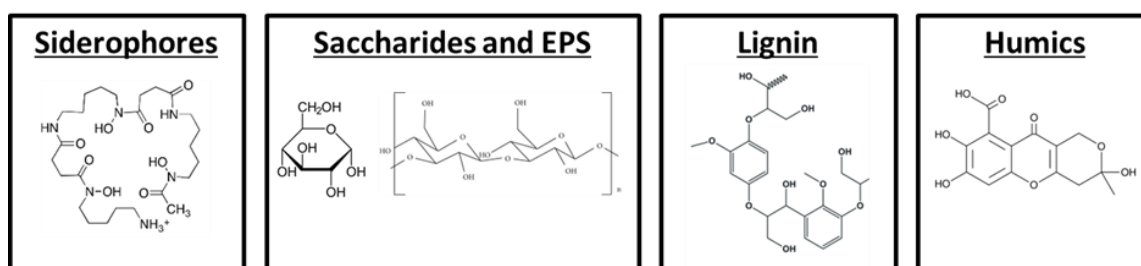


Figure 6: Representative structures of four key ligand groups.

#### 1. 4. 2. 1. Siderophores

Siderophores are small, soluble phase molecules synthesized by bacteria to obtain Fe. There are various known siderophores which can be divided by their binding moieties, namely hydroxymate,  $\alpha$ -hydroxy carboxylate, and/or catecholates (Vraspir and Butler 2009).

Siderophores strongly bind to Fe, and therefore are generally saturated with Fe if DFe concentrations are high enough (e.g. Boiteau et al. 2019). However, competition between Fe and Mn for siderophore binding sites is possible (*refs in* Duckworth et al. 2009). In general, siderophores are more abundant in biologically active surface waters compared to deep waters (Boiteau et al. 2019) and positively correlate to heterotrophic bacterial abundance (Mawji et al. 2008), reflecting their biological origin. Different siderophores show different abundances in different nutrient regimes (Boiteau et al. 2019), reflecting the ecological niches of the prokaryotes which produce them. Siderophores are thought to play an important role in microbial acquisition and dissolution of Fe from particles (Kraemer et al. 2005; Velasquez et al. 2016). The concentration of siderophores is typically low (Mawji et al. 2008), therefore they are not expected to exert a major control on Fe distribution. However, due to their specificity and strong affinity for Fe, siderophores generally reduce Fe

bioavailability to eukaryotic phytoplankton (Lis et al. 2015) while increasing Fe bioavailability to specific groups of microbes which are adapted to the uptake of siderophore bound Fe (Guan Le et al. 2001).

#### **1. 4. 2. 2. *Saccharides and exopolymeric substances***

Saccharides are primarily carbon, oxygen and hydrogen-containing organic molecules such as sugar molecules. They span a large physical size continuum from soluble (monosaccharides) to particulate aggregates or exopolymeric substances (EPS). The binding strength of saccharides and EPS ranges from strong to weak (Hassler et al. 2017).

Saccharides are produced by microbial populations either concomitantly by mortality processes releasing cellular contents (Lonborg et al. 2011; Nissimov et al. 2018) or deliberately by exudation for various ecologically advantageous reasons (Decho and Gutierrez 2017). As such, EPS are present at greatest concentrations in surface waters and at deep chlorophyll maxima (Mari et al. 2017). Monosaccharides (glucuronic acid) and EPS have been shown to enhance iron bioavailability for phytoplankton (Hassler et al. 2015; Hassler et al. 2011; Norman et al. 2015). Therefore, EPS production does show some temporal and spatial variation which likely interacts with Fe supply to impact Fe cycling.

#### **1. 4. 2. 3. *Lignin***

Lignin is a major structural element of vascular plants consisting of aromatic carbon rings with phenol groups. Lignin can bind to a variety of trace metals including Fe, Mn, and Cu (Merdy et al. 2000). Lignin binds Fe strongly (Merdy et al. 2000) and lignin-bound Fe may part of the soluble Fe pool (Williford et al. 2021) or form part of the colloidal Fe pool (Krachler et al. 2012). Lignin is predominantly found in terrestrial systems although seagrasses represent a marine source (Nakakuni et al. 2021). Therefore riverine sources are a dominant pathway for lignin to enter the marine environment (Canuel and Hardison 2016), although a major portion are lost by aggregation and deposition in river plumes (Nakakuni et al. 2021). Reflecting this primarily terrestrial origin, lignin concentration is greatest in the highly terrestrially and riverine influenced Arctic Ocean and lowest in terrestrially isolated Southern Ocean (Jang et al. 2023; Opsahl and Benner 1997). Lignin phenols have relatively short residence times in the ocean (Opsahl et al. 1999), and over time their molecular weight decreases (Hernes and Benner 2006). Overall, the influence of lignin on trace metal

biogeochemistry is likely highly spatially contextual however where it is abundant it likely has a stable temporal influence.

#### **1. 4. 2. 4. Humic substances**

Humic substances are a diverse and heterogeneous group of molecules with the general structure of aromatic or alicyclic carbon rings with abundant carboxyl groups with some aryl ketones and alkyl groups (Cao and Schmidt-Rohr 2018; Hertkorn et al. 2006; IHSS 2019). Humics are commonly operationally characterized into three groups (fulvic acids, humic acids, and humins based on their solubility at pH 1 (IHSS 2019)). Although this operational definition is part of the reason humics are a highly heterogeneous pool and such a definition could be argued to be not representative of the natural DOM pool (Kleber and Lehmann 2019; Lehmann and Kleber 2015), the molecular structure of fulvic acids and humic acids are distinct which supports the environmental relevance of these definitions. Fulvic acids are more aliphatic and heteroaliphatic (alicyclic rings with no double bonds), carboxyl rich, and phenolic poor (IHSS 2019), while humic acids are more aromatic, carboxyl poor, and phenol-rich. Fulvic acids are thought to be more bioavailable than humic acids and also precursors to humic acids (Harvey et al. 1983; Nissenbaum and Kaplan 1972), therefore the fulvic acid to humic acid ratio generally decreases with the diagenetic state of organic matter (e.g. with depth, Stuermer and Harvey 1974). Sources of humics include terrestrial and microbial activity. As such, trace metal binding humics are generally greatest proximal to terrestrial environments, e.g. Arctic ocean (Slagter et al. 2019), and in mesopelagic waters (Whitby et al. 2020b). It is noted that there is a paucity of observations, particularly in the Southern Ocean (Whitby et al. 2020b); considering the important role of Fe in Southern Ocean biogeochemistry, this is an important knowledge gap. Humics are ubiquitous and comprise a major portion of DOM (50%, Zigah et al. 2017), but only approximately 10 %, comprising ~5 % of dissolved organic carbon (DOC), are classed as electroactive and trace metal binding (Dulaquais et al. 2018; Laglera and van den Berg 2009). Humics can bind to a variety of trace metals including Fe, Cu, Mn, Mo, Pb, Cd, Zn, and Hg (Chakraborty et al. 2014; Chang Chien et al. 2006; Laglera and van den Berg 2009; Oldham et al. 2017; Quentel et al. 1987; Whitby and van den Berg 2015). Humic Fe binding strength ranges from 'strong' to 'weak' (Laglera et al. 2019; Laglera and van den Berg 2009; Sukekava et al. 2024), likely depending on humic molecular structure and source. Reflecting their ubiquity and abundance, humics are closely

linked to DFe distribution in many ocean basins (Whitby et al. 2020b; Yamashita et al. 2020) and culture based experiments suggest that humics are a highly bioavailable source of Fe (Lis et al. 2015).

#### 1. 4. 2. 5. Concluding remarks on the distribution of ligands

The distribution of Fe binding ligands therefore reflects the cycling pathways of each of these groups of ligands. It's distribution broadly follows the pattern of organic matter sources (Figure 7b), including elevated at riverine sources (Bundy et al. 2015), sedimentary boundary layers (Bundy et al. 2014), hydrothermal vents (Gerringa et al. 2015), in mesopelagic waters due to production via remineralization processes (Boyd et al. 2010; Bressac et al. 2019) and in euphotic zones, where it covaries with primary production (Gerringa et al. 2015) and associated food web processes such as zooplankton grazing (Sato et al. 2007) (Figure 7a).

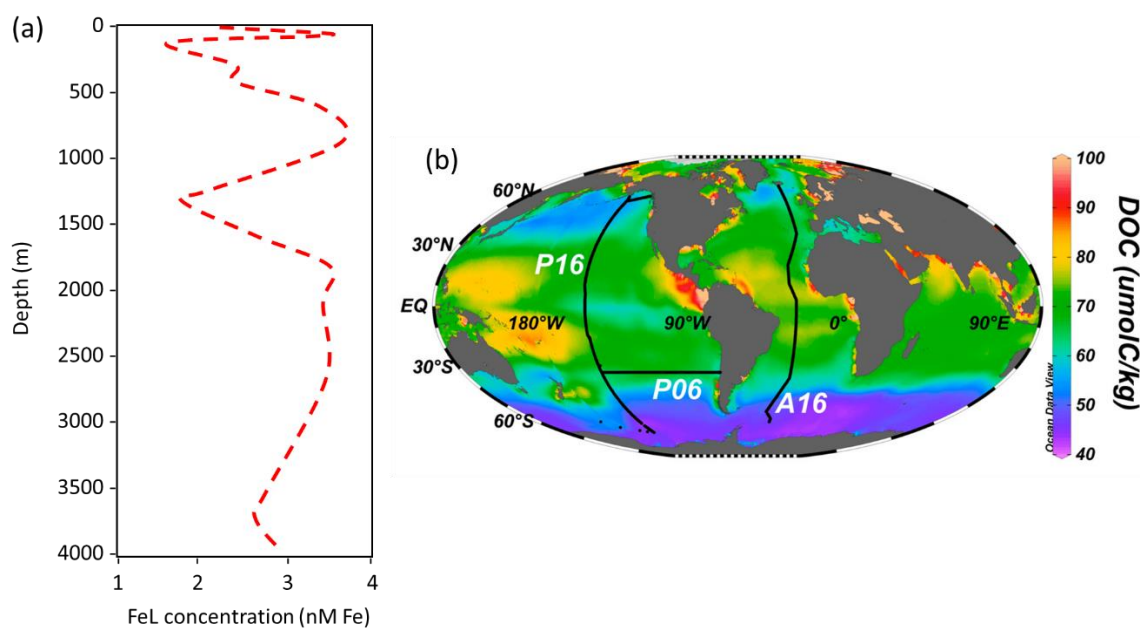


Figure 7: (a) Representative distribution of iron binding ligands (FeL) with depth adapted from Hassler et al. (2017). (b) modelled global distribution of DOC, with oceans sections P16, P06, and A16 annotated, taken from Hansell and Orellana (2021).

#### 1. 5. Humic substances: cycling pathways and interactions with trace metals

Of the diverse pools of trace metal binding organic ligands, previous data suggests that humics are important (Muller 2018; Whitby et al. 2020b). Humics are ubiquitous

components of the DOM pool (Hertkorn et al. 2006), therefore they have the potential to play a significant role in trace metal biogeochemistry throughout the global ocean. Humics are also highly abundant, as such they can comprise a large portion of the organic ligand pool (e.g. Whitby et al. 2020b) which implies a significant role in trace metal biogeochemistry via ligand kinetics. Indeed, humics are positively correlated to DFe in many ocean basins (Whitby et al. 2020b; Yamashita et al. 2020). Therefore, the processes which cycle humics could be an important control on trace metal biogeochemistry.

### **1. 5. 1. A note on the methods used to measure humic substances**

Humics can be measured using several different analytical methods, each targeting a different chemical characteristic of humics (discussed in more detail in Chapter 2). The most commonly applied is absorbance or fluorescence spectroscopy to measure the coloured and fluorescent component of the humic pool (termed coloured or fluorescent DOM; CDOM/FDOM) (Coble 2007). Although humic CDOM/FDOM covaries closely with DFe in some contexts (e.g. Mahieu et al. 2024; Takata et al. 2005; Takata et al. 2004; Yamashita et al. 2020) (all Pacific and/or have high terrestrial influence), the trace metal binding component of the humic pool is most directly measured using electrochemistry (Gledhill and Buck 2012). In the few studies which have measured this pool, trace metal binding humics detectable by electrochemistry ('electroactive') generally correlate well to DFe in most ocean basins (Whitby et al. 2020b). The majority of marine humic studies have measured the humic CDOM/FDOM component, therefore we know a lot about the distribution and biogeochemistry of humic CDOM/FDOM, which is generally extended to the entire humic pool, including the trace metal binding component. However, humic CDOM/FDOM does not always correlate to trace metal binding humics (e.g. Whitby et al. 2020b). As a result, it is important to directly measure the trace metal binding humic pool in order to understand the role of humics in Fe cycling.

### **1. 5. 2. Processes which cycle humics**

This section takes a more detailed look at the processes and biogeochemistry of humics, and how these may link to trace metal biogeochemistry. The major cycling pathways of humics comprise abiotic processes and biotic processes which span the entire marine food-web including terrestrial riverine sources, hydrothermal, photooxidation, sediments, phytoplankton, zooplankton, and prokaryote remineralisation (Figure 8).

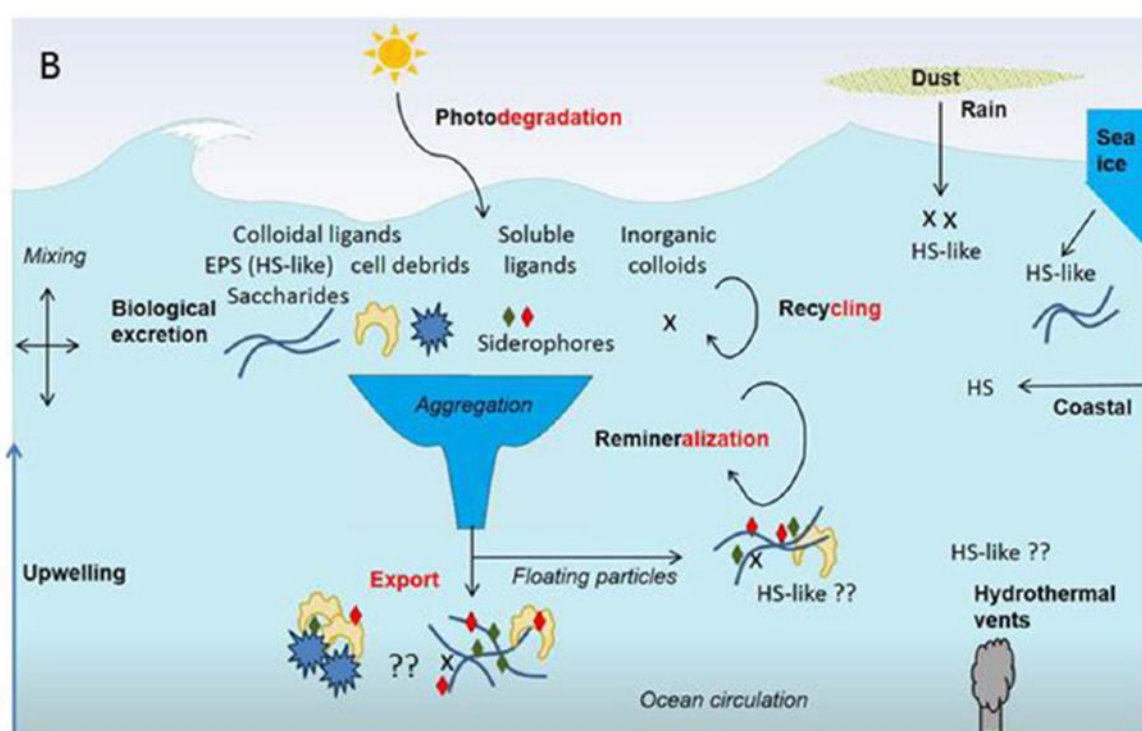


Figure 8: Processes which cycle humics, where ‘??’ indicate knowledge gaps, taken from Hassler et al. (2017).

### 1. 5. 2. 1. Terrestrial

Terrestrial sources of humics are primarily transported to the marine environment via rivers (Nelson and Gauglitz 2016), however isotopic evidence suggests that the majority of terrestrially derived humics are not transported far offshore (Nissenbaum and Kaplan 1972). The amount and composition of humics within rivers is determined by a complex set of factors including soil organic matter composition, environmental conditions, and anthropogenic disturbance (Jaffé et al. 2013). Further, the degree of flocculation and biological removal of humics are key factors determining transfer of riverine humics to the ocean (Boehme and Wells 2006; Riso et al. 2021). Terrestrial humics are produced from different precursor molecules and processes compared to marine humics (Muller 2018). Terrestrial humics are primarily produced from lignin precursors derived from vascular plants (Stevenson 1994), but there are minimal lignin marine sources. Consequently, the composition and/or structure of marine humics may be different to terrestrial humics. Riverine humic biogeochemistry has a strong impact on trace metal biogeochemistry. Humics supply a large portion of riverine derived trace metals to the ocean and are involved in colloidal aggregation losses of trace metals in estuaries (Batchelli et al. 2010).

### **1. 5. 2. 2. Photooxidation**

Photooxidation is a major humic cycling process in the surface, euphotic layer (Jørgensen et al. 2011; Nelson and Gauglitz 2016). Photooxidation has a net removal impact on humics; this effect is more pronounced in the low latitudes or equator where solar radiation is high, compared to the high latitudes (Omori et al. 2020). Consequently, trace metal binding humic concentration is generally lowest in surface waters (Dulaquais et al. 2018; Whitby et al. 2020b). Photooxidation acts to remove humic properties by altering aromatic rings and other functional groups (*refs in* Moran and Zepp 1997) and cleaving molecules (Omori et al. 2015). However, photooxidation of DOM can also be a source of humics via polymerisation reactions (Moran and Zepp 1997; Zhao et al. 2017). Such changes to the humic pool in the euphotic zone have the potential to impact trace metal biogeochemistry because oceanic primary production also occurs in this zone.

### **1. 5. 2. 3. Hydrothermal activity**

Hydrothermal vents are variable sources of humics (Yang et al. 2017), although as yet it is unclear what conditions predicate humic production within thermally and geochemically diverse hydrothermal sources. Humics may be produced and/or degraded via thermal and/or geochemical alteration of organic matter (Hawkes et al. 2016; Sarma et al. 2018). Further, hydrothermal systems are sites of active microbial cycling of organic matter (Bennett et al. 2011; Cathalot et al. 2021; McCarthy et al. 2011), which suggests that these communities might actively cycle humics. The only studies to date which measured trace metal binding humics in hydrothermally influenced waters, specifically a shallow vent system with submarine stratovolcano conditions, observed no clear signals of trace metal binding humic production (Dulaquais et al. 2023; Portlock 2023), however, observations in deep hydrothermal systems with other geochemical conditions are non-existent. Trace metal binding humics bind to a portion of trace metals and influence trace metal physical speciation under experimental hydrothermal conditions (Duan et al. 2003; Dulaquais et al. 2023). Therefore, understanding humic cycling in hydrothermal systems and how it relates to trace metals is an important knowledge gap for hydrothermal trace metal biogeochemistry.

### **1. 5. 2. 4. Sediments**

Marine sediments are rich in humics (Degens et al. 1964; Nissenbaum and Kaplan 1972). These humics originate from degraded autochthonous material, riverine derived aggregates

in sediments proximal to riverine sources, and abiotic geochemical polymerisation processes (Moore et al. 2023; Nakakuni et al. 2021; Nissenbaum and Kaplan 1972). Abiotic geopolymerisation where simple molecules are converted into complex, humic-like molecules is a significant production mechanism in sediments because of the ample supply of Fe or Mn oxyhydroxides which catalyse the reaction (Moore et al. 2023). Sedimentary organic carbon, and likely humics by association, are released into the water column, however due to the scarcity of observations, particularly near-bottom (e.g. Whitby et al. 2020b), the significance of sediments sources of humics to the deep ocean is unknown. Considering the important role of sediments in trace metal biogeochemistry (see trace metal section), associations between humics and trace metal at source and during transport could play an important role in trace metal biogeochemistry.

#### **1. 5. 2. 5. Phytoplankton**

Phytoplankton release trace metal binding humics (Norman et al. 2015), which may be released by cellular exudation or cell lysis. As such trace metal binding humics can be positively correlated with chlorophyll concentration in the marine environment (Dulaquais et al. 2018). However, different phytoplankton taxa can produce humics at different rates and of different composition (Castillo et al. 2010; Norman et al. 2015; Zhao et al. 2017). Therefore, it is expected that humic distribution will not always covary with primary production, rather that the biogeographic patterns of different phytoplankton groups play a role in controlling spatial-temporal patterns of humic distribution, with possible implications for trace metal speciation and trace metal uptake, and consequently trace metal biogeochemistry.

#### **1. 5. 2. 6. Zooplankton**

Taxonomically diverse zooplankton groups produce humics, for example crustacean zooplankton (Urban-Rich et al. 2006), gelatinous zooplankton, gelatinous radiolarians (Steinberg et al. 2004) and Antarctic krill (Ortega-Retuerta et al. 2009), either by direct excretion from the zooplankton organism (Steinberg et al. 2004; Urban-Rich et al. 2006) or by leaching from fecal pellets (Cabanès et al. 2017). These processes likely have a large impact on the distribution of humics. For example, zooplankton which form swarms such as Antarctic krill are likely to produce intense and patchy humic distribution patterns (Ortega-Retuerta et al. 2009). Zooplankton play an important role in Fe recycling (as highlighted by a

recent review, Cavan et al. 2019), therefore trace metal binding humics produced by this zooplankton are poised to also play an important, but unresolved role in Fe recycling, and consequently trace metal biogeochemistry.

#### **1. 5. 2. 7. Prokaryote remineralisation**

Prokaryote remineralisation of organic matter is the major cycling pathway of humics (Omori et al. 2020), however it is complex and variable. Humic production rate by prokaryote remineralisation is impacted by organic matter parameters such as: prokaryote growth stage, DOM composition, and biogenic content of POM (Aparicio et al. 2015; Martínez-Pérez et al. 2017; Romera-Castillo et al. 2011; Whitby et al. 2020a). Humic production rate is also impacted by prokaryote community composition with different strains producing different amounts of compositionally distinct humics (Goto et al. 2020; Shimotori et al. 2012). Prokaryotes are also major sinks of humics in a diverse range of water masses (Aparicio et al. 2015; Bussmann 1999; Romera-Castillo et al. 2011). The removal of humics by prokaryotes is controlled by humic molecular composition (Bussmann 1999; Hunt et al. 2000; Romera-Castillo et al. 2011), and likely also prokaryote community composition (Liu et al. 2020; Manna et al. 2020; Sala et al. 2020) and environmental conditions such as concentration of DOM (dilution hypothesis, Arrieta et al. 2015), and temperature (Sala et al. 2020). Perhaps reflecting these complex conditions, variable relationships between trace metal binding humics and prokaryote remineralization have been observed (Dulaquais et al. 2018; Whitby et al. 2020b), which demonstrates that prokaryote cycling of trace metal binding humics is not well understood. Further, prokaryote trace metal binding humic cycling has a high potential to impact trace metal biogeochemistry. Prokaryote remineralization is an important source of recycled trace metals, and therefore prokaryote mediated changes to the trace metal binding humic pool could impact the speciation of these recycled trace metal at source, with potential consequential impacts on trace metal supply by remineralization (Whitby et al. 2020a).

#### **1. 6. Summary of key knowledge gaps identified**

In general, the mechanisms governing links between trace metal speciation, in particularly organic complexation, and trace metal biogeochemistry are not well resolved. Dynamic exchange of trace metals between speciation pools is an important consideration in their biogeochemistry. Dynamic exchange between trace metal speciation pools and between

organic ligand pools is partially mediated by organic ligand binding strength and concentration. The organic ligand concentration and binding strength differs between different organic ligand pools, therefore understanding the distribution and cycling of these different pools is important to understanding trace metal biogeochemistry. Overall, there is a lack of knowledge regarding the distribution and cycling of all classes of organic ligands, but two broad knowledge gaps exist for humic ligands:

1. There is a lack of observations of humic ligands, particularly in the Southern Ocean. Addressing this knowledge gap is important because humics are ubiquitous in marine environments and can bind to a variety of trace metals which indicates that it could play an important yet complex role in trace metal biogeochemistry, particularly in the trace metal limited Southern Ocean where the biogeochemistry of trace metals has particular importance for the global carbon cycle.
2. There is conflicting information on the drivers of prokaryote humic cycling and the conditions under which prokaryotes produce or degrade humics. This is an important knowledge gap because prokaryotes are a major mediator of humic cycling and therefore exert major control on humic distribution. Changes to the magnitude of the trace metal binding humic pool can change humic trace metal complexation capacity, which in turn could influence the stabilisation and transport of trace metals.
3. There is a lack of knowledge on the processes which cycle trace metal binding humics. Addressing this knowledge gap is essential for two reasons. Firstly, because it will provide understanding of why the distribution patterns emerge. Secondly, because the processes which cycle humics are also important for trace metal cycling, which implies significant, but currently unknown, interaction effects with trace metals. Of particular note is at deep hydrothermal vents, where no observations exist.

### **1. 7. Aims and objectives of this thesis**

The general aim of this thesis is to expand the knowledge regarding the distribution of humics by presenting measurements from several understudied areas of the ocean. In these study sites, the processes controlling the distribution of humics will be assessed. Finally, I

will investigate the links between the biogeochemistry of humics with that of the wider DOM pool and trace metals, in order to place the biogeochemistry of humics in the context of carbon and trace metals. The following objectives were set in order to achieve these aims:

*1. Investigate the distribution and cycling of humics in the biogeochemically diverse Southwest Indian region of the Southern Ocean (Chapter 3)*

This objective will present the first basin scale observations of trace metal binding humics in the Southwest Indian region of the Southern Ocean. It will use the diverse biogeochemical settings in the region of prevailing low Fe, low productivity with patches of Fe replete high productivity stimulated by trace metals from sub-Antarctic islands as a natural laboratory to investigate the microbial processes involved in the cycling of humics. Further, it will compare the distribution of trace metal binding humics with DOC and trace metals in order to bring insights into the role of trace metal binding humics in Southern Ocean carbon and trace metal biogeochemistry. This will give insights into the mechanisms underpinning Southern Ocean microbial-trace metal interactions, which are important for global carbon cycling.

*2. Investigate the impact of dissolved organic matter composition on cycling of humics by prokaryotes in the sub-Antarctic Southern Ocean (Chapter 4)*

This objective will use the results from a shipboard incubation experiment to take a deeper, more focused look at the mechanisms underpinning prokaryote humic cycling in the Southwest Indian region of the Southern Ocean. Specifically, the incubation investigates the effect of DOM composition and availability on prokaryote humic cycling, links to prokaryote community composition, and relates these findings to carbon and trace metal biogeochemistry in the wider study area. This will bring a mechanistic understanding to observations gained in Chapter 3, and inform how humic cycling may be coupled or decoupled from Fe supply from islands or remineralised sources.

*3. Investigate the distribution and cycling of humics in a hydrothermal plume (Chapter 5)*

This objective will present the first observations of trace metal binding humics in a deep sea hydrothermal plume to help to answer a key knowledge gap in the humic research field: Are humics actively cycled in and around deep sea hydrothermal plumes and if so, what processes are involved in its cycling. Further, it will investigate the links between the trace

metal binding humic and trace metal pools in order to bring further understanding on the role of trace metal binding humics in hydrothermal trace metal biogeochemistry. Hydrothermal vents represent a significant source of trace metals to the deep ocean inventory and stabilisation of trace metals by humics is an unknown, but potentially important part of the transport of trace metals throughout the deep ocean.

## 1. 8. References

- Anderson, D. M., and F. M. M. Morel. 1978. Copper sensitivity of *Gonyaulax tamarensis* 1. *Limnology and Oceanography* **23**: 283-295.
- Aparicio, F. L. and others 2015. Microbially-Mediated Fluorescent Organic Matter Transformations in the Deep Ocean. Do the Chemical Precursors Matter? *Front. Mar. Sci.* **2**.
- Arrieta, J. M., E. Mayol, R. L. Hansman, G. J. Herndl, T. Dittmar, and C. M. Duarte. 2015. Dilution limits dissolved organic carbon utilization in the deep ocean. *Science* **348**: 331-333.
- Azam, F., T. Fenchel, J. G. Field, J. S. Gray, L. A. Meyer-Reil, and F. Thingstad. 1983. The Ecological Role of Water-Column Microbes in the Sea. *Marine Ecology Progress Series* **10**: 257-263.
- Balasubramanian, R., G. E. Kenney, and A. C. Rosenzweig. 2011. Dual Pathways for Copper Uptake by Methanotrophic Bacteria. *Journal of Biological Chemistry* **286**: 37313-37319.
- Barbeau, K., J. W. Moffett, D. A. Caron, P. L. Croot, and D. L. Erdner. 1996. Role of protozoan grazing in relieving iron limitation of phytoplankton. *Nature* **380**: 61-64.
- Batchelli, S., F. L. L. Muller, K.-C. Chang, and C.-L. Lee. 2010. Evidence for Strong but Dynamic Iron-Humic Colloidal Associations in Humic-Rich Coastal Waters. *Environmental Science & Technology* **44**: 8485-8490.
- Bennett, S. A. and others 2011. Dissolved and particulate organic carbon in hydrothermal plumes from the East Pacific Rise, 9°50'N. *Deep Sea Research Part I: Oceanographic Research Papers* **58**: 922-931.

- Bergquist, B. A., J. Wu, and E. A. Boyle. 2007. Variability in oceanic dissolved iron is dominated by the colloidal fraction. *Geochimica et Cosmochimica Acta* **71**: 2960-2974.
- Boehme, J., and M. Wells. 2006. Fluorescence variability of marine and terrestrial colloids: Examining size fractions of chromophoric dissolved organic matter in the Damariscotta River estuary. *Marine Chemistry* **101**: 95-103.
- Boiteau, R. M., C. P. Till, T. H. Coale, J. N. Fitzsimmons, K. W. Bruland, and D. J. Repeta. 2019. Patterns of iron and siderophore distributions across the California Current System. *Limnology and Oceanography* **64**: 376-389.
- Boyd, P. W., E. Ibsanmi, S. G. Sander, K. A. Hunter, and G. A. Jackson. 2010. Remineralization of upper ocean particles: Implications for iron biogeochemistry. *Limnology and Oceanography* **55**: 1271-1288.
- Boyd, P. W. and others 2015. Why are biotic iron pools uniform across high- and low-iron pelagic ecosystems? *Global Biogeochemical Cycles* **29**: 1028-1043.
- Boye, M. and others 2010. Significant portion of dissolved organic Fe complexes in fact is Fe colloids. *Marine Chemistry* **122**: 20-27.
- Bressac, M. and others 2019. Resupply of mesopelagic dissolved iron controlled by particulate iron composition. *Nature Geoscience* **12**: 995-1000.
- Bundy, R. M., H. A. N. Abdulla, P. G. Hatcher, D. V. Biller, K. N. Buck, and K. A. Barbeau. 2015. Iron-binding ligands and humic substances in the San Francisco Bay estuary and estuarine-influenced shelf regions of coastal California. *Marine Chemistry* **173**: 183-194.
- Bundy, R. M., D. V. Biller, K. N. Buck, K. W. Bruland, and K. A. Barbeau. 2014. Distinct pools of dissolved iron-binding ligands in the surface and benthic boundary layer of the California Current. *Limnology and Oceanography* **59**: 769-787.
- Bussmann, I. 1999. Bacterial utilization of humic substances from the Arctic Ocean. *Aquatic Microbial Ecology* **19**: 37-45.
- Cabanes, D. J. E. and others 2017. First Evaluation of the Role of Salp Fecal Pellets on Iron Biogeochemistry. *Front. Mar. Sci.* **3**.
- Canuel, E. A., and A. K. Hardison. 2016. Sources, Ages, and Alteration of Organic Matter in Estuaries. *Annual Review of Marine Science* **8**: 409-434.

- Cao, X., and K. Schmidt-Rohr. 2018. Abundant Nonprotonated Aromatic and Oxygen-Bonded Carbons Make Humic Substances Distinct from Biopolymers. *Environmental Science & Technology Letters* **5**: 476-480.
- Castillo, C. R., H. Sarmiento, X. A. Álvarez-Salgado, J. M. Gasol, and C. Marraséa. 2010. Production of chromophoric dissolved organic matter by marine phytoplankton. *Limnology and Oceanography* **55**: 446-454.
- Cathalot, C. and others 2021. Hydrothermal plumes as hotspots for deep-ocean heterotrophic microbial biomass production. *Nature Communications* **12**: 6861.
- Cavan, E. L. and others 2019. The importance of Antarctic krill in biogeochemical cycles. *Nature Communications* **10**: 4742.
- Chakraborty, P., K. M. Yao, K. Chennuri, K. Vudamala, and P. V. Raghunadh Babu. 2014. Interactions of mercury with different molecular weight fractions of humic substances in aquatic systems. *Environmental Earth Sciences* **72**: 931-939.
- Chang Chien, S. W., M. C. Wang, and C. C. Huang. 2006. Reactions of compost-derived humic substances with lead, copper, cadmium, and zinc. *Chemosphere* **64**: 1353-1361.
- Chassot, E. and others 2010. Global marine primary production constrains fisheries catches. *Ecology Letters* **13**: 495-505.
- Coble, P. G. 2007. *Marine Optical Biogeochemistry: The Chemistry of Ocean Color*. *Chemical Reviews* **107**: 402-418.
- Cullen, J. T., B. A. Bergquist, and J. W. Moffett. 2006. Thermodynamic characterization of the partitioning of iron between soluble and colloidal species in the Atlantic Ocean. *Marine Chemistry* **98**: 295-303.
- Decho, A. W., and T. Gutierrez. 2017. Microbial Extracellular Polymeric Substances (EPSs) in Ocean Systems. *Frontiers in Microbiology* **8**.
- Degens, E. T., J. H. Reuter, and K. N. F. Shaw. 1964. Biochemical compounds in offshore California sediments and sea waters. *Geochimica et Cosmochimica Acta* **28**: 45-66.
- Duan, J., N. J. D. Graham, and F. Wilson. 2003. Coagulation of humic acid by ferric chloride in saline (marine) water conditions. *Water Science and Technology* **47**: 41-48.
- Duckworth, O. W., J. R. Bargar, and G. Sposito. 2009. Coupled biogeochemical cycling of iron and manganese as mediated by microbial siderophores. *BioMetals* **22**: 605-613.

- Dulaquais, G. and others 2023. The role of humic-type ligands in the bioavailability and stabilization of dissolved iron in the Western Tropical South Pacific Ocean. *Front. Mar. Sci.* **10**.
- Dulaquais, G., M. Waeles, L. J. A. Gerringa, R. Middag, M. J. A. Rijkenberg, and R. Riso. 2018. The Biogeochemistry of Electroactive Humic Substances and Its Connection to Iron Chemistry in the North East Atlantic and the Western Mediterranean Sea. *Journal of Geophysical Research: Oceans* **123**: 5481-5499.
- Falkowski, P., and J. A. Raven. 2007. *Aquatic Photosynthesis*. Princeton University Press, Princeton, New Jersey, USA.
- Fang, K., D. Yuan, L. Zhang, L. Feng, Y. Chen, and Y. Wang. 2015. Effect of environmental factors on the complexation of iron and humic acid. *Journal of Environmental Sciences* **27**: 188-196.
- Field, C. B., M. J. Behrenfeld, J. T. Randerson, and P. Falkowski. 1998. Primary Production of the Biosphere: Integrating Terrestrial and Oceanic Components. *Science* **281**: 237-240.
- Fourquez, M. and others 2023. Chasing iron bioavailability in the Southern Ocean: Insights from *Phaeocystis antarctica* and iron speciation. *Science Advances* **9**: eadf9696.
- García-Frank, A., S. Ureta, and R. Mas. 2012. Iron-Coated Particles from Condensed Aalenian–Bajocian Deposits: Evolutionary Model (Iberian Basin, Spain). *Journal of Sedimentary Research* **82**: 953-968.
- Gerringa, L. J. A., M. J. A. Rijkenberg, V. Schoemann, P. Laan, and H. J. W. de Baar. 2015. Organic complexation of iron in the West Atlantic Ocean. *Marine Chemistry* **177**: 434-446.
- Gillooly, J. F., J. H. Brown, G. B. West, V. M. Savage, and E. L. Charnov. 2001. Effects of Size and Temperature on Metabolic Rate. *Science* **293**: 2248-2251.
- Giorgio, P. A. d., and J. J. Cole. 1998. BACTERIAL GROWTH EFFICIENCY IN NATURAL AQUATIC SYSTEMS. *Annual Review of Ecology and Systematics* **29**: 503-541.
- Gledhill, M., and K. Buck. 2012. The Organic Complexation of Iron in the Marine Environment: A Review. *Frontiers in Microbiology* **3**.
- Gledhill, M., and C. M. G. van den Berg. 1994. Determination of complexation of iron(III) with natural organic complexing ligands in seawater using cathodic stripping voltammetry. *Marine Chemistry* **47**: 41-54.

- Goldberg, E. D. 1954. Marine Geochemistry 1. Chemical Scavengers of the Sea. *The Journal of Geology* **62**: 249-265.
- Goto, S., Y. Tada, K. Suzuki, and Y. Yamashita. 2020. Evaluation of the Production of Dissolved Organic Matter by Three Marine Bacterial Strains. *Frontiers in Microbiology* **11**.
- Guan Le, L., K. Kanoh, and K. Kamino. 2001. Effect of Exogenous Siderophores on Iron Uptake Activity of Marine Bacteria under Iron-Limited Conditions. *Applied and Environmental Microbiology* **67**: 1710-1717.
- Guidi, L. and others 2016. Plankton networks driving carbon export in the oligotrophic ocean. *Nature* **532**: 465-470.
- Guo, L., P. H. Santschi, and K. W. Warnken. 2000. Trace metal composition of colloidal organic material in marine environments. *Marine Chemistry* **70**: 257-275.
- Hamilton, D. S. and others 2022. Earth, Wind, Fire, and Pollution: Aerosol Nutrient Sources and Impacts on Ocean Biogeochemistry. *Annual Review of Marine Science* **14**: 303-330.
- Hansell, D. A. 2013. Recalcitrant Dissolved Organic Carbon Fractions. *Annual Review of Marine Science* **5**: 421-445.
- Hansell, D. A., and M. V. Orellana. 2021. Dissolved Organic Matter in the Global Ocean: A Primer. *Gels* **7**: 128.
- Harvey, G. R., D. A. Boran, L. A. Chesal, and J. M. Tokar. 1983. The structure of marine fulvic and humic acids. *Marine Chemistry* **12**: 119-132.
- Hassler, C. S. and others 2015. Iron associated with exopolymeric substances is highly bioavailable to oceanic phytoplankton. *Marine Chemistry* **173**: 136-147.
- Hassler, C. S., V. Schoemann, C. M. Nichols, E. C. V. Butler, and P. W. Boyd. 2011. Saccharides enhance iron bioavailability to Southern Ocean phytoplankton. *Proceedings of the National Academy of Sciences* **108**: 1076-1081.
- Hassler, C. S., C. M. G. van den Berg, and P. W. Boyd. 2017. Toward a Regional Classification to Provide a More Inclusive Examination of the Ocean Biogeochemistry of Iron-Binding Ligands. *Front. Mar. Sci.* **4**.
- Hawkes, J. A., C. T. Hansen, T. Goldhammer, W. Bach, and T. Dittmar. 2016. Molecular alteration of marine dissolved organic matter under experimental hydrothermal conditions. *Geochimica et Cosmochimica Acta* **175**: 68-85.

- Henson, S. A., R. Sanders, E. Madsen, P. J. Morris, F. Le Moigne, and G. D. Quartly. 2011. A reduced estimate of the strength of the ocean's biological carbon pump. *Geophysical Research Letters* **38**.
- Hernes, P. J., and R. Benner. 2006. Terrigenous organic matter sources and reactivity in the North Atlantic Ocean and a comparison to the Arctic and Pacific oceans. *Marine Chemistry* **100**: 66-79.
- Hertkorn, N. and others 2006. Characterization of a major refractory component of marine dissolved organic matter. *Geochimica et Cosmochimica Acta* **70**: 2990-3010.
- Hettiarachchi, E., R. L. Reynolds, H. L. Goldstein, B. Moskowicz, and G. Rubasinghege. 2019. Bioavailable iron production in airborne mineral dust: Controls by chemical composition and solar flux. *Atmospheric Environment* **205**: 90-102.
- Homoky, W. B. and others 2021. Iron colloids dominate sedimentary supply to the ocean interior. *Proceedings of the National Academy of Sciences* **118**: e2016078118.
- Huizenga, D. L., and D. R. Kester. 1979. Protonation equilibria of marine dissolved organic matter. *Limnology and Oceanography* **24**: 145-150.
- Hunt, A. P., J. D. Parry, and J. Hamilton-Taylor. 2000. Further evidence of elemental composition as an indicator of the bioavailability of humic substances to bacteria. *Limnology and Oceanography* **45**: 237-241.
- IHSS, I. H. S. S. 2019, <https://humic-substances.org/>.
- Jaffé, R. and others 2013. Global Charcoal Mobilization from Soils via Dissolution and Riverine Transport to the Oceans. *Science* **340**: 345-347.
- Jang, J. and others 2023. Ocean-atmosphere interactions: Different organic components across Pacific and Southern Oceans. *Science of The Total Environment* **878**: 162969.
- Jiao, N. and others 2010. Microbial production of recalcitrant dissolved organic matter: long-term carbon storage in the global ocean. *Nature Reviews Microbiology* **8**: 593-599.
- Jørgensen, L., C. A. Stedmon, T. Kragh, S. Markager, M. Middelboe, and M. Søndergaard. 2011. Global trends in the fluorescence characteristics and distribution of marine dissolved organic matter. *Marine Chemistry* **126**: 139-148.
- Kleber, M., and J. Lehmann. 2019. Humic Substances Extracted by Alkali Are Invalid Proxies for the Dynamics and Functions of Organic Matter in Terrestrial and Aquatic Ecosystems. *Journal of Environmental Quality* **48**: :207–216.

- Krachler, R., F. Jirsa, and S. Ayromlou. 2005. Factors influencing the dissolved iron input by river water to the open ocean. *Biogeosciences* **2**: 311-315.
- Krachler, R. and others 2015. River-derived humic substances as iron chelators in seawater. *Marine Chemistry* **174**: 85-93.
- Krachler, R. and others 2012. Nanoscale lignin particles as sources of dissolved iron to the ocean. *Global Biogeochemical Cycles* **26**.
- Kraemer, S. M., A. Butler, P. Borer, and J. Cervini-Silva. 2005. Siderophores and the Dissolution of Iron-Bearing Minerals in Marine Systems. *Reviews in Mineralogy and Geochemistry* **59**: 53-84.
- Kuma, K., J. Nishioka, and K. Matsunaga. 1996. Controls on iron(III) hydroxide solubility in seawater: The influence of pH and natural organic chelators. *Limnology and Oceanography* **41**: 396-407.
- Laglera, L. M., and M. Filella. 2015. The relevance of ligand exchange kinetics in the measurement of iron speciation by CLE-AdCSV in seawater. *Marine Chemistry* **173**: 100-113.
- Laglera, L. M., C. Sukekava, H. A. Slagter, J. Downes, A. Aparicio-Gonzalez, and L. J. A. Gerringa. 2019. First Quantification of the Controlling Role of Humic Substances in the Transport of Iron Across the Surface of the Arctic Ocean. *Environmental Science & Technology* **53**: 13136-13145.
- Laglera, L. M., and C. M. G. van den Berg. 2009. Evidence for geochemical control of iron by humic substances in seawater. *Limnology and Oceanography* **54**: 610-619.
- Le Moigne, F. A. C. and others 2016. What causes the inverse relationship between primary production and export efficiency in the Southern Ocean? *Geophysical Research Letters* **43**: 4457-4466.
- Lehmann, J., and M. Kleber. 2015. The contentious nature of soil organic matter. *Nature* **528**: 60-68.
- Lis, H., Y. Shaked, C. Kranzler, N. Keren, and F. M. M. Morel. 2015. Iron bioavailability to phytoplankton: an empirical approach. *The ISME Journal* **9**: 1003-1013.
- Liu, S. and others 2020. Different carboxyl-rich alicyclic molecules proxy compounds select distinct bacterioplankton for oxidation of dissolved organic matter in the mesopelagic Sargasso Sea. *Limnology and Oceanography* **65**: 1532-1553.

- Liu, X., and F. J. Millero. 2002. The solubility of iron in seawater. *Marine Chemistry* **77**: 43-54.
- Lonborg, C., S. Martinez-Garcia, E. Teira, and X. A. Alvarez-Salgado. 2011. Bacterial carbon demand and growth efficiency in a coastal upwelling system. *Aquatic Microbial Ecology* **63**: 183-191.
- López-Urrutia, Á., and X. A. G. Morán. 2007. RESOURCE LIMITATION OF BACTERIAL PRODUCTION DISTORTS THE TEMPERATURE DEPENDENCE OF OCEANIC CARBON CYCLING. *Ecology* **88**: 817-822.
- Mahieu, L. and others 2024. Iron-binding by dissolved organic matter in the Western Tropical South Pacific Ocean (GEOTRACES TONGA cruise GPpr14). *Front. Mar. Sci.* **11**.
- Maldonado, M. T., and N. M. Price. 1996. Influence of N substrate on Fe requirements of marine centric diatoms. *Marine Ecology Progress Series* **141**: 161-172.
- Manna, V. and others 2020. Prokaryotic Response to Phytodetritus-Derived Organic Material in Epi- and Mesopelagic Antarctic Waters. *Frontiers in Microbiology* **11**.
- Marchetti, A. and others 2009. Ferritin is used for iron storage in bloom-forming marine pennate diatoms. *Nature* **457**: 467-470.
- Mari, X., U. Passow, C. Migon, A. B. Burd, and L. Legendre. 2017. Transparent exopolymer particles: Effects on carbon cycling in the ocean. *Progress in Oceanography* **151**: 13-37.
- Martínez-Pérez, A. M., X. A. Álvarez-Salgado, J. Arístegui, and M. Nieto-Cid. 2017. Deep-ocean dissolved organic matter reactivity along the Mediterranean Sea: does size matter? *Scientific Reports* **7**: 5687.
- Mawji, E. and others 2008. Hydroxamate Siderophores: Occurrence and Importance in the Atlantic Ocean. *Environmental Science & Technology* **42**: 8675-8680.
- McCarthy, M. D., S. R. Beupré, B. D. Walker, I. Voparil, T. P. Guilderson, and E. R. M. Druffel. 2011. Chemosynthetic origin of <sup>14</sup>C-depleted dissolved organic matter in a ridge-flank hydrothermal system. *Nature Geoscience* **4**: 32-36.
- McKay, R. M. L., J. La Roche, A. F. Yakunin, D. G. Durnford, and R. J. Geider. 1999. ACCUMULATION OF FERREDOXIN AND FLAVODOXIN IN A MARINE DIATOM IN RESPONSE TO FE. *Journal of Phycology* **35**: 510-519.
- Merdy, P., E. Guillon, M. Aplincourt, and J. Duomonceau. 2000. Interaction of metallic cations with lignins. Part 1: Stability of iron (III), manganese (II) and copper (II)

- complexes with phenolic lignin model compounds: Coumaric, ferulic and sinapic acids and coniferyl alcohol. *Journal of Chemical Research* **2000**: 76-77.
- Mills, M. M. and others 2008. Nitrogen and phosphorus co-limitation of bacterial productivity and growth in the oligotrophic subtropical North Atlantic. *Limnology and Oceanography* **53**: 824-834.
- Moore, C. M. and others 2013. Processes and patterns of oceanic nutrient limitation. *Nature Geoscience* **6**: 701-710.
- Moore, O. W. and others 2023. Long-term organic carbon preservation enhanced by iron and manganese. *Nature* **621**: 312-317.
- Moran, M. A., and R. G. Zepp. 1997. Role of photoreactions in the formation of biologically labile compounds from dissolved organic matter. *Limnology and Oceanography* **42**: 1307-1316.
- Muller, F. L. L. 2018. Exploring the Potential Role of Terrestrially Derived Humic Substances in the Marine Biogeochemistry of Iron. *Frontiers in Earth Science* **6**.
- Nakakuni, M. and others 2021. Seagrass contributes substantially to the sedimentary lignin pool in an estuarine seagrass meadow. *Science of The Total Environment* **793**: 148488.
- Nelson, N. B., and J. M. Gauglitz. 2016. Optical Signatures of Dissolved Organic Matter Transformation in the Global Ocean. *Front. Mar. Sci.* **2**.
- Nissenbaum, A., and I. R. Kaplan. 1972. CHEMICAL AND ISOTOPIC EVIDENCE FOR THE IN SITU ORIGIN OF MARINE HUMIC SUBSTANCES<sup>1,2</sup>. *Limnology and Oceanography* **17**: 570-582.
- Nissimov, J. I., R. Vandzura, C. T. Johns, F. Natale, L. Haramaty, and K. D. Bidle. 2018. Dynamics of transparent exopolymer particle production and aggregation during viral infection of the coccolithophore, *Emiliana huxleyi*. *Environmental Microbiology* **20**: 2880-2897.
- Norman, L. and others 2015. The role of bacterial and algal exopolymeric substances in iron chemistry. *Marine Chemistry* **173**: 148-161.
- Oldham, V. E., A. Mucci, B. M. Tebo, and G. W. Luther. 2017. Soluble Mn(III)–L complexes are abundant in oxygenated waters and stabilized by humic ligands. *Geochimica et Cosmochimica Acta* **199**: 238-246.

- Omori, Y., T. Hama, and M. Ishii. 2015. Photochemical bleaching of fluorescent dissolved organic matter in the subtropical North Pacific Ocean. *GEOCHEMICAL JOURNAL* **49**: 175-184.
- Omori, Y., A. Saeki, S. Wada, Y. Inagaki, and T. Hama. 2020. Experimental Analysis of Diurnal Variations in Humic-Like Fluorescent Dissolved Organic Matter in Surface Seawater. *Front. Mar. Sci.* **7**.
- Opsahl, S., and R. Benner. 1997. Distribution and cycling of terrigenous dissolved organic matter in the ocean. *Nature* **386**: 480-482.
- Opsahl, S., R. Benner, and R. M. W. Amon. 1999. Major flux of terrigenous dissolved organic matter through the Arctic Ocean. *Limnology and Oceanography* **44**: 2017-2023.
- Ortega-Retuerta, E. and others 2009. Biogeneration of chromophoric dissolved organic matter by bacteria and krill in the Southern Ocean. *Limnology and Oceanography* **54**: 1941-1950.
- Peers, G., and N. M. Price. 2006. Copper-containing plastocyanin used for electron transport by an oceanic diatom. *Nature* **441**: 341-344.
- Poorvin, L., J. M. Rinta-Kanto, D. A. Hutchins, and S. W. Wilhelm. 2004. Viral release of iron and its bioavailability to marine plankton. *Limnology and Oceanography* **49**: 1734-1741.
- Portlock, G. 2023. The sources and sinks of thiols, reduced sulphur substances, and humic-like substances in hydrothermal waters. University of Liverpool.
- Quentel, F., C. Madec, and J. Courtot-coupez. 1987. Determination of Humic Substances in Seawater by Electrochemistry (Mechanisms). *Analytical Letters* **20**: 47-62.
- Ratnarajah, L., A. R. Bowie, D. Lannuzel, K. M. Meiners, and S. Nicol. 2014. The Biogeochemical Role of Baleen Whales and Krill in Southern Ocean Nutrient Cycling. *PLOS ONE* **9**: e114067.
- Ratnarajah, L. and others 2017. Physical speciation and solubility of iron from baleen whale faecal material. *Marine Chemistry* **194**: 79-88.
- Riso, R. and others 2021. Distribution, speciation and composition of humic substances in a macro-tidal temperate estuary. *Estuarine, Coastal and Shelf Science* **255**: 107360.
- Rivkin, R. B., and L. Legendre. 2001. Biogenic Carbon Cycling in the Upper Ocean: Effects of Microbial Respiration. *Science* **291**: 2398-2400.

- Robinson, C. and others 2010. Mesopelagic zone ecology and biogeochemistry – a synthesis. *Deep Sea Research Part II: Topical Studies in Oceanography* **57**: 1504-1518.
- Romera-Castillo, C., H. Sarmiento, X. A. Álvarez-Salgado, J. M. Gasol, and C. Marrasé. 2011. Net Production and Consumption of Fluorescent Colored Dissolved Organic Matter by Natural Bacterial Assemblages Growing on Marine Phytoplankton Exudates. *Applied and Environmental Microbiology* **77**: 7490-7498.
- Rose, A. L., and T. D. Waite. 2003. Kinetics of Hydrolysis and Precipitation of Ferric Iron in Seawater. *Environmental Science & Technology* **37**: 3897-3903.
- Sala, M. M. and others 2020. Prokaryotic Capability to Use Organic Substrates Across the Global Tropical and Subtropical Ocean. *Frontiers in Microbiology* **11**.
- Santschi, P. H. 2018. Marine colloids, agents of the self-cleansing capacity of aquatic systems: Historical perspective and new discoveries. *Marine Chemistry* **207**: 124-135.
- Sarma, N. S. and others 2018. Hydrothermal Alteration Promotes Humic Acid Formation in Sediments: A Case Study of the Central Indian Ocean Basin. *Journal of Geophysical Research: Oceans* **123**: 110-130.
- Sato, M., S. Takeda, and K. Furuya. 2007. Iron regeneration and organic iron(III)-binding ligand production during in situ zooplankton grazing experiment. *Marine Chemistry* **106**: 471-488.
- Schallenberg, C. and others 2018. Sustained Upwelling of Subsurface Iron Supplies Seasonally Persistent Phytoplankton Blooms Around the Southern Kerguelen Plateau, Southern Ocean. *Journal of Geophysical Research: Oceans* **123**: 5986-6003.
- Schmidt, K. and others 2011. Seabed foraging by Antarctic krill: Implications for stock assessment, benthic-pelagic coupling, and the vertical transfer of iron. *Limnology and Oceanography* **56**: 1411-1428.
- Shaked, Y., K. N. Buck, T. Mellett, and M. T. Maldonado. 2020. Insights into the bioavailability of oceanic dissolved Fe from phytoplankton uptake kinetics. *The ISME Journal* **14**: 1182-1193.
- Shaked, Y., and H. Lis. 2012. Disassembling Iron Availability to Phytoplankton. *Frontiers in Microbiology* **3**.
- Shatova, O., S. R. Wing, M. Gault-Ringold, L. Wing, and L. J. Hoffmann. 2016. Seabird guano enhances phytoplankton production in the Southern Ocean. *Journal of Experimental Marine Biology and Ecology* **483**: 74-87.

- Shimotori, K., K. Watanabe, and T. Hama. 2012. Fluorescence characteristics of humic-like fluorescent dissolved organic matter produced by various taxa of marine bacteria. *Aquatic Microbial Ecology* **65**: 249-260.
- Slagter, H. A., L. M. Laglera, C. Sukekava, and L. J. A. Gerringa. 2019. Fe-Binding Organic Ligands in the Humic-Rich TransPolar Drift in the Surface Arctic Ocean Using Multiple Voltammetric Methods. *Journal of Geophysical Research: Oceans* **124**: 1491-1508.
- Steinberg, D. K., N. B. Nelson, C. A. Carlson, and A. Prusak. 2004. Production of chromophoric dissolved organic matter (CDOM) in the open ocean by zooplankton and the colonial cyanobacterium *Trichodesmium* spp. *Marine Ecology Progress Series* **267**: 45-56.
- Stevenson, J. 1994. *Humus Chemistry: Genesis, Composition, Reactions*. John Wiley and Sons.
- Strzepek, R. F. and others 2005. Spinning the “Ferrous Wheel”: The importance of the microbial community in an iron budget during the FeCycle experiment. *Global Biogeochemical Cycles* **19**.
- Stuermer, D. H., and G. R. Harvey. 1974. Humic substances from seawater. *Nature* **250**: 480-481.
- Stumm, W., and J. Morgan. 1995. *Dissolved Carbon Dioxide. Aquatic Chemistry : Chemical Equilibria and Rates in Natural Waters*. John Wiley & Sons, Incorporated.
- Sukekava, C. F., J. Downes, M. Filella, B. Vilanova, and L. M. Laglera. 2024. Ligand exchange provides new insight into the role of humic substances in the marine iron cycle. *Geochimica et Cosmochimica Acta* **366**: 17-30.
- Sunda, W. 2012. Feedback Interactions between Trace Metal Nutrients and Phytoplankton in the Ocean. *Frontiers in Microbiology* **3**.
- Sunda, W. G., and J. A. M. Lewis. 1978. Effect of complexation by natural organic ligands on the toxicity of copper to a unicellular alga, *Monochrysis lutheri*. *Limnology and Oceanography* **23**: 870-876.
- Tagliabue, A. and others 2010. Hydrothermal contribution to the oceanic dissolved iron inventory. *Nature Geoscience* **3**: 252-256.
- Tagliabue, A., A. R. Bowie, P. W. Boyd, K. N. Buck, K. S. Johnson, and M. A. Saito. 2017. The integral role of iron in ocean biogeochemistry. *Nature* **543**: 51-59.

- Tagliabue, A. and others 2019. The interplay between regeneration and scavenging fluxes drives ocean iron cycling. *Nature Communications* **10**: 4960.
- Tagliabue, A. and others 2023. Authigenic mineral phases as a driver of the upper-ocean iron cycle. *Nature* **620**: 104-109.
- Tagliabue, A., J.-B. Sallée, A. R. Bowie, M. Lévy, S. Swart, and P. W. Boyd. 2014. Surface-water iron supplies in the Southern Ocean sustained by deep winter mixing. *Nature Geoscience* **7**: 314-320.
- Takata, H., K. Kuma, S. Iwade, Y. Isoda, H. Kuroda, and T. Senjyu. 2005. Comparative vertical distributions of iron in the Japan Sea, the Bering Sea, and the western North Pacific Ocean. *Journal of Geophysical Research: Oceans* **110**.
- Takata, H. and others 2004. Spatial variability of iron in the surface water of the northwestern North Pacific Ocean. *Marine Chemistry* **86**: 139-157.
- Tortell, P. D., M. T. Maldonado, and N. M. Price. 1996. The role of heterotrophic bacteria in iron-limited ocean ecosystems. *Nature* **383**: 330-332.
- Tovar-Sanchez, A., C. M. Duarte, S. Hernández-León, and S. A. Sañudo-Wilhelmy. 2007. Krill as a central node for iron cycling in the Southern Ocean. *Geophysical Research Letters* **34**.
- Tréguer, P. and others 2018. Influence of diatom diversity on the ocean biological carbon pump. *Nature Geoscience* **11**: 27-37.
- Tufano, T. P., and K. N. Raymond. 1981. Coordination chemistry of microbial iron transport compounds. 21. Kinetics and mechanism of iron exchange in hydroxamate siderophore complexes. *Journal of the American Chemical Society* **103**: 6617-6624.
- Twining, B. S., and S. B. Baines. 2013. The Trace Metal Composition of Marine Phytoplankton. *Annual Review of Marine Science* **5**: 191-215.
- Urban-Rich, J., J. T. McCarty, D. Fernández, and J. L. Acuña. 2006. Larvaceans and copepods excrete fluorescent dissolved organic matter (FDOM). *Journal of Experimental Marine Biology and Ecology* **332**: 96-105.
- Velasquez, I. B., E. Ibanami, E. W. Maas, P. W. Boyd, S. Nodder, and S. G. Sander. 2016. Ferrioxamine Siderophores Detected amongst Iron Binding Ligands Produced during the Remineralization of Marine Particles. *Front. Mar. Sci.* **3**.

- Volk, T., and M. I. Hoffert. 1985. Ocean Carbon Pumps: Analysis of Relative Strengths and Efficiencies in Ocean-Driven Atmospheric CO<sub>2</sub> Changes, p. 99-110. *The Carbon Cycle and Atmospheric CO<sub>2</sub>: Natural Variations Archean to Present*.
- von der Heyden, B. P., and A. N. Roychoudhury. 2015. A review of colloidal iron partitioning and distribution in the open ocean. *Marine Chemistry* **177**: 9-19.
- Vraspir, J. M., and A. Butler. 2009. Chemistry of Marine Ligands and Siderophores. *Annual Review of Marine Science* **1**: 43-63.
- Wagener, T., C. Guieu, and N. Leblond. 2010. Effects of dust deposition on iron cycle in the surface Mediterranean Sea: results from a mesocosm seeding experiment. *Biogeosciences* **7**: 3769-3781.
- Whitby, H., M. Bressac, G. Sarthou, M. J. Ellwood, C. Guieu, and P. W. Boyd. 2020a. Contribution of Electroactive Humic Substances to the Iron-Binding Ligands Released During Microbial Remineralization of Sinking Particles. *Geophysical Research Letters* **47**: e2019GL086685.
- Whitby, H. and others 2020b. A call for refining the role of humic-like substances in the oceanic iron cycle. *Scientific Reports* **10**: 6144.
- Whitby, H., and C. M. G. van den Berg. 2015. Evidence for copper-binding humic substances in seawater. *Marine Chemistry* **173**: 282-290.
- Williford, T. and others 2021. Insights into the origins, molecular characteristics and distribution of iron-binding ligands in the Arctic Ocean. *Marine Chemistry* **231**: 103936.
- Wu, J., E. Boyle, W. Sunda, and L.-S. Wen. 2001. Soluble and Colloidal Iron in the Oligotrophic North Atlantic and North Pacific. *Science* **293**: 847-849.
- Yamashita, Y., J. Nishioka, H. Obata, and H. Ogawa. 2020. Shelf humic substances as carriers for basin-scale iron transport in the North Pacific. *Scientific Reports* **10**: 4505.
- Yang, L., W.-E. Zhuang, C.-T. A. Chen, B.-J. Wang, and F.-W. Kuo. 2017. Unveiling the transformation and bioavailability of dissolved organic matter in contrasting hydrothermal vents using fluorescence EEM-PARAFAC. *Water Research* **111**: 195-203.
- Zhao, Z. and others 2017. Picocyanobacteria and deep-ocean fluorescent dissolved organic matter share similar optical properties. *Nature Communications* **8**: 15284.

- Zhu, K., M. J. Hopwood, J. E. Groenenberg, A. Engel, E. P. Achterberg, and M. Gledhill. 2021. Influence of pH and Dissolved Organic Matter on Iron Speciation and Apparent Iron Solubility in the Peruvian Shelf and Slope Region. *Environmental Science & Technology* **55**: 9372-9383.
- Zigah, P. K. and others 2017. Allochthonous sources and dynamic cycling of ocean dissolved organic carbon revealed by carbon isotopes. *Geophysical Research Letters* **44**: 2407-2415.

## Chapter 2 Methodological approaches used to quantify humics

### 2.1 Abstract

Humics are a heterogeneous pool of organic matter with structural characteristics that underpin its biogeochemical role in trace metal and carbon cycling, these properties are also targeted by analytical methods. The two analytical methods used in this thesis are voltammetry and absorbance/fluorescence spectroscopy. This chapter describes the principles of these two methods, details the methodological steps involved, and discusses any limitations. The chapter concludes by taking a holistic look at what these two methods reveal about the humic pool, and outlines a framework by which tandem voltammetric and absorbance/fluorescence spectroscopic measurements will be utilised in this thesis. Ultimately, understanding the biogeochemistry of these pools of organic matter will give insights into trace metal and carbon cycling.

## **2.2 Background**

Quantification and characterisation of the humic pool is an important first step to understanding the distribution and biogeochemistry of humics. Common methods to quantify and/or characterise the humic pool include Fourier transform ion cyclotron mass spectrometry (Hertkorn et al. 2006), Fourier transform infrared spectroscopy (Davis et al. 1999), CDOM/FDOM analysis (fluorescence spectrometry and UV-visible absorbance spectrometry) (Coble 1996), and voltammetry (Laglera et al. 2007; Pernet-Coudrier et al. 2013; Whitby and van den Berg 2015). Each method measures a different chemical property of humics and has varying specificity and therefore have distinct applications. To date, no method is truly quantitative and can measure the entire humic pool. This section will focus on the two methods used in this thesis: CDOM/FDOM analysis and voltammetry.

### **2. 3. Voltammetric measurement of humic substances**

#### **2. 3. 1. Voltammetric principles**

The principle of voltammetry includes the use of electrodes to measure the concentration of analytes. The set up was a three-electrode system with a working electrode (where the electrochemical reactions of interest take place), a reference electrode, and an auxiliary electrode. While a potential is applied across the sample, the current flows between the working electrode (hanging mercury drop electrode) and the auxiliary electrode (glassy carbon auxiliary electrode). The purpose of the reference electrode (Ag/AgCl//KCl 3M) is to inform the potential of the working electrode. The specific voltammetry method used in this thesis was cathodic stripping voltammetry (CSV) which consists of two steps: firstly, a deposition or accumulation step, and secondly a stripping step where the analyte is quantified. In the deposition step, a fixed potential (deposition potential) is imposed at the working electrode, during which the analytes (in this case humics bound to certain trace metals) are attracted to the electrode and are deposited/adsorbed on the electrode (in this case Hg) surface (Figure 1). The duration of the deposition step (deposition time) is dependent on the analyte concentration. Subsequently in the stripping step, the potential is varied from positive to negative during which the current is measured continuously. During this 'stripping step', the current measured originates from the current produced when the trace metal bound to the humics are reduced (Figure 1). This occurs at a specific potential

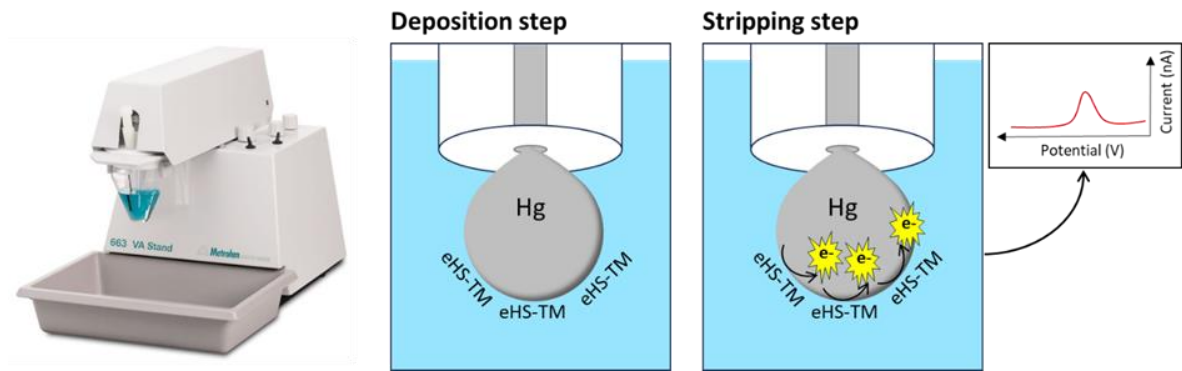


Figure 1: Voltammeter machine (picture from Metrohm) and schematic demonstrating the interaction of eHS and trace metal complex (TM-eHS) during CSV analytical deposition and stripping steps at the mercury drop of the working electrode, and the resultant voltammogram.

and appears as a peak in the potential vs current graph (voltammogram). The concentration of electroactive trace metal binding humics is then calculated from the size of initial humic peak using standard additions of a humic standard. The standard used in this thesis is Suwannee River fulvic acid (SRFA), Suwannee River humic acid (SRHA) is also commonly used (IHSS 2019).

CSV detects the trace metal and humic complex. The components of the humic molecule that are responsible for trace metal binding are oxygen containing (carboxylic, hydroxyl, phenol, catechol), aromatic, and quinone groups (Frimmel et al. 2005; Orłowska et al. 2017; Schnitzer 1978; Schnitzer and Riffaldi 1972; van Schaik et al. 2008; Vinkler et al. 1976).

However, in some cases the loss of one carboxyl from a molecule removes its trace metal complexation ability (Amin et al. 2009), therefore the amount of carboxyl groups does not necessarily predict trace metal binding. One important chemical property that determines whether CSV can detect the molecule is whether the molecule, or part of the molecule, can form a planar species that can adsorb onto the electrode and concomitantly hold the complexing metal against the electrode surface (Laglera et al. 2007; van den Berg 1984).

### 2. 3. 2. Electrochemical vs trace metal binding

The concentration of trace metal binding humics measured using voltammetry is termed the electroactive fraction (e.g. Dulaquais et al. 2018). Voltammetry is the most direct method to measure trace metal binding capabilities of DOM, however it is possible that not all the trace

metal binding humics are detected. This could be caused by a lack of interaction between the trace metal binding humics and the electrode surface, possibly due to encapsulation of the trace metal binding humics and/or certain humic chemical characteristics. These fractions can be thought of as 'electrochemically invisible' trace metal binding humics or electroinactive. The presence of this fraction is inferred from observations of lack of correlation between electroactive humics with dissolved Fe (DFe) simultaneous to observations of close correlation between CDOM/FDOM humics with DFe (Mahieu et al. 2024). The concentration and distribution of these fractions, and the existence or prevalence of exchange between the electroactive and electroinactive fractions are unknown. As a result, these processes could have an important, but completely unresolved impact on the electroactive humic concentration relative to trace metal binding humic concentration. These factors should be kept in mind whilst interpreting electroactive humic concentration data and remain an important question for the field to answer. One important benefit that voltammetry brings is that the electroactive fraction is thought to be the most comparable to the bioavailable fraction because it is readily reduced, which is likely comparable to reductive uptake commonly utilised by microorganisms (Sutak et al. 2020).

### **2. 3. 3. Choice of analytical trace metal and voltammetric method**

Voltammetric measurement of the concentration of trace metal binding humics can be measured using Fe (Laglera et al. 2007), Mo (Pernet-Coudrier et al. 2013; Quentel et al. 1987), or Cu (Whitby and van den Berg 2015) as the complexing metal. Within each method, the selected complexing trace metal is added at saturating concentrations to ensure that humic binding sites are saturated by the complexing trace metals. The analytical conditions (such as pH, deposition potential, and stripping parameters) used are specific and optimised to the trace metal used.

Several intercomparison efforts have been performed to assess agreement between the Fe, Cu, and Mo methods. There is evidence that the concentration of Fe-eHS agrees well with Cu-eHS (Whitby et al. 2020) and Mo-eHS (Dulaquais et al. 2023). Further, comparison of the Fe-, Mo-, and Cu-eHS method in the Western Tropical Pacific showed no statistical difference in eHS concentration between the three methods (Portlock 2023). Indeed, theory predicts that the methods should covary. Mo, Cu, and Fe are all intermediate acids according to hard and soft (Lewis) acids and bases (HSAB) theory due to their intermediate ionic radius and

positive charge and therefore are expected to behave similarly (as observed in the Amazon, Gledhill et al. 2022) and bind to similar ligand (humic) bindings sites. However, there is also evidence that the methods do not agree. In the same study in the Western Tropical Pacific, Cu-eHS tended to exceed Mo- and Fe-eHS (Portlock 2023) and in another study in coastal waters Mo-eHS and Fe-eHS diverged (Laglera et al. 2007).

The Mo and Cu methods are the two methods used in this thesis (Pernet-Coudrier et al. 2013; Whitby and van den Berg 2015). The Cu method was selected for the hydrothermal samples because, unlike the Fe-humic method, the Cu-humic method does not suffer from sulfide interference. This is because the sulfide peak occurs at a different potential compared to the Cu-humic peak. Sulfide interference is expected to be high in hydrothermal samples due to the high concentration of sulfides in hydrothermal fluid. This effect would be especially pronounced in the sulfide rich TAG plume (Konn et al. 2022).

The Mo method was selected for the Southern Ocean samples. This method was favoured as, unlike the Fe-humic method (Laglera et al. 2007), it does not suffer from interference from glutathione or other reduced sulfur compounds, as these peaks occur at different potential compared to the Mo-humic peak (Pernet-Coudrier et al. 2013). It was predicted that these compounds could be produced during the Southern Ocean bacterial organic matter incubations and therefore the Mo humic method was selected for all Southern Ocean samples to allow comparison between the samples. Further, unlike Fe, dissolved Mo can be present in excess of humics and as a result the Mo-humic analytical procedure is simpler to perform compared to the Fe-humic method, which allowed greater throughput of samples.

#### **2. 3. 4. Quantification of the size of the eHS peak**

Once a voltammogram has been obtained, there are several methods used to quantify the size of the humic peak. The two used in this thesis are peak height and 1<sup>st</sup> peak derivative (Figure 2). Peak height measures the height of the peak (green arrow) from a baseline tangent from the baseline (green dotted line) to the maximum current within the peak. The 1<sup>st</sup> peak derivative measures the gradient of the peak at its inflection, visualised here by tangents (solid green lines) (Salaün and van den Berg 2006).

One major difference between these two methods is that peak height is sensitive to the shape of the baseline while 1<sup>st</sup> derivative is not affected (Alves et al. 2011). For this reason,

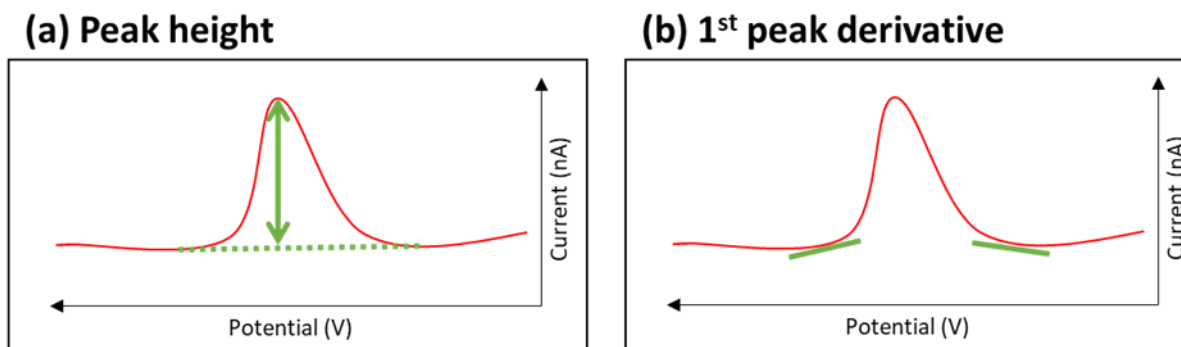


Figure 2. Schematic of mathematical procedure involved in calculating (a) peak height and (b) 1<sup>st</sup> peak derivative.

1<sup>st</sup> peak derivative has better reproducibility at low concentrations (Alves et al. 2011). This is especially useful when working close to the limit of detection. Therefore, for this thesis, peak derivative was used to quantify the eHS peak during analysis of Southern Ocean samples, for which low eHS concentration was norm. Further, sensitivity of peak height to the baseline could be problematic under situations where the baseline fluctuates.

### 2. 3. 5. Quantification of eHS concentration

The concentration of trace metal binding humics is calculated using standard additions of a humic standard (Figure 3). To date, the widely used standard is Suwannee River fulvic or humic acid (SRFA/HA) produced by the International Humic Substances Society (IHSS 2019). These standards are derived from organic matter extracted from the humic rich ‘black water’ (peat/organic matter rich) Suwannee River generally according to Thurman and Malcolm (1981)’s procedure. Briefly, DOM is passed over a XAD-8 resin column, which absorbs the hydrophobic DOM on the resin. The absorbed DOM is then eluted (taken off) from the resin using alkaline extraction (aqueous NaOH). The resultant hydrophobic DOM mixture is then acidified to pH 1, which precipitates the SRHA and leaving the SRFA in solution, thereby separating the SRFA and SRHA fractions. It is advantageous to use these standards because their composition is well characterised and they are easily accessible by researchers around the world, which allows standardisation of analytical methods and objective comparison of results within the eHS-analysis community (MacCarthy 1976). However, there are several limitations of the use of these standards which must be considered, primarily due to compositional differences between the standards and marine humics.

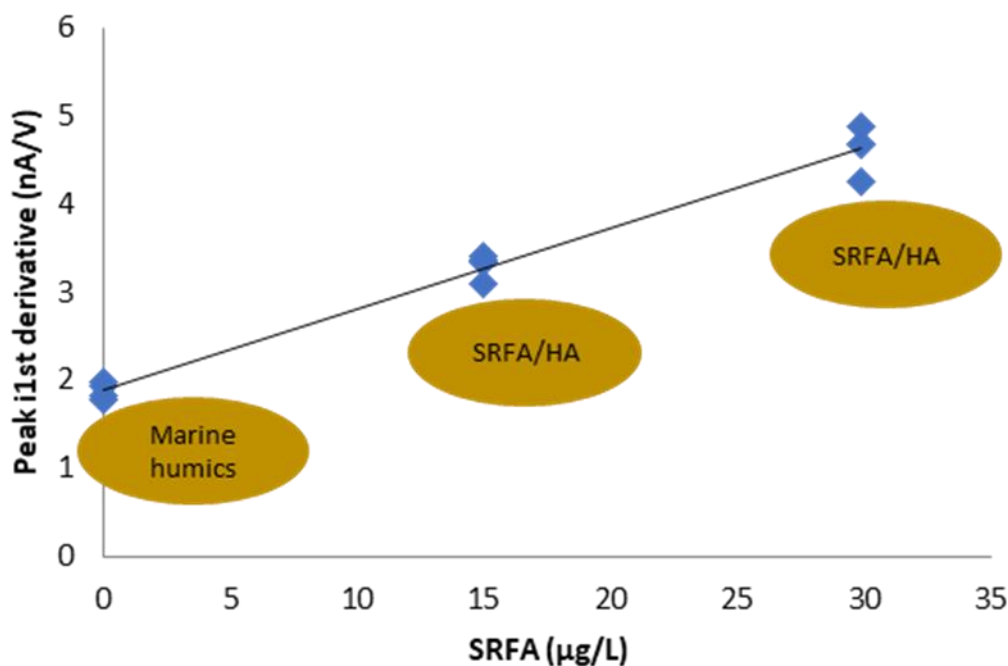


Figure 3: Size of eHS peak (measured in 1<sup>st</sup> peak derivative) against SRFA additions in a Mo-eHS CSV analysis. The size of the peak is at 0 SRFA addition is related to the concentration of marine eHS, the size of the eHS peak increases with subsequent additions of SRFA standard.

### 2. 3. 6. Composition of the eHS standard

The molecular structure and composition of SRFA and marine humics are distinct (Felgate et al. 2023). In a recent study which characterised a marine DOM standard 'TRM', the marine DOM standard was richer in N- and S-compounds compared to SRFA. Indeed, a major characteristic of marine humics is that the majority of compounds are found within a narrow elemental ratio range:  $1.17 \pm 0.13$  H/C and  $0.52 \pm 0.10$  O/C (Lechtenfeld et al. 2014) termed carboxylic rich alicyclic molecules (Hertkorn et al. 2006). In the marine DOM standard TRM, the majority of compounds fall within this range, while in SRFA a considerable portion of the CHO compounds extend outside of this range (Figure 4). As such, the SRFA contains more complex array of CHO molecules, of lower H/C (indicating higher aromaticity) and generally higher O/C (indicating greater number of O containing moieties such as -OH and -COOH) (Figure 4). Differences in the structure and composition of marine humics vs SRFA are underpinned by the different precursor molecules and processes involved in their

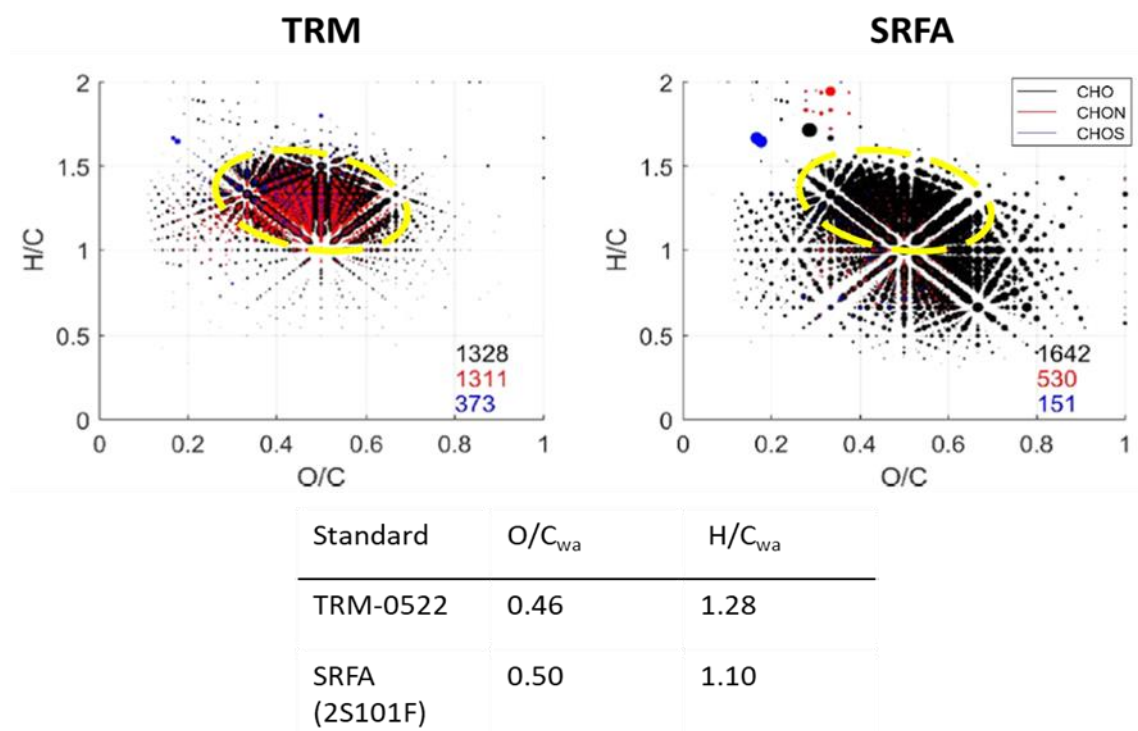


Figure 4: FTICR-MS elemental composition of a marine DOM extract (TRM) and a terrestrial humic standard (SRFA). Taken from Felgate et al. (2023). Yellow area indicates the approximate position of refractory CRAM molecule region as determined by Hertkorn et al. (2006) and Lechtenfeld et al. (2014).

production in either environment (described in Chapter 1). Another mechanism which could generate compositional differences between SRFA/HA standard and marine humics is chemical alteration of the SRFA/HA during the harsh extraction steps. This is currently under debate within the field (De Nobili et al. 2020; Kleber and Lehmann 2019; Lehmann and Kleber 2015). Finally, spatial and temporal variations in humic composition within the marine environment will result in varying degrees of compositional differences between the in-situ marine humics and the SRFA/HA standard (see Chapter 1). Therefore any particular marine humic isolated from a particular region at a particular time is likely to be compositionally different from the SRFA/HA standard.

### **2. 3. 6. 1. The impact of composition of the eHS standard on the eHS concentration calculation**

The analytical consequences of using a humic standard that is compositionally distinct from the humic analyte (natural marine humics) are largely unresolved. Few studies have

investigated this. In the Fe CSV method, the sensitivity to Fe-SRHA was approximately double that of SRFA (consistent with their Fe binding capacity) and as such the resultant eHS concentration when either standard is used is different (Laglera et al. 2007). Considering the compositional differences between SRFA and SRHA, these results highlight that the composition of the standard is an important factor in eHS quantification by CSV.

However, multiple lines of evidence support the application of the SRFA/HA standard. Firstly, linear increases after multiple additions of the standard suggest that the standard is comparable to the natural marine humics (Figure 3). Secondly, in the copper method, both the SRFA and SRHA standard have the same sensitivity (Whitby and van den Berg 2015), which lends confidence to the use of SRFA/HA standards. Finally, the SRFA/HA peaks are both the same shape and occur at the same potential on the voltammogram to those obtained with marine humics (Laglera et al. 2007; Quentel et al. 1987; Whitby and van den Berg 2015). Nevertheless, considering the variability in the composition of humics found in the marine environment, use of the SRFA/HA standard could have variable and unresolved consequences on the calculated eHS concentration. The need for a marine humic standard has been recently highlighted by the wider ‘humic’ community (Chin et al. 2023) and development is underway (e.g. a coastal marine DOM, Felgate et al. 2023), however the application presents similar compositional difference problems. This is a challenge that the community needs to address, but are still very much open questions.

### 2. 3. 7. Calculation of trace metal binding capacity

Several studies have performed voltammetry experiments to measure the binding capacity of SRFA/HA for Cu and Fe (Table 1). This can be measured using voltammetry by two methods. Firstly, using complexing ligand titrations where SRFA/HA compete against a strong ligand of known, well defined trace metal complexing capacity (in this case, salicylaldoxime; Whitby and van den Berg 2015).

Alternatively, by careful step-wise addition of trace metals until the trace metal eHS complex voltammetric signal reaches a maximum, which indicates saturation of trace

Trace metal	Binding capacity (nmol trace metal/mg SRFA/HA)	
	SRFA	SRHA
Cu	16 <sup>1</sup>	18 <sup>2</sup>
Fe	14.6 <sup>3</sup>	32 <sup>4</sup>

Table 1: Trace metal binding capacity of SRFA and SRHA for Cu and Fe. <sup>1</sup>Abualhaija et al. 2015, <sup>2</sup>Whitby and van den Berg 2015, <sup>3</sup>Sukekava et al. 2018, and <sup>4</sup>Laglera and van den Berg 2009.

metal binding sites (Laglera et al. 2007; Laglera and van den Berg 2009; Sukekava et al. 2018).

It is possible to use the trace metal binding capacity of SRFA/HA to calculate a eHS trace metal binding capacity/envelope for a given eHS concentration ( $[eHS]$ ) using equations 1 and 2, modified from (Whitby et al. 2020). For this calculation, the SRFA trace metal binding capacity is taken as a minimum bound and the SRHA trace metal binding capacity is taken as an upper bound. The result is two numbers, a minimum and maximum eHS trace metal binding capacity, which are reasonable first estimates.

$$(1) \text{ Maximum eHS trace metal binding capacity} = [eHS] \times \text{SRHA trace metal binding capacity}$$

$$(2) \text{ Minimum eHS trace metal binding capacity} = [eHS] \times \text{SRFA trace metal binding capacity}$$

The eHS trace metal binding capacity/envelope is useful because it allows intuitive comparison between eHS and trace metal concentrations. Further, comparison between the eHS trace metal binding capacity and in-situ trace metal concentrations can indicate whether a trace metal is in excess to the eHS binding capacity. However, these calculations carry certain assumptions, namely that the trace metal binding capacity of the marine humics is equal to, or covaries with that of the SRFA/HA standard which might not be the case given the compositional difference between the SRFA/HA and marine eHS (see next section), competition between different trace metals for eHS binding sites, and competition between different ligands and/or chemical speciation forms for certain trace metals. The latter two limitations are highly contextual and therefore will be discussed in the respective chapter discussion sections.

### **2. 3. 7. 1. Impact of the composition of the eHS standard on trace metal binding capacity calculation**

Molecular composition underpins trace metal binding capacity of organic ligands. This is because only certain molecular structures (moieties) are capable of donating electrons necessary to form a coordination (ligand) bond. Therefore, the abundance of ligand moieties exerts major control on trace metal binding capacity. Humic trace metal binding moieties include aromatic structures as well as oxygen containing groups such as phenolic, carboxylic, carbonyl, enolic, and alcoholic groups (see section 2. 3. 1.). Due to compositional differences

between terrestrial SRFA/HA and marine humics, it is likely that the abundance and composition of trace metal binding moieties, and consequently trace metal binding capacity, differs between the two. Further, the binding properties of humics are known to change during biogeochemical processing (Fourrier et al. 2022; Kikuchi et al. 2017). Therefore, the difference between the trace metal binding capacity of the marine humics and the standard varies with depth and time. These factors limit the application of SRFA/HA trace metal binding capacity to calculating the eHS trace metal binding capacity. As such, lack of knowledge on eHS molecular characteristics and their interaction with trace metal binding, represents an important knowledge gap. However, data indicates that eHS trace metal binding capacity falls below the SRHA upper limit in the Arctic, Pacific, and Atlantic Oceans which supports the use of the SRFA/HA trace metal binding capacity (Whitby et al. 2020) (Figure 5).

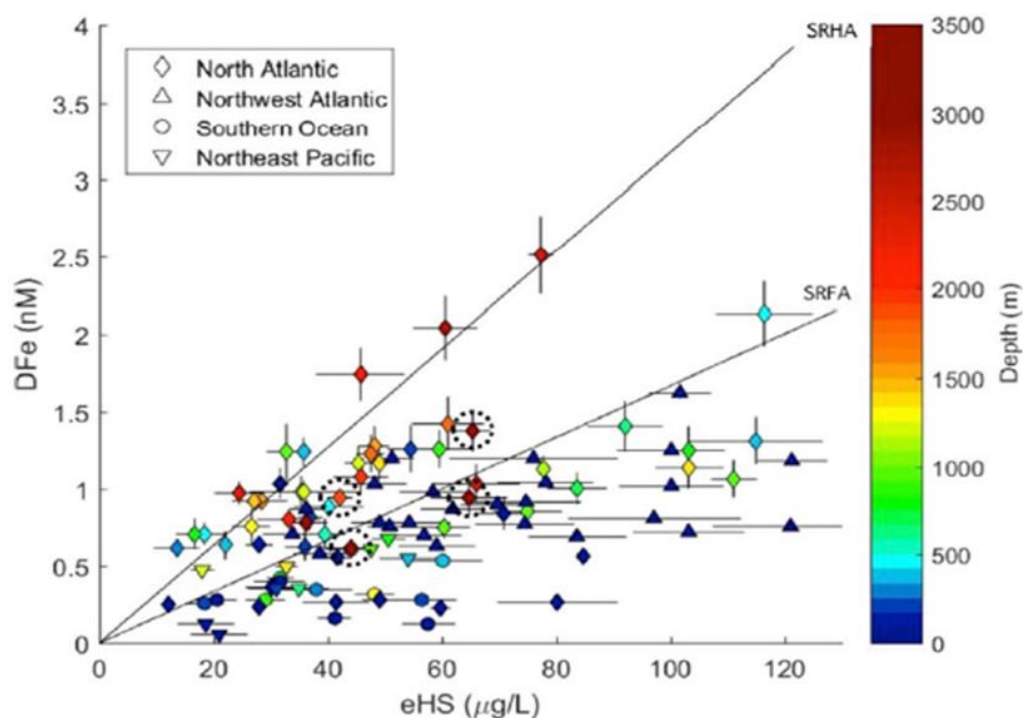


Figure 5: The relationship between dissolved Fe (DFe) with eHS, where the lines labelled SRHA and SRFA denote the respective binding capacities of these terrestrial standards. Taken from Whitby et al. (2020).

### 2. 3. 8. Calculation of carbon content of eHS

The International Humic Substances Society (IHSS) have characterised the molecular composition and structure of SRFA/HA standards in detail (IHSS 2019). The reported carbon content of the SRFA standard batch (2S101H) used in this thesis is 52.34 % (w/w). This can be used to convert measured eHS concentration ( $[eHS]$ ;  $\mu\text{g L}^{-1}$ ) into the estimated carbon content of the eHS pool (*eHS C content (SRFA)*;  $\mu\text{M}$ ), also using the molar mass of carbon (12 g/mol) (Equation 3) as in Dulaquais et al. (2018).

$$(3) \text{ eHS C content (SRFA)} = \frac{[eHS] \times 0.5234}{12}$$

This calculation is useful because it allows intuitive comparison of eHS with DOC. Further, it gives a first estimate of the carbon concentration of eHS which facilitates the discussion of eHS cycling in the context of carbon biogeochemistry, a potentially important role of eHS. However, this calculation assumes that the carbon content of the standard is equal to that of the in-situ eHS, which might not be the case given the compositional difference between the SRFA/HA and marine eHS which will be discussed in the next section.

#### 2. 3. 8. 1. Impact of the composition of the eHS standard on the eHS Carbon concentration calculation

In order to assess the impact of compositional differences between the eHS standard and the analyte on the eHS Carbon concentration calculation, Table 2 presents the carbon content of humics from different sources. Firstly, the carbon contents of SRFA and SRHA are very similar despite their compositional/structural differences (Table 3) which suggests that the carbon content of terrestrial humics may be relatively conservative. However, the carbon content of marine humics was generally lower than SRFA/HA (Table 2), likely originating from the differences in chemical composition between marine humics and the SRFA/HA standard, described in the previous section. Open ocean humics carbon content ranged from lower (-14 – -1 %) to higher (+ 8.5 %) carbon content than SRFA/HA (Table 2). On the other hand, coastal humics generally had lower (-11.5 – + 0.5 %) carbon content than SRFA/HA (Table 2). These spatial and temporal variations in marine humic carbon content highlight that the applicability of a single carbon content value to in-situ marine humics is limited. However, determining the carbon content of every humic sample across a transect is not feasible and the method to determine carbon content is time-consuming and expensive. Further, as SRFA is used in the analytical procedure to quantify the eHS, SRFA is

the best option until an appropriate marine humic standard is used to quantify the eHS peak.

Sample	Depth	Source	Location	Extraction	Fraction	C (% w/w)		
						Raw	Average	
SRFA <sup>1</sup>	n/a	Terrestrial	River	XAD-8, alkaline	FA	52.34	52.5	
SRHA <sup>1</sup>					HA	52.63		
TRM-0522 <sup>2</sup>	45	Marine	Coastal	C-18	Bulk DOM	41	46.8	
BE-Mar <sup>3</sup>	1			50				
BE-Apr <sup>3</sup>				43				
BE-May <sup>3</sup>				45				
BE-Jun <sup>3</sup>				51				
BE-Sep <sup>3</sup>				53				
SJF <sup>4</sup>	100			45				
EEP-1 <sup>4</sup>	5			XAD-2, alkaline		FA/HA		49.9
EEP-1 <sup>4</sup>	150							50.0
EEP-2 <sup>4</sup>	5							51.1
EEP-2 <sup>4</sup>	150	51.5						
HOTS-1 <sup>5</sup>	7.5	Open Ocean		45	49.0			
HOTS-1 <sup>5</sup>	2500			44				
NELHA-1 <sup>6</sup>	21	PPL	Bulk DOM	61				
NELHA-2 <sup>6</sup>	674			61				
NA-1 <sup>7</sup>	2			38.4				
NA-2 <sup>7</sup>	500	37.9						

Table 2: Carbon (C) content of humics. 1- IHSS, 2 – Felgate et al. (2023); 3 – Lodeiro et al. (2021); 4 – Meyers-Schulte and Hedges (1986); 5 – Broek et al. (2017); 6 – Green et al. (2014); 7 – Lodeiro et al. (2023).

### 2. 3. 9. Non-specificity of the eHS method

In CSV, using the 'Fe method' (Laglera et al. 2007) expolymeric substances (EPS) produces a peak at the same position as eHS (Hassler et al. 2011b). Therefore, EPS are indistinguishable from eHS by voltammetry. It is unknown whether this is the case under different voltammetric methods (Cu or Mo). In the Fe method, the peak of another molecule, glutathione, appears at a similar potential to eHS (Laglera et al. 2007). However, in the Mo method, which is performed at pH 2.0, glutathione appears at a different potential, far from

the eHS peak (Pernet-Coudrier et al. 2013). It is unknown whether this is also the case for EPS.

EPS are a distinct group of molecules with different biogeochemical cycling compared to humics. Therefore, the detection of EPS within the CSV eHS analytical window complicates interpretation of eHS data. EPS are hypothesised to be precursor molecules to humics; therefore, the two pools are biogeochemically related and knowledge on their bulk concentration is useful. As discussed in more detail in Chapter 1, EPS are maximum in the surface and covary with productivity, however they are rapidly degraded by prokaryotes and therefore decrease with depth (Hassler et al. 2011a). The contribution of EPS to the eHS signal is therefore expected to be greatest in highly productive, surface waters and minimal at depth.

## **2. 4. CDOM/FDOM measurement of humic substances**

### **2. 4. 1. CDOM/FDOM analytical principles**

CDOM/FDOM were first identified as components in water which appeared coloured to the naked eye, and are now operationally defined as the pool of DOM which absorbs light in the visible and UV wavelengths (Coble 2007). To measure this pool, light is passed through a water sample and the absorption is measured. By incrementally varying the wavelength from the visible to UV range and measuring the absorbance at each wavelength, an absorbance spectrum is generated (Figure 6). Several parameters can be extracted from this, including the absorbance at 254 nm and the slope ratio, which covary with chemical properties of the DOM. A specific component of the CDOM pool can also fluoresce under visible and UV light, this organic matter is termed fluorescent DOM (FDOM). When FDOM is exposed to light (termed the excitation), it fluoresces thereby producing light at a range of wavelengths (termed the emission). By incrementally varying the excitation wavelength and measuring the various emission fluorescence at different emission wavelengths, and excitation emission spectra (Ex/Em) can be generated. Several parameters relevant to humics can be extracted from these Ex/Em, including the humification index (a measure of the humic content of the organic matter; (Ohno 2002) and Coble peaks (Coble 1996; Coble 2007). The fluorescence emission intensity of humics are 'redshifted', i.e. shifted to longer wavelengths. A red shift in emission maximum can be caused by structural changes such as increase in aromaticity,

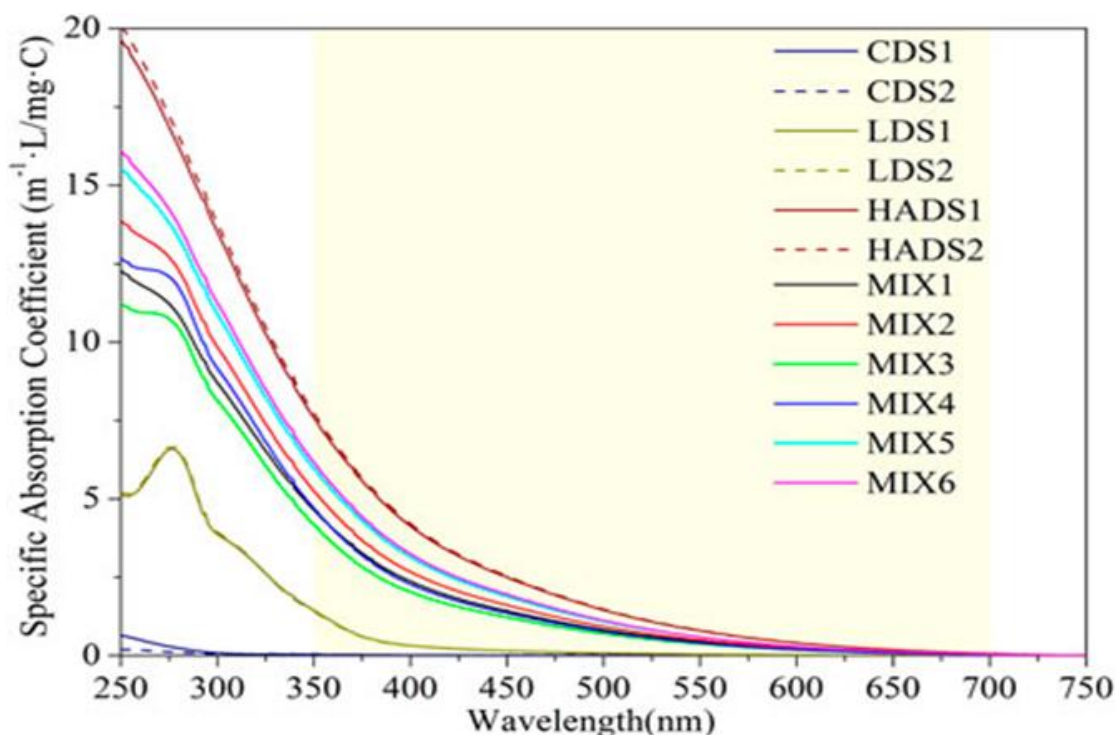


Figure 6: Light absorption of environmental samples of various sources at different wavelengths (UV to visible). Taken from Zeng et al. (2023).

increase in the number of conjugated bonds in a chain, or change of a non-linear to a linear ring system (all affecting fluorescence via increased  $\pi$ -electron system content), and/or addition of fluorescent functional groups including carbonyl, hydroxyl, and amine (Coble 1996; Senesi 1990) (Figure 7). Further, the presence of some functional groups such as carboxyl weaken the fluorescence emission intensity of a molecule, particularly when positioned on the exact opposite side to a hydroxyl group (Senesi 1990). Finally, humic spectra are generally broad (Coble 1996) reflecting the high complexity and low symmetry of the pool (Senesi 1990).

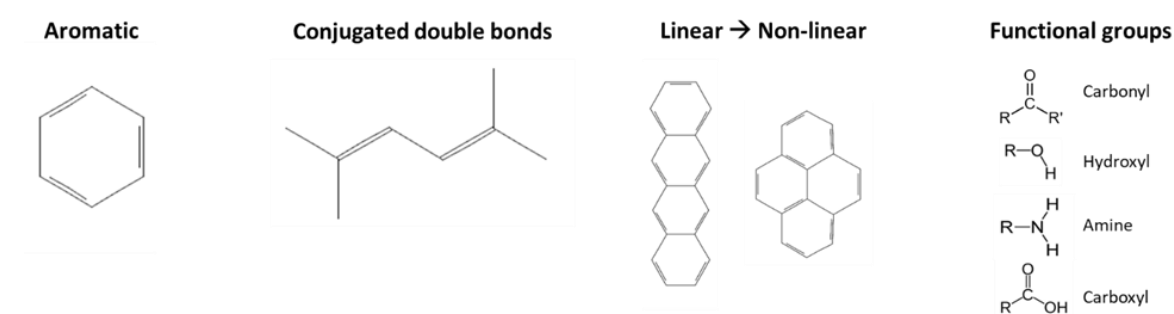


Figure 7: Functional groups identified as important at mediating fluorescence properties.

A further mathematical step can be taken to resolve part of this complexity. PARAllel FACtor analysis (PARAFAC) takes all of the samples' Em/Ex spectra and builds a model which resolves these spectra into several different spectral 'components' which adequately describe the complexity of the spectra (Murphy et al. 2013) (Figure 8). These

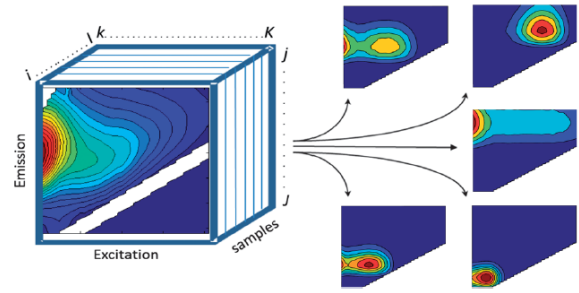


Figure 8: Schematic showing the analytical steps in PARAFAC taken from (Murphy et al. 2013)

spectral components can then be compared to a database which allows identification of these spectral components and inference of their structure and/or biogeochemical function (Murphy et al. 2014).

#### 2. 4. 2. Slope parameters: proxies of DOM, and humic, molecular composition

Two slope parameters were used by this study: absorbance at 254 nm and slope ratio. Absorbance at 254 nm ( $a_{254}$ ) normalised to DOC concentration ( $[DOC]$ ) is referred to as Specific Ultraviolet Absorbance ( $SUVA$ ) (Equation 4) (Weishaar et al. 2003).

$$(4) \quad SUVA = \frac{a_{254}}{[DOC]}$$

$SUVA$  is a robust and commonly utilised proxy for the aromatic content of DOM across aquatic systems (D'Andrilli et al. 2017; Weishaar et al. 2003; Zeng et al. 2023). Absorbance at 254 nm is sometimes used as a proxy for humic DOC (Summers et al. 1987; Zeng et al. 2023). However, the aromatic DOM pool is diverse, therefore DOM aromatic content can increase without increases in humified products (D'Andrilli et al. 2017). Further  $SUVA$  can be influenced by other factors such as iron concentration (Weishaar et al. 2003).

Spectral slope ratio ( $S_R$ ) is calculated according to Helms et al. (2008). The spectral slopes of the wavelength regions 275-295 nm ( $S_{275-295}$ ) and 350-400 nm ( $S_{350-400}$ ) were calculated using linear regression of the natural log transformed spectra (Figure 9). The spectral slope ratio ( $S_R$ ) was calculated as the ratio between  $S_{275-295}$  to  $S_{350-400}$  (Equation 5).

$$(5) \quad S_R = \frac{S_{275-295}}{S_{350-400}}$$

The inverse of the spectral slope ratio is commonly applied as a proxy for DOM molecular weight, as higher spectral slope ratio coincides with lower DOM molecular weight (Helms et

al. 2008). This is thought to occur due to a reduced potential for intramolecular charge transfer interactions in DOM of a lower molecular weight, which causes relatively greater absorption at shorter wavelengths, thereby increasing spectral slope ratio (Del Vecchio and Blough 2004; Helms et al. 2008). Note, spectral slope ratio were only linearly related to DOM molecular weight of less than 3 KDa (Helms et al. 2008). And, as Helms et al. (2008) point out in their article, further research is required to establish if spectral slope ratio is a widely applicable proxy for DOM molecular weight. Spectral slope ratio also strongly positively correlates with the elementary ratio of O/C and weakly positively correlates to the

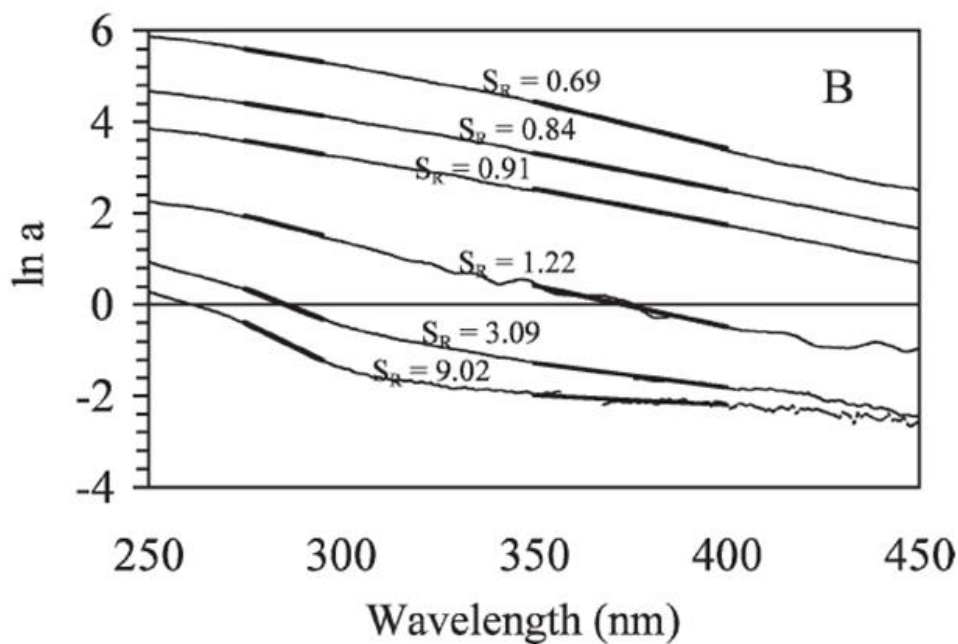


Figure 9: Procedure to calculate SR from multiple samples taken from Helms et al. (2008)

elementary ratio of H/C (Zeng et al. 2023). Although, again, these results are based on laboratory experiments performed on terrestrial organic matter extracts, which may limit their application to marine systems.

#### 2. 4. 3. Humification index: a proxy for humic DOM content

The humification index is a proxy for the humic content of DOM. It relies on the red-shifted fluorescence emission spectra of humics. Humification index (*HIX*) is calculated as the fluorescence intensity in the 300 – 345 nm region ( $I_{300-345}$ ) relative to the sum of the intensity in both the 300 – 345 nm ( $I_{300-345}$ ) and 435 – 480 nm regions ( $I_{435-480}$ ) (Equation 6), after correction for inner-filtration effects is performed (Ohno 2002). Under this

procedure, humification index is a robust, quantitative measure of the humic content of DOM when absorbance at 254 nm is  $\leq 0.3 \text{ cm}^{-1}$ . Otherwise, humification index is considered a qualitative measurement.

$$(6) \text{ HIX} = \frac{\sum I_{300-345}}{\sum I_{300-345} + \sum I_{435-480}}$$

#### **2. 4. 4. Humic Coble peaks a, m, c: proxies for humic chemical composition**

The humic coble peaks are fluorescent intensities within predefined ranges of Ex/Em and are characteristic of humics of different chemical composition as identified by Coble (1996) and later updated in Coble (2007). As aforementioned, the red-shift of an Ex/Em spectra can indicate chemical structure changes to DOM. Humic Coble peak c is red shifted relative to humic coble peak m (Coble 2007) (Figure 9). As such, it is expected that the humics responsible for peak c fluorescence exhibit any one or multiple of the following characteristics: higher aromaticity, more linear rings, more conjugated bonds, and/or more fluorescent functional groups, compared to the humics responsible for peak m fluorescence (Senesi 1990). However, the exact structural change(s) responsible for the spectral shift are unknown, as fluorescence is a nonspecific characteristic.

Coble peaks are selected via 'peak picking'. This has several drawbacks investigated by Korak et al. (2014). Firstly, many DOM samples do not exhibit a peak maximum within a Coble (1996) peak range. Secondly, as some peaks occur on the boundary of other peaks, peaks can influence the calculated intensity of 'neighboring' peaks. Although this effect is usually minimal for humic peak measurement, as they generally strongly influence other peaks.

#### **2. 4. 5. Humic PARAFAC peaks: proxies for humic chemical composition and origin**

PARAFAC analysis allows identification of multiple 'humic-like' components in a complex mixture (such as seawater) (Murphy et al. 2013). Each component is generally reported as the fluorescence intensity at the maximum (Fmax). Comparing the Fmax of different components is complex, as Fmax is a function of how abundant the component is (concentration) and how efficient the component is at absorbing and converting incident radiation into fluorescence (fluorescence efficiency) (Murphy et al. 2013).

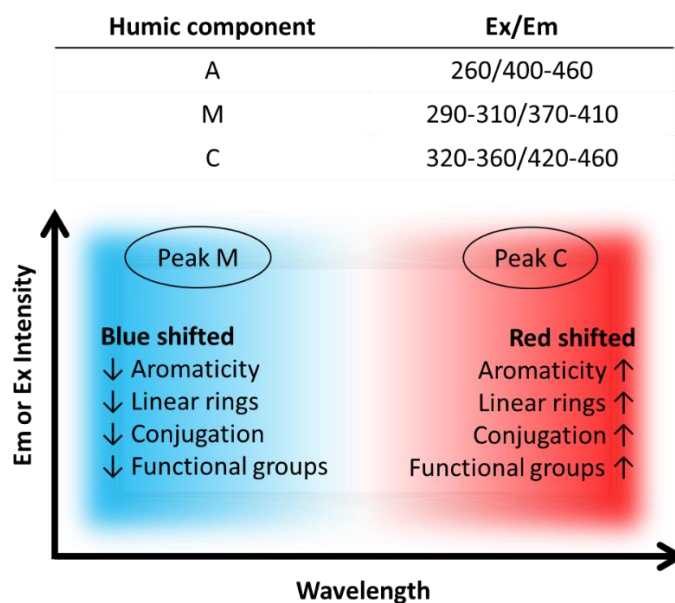


Figure 9: Relative Ex/Em of humic coble groups. Data from Coble (2007).

Once humic components are identified via PARAFAC, it is useful to cross reference and match these components against a database of previously reported PARAFAC components, such as OpenFluor (Murphy et al. 2014). This procedure returns a list of ‘matched’ spectra from the literature, along with environmental context in which these components were found. This facilitates the identification of these humic components. However, spectral matching does not guarantee that the components are chemically identical, rather it indicates shared spectral characteristics indicative of shared chemical structures (Murphy et al. 2014).

## 2. 5. Tandem CDOM/FDOM and voltammetric analysis

Quantification and characterisation of the humic pool represents an analytical challenge because of the heterogeneity of the humic pool. Characterisation of complex and heterogenous pools is a challenge because of the amount of information contained in complex mixtures, together with the overlap of properties making it difficult to distinguish individual molecules. The main aim of this thesis is to gain an understanding of trace metal binding humics specifically, and thus voltammetry measurements of eHS were the dominant analyses performed. However, measurement of CDOM/FDOM humics is also useful. CDOM/FDOM and voltammetry target different aspects of the humic structure (Figure 10), as demonstrated by lack of correlation between eHS and CDOM/FDOM humics in some environmental studies (e.g. Whitby et al. 2020). Therefore, tandem measurements of these

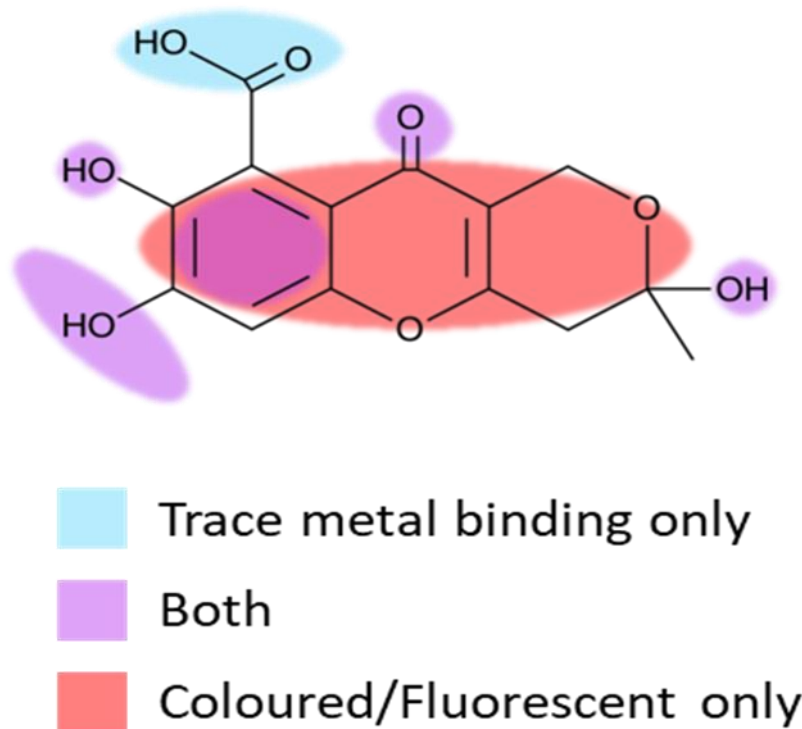


Figure 10: Schematic showing the functional groups targeted by voltammetry and/or CDOM/FDOM analyses.

two methods ‘widens the lens’ used to quantify humics, allowing a more holistic view of humic cycling in the context of the wider humic pool.

Further, voltammetric and CDOM/FDOM humic analysis are both bulk measurements, in that there is typically no fractionation of the DOM pool prior to analysis therefore any analytical response reflects the entire DOM pool. As such, in the ‘traditional’ eHS quantification step, humics are represented as a single peak which essentially only contains one ‘bit’ of information: the concentration of eHS. Whereas, for CDOM/FDOM humic quantification, more information is gathered which relates to the molecular characteristics. One notable difference between voltammetry and CDOM/FDOM analysis is the impact of the carboxyl group, which is thought to be responsible for the majority of trace metal binding and electroactive properties of eHS, while also acting to decrease the fluorescence properties of humics (references in relevant sections of this chapter). Therefore, observations of divergence or convergence of CDOM/FDOM and eHS profiles can be leveraged to give information about these molecular properties (e.g. Fourier et al. 2022).

Finally, establishing these links between voltammetric and CDOM/FDOM analysis can give insights into the molecular characteristics which drive trace metal binding and adds mechanistic understanding to the objectives of this thesis.

## 2. 6. References

- Abualhaija, M. M., H. Whitby, and C. M. G. van den Berg. 2015. Competition between copper and iron for humic ligands in estuarine waters. *Marine Chemistry* **172**: 46-56.
- Alves, G. M. S., J. M. C. S. Magalhães, P. Salaün, C. M. G. van den Berg, and H. M. V. M. Soares. 2011. Simultaneous electrochemical determination of arsenic, copper, lead and mercury in unpolluted fresh waters using a vibrating gold microwire electrode. *Analytica Chimica Acta* **703**: 1-7.
- Amin, S. A., D. H. Green, F. C. Küpper, and C. J. Carrano. 2009. Vibrioferrin, an Unusual Marine Siderophore: Iron Binding, Photochemistry, and Biological Implications. *Inorganic Chemistry* **48**: 11451-11458.
- Broek, T. A. B., B. D. Walker, T. P. Guilderson, and M. D. McCarthy. 2017. Coupled ultrafiltration and solid phase extraction approach for the targeted study of semi-labile high molecular weight and refractory low molecular weight dissolved organic matter. *Marine Chemistry* **194**: 146-157.
- Chin, Y.-P. and others 2023. Identification of next-generation International Humic Substances Society reference materials for advancing the understanding of the role of natural organic matter in the Anthropocene. *Aquatic Sciences* **85**: 32.
- Coble, P. G. 1996. Characterization of marine and terrestrial DOM in seawater using excitation-emission matrix spectroscopy. *Marine Chemistry* **51**: 325-346.
- . 2007. *Marine Optical Biogeochemistry: The Chemistry of Ocean Color*. *Chemical Reviews* **107**: 402-418.
- D'Andrilli, J., C. M. Foreman, M. Sigl, J. C. Priscu, and J. R. McConnell. 2017. A 21 000-year record of fluorescent organic matter markers in the WAIS Divide ice core. *Clim. Past* **13**: 533-544.
- Davis, W. M., C. L. Erickson, C. T. Johnston, J. J. Delfino, and J. E. Porter. 1999. Quantitative Fourier Transform Infrared spectroscopic investigation humic substance functional group composition. *Chemosphere* **38**: 2913-2928.

- De Nobili, M., C. Bravo, and Y. Chen. 2020. The spontaneous secondary synthesis of soil organic matter components: A critical examination of the soil continuum model theory. *Applied Soil Ecology* **154**: 103655.
- Del Vecchio, R., and N. V. Blough. 2004. On the Origin of the Optical Properties of Humic Substances. *Environmental Science & Technology* **38**: 3885-3891.
- Dulaquais, G. and others 2023. The role of humic-type ligands in the bioavailability and stabilization of dissolved iron in the Western Tropical South Pacific Ocean. *Front. Mar. Sci.* **10**.
- Dulaquais, G., M. Waeles, L. J. A. Gerringa, R. Middag, M. J. A. Rijkenberg, and R. Riso. 2018. The Biogeochemistry of Electroactive Humic Substances and Its Connection to Iron Chemistry in the North East Atlantic and the Western Mediterranean Sea. *Journal of Geophysical Research: Oceans* **123**: 5481-5499.
- Felgate, S. L., A. J. Craig, L. W. K. Moodie, and J. Hawkes. 2023. Characterization of a Newly Available Coastal Marine Dissolved Organic Matter Reference Material (TRM-0522). *Analytical Chemistry* **95**: 6559-6567.
- Fourrier, P. and others 2022. Characterization of the vertical size distribution, composition and chemical properties of dissolved organic matter in the (ultra)oligotrophic Pacific Ocean through a multi-detection approach. *Marine Chemistry* **240**: 104068.
- Frimmel, F. H., U. Lankes, H. D. Lüdemann, and M. B. Müller. 2005. Structural characterization of humic substances from waste water. , p. 3-22. . *In* G. Davies and E. Ghabbour [eds.], *Humic substances: molecular details and applications in land and water conservation*. . Taylor & Francis
- Gledhill, M. and others 2022. Trace metal stoichiometry of dissolved organic matter in the Amazon plume. *Science Advances* **8**: eabm2249.
- Green, N. W. and others 2014. An intercomparison of three methods for the large-scale isolation of oceanic dissolved organic matter. *Marine Chemistry* **161**: 14-19.
- Hassler, C. S., E. Alasonati, C. A. Mancuso Nichols, and V. I. Slaveykova. 2011a. Exopolysaccharides produced by bacteria isolated from the pelagic Southern Ocean — Role in Fe binding, chemical reactivity, and bioavailability. *Marine Chemistry* **123**: 88-98.

- Hassler, C. S., V. Schoemann, C. M. Nichols, E. C. V. Butler, and P. W. Boyd. 2011b. Saccharides enhance iron bioavailability to Southern Ocean phytoplankton. *Proceedings of the National Academy of Sciences* **108**: 1076-1081.
- Helms, J. R., A. Stubbins, J. D. Ritchie, E. C. Minor, D. J. Kieber, and K. Mopper. 2008. Absorption spectral slopes and slope ratios as indicators of molecular weight, source, and photobleaching of chromophoric dissolved organic matter. *Limnology and Oceanography* **53**: 955-969.
- Hertkorn, N. and others 2006. Characterization of a major refractory component of marine dissolved organic matter. *Geochimica et Cosmochimica Acta* **70**: 2990-3010.
- IHSS, I. H. S. S. 2019, <https://humic-substances.org/>.
- Kikuchi, T., M. Fujii, K. Terao, R. Jiwei, Y. P. Lee, and C. Yoshimura. 2017. Correlations between aromaticity of dissolved organic matter and trace metal concentrations in natural and effluent waters: A case study in the Sagami River Basin, Japan. *Science of The Total Environment* **576**: 36-45.
- Kleber, M., and J. Lehmann. 2019. Humic Substances Extracted by Alkali Are Invalid Proxies for the Dynamics and Functions of Organic Matter in Terrestrial and Aquatic Ecosystems. *Journal of Environmental Quality* **48**: :207–216.
- Konn, C. and others 2022. Extending the dataset of fluid geochemistry of the Menez Gwen, Lucky Strike, Rainbow, TAG and Snake Pit hydrothermal vent fields: Investigation of temporal stability and organic contribution. *Deep Sea Research Part I: Oceanographic Research Papers* **179**: 103630.
- Korak, J. A., A. D. Dotson, R. S. Summers, and F. L. Rosario-Ortiz. 2014. Critical analysis of commonly used fluorescence metrics to characterize dissolved organic matter. *Water Research* **49**: 327-338.
- Laglera, L. M., G. Battaglia, and C. M. G. van den Berg. 2007. Determination of humic substances in natural waters by cathodic stripping voltammetry of their complexes with iron. *Analytica Chimica Acta* **599**: 58-66.
- Laglera, L. M., and C. M. G. van den Berg. 2009. Evidence for geochemical control of iron by humic substances in seawater. *Limnology and Oceanography* **54**: 610-619.
- Lechtenfeld, O. J., G. Kattner, R. Flerus, S. L. McCallister, P. Schmitt-Kopplin, and B. P. Koch. 2014. Molecular transformation and degradation of refractory dissolved organic

- matter in the Atlantic and Southern Ocean. *Geochimica et Cosmochimica Acta* **126**: 321-337.
- Lehmann, J., and M. Kleber. 2015. The contentious nature of soil organic matter. *Nature* **528**: 60-68.
- Lodeiro, P., C. Rey-Castro, C. David, J. Puy, E. P. Achterberg, and M. Gledhill. 2021. Seasonal Variations in Proton Binding Characteristics of Dissolved Organic Matter Isolated from the Southwest Baltic Sea. *Environmental Science & Technology* **55**: 16215-16223.
- MacCarthy, P. 1976. A proposal to establish a reference collection of humic materials for interlaboratory comparisons. *Geoderma* **16**: 179-181.
- Mahieu, L. and others 2024. Iron-binding by dissolved organic matter in the Western Tropical South Pacific Ocean (GEOTRACES TONGA cruise GPpr14). *Front. Mar. Sci.* **11**.
- Meyers-Schulte, K. J., and J. I. Hedges. 1986. Molecular evidence for a terrestrial component of organic matter dissolved in ocean water. *Nature* **321**: 61-63.
- Murphy, K. R., C. A. Stedmon, D. Graeber, and R. Bro. 2013. Fluorescence spectroscopy and multi-way techniques. *PARAFAC. Analytical Methods* **5**: 6557-6566.
- Murphy, K. R., C. A. Stedmon, P. Wenig, and R. Bro. 2014. OpenFluor— an online spectral library of auto-fluorescence by organic compounds in the environment. *Analytical Methods* **6**: 658-661.
- Ohno, T. 2002. Fluorescence Inner-Filtering Correction for Determining the Humification Index of Dissolved Organic Matter. *Environmental Science & Technology* **36**: 742-746.
- Orlowska, E. and others 2017.  $\beta$ -O-4 type dilignol compounds and their iron complexes for modeling of iron binding to humic acids: synthesis, characterization, electrochemical studies and algal growth experiments. *New Journal of Chemistry* **41**: 11546-11555.
- Pernet-Coudrier, B., M. Waeles, M. Filella, F. Quentel, and R. D. Riso. 2013. Simple and simultaneous determination of glutathione, thioacetamide and refractory organic matter in natural waters by DP-CSV. *Science of The Total Environment* **463-464**: 997-1005.
- Portlock, G. 2023. The sources and sinks of thiols, reduced sulphur substances, and humic-like substances in hydrothermal waters. University of Liverpool.

- Quentel, F., C. Madec, and J. Courtot-coupez. 1987. Determination of Humic Substances in Seawater by Electrochemistry (Mechanisms). *Analytical Letters* **20**: 47-62.
- Salaün, P., and C. M. G. van den Berg. 2006. Voltammetric Detection of Mercury and Copper in Seawater Using a Gold Microwire Electrode. *Analytical Chemistry* **78**: 5052-5060.
- Schnitzer, M. 1978. Humic substances: chemistry and reactions. , p. 1-64. In *Developments in soil science* Elsevier. .
- Schnitzer, M., and R. Riffaldi. 1972. The Determination of Quinone Groups in Humic Substances. *Soil Science Society of America Journal* **36**: 772-777.
- Senesi, N. 1990. Molecular and quantitative aspects of the chemistry of fulvic acid and its interactions with metal ions and organic chemicals: Part II. The fluorescence spectroscopy approach. *Analytica Chimica Acta* **232**: 77-106.
- Sukekava, C., J. Downes, H. A. Slagter, L. J. A. Gerringa, and L. M. Laglera. 2018. Determination of the contribution of humic substances to iron complexation in seawater by catalytic cathodic stripping voltammetry. *Talanta* **189**: 359-364.
- Summers, R. S., P. K. Cornel, and P. V. Roberts. 1987. Molecular size distribution and spectroscopic characterization of humic substances. *Science of The Total Environment* **62**: 27-37.
- Sutak, R., J.-M. Camadro, and E. Lesuisse. 2020. Iron Uptake Mechanisms in Marine Phytoplankton. *Frontiers in Microbiology* **11**.
- Thurman, E. M., and R. L. Malcolm. 1981. Preparative isolation of aquatic humic substances. *Environ. Sci. Technol.* **15**: 463-466.
- van den Berg, C. M. G. 1984. Determination of copper in sea water by cathodic stripping voltammetry of complexes with catechol. *Analytica Chimica Acta* **164**: 195-207.
- van Schaik, J. W. J., I. Persson, D. B. Kleja, and J. P. Gustafsson. 2008. EXAFS Study on the Reactions between Iron and Fulvic Acid in Acid Aqueous Solutions. *Environmental Science & Technology* **42**: 2367-2373.
- Vinkler, P., B. Lakatos, and J. Meisel. 1976. Infrared spectroscopic investigations of humic substances and their metal complexes. *Geoderma* **15**: 231-242.
- Weishaar, J. L., G. R. Aiken, B. A. Bergamaschi, M. S. Fram, R. Fujii, and K. Mopper. 2003. Evaluation of Specific Ultraviolet Absorbance as an Indicator of the Chemical Composition and Reactivity of Dissolved Organic Carbon. *Environmental Science & Technology* **37**: 4702-4708.

- Whitby, H. and others 2020. A call for refining the role of humic-like substances in the oceanic iron cycle. *Scientific Reports* **10**: 6144.
- Whitby, H., and C. M. G. van den Berg. 2015. Evidence for copper-binding humic substances in seawater. *Marine Chemistry* **173**: 282-290.
- Zeng, R., C. M. Mannaerts, and C. Lievens. 2023. Assessment of UV-VIS spectra analysis methods for quantifying the absorption properties of chromophoric dissolved organic matter (CDOM). *Frontiers in Environmental Science* **11**.

## **Chapter 3 Variable microbial cycling of metal binding humic substances and its interaction with iron in the Southern Ocean**

Millie Goddard-Dwyer<sup>1</sup>, Alessandro Tagliabue<sup>1</sup>, H el ene Planquette<sup>2</sup>, Thomas Ryan-Keogh<sup>3</sup>, Stacey Felgate<sup>4</sup>, Corentin Baudet<sup>2</sup>, David Gonz alez-Santana<sup>2</sup>, Bruno Hamelin<sup>5</sup>, Nolwenn Lemaitre<sup>6</sup>, Wen-Hsuan Liao<sup>2</sup>, Maria Vorrath<sup>2</sup>, St ephane Blain<sup>7</sup>, Audrey Gueneugues<sup>7</sup>, Ingrid Obernosterer<sup>7</sup>, Rui Zhang<sup>7</sup>, Catherine Jeandel<sup>8</sup>, Hannah Whitby<sup>1</sup>,

1. University of Liverpool, UK
2. LEMAR, France
3. CSIR, South Africa
4. Heriot-Watt University, Edinburgh, UK
5. CEREGE, France
6. ETH, Switzerland
7. LOMIC, France
8. LEGOS, France

### Statement of contributions:

CB, DGS, BH, NL, WHL, and MV collected the eHS and DFe samples. MGD performed the eHS and CDOM/FDOM analysis. HP and CB performed the DFe analysis. TRK performed the CHEMTAX, derived bloom phenology and net primary production, and calculated AOU and MLD. AG and SB collected and analysed DOC samples. RZ and IO collected and analysed bacterial counts. SF performed the PARFAC. SF and MGD performed CDOM/FDOM data analysis. MGD performed the data analysis and wrote the manuscript. MGD, AT, HP, and HW edited the manuscript.

### Highlights:

- eHS production was closely linked to specific phytoplankton taxa.
- Zooplankton grazing and phytoplankton senescence were important sources of eHS in surface waters.
- Bacterial remineralisation was a source of eHS in mesopelagic waters off the island plateaus.

- Aside from over shallow island plateaus, eHS and DFe were uncoupled throughout the transect

### **3. 1. Abstract:**

Trace metal availability is an important control on the marine carbon cycle via limitation of primary production. A key factor controlling the availability of trace metals is complexation by components of the dissolved organic carbon (DOC) pool called organic ligands. Within this pool, trace metal binding humic substances (eHS) are thought to play an important role. However, the processes that control humic cycling are poorly constrained and their overall impact on trace metals and DOC cycling is unknown. The Southwest Indian sector of the Southern Ocean is largely depleted in trace metals and organic carbon, with point sources of trace metals associated with islands that stimulate high productivity. These gradients in trace metals and productivity present a unique opportunity to investigate the processes involved in eHS cycling. Here we determine the distribution of eHS along the GEOTRACES GS02 section and its relationship with phytoplankton community composition, pigment proxies for grazing, apparent oxygen utilisation, and both dissolved organic carbon and dissolved Fe (DFe) concentrations. The phytoplankton blooms associated with the islands were linked to elevated levels of eHS, potentially modulated by phytoplankton community composition and grazing. Over shallow island plateaus, DFe was closely related to eHS, implying eHS may contribute to local Fe supply. Off plateau, microbial remineralisation was a potential important source of eHS, which could play a role in local carbon storage. However, eHS and DFe were uncoupled offshore, likely as a result of elevated DFe relative to eHS from microbial remineralisation processes. Uncoupling between eHS and DFe together with DFe in excess of eHS Fe binding capacity imply other Fe stabilisation mechanisms may be more important in regional Fe supply. Ultimately, this study provides a first estimate of the processes that control eHS distribution in the region and highlights potential impacts of eHS on DFe stabilisation and carbon cycling and storage.

### **3. 2. Introduction**

Trace metal availability is a major control on the marine carbon cycle (Moore et al. 2013; Tortell et al. 1996). The Southern Ocean is the largest trace metal limited ocean region (Tagliabue et al. 2017). Here, primary production is primarily limited by lack of iron (Fe) and

manganese (Mn) (Browning et al. 2021; Hawco et al. 2022) and marine heterotrophic activity is usually limited by Fe and organic carbon (Church et al. 2000; Fourquez et al. 2020; Obernosterer et al. 2015; Tortell et al. 1996). Due to minimal external sources of trace metals, internal processes which recycle trace metals are important (Boyd et al. 2015). These include microbial remineralisation and food web processes such as zooplankton grazing (Barbeau et al. 1996). The region also has important localised sources of new trace metals including aeolian deposition of dust and fire derived particles (Tagliabue et al. 2009; Tang et al. 2021), hydrothermal (Tagliabue et al. 2022), and sedimentary inputs from seafloor sediments, sub-Antarctic island plateaus, and the Antarctic continental land-mass (Bowie et al. 2015; Tagliabue et al. 2009). Proximal to these trace metal sources, primary production is elevated due to alleviation of trace metal limitation and carbon export is promoted (Ardyna et al. 2019; Blain et al. 2007), heterotrophic activity is also elevated due to supply of phytoplankton derived organic carbon alleviating organic carbon limitation (Obernosterer et al. 2008; Obernosterer et al. 2015). Overall, trace metal stimulated microbial activity amplifies the Southern Oceans important role in carbon storage (Sabine et al. 2004). Therefore, understanding the mechanisms of trace metal supply to the Southern Ocean is key to understanding carbon export and storage in the region.

Trace metal biogeochemistry is controlled by a complex network of factors including magnitude of supply and physical and chemical speciation (Tagliabue et al. 2017). Of the diverse suite of Fe chemical species, Fe organic complexation is an important factor influencing Fe solubility, transport, and bioavailability (Moffett and Boiteau 2024; Whitby et al. 2024). Organic molecules which complex Fe (Fe binding ligands) are a diverse pool including siderophores, exopolymeric substances, saccharides, and humic substances (Gledhill and Buck 2012). Humics are a heterogeneous pool of organic matter dominated by carboxyl rich alicyclic molecules with aromatic, phenol, and alkyl groups (Frimmel et al. 2005; Hertkorn et al. 2006) which have been identified as important Fe binding ligands mediating Fe distribution in productive, terrestrially influenced basins such as the Arctic, North Atlantic, and North Pacific Oceans (Kitayama et al. 2009; Laglera et al. 2019; Whitby et al. 2020b; Yamashita et al. 2020). However, in the sub-tropical Pacific and at select biogeochemical sites in the Southern Ocean, data suggest that Fe distribution is uncoupled from humics (Cabanes et al. 2020; Fourquez et al. 2023). Due to the lack of trace metal

binding humic data from the Southern Ocean, it is unknown whether this relationship holds true on a basin scale. Humics have the potential to be important in Southern Ocean Fe cycling as the same processes which cycle Fe are involved in humic cycling. Terrestrial derived humics and humic-like substances can be transported to the ocean via aeolian (Graber and Rudich 2006), riverine (Batchelli et al. 2010; Krachler et al. 2015), and glacial inputs (Jeon et al. 2021). In-situ pathways which cycle humics include microbial remineralisation of organic matter (Whitby et al. 2020a), phytoplankton (Castillo et al. 2010), zooplankton grazing (Urban-Rich et al. 2006), hydrothermal activity (Yang et al. 2012), and marine sedimentary efflux (Nissenbaum and Kaplan 1972), all of which are also sources of Fe (see references above).

Evidence suggests that humic cycling pathways are likely to be variable across the Southern Ocean in response to trace metal availability. Firstly, phytoplankton can exude different amounts of humics according to community composition (Castillo et al. 2010; Norman et al. 2015), and community composition varies in response to trace metal availability in the Southern Ocean (Armand et al. 2008; Irion et al. 2020). Secondly, zooplankton grazing may release humics via excretion (*refs in* Steinberg et al. 2004; Urban-Rich et al. 2006; Urban-Rich et al. 2004), egestion and subsequent dissolution of faecal pellets (Cabanes et al. 2017), and release of phytoplankton cell content by sloppy feeding (Møller et al. 2003). Zooplankton grazing varies in response to trace metal availability in the Southern Ocean (Carlotti et al. 2015). Finally, the strength of microbial remineralisation is linked to trace metal availability in the Southern Ocean (Jacquet et al. 2008; Obernosterer et al. 2008) and humic production by microbial remineralisation is influenced by the quantity and composition of particulate organic matter such as the lithogenic vs biogenic fractions (Whitby et al. 2020a). The resultant impact of these processes on humic distribution and subsequent interactions with wider dissolved organic carbon (DOC) cycling and Fe are unknown.

The Southwest Indian Sector of the Southern Ocean is a region of predominantly low primary productivity due to persistent trace metal limitation, with diverse point sources of trace metals which support primary productivity and promote carbon storage. This includes hydrothermal activity at the Southwest Indian Ridge (e.g. Léon et al. 2024), glacial and volcanic sources at Heard and McDonald Islands (Holmes et al. 2019), and island mass effect sources with increasing magnitude from Marion Island, to Crozet Archipelago, to Kerguelen

plateau (Blain et al. 2007; Planquette et al. 2007). These highly local trace metal sources across environmental gradients act as a unique ‘natural laboratory’ across which processes such as phytoplankton community composition, zooplankton grazing, and remineralisation vary (Armand et al. 2008; Carlotti et al. 2015; Jacquet et al. 2008), offering a unique opportunity to untangle the biological processes involved in the cycling of humics and the wider DOC pool. Further, the impact of trace metal binding humics on Fe solubility and transport is unknown but potentially an important part of Fe biogeochemistry in the region. Addressing these knowledge gaps is important to understand the mechanisms controlling trace metal cycling, and consequently microbial activity and carbon storage in this climatically important region.

In this context, this study provides a first basin scale quantification of trace metal binding humics (electroactive humic substances, eHS) and its relationship with Fe and wider DOC cycling in the Southwest Indian part of the Southern Ocean. Using CHEMTAX derived phytoplankton community composition, pigment-derived grazing proxies, and apparent oxygen utilisation as a microbial remineralisation proxy, we assess how these microbial processes link to eHS distributions, providing insight into the relationship between eHS and both Fe and wider DOC cycling, in different horizontal and vertical biogeochemical regions of the transect.

### **3. 3. Methods**

#### **3. 3. 1. Hydrographic setting**

The Antarctic circumpolar current (ACC) is split into multiple jets associated with fronts and frontal zones ordered from north to south, the location of these fronts was determined as in Park et al. (2019) and are shown in Figure 1a. However, in this region the Sub Antarctic front (SAF) often merges with the Sub-tropical Front (STF) therefore the region north of the SAF is termed the sub-Antarctic frontal zone (SAFZ) or the Sub-tropical frontal zone (STFZ). The area between the SAF and the Polar Front (PF) is termed the Polar Frontal Zone (PFZ). Antarctic water (AW) is found between the PF and the Southern Antarctic Circumpolar Current Front (SACCF). Note that the fronts listed here can separate into northern, middle, and southern branches of the frontal jets (e.g. Sokolov and Rintoul 2009). Station 14 was within the SAFZ; Stations 16 – 27 and 31 – 42 were within the PFZ; Station 29, Stations 44 –

48 and 63 – 68 were within AW. Station 58 beyond the SACCF. The position of the stations around the islands is shown in Figure S1.

Three water masses were identified according to their neutral density characteristics: Upper Circumpolar Deep Water (UCDW) and Lower Circumpolar Deep Water (LCDW) which dominated across the majority of the transect, and Antarctic Bottom Water (AABW). Due to the low number of samples within the AABW it was excluded from analysis. UCDW was found between 200 and 1200m in mesopelagic waters. LCDW generally extended from ~600 – 3500m (excluding Station 58 where the LCDW shoals dramatically).

### **3. 3. 2. Sampling**

Sampling was conducted during the SWINGS GS02 GEOTRACES (MD229) research cruise Jan 11<sup>th</sup>-March 8<sup>th</sup> 2021 (Fig 1a) aboard the N/O Marion Dufresne according to GEOTRACES protocols (Cutter et al. 2017). Trace metal clean water for dissolved trace metals (DTM), humics, and DOC samples was collected using a clean system made of 24 Go-Flo bottles mounted on a trace metal clean rosette. Seawater for DTM, and humics were subsequently filtered through acid cleaned 0.45 µm filters into acid cleaned LDPE bottles prior to freezing and storage at -20 °C inside a class-100 clean container on board the ship.

### **3. 3. 3. Electroactive humic substances (eHS)**

#### **3. 3. 3. 1. Reagents**

Molybdenum standard solutions were prepared by dilution in Milli-Q and acidified to pH 2 using HCl. Suwannee River Fulvic acid (SRFA) standards (2S101H, IHSS) were dissolved in Milli-Q and acidified to pH 2 using HCl. Samples and standards were acidified using TraceMetal™ Grade HCl (Fisher Chemical™).

#### **3. 3. 3. 2. Instrumentation**

Analyses were conducted using cathodic stripping voltammetry as described in Pernet-Coudrier et al. (2013) using a Metrohm µAutolab 3 potentiostat controlled by NOVA software (version 2.1.7) and Metrohm V663 stand controlled via Metrohm IME663. The system comprised of a hanging mercury drop working electrode, a glassy carbon auxiliary electrode, and an Ag/AgCl (3 mol L<sup>-1</sup> KCl) reference electrode. Samples were defrosted in the dark and mixed thoroughly prior to aliquoting. 10 mL seawater sample was added to an acid cleaned glass electrochemical cell, acidified to pH 2, and 200 nmol L<sup>-1</sup> Mo(VI) added. Modifications to the method described by Pernet-Coudrier et al. (2013) include using a

deposition time of 400s, and using the 1<sup>st</sup> derivative of the peak processed in ECD software (Omanović 2011) to quantify the eHS peak. The humic concentration was quantified using two standard additions of SRFA standard. The concentration and standard deviation was calculated as described by Harris (2003). The limit of detection (three times the standard deviation of the sample with the lowest eHS concentration) was calculated as 3.81 µg/L.

### **3. 3. 3. 3. Validation**

Daily measurement of a reference material was used to validate the cathodic stripping voltammetry data. This reference material was Hansell lab dissolved organic carbon certified reference material deep (batch 21 lot 11-21 and batch 22 lot 10-22). The average concentration of the reference material was  $22.6 \pm 5.0$  µg/L for batch 21 lot 11-21 and  $22.4 \pm 3.23$  µg/L for batch 22 lot 10-22. Approximately daily measurements of the reference material were conducted, data where average eHS concentrations and/or standard deviation within this certified reference material range were accepted.

### **3. 3. 3. 4. Calculation of eHS Fe binding envelope**

The eHS Fe binding envelope (nM Fe equivalent) was calculated from reported values for humic standards SRFA and SRHA standards, 0.0146 nmol Fe/ µg SRFA and 0.032 nmol Fe/ µg Suwannee River Humic acid (SRHA) (Laglera and van den Berg 2009; Sukekava et al. 2018) using Eq. 1 and 2 modified from Whitby et al. (2020b).

$$\text{Eq. 1 Lower HS Fe binding capacity (SRFA)} = [eHS] \times 0.0146$$

$$\text{Eq. 2 Upper HS Fe binding capacity (SRHA)} = [eHS] \times 0.032$$

We estimate a Fe eHS binding envelope using the maximum and minimum reported Fe binding capacity of terrestrial humic standards to allow comparison of eHS to DFe in terms of nM Fe (Fourquez et al. 2023; Whitby et al. 2020b). It is important to note that the Fe binding capacity of the terrestrial humic standards may not covary with the Fe binding capacity of the in-situ marine eHS (see Chapter 2), particularly considering the structural differences between the terrestrial and marine humics as a result of the different precursor molecules and processes which are involved in humics production pathways in each environment (Muller 2018). eHS represent the concentration of humic-like ligands that are able to bind Fe, however competition for Fe between different Fe binding organic ligands will also occur, while other metals may compete with Fe for humic binding sites (Gao and

Guéguen 2018; Whitby and van den Berg 2015). The paucity of direct observations of Fe binding capacity, arrangement, and strength of in-situ eHS is a key knowledge gap inhibiting our understanding of the role of eHS in trace metal cycling. However, in the absence of direct observations of eHS trace metal binding capacity, employing the humics Fe binding envelope facilitates a valuable first step in the understanding interactions between eHS and DFe across the Southwest Indian Sector of the Southern Ocean.

### **3. 3. 3. 5. Calculation of eHS carbon content**

The approximate carbon concentration of the eHS pool ( $\mu\text{M}$ ) can be calculated using the reported carbon concentration of the SRFA standard (2S101H; IHSS 2019; 52.34 %) and the molar mass of carbon (12 g/mol) using Eq. 3.

$$\text{Eq. 3 HS C content (SRFA)} = \frac{[eHS] \times 0.5234}{12}$$

We estimate carbon content of eHS to enable more intuitive comparison between eHS and DOC, however this assumes constant eHS carbon content which is likely not the case because of structural differences between marine and terrestrial humics (e.g. Felgate et al. 2023) and spatial variation in marine eHS C content (e.g. Stuermer and Harvey 1974). However, there is currently no simple and/or agreed method within the field to directly measure eHS carbon content, therefore with these assumptions in mind, our method of representing eHS carbon content is a reasonable first step towards understanding the role of eHS in carbon cycling.

### **3. 3. 4. Dissolved organic carbon (DOC)**

Seawater for DOC analyses was filtered through two ashed (24h, 450 °C) 0.7  $\mu\text{m}$  GF/F filters using a custom-made all-glass/Teflon filtration syringe system into ashed ampoules, acidified to pH 2 using phosphoric acid, sealed ampoules were stored at room temperature in the dark until analyses by high temperature catalytic oxidation (HTCO) on a Shimadzu TOC-V-CSH analyzer (Benner and Strom 1993).

### **3. 3. 5. Coloured/Fluorescent dissolved organic matter and PARAFAC**

Coloured dissolved organic matter (DOM)/Fluorescent DOM (CDOM/FDOM) analysis was conducted on stations around Crozet (Stations 29, 31, 33, 36, and 38). CDOM/FDOM samples were aliquoted into HCl cleaned glass vials with HDPE septa from eHS sample bottles. Samples were stored at 5 °C before analysis took place the following day using a

Cary Eclipse Fluorescence Spectrophotometer and a Cary 60 UV-vis spectrophotometer (Agilent; 1 cm cells). All analysis was performed in R version 4.3.1 using the latest StarDom package according to Murphy et al. (2013; 2014).

### **3. 3. 6. Prokaryote abundance**

Seawater was collected as described for DOC. 1.8 mL were fixed with glutaraldehyde (1% w/v final concentration) in the dark at 4 °C for 30 mins prior to flash freezing in liquid nitrogen. Samples were stored at -80°C until analysis using BD FACS Canto as described in Obernosterer et al. (2008). For integration with eHS and DFe datasets, depths were rounded to the nearest 10m.

### **3. 3. 7. Phytoplankton pigment and community composition**

Seawater was collected using Niskin bottles mounted on the standard rosette. 1 – 1.5 L seawater was filtered through 0.7 µm GF/F (Whatman) filters prior to flash freezing the filters in liquid nitrogen. Samples were stored at -80°C prior to analysis. Filters were extracted in 100 % methanol for 2 h prior to sonication and subsequently clarified by filtration using GF/F (Whatman). HPLC analysis using a HPLC Agilent Technologies 1200 was completed within 24 h of beginning the extraction as described in Ras et al. (2008).

CHEMTAX software was used to determine relative community structure. Pigment data was manually grouped into biogeographical regions (Mackey et al. 1996; Wright 2008). Stations where Divinyl-Chl-a was present were allocated to STZ group. Stations below the PF were allocated to the AW group. Stations within the PFZ which were visual identified as close to the sub-Antarctic Islands or in shallow bathymetry were classified as 'island'. All remaining stations were allocated to the PFZ group. CHEMTAX v1.9.5 was used to perform the analysis. Initial starting ratios for each group taken from Viljoen (2023) were randomised into an additional 59 ratio matrices using a randomisation factor of 0.7. CHEMTAX was performed with each of these 60 matrices with a  $\leq 200$  iterations per matrix. The resultant 6 pigment ratios with the lowest root mean square (RMS) error were averaged. If this did not produce a RMS of less than 0.05, the CHEMTAX was repeated using previously identified top 6 pigment ratios with a randomisation factor of 0.4. The relative contributions of micro, nano, and pico size classes were then determined using Brewin et al. (2015) and these proportions were transformed into mean community size index as in Bricaud et al. (2004).

### 3. 3. 8. Satellite derived net Primary Production

Satellite derived net Primary Production was computed using the CBPM algorithm (Behrenfeld et al. 2005) and averaged over the duration of the cruise.

### 3. 3. 9. Bloom Phenology

Bloom phenology was derived from satellite-derived chlorophyll-a concentrations (European Space Agency ocean colour climate change initiative (OC-CCI; <https://esa-oceancolour-cci.org>; v6.0, Sathyendranath et al. 2019) at 4 km and 8 day resolution over the time period 01/01/1998 – 30/06/2022. Missing data was reduced by first re-gridding the chlorophyll-a values using bilinear interpolation to a regular 25 km grid using the xESMF Python package (Zhuang 2018) and secondly by applying a linear interpolation scheme in sequential steps of longitude, latitude and time (Racault et al. 2014) using a three-point window. If one of the points bordering the gap along the indicated axis was invalid it was omitted from the calculation, whilst if two surrounding points were invalid then the gap was not filled. Finally, a moving average filter of the successive time steps described in more detail by Salgado-Hernanz et al. (2019).

### 3. 3. 10. Apparent Oxygen Utilisation

Apparent Oxygen Utilisation (AOU) evaluates integral oxygen consumption by biological activity and is computed as the difference between the oxygen saturation concentration and the actually observed oxygen concentration (Eq. 4).

$$Eq. 4 \quad AOU = O_{2,sat}(CT \times SA) - [O_2]$$

Where  $O_{2,sat}$  is determined as a function of Absolute Salinity ( $SA$ ) and Conservative Temperature ( $CT$ ). All calculations of  $O_{2,sat}$ ,  $SA$  and  $CT$  were performed in Python using the Gibbs SeaWater TEOS-10 toolbox.

### 3. 3. 11. Definition of water column structures

Temperature, salinity, and density profiles were visually inspected to determine the mixed layer depth according to the usual change in temperature and change in density criteria. In cases where a shallower mixed layer with weaker basal stratification sat above a deeper, older mixed layer with stronger basal stratification, the latter was chosen as the mixed layer depth. Mesopelagic waters were defined according as between the mixed layer depth and above the minimum oxygen depth. Minimum oxygen depth for a station was taken as depth

where oxygen concentration reached minima in the trace metal rosette CTD Oxygen profile. Deep waters were defined as between the depth of oxygen minimum and the seafloor.

### **3. 3. 12. Statistical approaches**

All statistical analyses were carried out in R version 4.3.1. Normality was assessed using Shapiro-Wilks test. Spearman rank correlations were used for pairwise correlation matrixes using the Hmisc package (rcorr function). Otherwise, spearman rank correlations were performed on non-parametric pairwise data and Pearson correlations were performed on parametric pairwise data both using the r stats package (cor.test function).

### **3. 4. Results**

#### **3. 4. 1. Phytoplankton bloom characteristics**

Chlorophyll-a concentration was elevated downstream of Crozet and over the Kerguelen plateau downstream of Heard and McDonald Islands (Figure 1d). Chlorophyll-a concentration was much greater at Kerguelen compared to that of Crozet. Conversely, satellite primary production estimates were greater around Crozet compared to Kerguelen (Figure 1b). Further, phytoplankton bloom phenology taken from satellite estimates of primary production indicate that these two phytoplankton blooms were at different stages of bloom development (Figure 1c). The peak of the bloom occurred more recently at Kerguelen ( $47 \pm 14$  days ago) compared to Crozet ( $68 \pm 9$  days ago) (Figure 1c).

#### **3. 4. 2. eHS distribution**

eHS concentration averaged  $20.2 \pm 8.3$   $\mu\text{g/L}$  across the transect and ranged from 6.8 – 67.8  $\mu\text{g/L}$  (Figure 2a). eHS exhibited a patchy distribution, with peaks observed throughout the water column in the surface mixed layer (average  $21.5 \pm 14.9$   $\mu\text{g/L}$ ), mesopelagic waters (average  $20.1 \pm 7.0$   $\mu\text{g/L}$ ), and deep waters (average  $19.7 \pm 6.5$   $\mu\text{g/L}$ ). The islands and their associated plateaus influenced eHS distribution (Figure 2a). Small plumes of eHS were observed downstream of both Marion and Crozet at <1000m. In the upper 500m, eHS was clearly and consistently elevated downstream of the Crozet and Kerguelen (Figure 2a). This effect was greatest at Kerguelen (Figure 2a), consistent with the intensity of the sampled phytoplankton blooms (Figure 1d). eHS exhibited widespread maxima over the Kerguelen plateau particularly in the upper 300m and reached maxima in the subsurface downstream of Heard and McDonald Islands (Stations 66 – 68, and 44) (Figure 2a), consistent with chlorophyll concentration (Figure 1d).

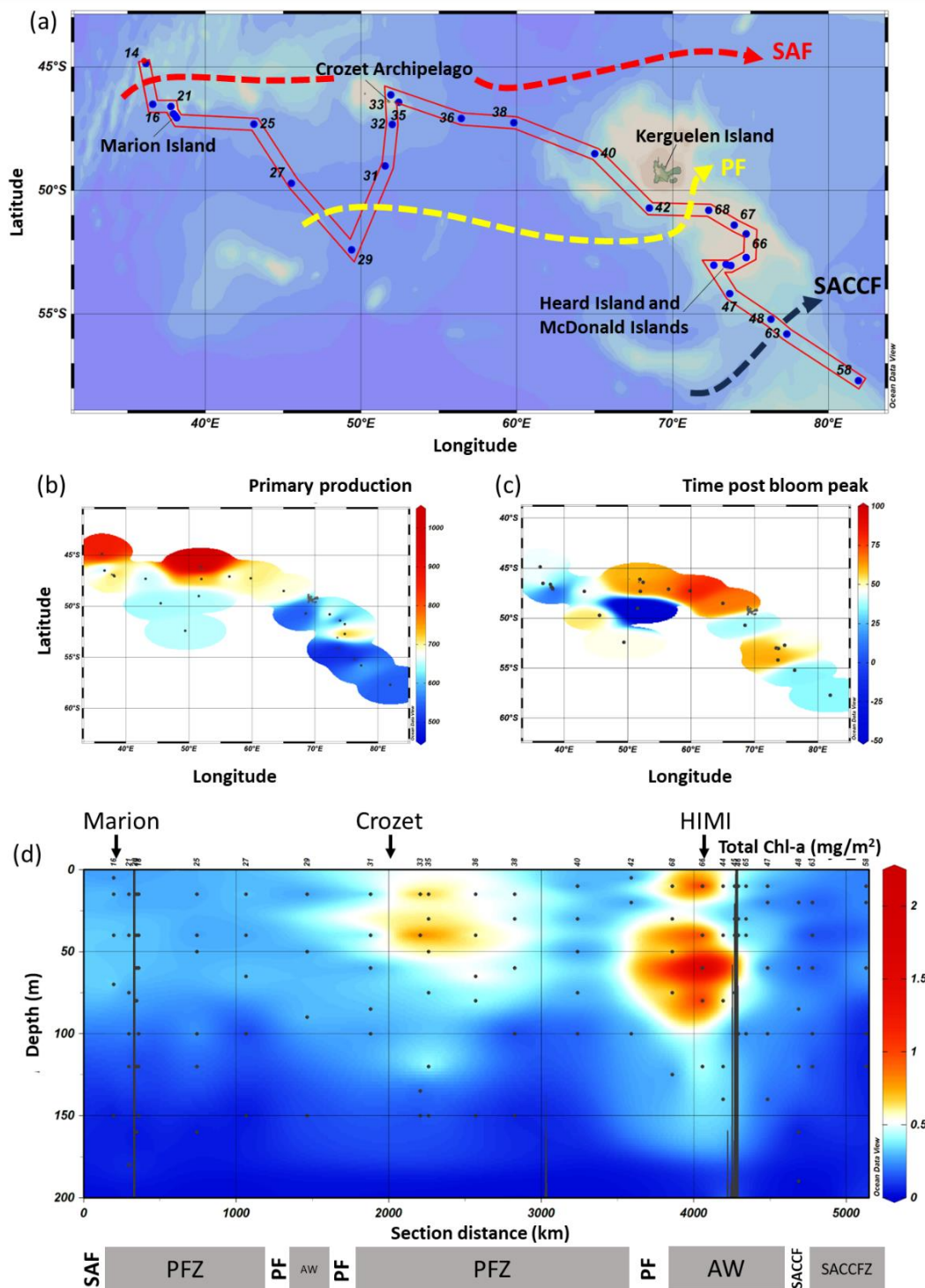


Figure 1: Station maps showing the location of the SWINGS GS02 cruise stations in the South West Indian part of the Southern Ocean (a) in relation to the major oceanographic fronts and sub-Antarctic islands (labelled) and associated plateaus targeted by the cruise. Bloom Phenology as indicated by satellite data (see methods) showing time in days post local bloom (b) termination and (c) peak when sampling occurred at each station. The intensity of the bloom as indicated by (d) Chlorophyll-a concentration with the locations

Figure legend continued: of Marion Island, Crozet Archipelago, Kerguelen Plateau, Heard Island and McDonald Islands (HIMI) and the Fawn Trough (FT) annotated. The positions of the fronts are also annotated (accurate within the transect between stations but otherwise approximated).

### **3. 4. 3. DFe/eHS distribution**

DFe distribution is not shown here but is discussed in detail in other papers (yet to be written). DFe averaged  $0.63 \pm 0.56$  nM across the whole transect. We estimated eHS Fe binding capacity using values from the literature and compared this to DFe concentration across the transect (Figure 2b) (explained and discussed in detail in methods). Across the transect, DFe exceeded eHS Fe binding capacity in 46 % of samples, while Fe fell within ( $\approx$ ) the eHS Fe binding capacity in 30 % of samples. In the westward 3000km of the transect, Fe averaged  $0.70 \pm 0.62$  nM and predominately exceeded eHS Fe binding capacity, however a transition to predominantly Fe  $\approx$  eHS Fe binding capacity occurred in the remaining eastward section (Figure 2b) where Fe averaged  $0.51 \pm 0.42$  nM. Fe  $\approx$  eHS Fe binding capacity was clearly associated with the islands and occurred downstream of Marion Island, Crozet Archipelago, Heard and McDonald Islands, and over Kerguelen plateau (Figure 2b). As such, eHS and DFe were positively correlated (Spearman;  $r = 0.93$   $p < 0.01$ ,  $n=7$ ) over shallow island plateaus (where bottom depth  $< 200$ m). However, this was unique to these locations, as over most of the transect eHS was not correlated with DFe (Figure 3).

When considering the pattern of eHS Fe binding capacity and DFe with depth across the whole transect, eHS Fe binding capacity rarely exceeded Fe concentration, but was predominantly associated with surface waters (Figure 2b). Mesopelagic waters commonly exhibited DFe within the eHS Fe binding capacity, whereas DFe often exceeded eHS Fe binding capacity in deeper waters. Further, DFe/eHS was positively correlated with depth across the transect (Spearman,  $\rho=0.38$ ,  $p < 0.001$ ). Therefore, there was a general trend of increasing DFe relative to eHS with depth.

### **3. 4. 4. eHS/DOC**

We estimated the proportion contribution of eHS to DOC using the carbon content of a terrestrial SRFA standard (explained in detail in methods). eHS/DOC ranged from 0.007 to

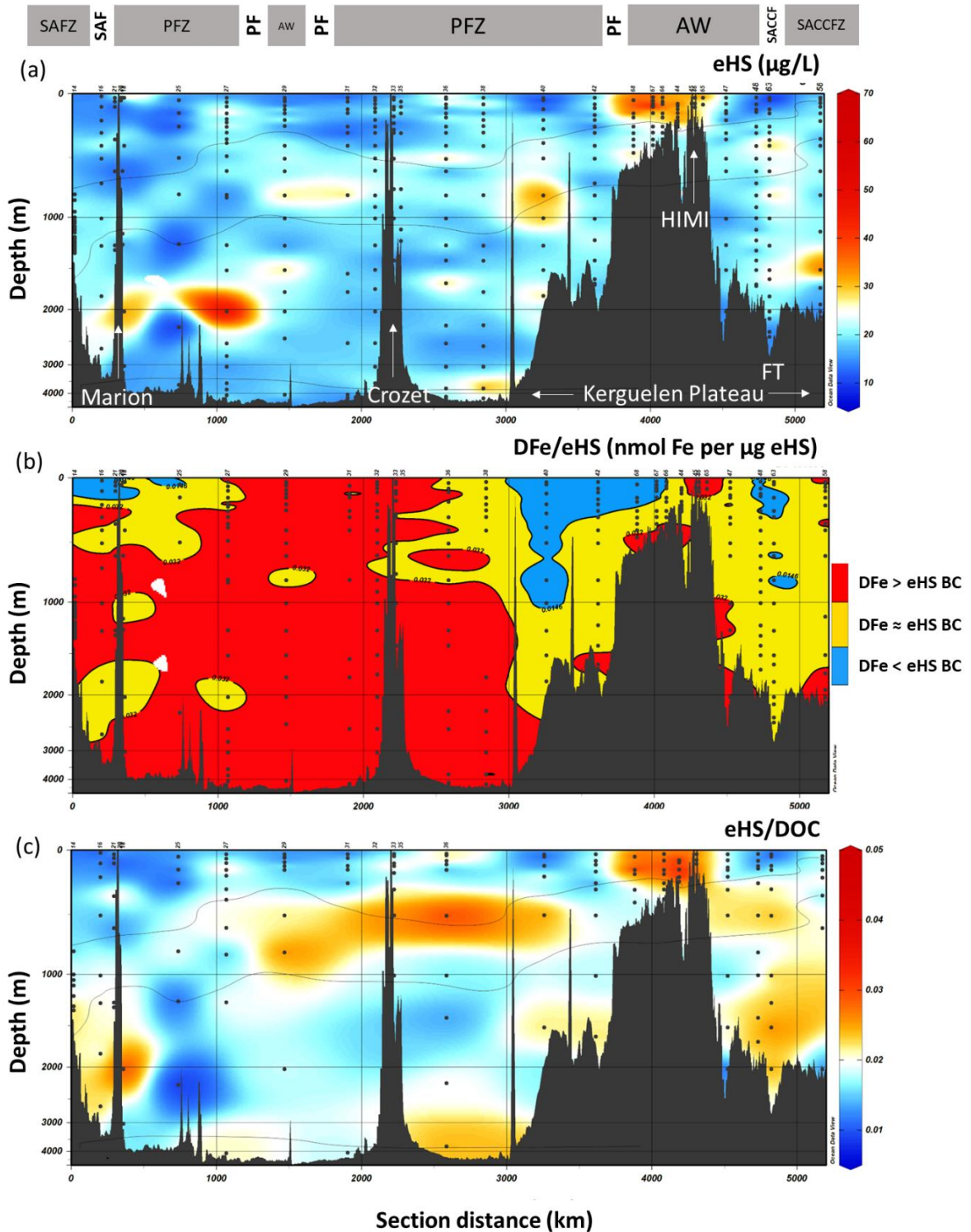


Figure 2 (a) electroactive humic substances (eHS) concentration ( $\mu\text{g/L}$ ), (b) relationship between DFe concentration and eHS Fe binding capacity, and (c) contribution of eHS to DOC across the transect with the locations of Marion Island, Crozet Archipelago, Kerguelen Plateau, Heard Island and McDonald Islands (HIMI), and the Fawn Trough (FT) annotated. The approximate positions of the fronts are also annotated (see text for abbreviations).

Figure legend continued: The depths of UCDW (area between top and middle contour), LCDW (area between middle and bottom contour), and AABW (area below bottom contour) water masses at the sampled stations are shown by the black contours on panels a and c only. Following the assumptions of the Fe eHS binding capacity (BC) calculation, DFe/eHS below 0.0146 (blue) suggests that DFe was below the eHS Fe binding capacity, DFe/eHS between 0.0146 – 0.032 (yellow) indicates that DFe was within the eHS Fe binding capacity, and DFe/eHS above 0.032 (red) indicates that DFe was above the eHS Fe binding capacity. Note non-linear depth axis.

0.048 across the transect (Figure 2c). Generally, surface water exhibited low eHS/DOC (averaged  $0.016 \pm 0.009$ ) apart from downstream of Heard and McDonald Islands above Kerguelen plateau, where a large plume of elevated eHS/DOC was observed. This was also observed to a lesser extent downstream of Crozet. In the mesopelagic, eHS/DOC averaged  $0.020 \pm 0.008$  and a large plume of elevated eHS/DOC (28 – 51 % greater than background mesopelagic levels) was observed downstream of Crozet. In deeper waters, eHS/DOC was generally consistent (averaged  $0.020 \pm 0.005$ ) (Figure 2c).

### **3. 4. 5. Influence of AOU on eHS and DFe**

AOU is a measure of biological oxygen consumption which is generally used as a proxy for microbial remineralisation. The relationship between AOU with eHS, DFe, and DFe/eHS varied across the transect (Figure 3). Data was partitioned according to bottom depth in order to separate plateau/island associated stations (bottom depth < 1000 m) from those off the plateaus (bottom depth > 1000m). Further, as noted earlier, a clear east-west transition in eHS/DFe behaviour was observed across the transect. As such, data was also partitioned into east and west sections for these correlation analyses. We considered four portions of the water column: Mesopelagic, UCDW, LCDW, and Deep.

In island/plateau associated mesopelagic waters, both eHS and DFe were negatively correlated with AOU (Figure 3, see figure for statistical results). However, in mesopelagic waters off plateau both DFe and DFe/eHS were positively correlated with AOU, while eHS was only correlated with AOU in mesopelagic waters off plateau in the eastward part of the transect (Figure 3). In the UCDW, DFe was positively correlated with AOU off plateau in the westward part of the transect and in island/plateau associated waters, while eHS was not

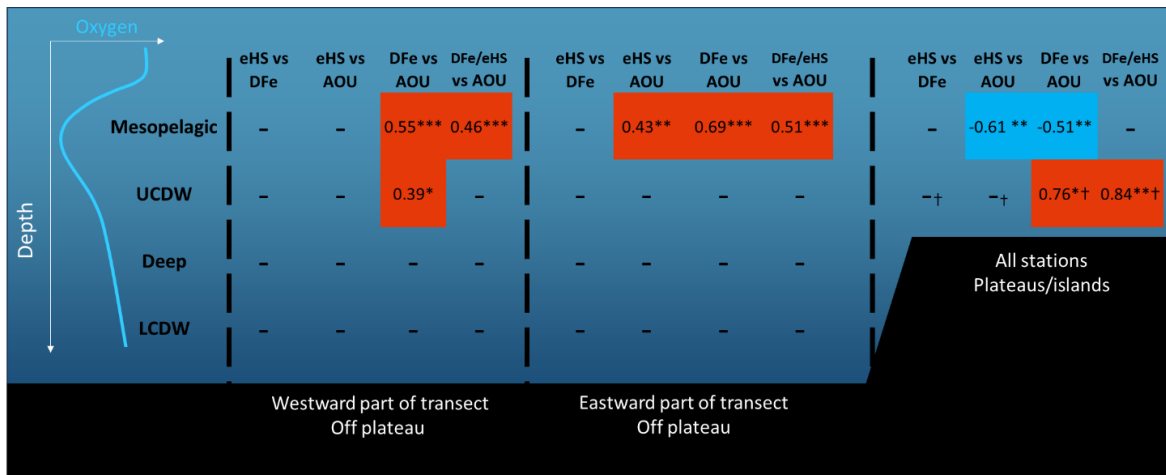


Figure 3: Correlations between eHS and DFe, eHS and AOU, DFe and AOU, and DFe/eHS and AOU performed on depth or water mass regions in data from the westward portion of the transect (stations 14 - 38) where bottom depth >1000m (off-plateaus), in the eastward portion of the transect (Stations > 40) where bottom depth >1000m (off plateau), and all stations where bottom depth <1000m (plateaus or islands). Mesopelagic waters were defined as between the mixed layer depth (see methods for definition) and depth of oxygen minimum. The positions of the water masses varied across the transect but generally Upper Circumpolar Deep Water (UCDW) was found between 200 and 1200m in mesopelagic waters (only below MLD are considered here) and Lower Circumpolar Deep Water (LCDW) was found at 600 – 3500 m in deep waters. Deep water was defined as below the depth of oxygen minimum. Spearman correlations were performed on non-parametric pairwise data and Pearson (indicated by †) were performed on parametric pairwise data both using the cor.test function in r stats package. dashes (-) indicate  $p > 0.05$  \* $p < 0.05$  \*\* $p < 0.01$  \*\*\* $p < 0.001$ .

linked to AOU (Figure 3). Neither eHS or DFe were linked to AOU in deep or Lower Circumpolar Deep Water (Figure 3).

The rate of eHS cycling by bacterial remineralisation in the mesopelagic can be converted to nM Fe equivalents using literature values of eHS Fe binding capacities. In mesopelagic waters off plateau (in the eastward part of the transect) 0.6 – 1.4 pM Fe eHS binding capacity was produced per unit AOU, 33 – 73 % of the 1.9 pM Fe produced per unit AOU.

### **3. 4. 6. Links between phytoplankton pigments and phytoplankton community composition with DOC, eHS, and DFe variables**

The network of links between eHS and DFe with different phytoplankton groups varied across the transect. When the entire transect is considered, both DFe and eHS were negatively correlated to phytoplankton groups (Figure 4a) (see figure for statistical results). However, both parameters were largely linked with different phytoplankton groups. When only the Kerguelen plateau is considered (Figure 4b), the network of links between DFe and eHS with different phytoplankton groups diverges further. Here, eHS was only positively correlated to phytoplankton groups, while DFe exhibited both positive and negative correlations. Notably, all of the phytoplankton groups which were positively correlated to DFe are also positively correlated to eHS (Prasinophytes, Chlorophytes) (Figure 4b). These relationships are concomitant with DFe falling within the eHS Fe binding capacity (Figure 2a). However, when only Crozet is considered, neither eHS or DFe were correlated with any phytoplankton groups (Figure 4c), coincident with the differences in bloom phenology between Crozet and Kerguelen (Figure 1bc). Several phytoplankton groups were negatively correlated to DFe/eHS, including Dinoflagellate and Diatoms A (Figure 4a, b).

The network of links between eHS and DOC with different phytoplankton groups also varied across the transect. Across the whole transect and at Kerguelen, DOC was positively correlated with chlorophyll-a and most of the phytoplankton groups (Figure 4a, b). Whereas, chlorophyll-a was not correlated to eHS (Figure 4; see figure for statistical results), despite general coherence between chlorophyll-a and eHS profiles (Figure 1d and 2a). Over Kerguelen, DOC and eHS shared positive relationships with a few phytoplankton groups (Haptophytes 6, Pelagophytes, Cryptophytes).

The phytoplankton pigments Phaeophytin-a, a product of phytoplankton grazing (Hayashi et al. 2001; Jeffrey 1974), and Phaeophorbid-a, a product of both phytoplankton senescence and phytoplankton grazing (Szymczak-Żyła et al. 2008), can be used as proxies for these processes. Across the whole transect, eHS was positively correlated to Phaeophytin-a and more weakly positively correlated to Phaeophorbid-a (Figure 4a). This relationship between eHS and Phaeophytin was strengthened when only Crozet was considered (Figure 4c). However, when only the Kerguelen plateau was considered, eHS was not significantly

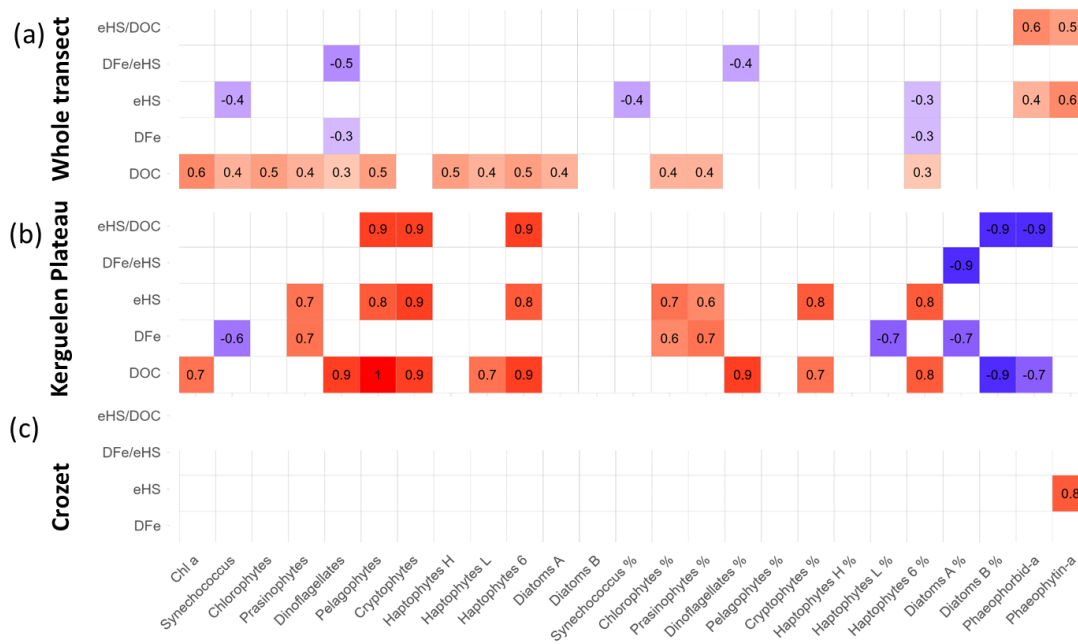


Figure 4 Three correlation matrices (Spearman's rank) using surface water data from (a) the entire transect, (b) only from Kerguelen (Stations >40, excluding Stations on or past the SAACF (48, 63, and 58)), and (c) only from Crozet-influenced (Stations >31 and <40). Colour denotes the strength of the correlation coefficient, with red signifying positive and blue signifying negative correlations. Results where  $p < 0.05$  are not shown. DOC vs phytoplankton groups sample size at Crozet was too small ( $n=4$ ) to perform correlation analyses.

correlated to either of these parameters (Figure 4b), coincident with differences in bloom phenology between Crozet and Kerguelen (Figure 1b, c).

### 3. 4. 7. Prokaryote abundance

Prokaryote abundance was elevated in surface waters (averaged  $5.6 \times 10^5 \pm 2.1 \times 10^5$  cells/mL), decreased rapidly below the mixed layer in mesopelagic waters (averaged  $2.9 \times 10^5 \pm 1.4 \times 10^5$  cells/mL), and was consistently at low concentrations deeper than 1000m (averaged  $2.3 \times 10^5 \pm 1.9 \times 10^5$  cells/mL; Figure S2). Notably, greater prokaryote abundance was observed at the Southwest Indian Ridge (station 14) at approximately 1000m depth. Prokaryote abundance did not correlate with eHS in the surface mixed layer or mesopelagic waters (Spearman,  $p > 0.05$ ) however a subsurface plume of elevated prokaryote abundance

was observed downstream of Crozet coincident to elevated eHS and eHS/DOC (Figure S2 and 2a,c).

### **3. 4. 8. The relationship between CDOM/FDOM with eHS, DFe, and AOU**

In order to understand the processes which impact eHS and DFe distribution in the context of the wider DOM pool, we measured CDOM and FDOM parameters in a subset of stations upstream and downstream of Crozet (stations listed in methods). The following CDOM/FDOM parameters were utilised: in-situ productivity or DOM freshness index (BIX; Fellman et al. 2010; Huguet et al. 2009), humification index (Ohno 2002), slope ratio (a proxy for molecular weight; Helms et al. 2008), absorbance at 254 nm (covaries with aromaticity; Weishaar et al. 2003), Specific Ultraviolet Absorbance (SUVA, a proxy for aromaticity; Weishaar et al. 2003), and classical Coble peaks (Coble 1996). Classical coble peaks include humic-like (a, m, c), protein-like (tryptophan-like, t and tyrosine-like, b).

Three fluorescence components were identified by the PARAFAC: Comp 1, Comp 2, and Comp 3. Comp 1 had an excitation maximum below the measured range but had a small peak at ~290nm (Figure S3). In comparison with the OpenFluor (Murphy et al. 2014) database, Comp 1 matched to an at the time unknown fluorophore identified in sea ice brines (Stedmon et al. 2011), a riverine tryptophan component (Kowalczyk et al. 2009), autochthonous protein-like DOM from Antarctic lakes (Wünsch et al. 2017), and protein- or phenolic-like DOM (Osburn et al. 2018) (Table S1). Comp 1 emission maximum was <360 nm which generally indicates amino acid fluorescence (Stedmon et al. 2011), however, the excitation and emission spectra was not characteristic of amino acids (Figure S3). Further, Comp 1 exhibited characteristics of phenolic material from lignin and tannin (Hernes et al. 2009; Maie et al. 2007), and did not match any coble peaks (Coble 2007). For this reason, we designate Comp 1 a phenolic like component. Comp 2 was a protein component, most closely matching tannin- and phenylalanine-like material (D'Andrilli et al. 2017) but also matching tyrosine-like DOM fluorescence (Painter et al. 2018), and most closely corresponded to coble peak t (Coble 2007). Comp 3 was a ubiquitous marine humic which matched to terrestrial and possibly agriculturally influenced humics (Vines and Terry 2020; Walker et al. 2009; Zhuang et al. 2021) and most closely matched Coble peak c (Coble 2007).

The associations between eHS with CDOM/FDOM parameters varied between different parts of the water column (Figure S4; see figure for statistical results). In the surface mixed layer, eHS was not linked to any CDOM/FDOM parameters (Figure S4b). Whereas, in the mesopelagic, eHS was correlated to a suite of humic and aromaticity related CDOM/FDOM parameters (Comp 1, Coble peak a and m, absorbance at 254) (Figure S4c). Finally, in the deep, eHS was positively correlated to Coble peak t and Coble peak m (Figure S4d). In contrast to eHS, DFe was not associated with CDOM/FDOM parameters throughout the water column (Figure S4).

With respect to AOU's relationship with CDOM/FDOM parameters, AOU was not related to CDOM/FDOM in the surface mixed layer (Figure S4b). In the mesopelagic, AOU was positively correlated to a suite of humic CDOM/FDOM parameters (Figure S4c). In the deep ocean AOU did not correlate to any humic CDOM/FDOM parameters (Figure S4d).

### **3. 5. Discussion**

#### **3. 5. 1. Sources and sinks of eHS across the transect**

##### **3. 5. 1. 1. Phytoplankton**

Phytoplankton are known to produce eHS (Norman et al. 2015) and humic CDOM/FDOM (Castillo et al. 2010), therefore we expected to observe close links between eHS and chlorophyll-a, a measure of phytoplankton abundance. However, we did not observe any correlations between these two parameters which suggests that phytoplankton abundance alone could not explain eHS distribution in surface waters (Figure 4abc). No positive relationships between eHS and phytoplankton groups were observed when the whole transect was considered which suggests that phytoplankton associated eHS production was not the dominant driver of eHS dynamics across the transect (Figure 4a). However, observed negative correlation between eHS and *Synechococcus* when the whole transect was considered (Figure 4a) could be due to the association of *Synechococcus* with low productivity regions where eHS tended to be lower (Figure 2a).

We found that a suite of specific phytoplankton groups were closely linked to eHS over the Kerguelen plateau (Figure 4b), such as Prasinophytes, Pelagophytes, Cryptophytes, and Haptophyte-6. This is consistent with variable eHS (Norman et al. 2015) and humic CDOM/FDOM (Castillo et al. 2010) production rate between different phytoplankton taxa. Haptophyte-6 represent Prymnesiophytes, including *Gephyrocapsa huxleyi* (previously

*Emiliana huxleyi*; Wright 2008). These phytoplankton could be playing a direct role in eHS production, as culture studies have shown that members of *G. huxleyi* and other Prymnesiophytes can produce eHS (Norman et al. 2015).

### **3. 5. 1. 2. Zooplankton grazing**

Zooplankton grazing is another process known to produce eHS (Cabanes et al. 2017), humic CDOM/FDOM (Ortega-Retuerta et al. 2009; Steinberg et al. 2004; Urban-Rich et al. 2006), and iron binding ligands (Sato et al. 2007). Consistent with this, we found that eHS was correlated to proxies for phytoplankton grazing and phytoplankton senescence (Phaeophytin-a and Phaeophorbid-a) (Hayashi et al. 2001; Jeffrey 1974; Szymczak-Żyła et al. 2008) both across the entire transect, and more strongly around Crozet (Figure 4a,c). This suggests that zooplankton grazing may be a key driver of eHS biogeochemistry across the entire transect. However, zooplankton grazing was not an important driver at Kerguelen, in contrast to Crozet (Figure 4b,c). This may have been related to the phenology of the bloom: sampling at Kerguelen ( $47 \pm 14$  days ago) occurred marginally temporally closer to the peak of the bloom compared to at Crozet ( $68 \pm 9$  days ago) (Figure 1c). We theorise that grazing pressure and grazing losses may have been more important in controlling eHS at Crozet, partly due to the later stage in the bloom (Razouls et al. 1998), and active phytoplankton growth more important at Kerguelen due to the earlier stage in the bloom. However, direct observations of grazing rates are required to confirm this.

### **3. 5. 1. 3. Microbial remineralisation**

The role of microbial remineralisation in eHS cycling varied with depth. In surface waters, eHS did not covary statistically with prokaryote abundance (Figure 2a and S2), which could reflect the minor role of microbial remineralisation in surface humic cycling (Omori et al. 2020) or the fact that microbial degradation is a rate based term that is not well represented by snap-shot measurements of cell abundance (Munson-McGee et al. 2022). The role of prokaryotes in surface eHS cycling is tested further in incubation experiments described in Chapter 4.

In mesopelagic waters, eHS was positively correlated with AOU only in the eastward portion of the transect and off the island plateaus (Figure 3). Consistent with this, microbial remineralisation is known to produce eHS (Whitby et al. 2020a) and CDOM/FDOM humics (Jørgensen et al. 2011; Nelson and Gauglitz 2016). The lack of any statistical relationship

between AOU and eHS in the UCDW further supports that particulate organic matter remineralisation plays a greater role in eHS production compared to dissolved organic matter remineralisation in this part of the transect. This is because water masses capture and transport dissolved organic matter, while the larger particulate organic matter is more prone to sinking processes. However, in contrast, eHS did not correlate with AOU in the westward part of the transect (Figure 3). The data was partitioned into eastward and westward to reflect distinct DFe and DFe/eHS behaviour between these two parts of the transect. Therefore, it is striking that clear differences in eHS vs AOU and DFe vs AOU relationships were also found between these parts of the transect, especially because eHS distribution did not exhibit such a marked contrast. However, the mechanism behind this is unclear. In mesopelagic waters over plateaus and around islands, eHS and DFe were both negatively correlated with AOU (Figure 3). Although microbial remineralisation in the mesopelagic can be a sink of eHS under conditions of low organic matter supply (Whitby et al. 2020a) and distinct mesopelagic carbon cycling on and off plateau has been noted in previous studies (Jacquet et al. 2008), it is more likely that this relationship results from mixing of water masses of different oxygen contents as deep water masses shoal at plateaus.

The relationship between eHS and CDOM/FDOM humic parameters can give insights into mesopelagic eHS and wider humic cycling. Mesopelagic eHS were positively correlated with a suite of humic CDOM/FDOM parameters which could indicate that these organic matter comprise the same pool, are produced by the same processes, and/or are chemical precursors (Figure S4c). It is possible that phenol containing Comp 1 was a precursor to humics here (Stevenson 1994). It is also possible that Comp 1 is of allochthonous terrestrial origin, as it closely matched the fluorescence signature of lignin and tannin, unequivocal terrestrial biomarkers (Opsahl and Benner 1997). Notably, eHS was not correlated with coble peak C in mesopelagic waters (and throughout the water column) (Figure S4c). Peak c fluorescence is red-shifted relative to other CDOM/FDOM humics (esp. peak m) (Coble 1996), which can be caused by higher aromaticity, more linear rings, more conjugated bonds, and/or more fluorescent functional groups, relative to peak m fluorescence (Senesi 1990) (discussed in detail in Chapter 2). Considering that these structural characteristics are responsible for humic trace metal binding (Aeschbacher et al. 2010; Frimmel et al. 2005; Lakatos et al. 1977; Orłowska et al. 2017; Schnitzer 1978; Schnitzer and Riffaldi 1972; van

Schaik et al. 2008), it is surprising that eHS did not correlate to peak c (Figure S4). These results suggest that the chemical properties responsible for eHS detection by voltammetry require further investigation.

In the deep ocean and within the LCDW (for eHS only), AOU did not correlate to eHS (Figure 3) or any humic CDOM/FDOM parameters (Figure S4d) which suggests that microbial remineralisation was not an important factor in humic cycling. This has been observed before in deep waters in the Mediterranean (Dulaquais et al. 2018). Lack of correlation between eHS and AOU suggests that the deep ocean eHS pool is refractory in this region, consistent with previous observations of refractory deep ocean humics (Yamashita and Tanoue 2008) and the recalcitrant nature of bulk DOC in the deep ocean (Hansell 2013; Hansell and Carlson 2013). This concept is explored in more detail in Chapter 4. Interestingly, eHS did not correlate with humic CDOM/FDOM components in the deep ocean or in the surface mixed layer (Figure S4b,d). Overall, relationships between eHS, CDOM/FDOM, and AOU suggest a compositionally diverse eHS pool throughout the water column.

#### **3. 5. 1. 4. Hydrothermal activity**

One station under hydrothermal influence was visited during the SWINGS cruise which allows the role of hydrothermal activity in eHS cycling to be discussed, although this topic is discussed in more detail in Chapter 5. At SWIR (Station 14), a putative low temperature clear hydrothermal source was investigated (Baudet et al. *in press*; Léon et al. 2024) and the eHS behaviour is explained in detail by Baudet et al. (*in press*). Briefly, a small signal of elevated eHS was observed (Figure 2a). These eHS might be derived from the hydrothermal fluids directly, as has been observed in other vent systems (Sarma et al. 2018; Yang et al. 2012), and/or from increased biological activity associated with the hydrothermal source (Cathalot et al. 2021), as has been observed with DOC (Bennett et al. 2011).

#### **3. 5. 2. The potential role of eHS in DFe stabilisation**

Overall, eHS and DFe did not correlate across the transect (Figure 2b and 3), which suggests that sources of DFe were uncoupled to those of eHS, consistent with previous observations in the Southern Ocean (Fourquez et al. 2023). As such, DFe tended to exceed eHS Fe binding capacity at DFe sources and also in the eastward part of the transect. This implies that the majority of DFe is present in other chemical forms, including other organic ligands and/or organic and inorganic colloids (Bergquist et al. 2007). It is also possible that the Fe binding

capacity of eHS in the region is higher than that of the terrestrial standard (see methods section and Chapter 2). Unfortunately, there is no Fe binding ligand data available from the area to compare to, but studies in other parts of the Southern Ocean typically report Fe binding ligands in excess to DFe (Smith et al. 2022). However, DFe concentrations were relatively high for the Southern Ocean, particularly in the eastward part of the transect, which could suggest that this system functions differently and is potentially not comparable to other parts of the Southern Ocean.

Lack of correlation between eHS and DFe in mesopelagic waters is of particular interest because relationships with AOU suggested that both DFe and eHS were produced by bacterial remineralisation (Figure 3). Positive correlations between DFe/eHS with AOU (Figure 3) and depth taken together with greater Fe production per unit AOU compared to that of eHS suggests that DFe release by remineralisation processes was more efficient than eHS release in mesopelagic waters. Nevertheless, DFe was often within the eHS Fe binding capacity in mesopelagic waters (Figure 2b), which implies that eHS had the potential to stabilise remineralised DFe sources here. Direct measurements of Fe binding capacity are required to confirm this. Irrespectively, it is clear that the relationship between eHS and DFe is not straightforward in the mesopelagic Southern Ocean.

Patterns in DFe and eHS Fe binding capacities also imply a role of eHS in the stabilisation of DFe from new sources (Figure 2b). Although DFe exceeded eHS Fe binding capacity directly at DFe sources, DFe was generally below or within the eHS Fe binding capacity in waters surrounding islands and plateaus (see methods section for discussion of binding capacity). eHS can solubilise DFe from freshly formed Fe-oxyhydroxides if the age of the Fe-oxyhydroxides is <7 days (Dulaquais et al. 2023) therefore eHS has the potential to stabilise plateau derived DFe for transport further afield. Further, over the Kerguelen plateau we find evidence for active eHS production by phytoplankton groups in response to DFe (Figure 4b). We hypothesize a positive feedback between phytoplankton eHS production and DFe availability which could play a role in sustaining plateau associated phytoplankton blooms. We also observed a close link between eHS and DFe at shallow island plateaus (Heard and McDonald Islands and Marion; see results section), suggesting that here, sources of DFe such as sediments (Bown et al. 2012; Planquette et al. 2007), fluvial sources, and glacial runoff (van der Merwe et al. 2015) are spatially and temporally coupled to those of eHS. In

particular, glacial melt waters were likely to be important around Heard Island because of its high coverage of glaciers. Indeed, sediments (Nissenbaum and Swaine 1976), fluvial (Batchelli et al. 2010; Whitby and van den Berg 2015), and glacial runoff (Jeon et al. 2021) are known sources of eHS and/or humics. Therefore, it is possible that eHS are important in the stabilisation and transport of DFe from these shallow island plateaus. However, again, direct measurements of the Fe bound to eHS are required to evidence this.

### **3. 5. 3. The implications of uncoupling between DOC and eHS cycling**

The relative cycling of DOC and eHS can bring insights into overall DOM cycling and have significant implications for carbon storage. Our results suggest that eHS comprised ~2% of the DOC pool at depth, and maximally ~5% which is broadly in agreement with previous studies in other ocean regions (Dulaquais et al. 2018; Laglera and van den Berg 2009) (Figure 1c). eHS generally comprised a greater part of the DOC pool in mesopelagic waters (see methods for assumptions) (Figure 2c), and this behaviour was particularly pronounced in a plume extending downstream of Crozet. Although eHS are a complex and heterogenous pool of DOM comprised of semi-labile through to recalcitrant organic matter, humics produced by prokaryotes are generally considered to be refractory or slowly cycled (Jørgensen et al. 2014; Lechtenfeld et al. 2015). Supporting this, we find that in the mesopelagic upstream and downstream of Crozet, eHS and AOU were positively correlated to CDOM/FDOM humic components (Figure S4c), proxies for refractory DOM production by the microbial carbon pump (Xiao et al. 2023). Therefore, our results suggest that mesopelagic waters are a hotspot of refractory DOM production by microbial remineralisation and that its efficiency is variable across the region, in particular, downstream of phytoplankton blooms. Using eHS/DOC as a proxy, we estimate that refractory DOM production by mesopelagic DOM remineralisation could have been 28 – 51 % greater than background mesopelagic levels here. Variability in the efficiency of mesopelagic carbon storage by processes such as the microbial carbon pump might be an important, but hitherto under explored aspect impacting Southern Ocean carbon storage.

### **3. 6. Conclusions**

We find that eHS are actively cycled in the Southwest Indian region of the Southern Ocean by a suite of processes including phytoplankton blooms, grazing, and mesopelagic microbial remineralisation. Phytoplankton community composition and grazing strength were

implicated as important factors, possibly underpinned by bloom phenology. We found that eHS has the potential to play a role in DFe stabilisation and transport at local scales surrounding shallow island plateaus. However, lack of correlation between these two variables and disparate eHS Fe binding capacity relative to DFe imply that factors other than eHS are important at basin scale. Ultimately, this study provides a first estimate of the processes that control eHS distribution in the region and highlights potential feedbacks between the network of DFe, DFe-stimulated primary production and associated microbial activity, and eHS cycling, on DFe stabilisation and carbon cycling and storage.

### **3. 7. Acknowledgements**

Gemma Portlock and Pascal Salaün for voltammetry guidance, Frederic Vivier for water mass and oceanographic front definitions. We would like to thank the captain A. Eyssautier, LDA and GENAVIR officers, engineers, technicians and the crew of the R/V Marion Dufresne for their enthusiasm and their professional assistance during the SWINGS cruise. We also thank Emmanuel de Saint-Léger and Fabien Pérault (CNRS DT INSU) for their help with the preparation, deployment and maintenance of the rosette. The SWINGS project was supported by the Flotte Océanographique Française (10.17600/18001925), Agence Nationale de la Recherche (ANR 19-CE01-0012), CNRS/ INSU (Centre National de la Recherche Scientifique/Institut National des Sciences de l'Univers) through its LEFE actions, Université de Bretagne Occidentale, and IsBlue project, Interdisciplinary graduate school for the blue planet (ANR 17-EURE-0015) and co-funded by a grant from the French government under the program 'Investissements d'Avenir' embedded in France 2030. The International GEOTRACES Programme is possible in part thanks to the support from the U.S. National Science Foundation (Grant OCE-2140395) to the Scientific Committee on Oceanic Research (SCOR).

### **3. 8. References**

- Aeschbacher, M., M. Sander, and R. P. Schwarzenbach. 2010. Novel Electrochemical Approach to Assess the Redox Properties of Humic Substances. *Environmental Science & Technology* **44**: 87-93.
- Ardyna, M. and others 2019. Hydrothermal vents trigger massive phytoplankton blooms in the Southern Ocean. *Nature Communications* **10**: 2451.

- Armand, L. K., V. Cornet-Barthaux, J. Mosseri, and B. Quéguiner. 2008. Late summer diatom biomass and community structure on and around the naturally iron-fertilised Kerguelen Plateau in the Southern Ocean. *Deep Sea Research Part II: Topical Studies in Oceanography* **55**: 653-676.
- Barbeau, K., J. W. Moffett, D. A. Caron, P. L. Croot, and D. L. Erdner. 1996. Role of protozoan grazing in relieving iron limitation of phytoplankton. *Nature* **380**: 61-64.
- Batchelli, S., F. L. L. Muller, K.-C. Chang, and C.-L. Lee. 2010. Evidence for Strong but Dynamic Iron-Humic Colloidal Associations in Humic-Rich Coastal Waters. *Environmental Science & Technology* **44**: 8485-8490.
- Behrenfeld, M. J., E. Boss, D. A. Siegel, and D. M. Shea. 2005. Carbon-based ocean productivity and phytoplankton physiology from space. *Global Biogeochemical Cycles* **19**.
- Benner, R., and M. Strom. 1993. A critical evaluation of the analytical blank associated with DOC measurements by high-temperature catalytic oxidation. *Marine Chemistry* **41**: 153-160.
- Bennett, S. A., R. L. Hansman, A. L. Sessions, K.-i. Nakamura, and K. J. Edwards. 2011. Tracing iron-fueled microbial carbon production within the hydrothermal plume at the Loihi seamount. *Geochimica et Cosmochimica Acta* **75**: 5526-5539.
- Bergquist, B. A., J. Wu, and E. A. Boyle. 2007. Variability in oceanic dissolved iron is dominated by the colloidal fraction. *Geochimica et Cosmochimica Acta* **71**: 2960-2974.
- Bittar, T. B. and others 2016. Seasonal dynamics of dissolved, particulate and microbial components of a tidal saltmarsh-dominated estuary under contrasting levels of freshwater discharge. *Estuarine, Coastal and Shelf Science* **182**: 72-85.
- Blain, S. and others 2007. Effect of natural iron fertilization on carbon sequestration in the Southern Ocean. *Nature* **446**: 1070-1074.
- Bowie, A. R. and others 2015. Iron budgets for three distinct biogeochemical sites around the Kerguelen Archipelago (Southern Ocean) during the natural fertilisation study, KEOPS-2. *Biogeosciences* **12**: 4421-4445.
- Bown, J. and others 2012. Imprint of a dissolved cobalt basaltic source on the Kerguelen Plateau. *Biogeosciences* **9**: 5279-5290.

- Boyd, P. W. and others 2015. Why are biotic iron pools uniform across high- and low-iron pelagic ecosystems? *Global Biogeochemical Cycles* **29**: 1028-1043.
- Brewin, R. J. W. and others 2015. Influence of light in the mixed-layer on the parameters of a three-component model of phytoplankton size class. *Remote Sensing of Environment* **168**: 437-450.
- Bricaud, A., H. Claustre, J. Ras, and K. Oubelkheir. 2004. Natural variability of phytoplanktonic absorption in oceanic waters: Influence of the size structure of algal populations. *Journal of Geophysical Research: Oceans* **109**.
- Browning, T. J., E. P. Achterberg, A. Engel, and E. Mawji. 2021. Manganese co-limitation of phytoplankton growth and major nutrient drawdown in the Southern Ocean. *Nature Communications* **12**: 884.
- Cabanes, D. J. E., L. Norman, A. R. Bowie, S. Strmečki, and C. S. Hassler. 2020. Electrochemical evaluation of iron-binding ligands along the Australian GEOTRACES southwestern Pacific section (GP13). *Marine Chemistry* **219**: 103736.
- Cabanes, D. J. E. and others 2017. First Evaluation of the Role of Salp Fecal Pellets on Iron Biogeochemistry. *Front. Mar. Sci.* **3**.
- Carlotti, F. and others 2015. Mesozooplankton structure and functioning during the onset of the Kerguelen phytoplankton bloom during the KEOPS2 survey. *Biogeosciences* **12**: 4543-4563.
- Castillo, C. R., H. Sarmiento, X. A. Álvarez-Salgado, J. M. Gasol, and C. Marraséa. 2010. Production of chromophoric dissolved organic matter by marine phytoplankton. *Limnology and Oceanography* **55**: 446-454.
- Cathalot, C. and others 2021. Hydrothermal plumes as hotspots for deep-ocean heterotrophic microbial biomass production. *Nature Communications* **12**: 6861.
- Church, M. J., D. A. Hutchins, and H. W. Ducklow. 2000. Limitation of Bacterial Growth by Dissolved Organic Matter and Iron in the Southern Ocean. *Applied and Environmental Microbiology* **66**: 455-466.
- Coble, P. G. 1996. Characterization of marine and terrestrial DOM in seawater using excitation-emission matrix spectroscopy. *Marine Chemistry* **51**: 325-346.
- . 2007. *Marine Optical Biogeochemistry: The Chemistry of Ocean Color*. *Chemical Reviews* **107**: 402-418.

- Cutter, G. and others 2017. Sampling and Sample-handling Protocols for GEOTRACES Cruises. **Version 3.0**.
- D'Andrilli, J., C. M. Foreman, M. Sigl, J. C. Priscu, and J. R. McConnell. 2017. A 21 000-year record of fluorescent organic matter markers in the WAIS Divide ice core. *Clim. Past* **13**: 533-544.
- Dulaquais, G. and others 2023. The role of humic-type ligands in the bioavailability and stabilization of dissolved iron in the Western Tropical South Pacific Ocean. *Front. Mar. Sci.* **10**.
- Dulaquais, G., M. Waeles, L. J. A. Gerringa, R. Middag, M. J. A. Rijkenberg, and R. Riso. 2018. The Biogeochemistry of Electroactive Humic Substances and Its Connection to Iron Chemistry in the North East Atlantic and the Western Mediterranean Sea. *Journal of Geophysical Research: Oceans* **123**: 5481-5499.
- Felgate, S. L., A. J. Craig, L. W. K. Moodie, and J. Hawkes. 2023. Characterization of a Newly Available Coastal Marine Dissolved Organic Matter Reference Material (TRM-0522). *Analytical Chemistry* **95**: 6559-6567.
- Fellman, J. B., E. Hood, and R. G. M. Spencer. 2010. Fluorescence spectroscopy opens new windows into dissolved organic matter dynamics in freshwater ecosystems: A review. *Limnology and Oceanography* **55**: 2452-2462.
- Fourquez, M. and others 2020. Microbial Competition in the Subpolar Southern Ocean: An Fe–C Co-limitation Experiment. *Front. Mar. Sci.* **6**.
- Fourquez, M. and others 2023. Chasing iron bioavailability in the Southern Ocean: Insights from *Phaeocystis antarctica* and iron speciation. *Science Advances* **9**: eadf9696.
- Frimmel, F. H., U. Lankes, H. D. Lüdemann, and M. B. Müller. 2005. Structural characterization of humic substances from waste water. , p. 3-22. . *In* G. Davies and E. Ghabbour [eds.], *Humic substances: molecular details and applications in land and water conservation*. Taylor & Francis.
- Gao, Z., and C. Guéguen. 2018. Distribution of thiol, humic substances and colored dissolved organic matter during the 2015 Canadian Arctic GEOTRACES cruises. *Marine Chemistry* **203**: 1-9.
- Gledhill, M., and K. Buck. 2012. The Organic Complexation of Iron in the Marine Environment: A Review. *Frontiers in Microbiology* **3**.

- Graber, E. R., and Y. Rudich. 2006. Atmospheric HULIS: How humic-like are they? A comprehensive and critical review. *Atmos. Chem. Phys.* **6**: 729-753.
- Hansell, D. A. 2013. Recalcitrant Dissolved Organic Carbon Fractions. *Annual Review of Marine Science* **5**: 421-445.
- Hansell, D. A., and C. A. Carlson. 2013. Localized refractory dissolved organic carbon sinks in the deep ocean. *Global Biogeochemical Cycles* **27**: 705-710.
- Harris, D. C. 2003. Quantitative chemical analysis / Daniel C. Harris, 6th ed. ed. W.H. Freeman and Co.
- Hawco, N. J., A. Tagliabue, and B. S. Twining. 2022. Manganese Limitation of Phytoplankton Physiology and Productivity in the Southern Ocean. *Global Biogeochemical Cycles* **36**: e2022GB007382.
- Hayashi, M., K. Furuya, and H. Hattori. 2001. Spatial Heterogeneity in Distributions of Chlorophyll a Derivatives in the Subarctic North Pacific during Summer. *Journal of Oceanography* **57**: 323-331.
- Helms, J. R., A. Stubbins, J. D. Ritchie, E. C. Minor, D. J. Kieber, and K. Mopper. 2008. Absorption spectral slopes and slope ratios as indicators of molecular weight, source, and photobleaching of chromophoric dissolved organic matter. *Limnology and Oceanography* **53**: 955-969.
- Hernes, P. J., B. A. Bergamaschi, R. S. Eckard, and R. G. M. Spencer. 2009. Fluorescence-based proxies for lignin in freshwater dissolved organic matter. *Journal of Geophysical Research: Biogeosciences* **114**.
- Hertkorn, N. and others 2006. Characterization of a major refractory component of marine dissolved organic matter. *Geochimica et Cosmochimica Acta* **70**: 2990-3010.
- Holmes, T. M. and others 2019. Iron availability influences nutrient drawdown in the Heard and McDonald Islands region, Southern Ocean. *Marine Chemistry* **211**: 1-14.
- Huguet, A., L. Vacher, S. Relexans, S. Saubusse, J. M. Froidefond, and E. Parlanti. 2009. Properties of fluorescent dissolved organic matter in the Gironde Estuary. *Organic Geochemistry* **40**: 706-719.
- IHSS, I. H. S. S. 2019, <https://humic-substances.org/>.
- Irion, S., L. Jardillier, I. Sassenhagen, and U. Christaki. 2020. Marked spatiotemporal variations in small phytoplankton structure in contrasted waters of the Southern Ocean (Kerguelen area). *Limnology and Oceanography* **65**: 2835-2852.

- Jacquet, S. H. M. and others 2008. Mesopelagic organic carbon remineralization in the Kerguelen Plateau region tracked by biogenic particulate Ba. *Deep Sea Research Part II: Topical Studies in Oceanography* **55**: 868-879.
- Jeffrey, S. W. 1974. Profiles of photosynthetic pigments in the ocean using thin-layer chromatography. *Marine Biology* **26**: 101-110.
- Jeon, M. H., J. Jung, M. O. Park, S. Aoki, T.-W. Kim, and S.-K. Kim. 2021. Tracing Circumpolar Deep Water and glacial meltwater using humic-like fluorescent dissolved organic matter in the Amundsen Sea, Antarctica. *Marine Chemistry* **235**: 104008.
- Jørgensen, L., C. A. Stedmon, M. A. Granskog, and M. Middelboe. 2014. Tracing the long-term microbial production of recalcitrant fluorescent dissolved organic matter in seawater. *Geophysical Research Letters* **41**: 2481-2488.
- Jørgensen, L., C. A. Stedmon, T. Kragh, S. Markager, M. Middelboe, and M. Søndergaard. 2011. Global trends in the fluorescence characteristics and distribution of marine dissolved organic matter. *Marine Chemistry* **126**: 139-148.
- Kitayama, S. and others 2009. Controls on iron distributions in the deep water column of the North Pacific Ocean: Iron(III) hydroxide solubility and marine humic-type dissolved organic matter. *Journal of Geophysical Research: Oceans* **114**.
- Kowalczyk, P., M. J. Durako, H. Young, A. E. Kahn, W. J. Cooper, and M. Gonsior. 2009. Characterization of dissolved organic matter fluorescence in the South Atlantic Bight with use of PARAFAC model: Interannual variability. *Marine Chemistry* **113**: 182-196.
- Krachler, R. and others 2015. River-derived humic substances as iron chelators in seawater. *Marine Chemistry* **174**: 85-93.
- Laglera, L. M., C. Sukekava, H. A. Slagter, J. Downes, A. Aparicio-Gonzalez, and L. J. A. Gerringa. 2019. First Quantification of the Controlling Role of Humic Substances in the Transport of Iron Across the Surface of the Arctic Ocean. *Environmental Science & Technology* **53**: 13136-13145.
- Laglera, L. M., and C. M. G. van den Berg. 2009. Evidence for geochemical control of iron by humic substances in seawater. *Limnology and Oceanography* **54**: 610-619.
- Lakatos, B., T. Tibai, and J. Meisel. 1977. EPR spectra of humic acids and their metal complexes. *Geoderma* **19**: 319-338.
- Lechtenfeld, O. J., N. Hertkorn, Y. Shen, M. Witt, and R. Benner. 2015. Marine sequestration of carbon in bacterial metabolites. *Nature Communications* **6**: 6711.

- Léon, M. and others 2024. Investigation of hydrothermal activity in the South West Indian ridge region using Ra isotopes and <sup>227</sup>Ac as tracers. *Progress in Oceanography* **221**: 103191.
- Mackey, M. D., D. J. Mackey, H. W. Higgins, and S. W. Wright. 1996. CHEMTAX - a program for estimating class abundances from chemical markers: application to HPLC measurements of phytoplankton. *Marine Ecology Progress Series* **144**: 265-283.
- Maie, N., N. M. Scully, O. Pisani, and R. Jaffé. 2007. Composition of a protein-like fluorophore of dissolved organic matter in coastal wetland and estuarine ecosystems. *Water Research* **41**: 563-570.
- Moffett, J. W., and R. M. Boiteau. 2024. Metal Organic Complexation in Seawater: Historical Background and Future Directions. *Annual Review of Marine Science* **16**: null.
- Møller, E. F., P. Thor, and T. G. Nielsen. 2003. Production of DOC by *Calanus finmarchicus*, *C. glacialis* and *C. hyperboreus* through sloppy feeding and leakage from fecal pellets. *Marine Ecology Progress Series* **262**: 185-191.
- Moore, C. M. and others 2013. Processes and patterns of oceanic nutrient limitation. *Nature Geoscience* **6**: 701-710.
- Muller, F. L. L. 2018. Exploring the Potential Role of Terrestrially Derived Humic Substances in the Marine Biogeochemistry of Iron. *Frontiers in Earth Science* **6**.
- Munson-McGee, J. H. and others 2022. Decoupling of respiration rates and abundance in marine prokaryoplankton. *Nature*.
- Murphy, K. R., C. A. Stedmon, D. Graeber, and R. Bro. 2013. Fluorescence spectroscopy and multi-way techniques. PARAFAC. *Analytical Methods* **5**: 6557-6566.
- Murphy, K. R., C. A. Stedmon, P. Wenig, and R. Bro. 2014. OpenFluor— an online spectral library of auto-fluorescence by organic compounds in the environment. *Analytical Methods* **6**: 658-661.
- Nelson, N. B., and J. M. Gauglitz. 2016. Optical Signatures of Dissolved Organic Matter Transformation in the Global Ocean. *Front. Mar. Sci.* **2**.
- Nissenbaum, A., and I. R. Kaplan. 1972. CHEMICAL AND ISOTOPIC EVIDENCE FOR THE IN SITU ORIGIN OF MARINE HUMIC SUBSTANCES<sup>1,2</sup>. *Limnology and Oceanography* **17**: 570-582.

- Nissenbaum, A., and D. J. Swaine. 1976. Organic matter-metal interactions in Recent sediments: the role of humic substances. *Geochimica et Cosmochimica Acta* **40**: 809-816.
- Norman, L. and others 2015. The role of bacterial and algal exopolymeric substances in iron chemistry. *Marine Chemistry* **173**: 148-161.
- Obernosterer, I., U. Christaki, D. Lefevre, P. Catala, F. Van Wambeke, and P. Lebaron. 2008. Rapid bacterial mineralization of organic carbon produced during a phytoplankton bloom induced by natural iron fertilization in the Southern Ocean. *Deep-Sea Research Part II-Topical Studies in Oceanography* **55**: 777-789.
- Obernosterer, I., M. Fourquez, and S. Blain. 2015. Fe and C co-limitation of heterotrophic bacteria in the naturally fertilized region off the Kerguelen Islands. *Biogeosciences* **12**: 1983-1992.
- Ohno, T. 2002. Fluorescence Inner-Filtering Correction for Determining the Humification Index of Dissolved Organic Matter. *Environmental Science & Technology* **36**: 742-746.
- Omanović, D. 2011. ElectroChemical Data Software (ECDSOFT).
- Omori, Y., A. Saeki, S. Wada, Y. Inagaki, and T. Hama. 2020. Experimental Analysis of Diurnal Variations in Humic-Like Fluorescent Dissolved Organic Matter in Surface Seawater. *Front. Mar. Sci.* **7**.
- Opsahl, S., and R. Benner. 1997. Distribution and cycling of terrigenous dissolved organic matter in the ocean. *Nature* **386**: 480-482.
- Orlowska, E. and others 2017.  $\beta$ -O-4 type dilignol compounds and their iron complexes for modeling of iron binding to humic acids: synthesis, characterization, electrochemical studies and algal growth experiments. *New Journal of Chemistry* **41**: 11546-11555.
- Ortega-Retuerta, E. and others 2009. Biogeneration of chromophoric dissolved organic matter by bacteria and krill in the Southern Ocean. *Limnology and Oceanography* **54**: 1941-1950.
- Osburn, C. L., D. Oviedo-Vargas, E. Barnett, D. Dierick, S. F. Oberbauer, and D. P. Genereux. 2018. Regional Groundwater and Storms Are Hydrologic Controls on the Quality and Export of Dissolved Organic Matter in Two Tropical Rainforest Streams, Costa Rica. *Journal of Geophysical Research: Biogeosciences* **123**: 850-866.

- Painter, S. C. and others 2018. Terrestrial dissolved organic matter distribution in the North Sea. *Science of The Total Environment* **630**: 630-647.
- Park, Y.-H. and others 2019. Observations of the Antarctic Circumpolar Current Over the Udintsev Fracture Zone, the Narrowest Choke Point in the Southern Ocean. *Journal of Geophysical Research: Oceans* **124**: 4511-4528.
- Pernet-Coudrier, B., M. Waeles, M. Filella, F. Quentel, and R. D. Riso. 2013. Simple and simultaneous determination of glutathione, thioacetamide and refractory organic matter in natural waters by DP-CSV. *Science of The Total Environment* **463-464**: 997-1005.
- Planquette, H. and others 2007. Dissolved iron in the vicinity of the Crozet Islands, Southern Ocean. *Deep Sea Research Part II: Topical Studies in Oceanography* **54**: 1999-2019.
- Racault, M.-F., S. Sathyendranath, and T. Platt. 2014. Impact of missing data on the estimation of ecological indicators from satellite ocean-colour time-series. *Remote Sensing of Environment* **152**: 15-28.
- Ras, J., H. Claustre, and J. Uitz. 2008. Spatial variability of phytoplankton pigment distributions in the Subtropical South Pacific Ocean: comparison between in situ and predicted data. *Biogeosciences* **5**: 353-369.
- Razouls, S., G. Du Réau, P. Guillot, J. Maison, and C. Jeandel. 1998. Seasonal abundance of copepod assemblages and grazing pressure in the Kerguelen Island area (Southern Ocean). *Journal of Plankton Research* **20**: 1599-1614.
- Sabine, C. L. and others 2004. The Oceanic Sink for Anthropogenic CO<sub>2</sub>. *Science* **305**: 367-371.
- Salgado-Hernanz, P. M., M. F. Racault, J. S. Font-Muñoz, and G. Basterretxea. 2019. Trends in phytoplankton phenology in the Mediterranean Sea based on ocean-colour remote sensing. *Remote Sensing of Environment* **221**: 50-64.
- Sarma, N. S. and others 2018. Hydrothermal Alteration Promotes Humic Acid Formation in Sediments: A Case Study of the Central Indian Ocean Basin. *Journal of Geophysical Research: Oceans* **123**: 110-130.
- Sathyendranath, S. and others 2019. An Ocean-Colour Time Series for Use in Climate Studies: The Experience of the Ocean-Colour Climate Change Initiative (OC-CCI). *Sensors* **19**: 4285.

- Sato, M., S. Takeda, and K. Furuya. 2007. Iron regeneration and organic iron(III)-binding ligand production during in situ zooplankton grazing experiment. *Marine Chemistry* **106**: 471-488.
- Schnitzer, M. 1978. Humic substances: chemistry and reactions. , p. 1-64. In *Developments in soil science* Elsevier. .
- Schnitzer, M., and R. Riffaldi. 1972. The Determination of Quinone Groups in Humic Substances. *Soil Science Society of America Journal* **36**: 772-777.
- Senesi, N. 1990. Molecular and quantitative aspects of the chemistry of fulvic acid and its interactions with metal ions and organic chemicals: Part II. The fluorescence spectroscopy approach. *Analytica Chimica Acta* **232**: 77-106.
- Smith, A. J. R. and others 2022. Identifying potential sources of iron-binding ligands in coastal Antarctic environments and the wider Southern Ocean. *Front. Mar. Sci.* **9**.
- Sokolov, S., and S. R. Rintoul. 2009. Circumpolar structure and distribution of the Antarctic Circumpolar Current fronts: 1. Mean circumpolar paths. *Journal of Geophysical Research: Oceans* **114**.
- Stedmon, C. A., D. N. Thomas, S. Papadimitriou, M. A. Granskog, and G. S. Dieckmann. 2011. Using fluorescence to characterize dissolved organic matter in Antarctic sea ice brines. *Journal of Geophysical Research: Biogeosciences* **116**.
- Steinberg, D. K., N. B. Nelson, C. A. Carlson, and A. Prusak. 2004. Production of chromophoric dissolved organic matter (CDOM) in the open ocean by zooplankton and the colonial cyanobacterium *Trichodesmium* spp. *Marine Ecology Progress Series* **267**: 45-56.
- Stevenson, J. 1994. *Humus Chemistry: Genesis, Composition, Reactions*. John Wiley and Sons.
- Stuermer, D. H., and G. R. Harvey. 1974. Humic substances from seawater. *Nature* **250**: 480-481.
- Sukekava, C., J. Downes, H. A. Slagter, L. J. A. Gerringa, and L. M. Laglera. 2018. Determination of the contribution of humic substances to iron complexation in seawater by catalytic cathodic stripping voltammetry. *Talanta* **189**: 359-364.
- Szymczak-Żyła, M., G. Kowalewska, and J. W. Louda. 2008. The influence of microorganisms on chlorophyll a degradation in the marine environment. *Limnology and Oceanography* **53**: 851-862.

- Tagliabue, A., L. Bopp, and O. Aumont. 2009. Evaluating the importance of atmospheric and sedimentary iron sources to Southern Ocean biogeochemistry. *Geophysical Research Letters* **36**.
- Tagliabue, A., A. R. Bowie, P. W. Boyd, K. N. Buck, K. S. Johnson, and M. A. Saito. 2017. The integral role of iron in ocean biogeochemistry. *Nature* **543**: 51-59.
- Tagliabue, A. and others 2022. Constraining the Contribution of Hydrothermal Iron to Southern Ocean Export Production Using Deep Ocean Iron Observations. *Front. Mar. Sci.* **9**.
- Tang, W. and others 2021. Widespread phytoplankton blooms triggered by 2019–2020 Australian wildfires. *Nature* **597**: 370-375.
- Tortell, P. D., M. T. Maldonado, and N. M. Price. 1996. The role of heterotrophic bacteria in iron-limited ocean ecosystems. *Nature* **383**: 330-332.
- Urban-Rich, J., J. T. McCarty, D. Fernández, and J. L. Acuña. 2006. Larvaceans and copepods excrete fluorescent dissolved organic matter (FDOM). *Journal of Experimental Marine Biology and Ecology* **332**: 96-105.
- Urban-Rich, J., J. T. McCarty, and M. Shailer. 2004. Effects of food concentration and diet on chromophoric dissolved organic matter accumulation and fluorescent composition during grazing experiments with the copepod *Calanus finmarchicus*. *ICES Journal of Marine Science* **61**: 542-551.
- van der Merwe, P. and others 2015. Sourcing the iron in the naturally fertilised bloom around the Kerguelen Plateau: particulate trace metal dynamics. *Biogeosciences* **12**: 739-755.
- van Schaik, J. W. J., I. Persson, D. B. Kleja, and J. P. Gustafsson. 2008. EXAFS Study on the Reactions between Iron and Fulvic Acid in Acid Aqueous Solutions. *Environmental Science & Technology* **42**: 2367-2373.
- Viljoen, J. J. 2023. Phytoplankton and trace metal dynamics in the Southern Ocean: An observational study assessing the relationships between phytoplankton communities, small scale features, and micronutrients. Stellenbosch University.
- Vines, M., and L. G. Terry. 2020. Evaluation of the biodegradability of fluorescent dissolved organic matter via biological filtration. *AWWA Water Science* **2**: e1201.
- Walker, S. A., R. M. W. Amon, C. Stedmon, S. Duan, and P. Louchouart. 2009. The use of PARAFAC modeling to trace terrestrial dissolved organic matter and fingerprint

- water masses in coastal Canadian Arctic surface waters. *Journal of Geophysical Research: Biogeosciences* **114**.
- Weishaar, J. L., G. R. Aiken, B. A. Bergamaschi, M. S. Fram, R. Fujii, and K. Mopper. 2003. Evaluation of Specific Ultraviolet Absorbance as an Indicator of the Chemical Composition and Reactivity of Dissolved Organic Carbon. *Environmental Science & Technology* **37**: 4702-4708.
- Whitby, H., M. Bressac, G. Sarthou, M. J. Ellwood, C. Guieu, and P. W. Boyd. 2020a. Contribution of Electroactive Humic Substances to the Iron-Binding Ligands Released During Microbial Remineralization of Sinking Particles. *Geophysical Research Letters* **47**: e2019GL086685.
- Whitby, H., J. Park, S. Y., B. R.M., B. K.N., and B. R.M. 2024. New insights into the organic complexation of bioactive trace metals in the global ocean from the GEOTRACES era. *Oceanography* **37**: 142–155.
- Whitby, H. and others 2020b. A call for refining the role of humic-like substances in the oceanic iron cycle. *Scientific Reports* **10**: 6144.
- Whitby, H., and C. M. G. van den Berg. 2015. Evidence for copper-binding humic substances in seawater. *Marine Chemistry* **173**: 282-290.
- Wright, S. W. 2008. Chemtax version 1.95 for calculating the taxonomic composition of phytoplankton populations. . Australian Antarctic Data Centre.
- Wünsch, U. J., K. R. Murphy, and C. A. Stedmon. 2017. The One-Sample PARAFAC Approach Reveals Molecular Size Distributions of Fluorescent Components in Dissolved Organic Matter. *Environmental Science & Technology* **51**: 11900-11908.
- Xiao, X., Y. Yamashita, M. Gonsior, and N. Jiao. 2023. The efficiency of the microbial carbon pump as seen from the relationship between apparent oxygen utilization and fluorescent dissolved organic matter. *Progress in Oceanography* **210**: 102929.
- Yamashita, Y., J. Nishioka, H. Obata, and H. Ogawa. 2020. Shelf humic substances as carriers for basin-scale iron transport in the North Pacific. *Scientific Reports* **10**: 4505.
- Yamashita, Y., and E. Tanoue. 2008. Production of bio-refractory fluorescent dissolved organic matter in the ocean interior. *Nature Geoscience* **1**: 579-582.
- Yang, L., H. Hong, W. Guo, C.-T. A. Chen, P.-I. Pan, and C.-C. Feng. 2012. Absorption and fluorescence of dissolved organic matter in submarine hydrothermal vents off NE Taiwan. *Marine Chemistry* **128-129**: 64-71.

Zhuang, J. 2018. 2018. xESMF: Universal Regridder for Geospatial Data.

Zhuang, W.-E., W. Chen, Q. Cheng, and L. Yang. 2021. Assessing the priming effect of dissolved organic matter from typical sources using fluorescence EEMs-PARAFAC. *Chemosphere* **264**: 128600.

### 3. 9. Supplementary materials

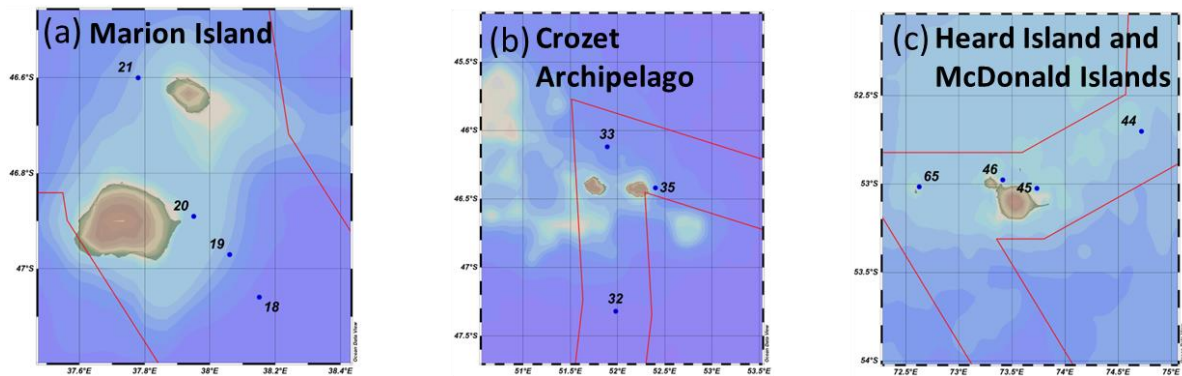


Figure S1: Close view showing the location of stations around (a) Marion and Prince Edward Islands, (b) Crozet Archipelago, and (c) Heard and McDonald Islands.

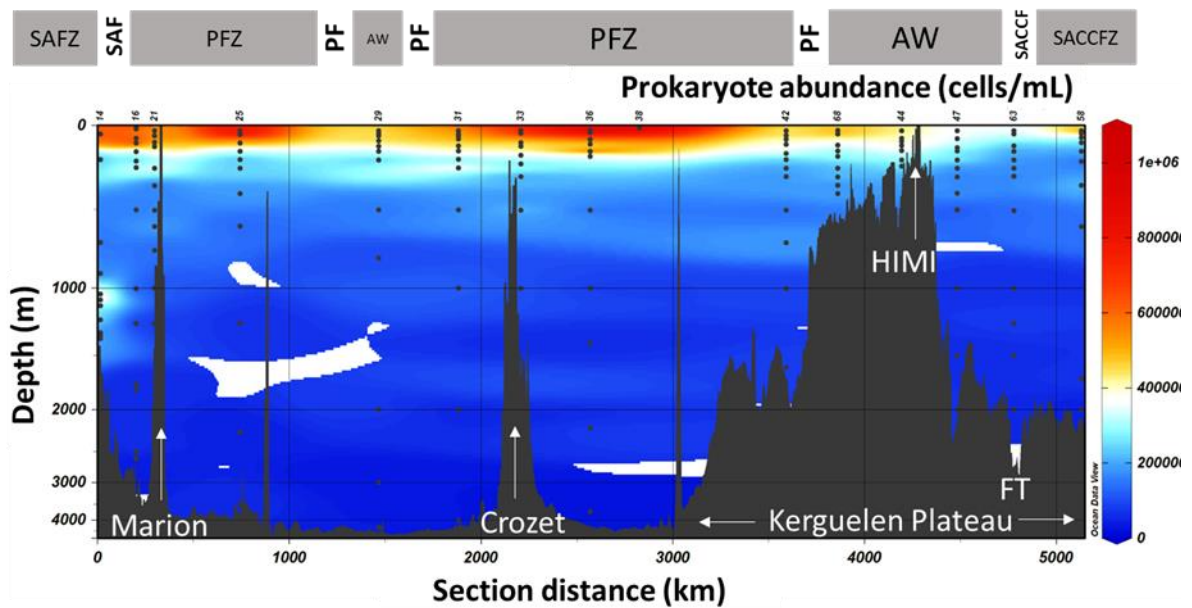


Figure S2 Prokaryote abundance with locations of Marion and Prince Edward Island, Crozet Archipelago, Kerguelen Plateau, Heard Island and McDonald Islands (HIMI) and the Fawn Trough (FT) annotated. The approximate positions of the fronts and water masses are also annotated. Note non-linear depth axis.

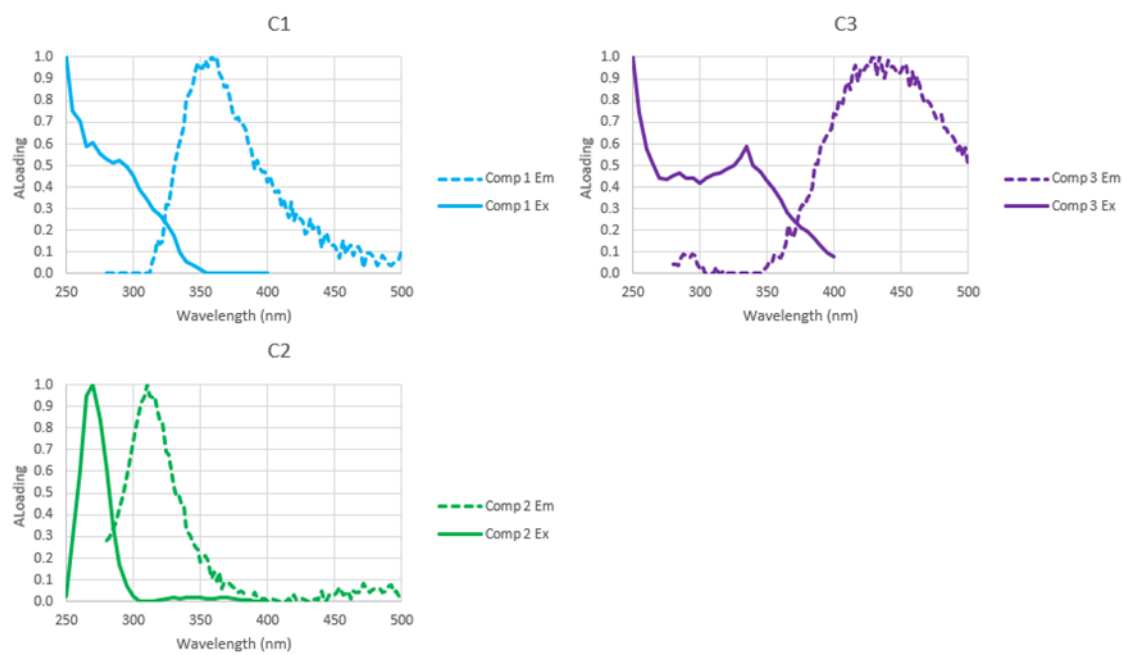


Figure S3: Excitation (Ex) (solid) and Emission (Em) (dashed) spectra for three fluorescent components identified by the PARAFAC.

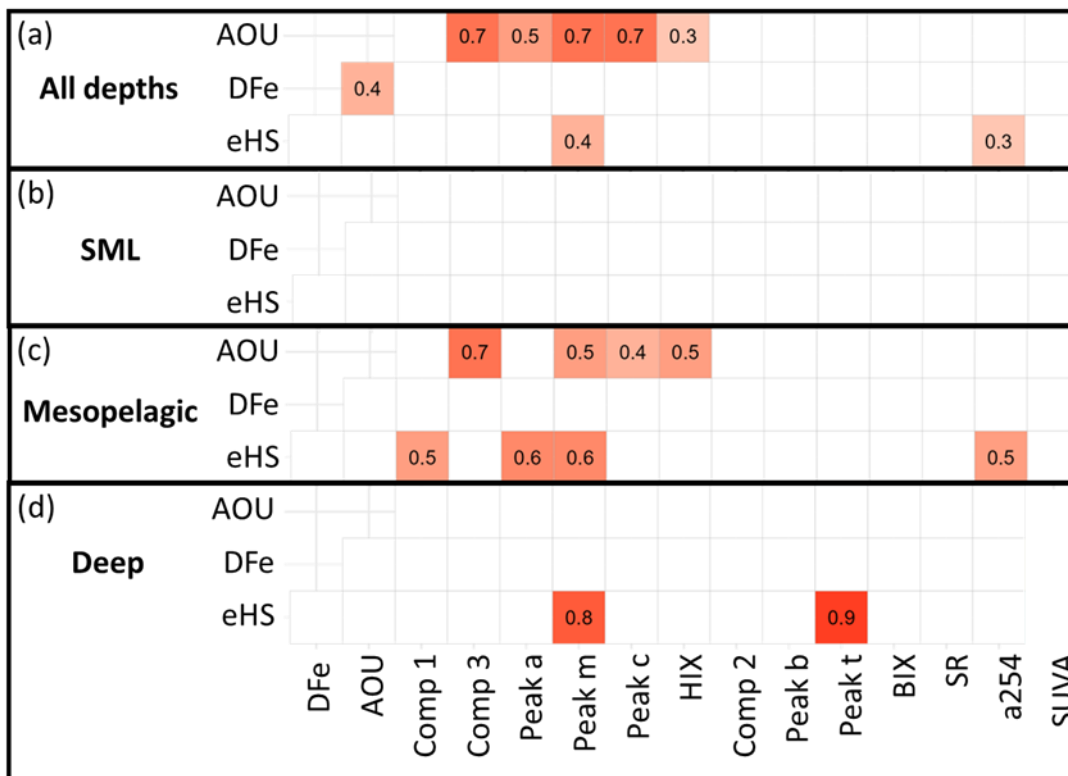


Figure S4: Correlation matrix between eHS, DFe, AOU, and CDOM/FDOM parameters in stations surrounding Crozet (listed in methods). Spearman rank correlations computed using the rcorr package in R.

Component	Ex/Em	% similarity	Matched component	Matched Ex/Em	Reference
1	250(290)/358	97.7	6	250(290)/356	Kowalczyk et al. 2009
		97.6	5	240/356	Stedmon et al. 2011
		97.6	1	~280/345	Wünsch et al. 2017
		97.0	6	~290/350	Osburn et al. 2018
2	270/310	98.3	2	260–270/ 310–320	D'Andrilli et al. 2017
		96.9	3	270/308	Painter et al. 2018
		98.9	1	320/444	Vines and Terry 2020
3	250(335)/434	98.4	1	320 (250)/428	Walker et al. 2009
		98.2	1	245 (330)/441	Zhuang et al. 2021
		98.1	1	315/436	Bittar et al. 2016

Table S1: Data table for the three fluorescent components identified by the PARAFAC with corresponding maximum excitation wavelength (Ex) and maximum emission wavelength (Em), the similarity (%) to named matched component in OpenFluor data base with reference paper and the Ex/Em of the matched components.

## **Chapter 4 Dissolved organic matter bioavailability influences Southern Ocean prokaryotic humic cycling with implications for trace metal biogeochemistry and carbon cycling**

Millie Goddard-Dwyer<sup>1,2</sup>; Claire Evans<sup>2</sup>, Ingrid Obernosterer<sup>3</sup>, Rui Zhang<sup>3</sup>, Rhea Thoppil<sup>3</sup>, Barbara Marie<sup>3</sup>, H el ene Planquette<sup>4</sup>, and Hannah Whitby<sup>1</sup>.

1. Department of Earth, Ocean and Ecological Sciences, University of Liverpool, Liverpool, L69 3BX, United Kingdom
2. National Oceanography Centre, European Way, Southampton, SO14 3ZH, United Kingdom
3. Laboratoire d'Oc eanographie Microbienne, BP 44, Avenue Pierre Fabre, 66651, Banyuls-sur-mer, France
4. LEMAR, Rue Dumont D'urville, 29280, Plouzan e, France

This chapter is in preparation for submission to Limnology and Oceanography.

### Statement of contributions:

MGD designed and performed the study, MGD did the eHS, prokaryote abundance and CDOM/FDOM analysis, RZ did the DNA extractions and preparation for sequencing, RT did the bioinformatics, BM did the DOC analysis. MGD performed the data analysis and wrote manuscript. MGD, CE, IO, and HW edited the manuscript.

### Highlights

1. The cycling of electroactive and coloured/fluorescent humic-like substances displayed opposite responses to changes in DOM supply and bioavailability.
2. eHS production appeared to be limited by carbon availability while coloured/fluorescent humics production may be limited by the scarcity of refractory chemical precursors.
3. Prokaryote carbon limitation promoted the removal of both eHS and coloured/fluorescent humics.

#### **4. 1. Abstract**

The stabilisation and availability of dissolved iron exerts a key control on ocean carbon cycling, particularly in iron-limited regions such as the Southern Ocean. Humic substances are thought to play an important role in the complexation of iron and other trace metals. Humics, a component of the dissolved organic matter (DOM) pool, can be characterized electrochemically (as electroactive humic substances; eHS) and by colour or fluorescence (coloured or fluorescent dissolved organic matter; CDOM/FDOM). DOM composition and prokaryote community composition are thought to be central drivers of CDOM/FDOM humic cycling. However, less is known about the drivers of eHS cycling. The Southwest Indian region of the sub-Antarctic sector of the Southern Ocean is a predominantly iron limited, low productivity region with islands supplying iron that can stimulate phytoplankton blooms and bioavailable DOM production. This study incubated in-situ prokaryote communities with in-situ DOM of varying bioavailability and measured changes in eHS, CDOM/FDOM, and prokaryote community composition. Greater DOC supply and DOM bioavailability increased eHS production while reducing CDOM/FDOM humic production, suggesting that eHS cycling is constrained by carbon availability while CDOM/FDOM humic production is controlled by the abundance of refractory chemical precursors. Lower bioavailability DOM and DOC supply promoted the removal of both eHS and CDOM/FDOM humics, likely due to prokaryote carbon limitation. Changes in DOM bioavailability and DOC supply resulted in variation in prokaryotic community composition which was coincident with variations in humic cycling. These results suggest that DOM bioavailability may interact with prokaryote humic cycling to influence local iron stabilisation and transport, with possible impacts on the magnitude of iron-driven phytoplankton blooms.

## 4. 2. Introduction

The Southern Ocean plays an important role in global carbon storage (Sarmiento and Toggweiler 1984) yet is a predominantly iron-limited, low primary productivity zone (termed high nutrient, low chlorophyll; HNLC) (Martin et al. 1990), where prokaryote heterotrophic communities are also consequently co-limited by iron and carbon (Church et al. 2000). However, point sources supply iron that support local phytoplankton blooms, leading to significant carbon sequestration (Blain et al. 2007) as well as producing phytoplankton derived bioavailable organic carbon, which alleviates prokaryote carbon limitation and promotes a distinct prokaryote community (Obernosterer et al. 2011; Obernosterer et al. 2015). Being the largest iron-limited region, the supply and bioavailability of iron to the Southern Ocean exerts key control on global carbon storage (Martin 1990; Watson et al. 2000). Therefore, understanding the factors which control iron supply and bioavailability, and relating it to microbial processes, is crucial.

Organic complexation of iron by ligands is an important factor mediating iron solubility (Gledhill and van den Berg 1994; Millero 1998). A range of studies have demonstrated that humic substances comprise a large part of the organic ligand pool (e.g. Whitby et al. 2020b), increase iron solubility (Krachler et al. 2015) and bioavailability (Chen and Wang 2008; Lis et al. 2015), and support the transport of iron over long distances (Slagter et al. 2019). Humics are a heterogeneous group of organic molecules, mostly comprised of carboxyl-rich alicyclic molecules (Hertkorn et al. 2006), which form a major part of marine dissolved organic matter (DOM) (Nissenbaum 1979; Zigarh et al. 2017). Measurements of fluorescent humic-like DOM (FDOM) can correlate with iron solubility (Kitayama et al. 2009; Tani et al. 2003) and distribution (Yamashita et al. 2020) although these relationships do not hold in the Atlantic (Heller et al. 2013; Whitby et al. 2020b). Measurements of electroactive humics (eHS) are thought to represent the iron-binding fraction specifically but do not always correlate with FDOM humics (e.g. Whitby et al. 2020b), which suggests these can represent different components of humic-like DOM (Fourrier et al. 2022), with potentially different cycling mechanisms.

Allochthonous sources of humics include riverine or aeolian deposition of terrestrial organics, while autochthonous sources include production and/or degradation by marine microbes, in particular prokaryote remineralisation (Romera-Castillo et al. 2011; Whitby et

al. 2020a). However, the mechanisms involved in Southern Ocean prokaryote humic cycling and its interplay with iron inputs and the bioavailable carbon produced by iron-stimulated phytoplankton blooms represents an important knowledge gap. DOM with greater aromaticity (Bussmann 1999; Romera-Castillo et al. 2011) and lower molecular size (Shen and Benner 2020) is generally of lower quality and is less bioavailable. Consequently, humics, with their aromatic and alicyclic structures (Hertkorn et al. 2006), are generally not degraded over short timescales by the microbial community (Lechtenfeld et al. 2014; Zheng et al. 2022). However, the prokaryote community may shift in response to changes in DOM quality (Bouchachi et al. 2023; Liu et al. 2020a; Manna et al. 2020; Sala et al. 2020). For example, higher initial humic concentration promotes a prokaryote community which possess the metabolic strategies to degrade humics (Bouchachi et al. 2023). However, this might come at the expense of supporting iron complexation as in some cases the amount of iron resupplied during remineralisation is limited by ligand (often humic) concentration (Whitby et al. 2020a). DOM quality also exerts strong control on humic production (Aparicio et al. 2015; Jørgensen et al. 2014; Martínez-Pérez et al. 2017; Xu et al. 2022). Further, DOM quality prompts changes in prokaryotic community composition (Romera-Castillo et al. 2011), with different strains yielding various amounts of (Goto et al. 2020) and compositionally distinct humics (Shimotori et al. 2012).

No studies have directly measured the impact of DOM composition and prokaryote community composition on eHS. This is an important knowledge gap, as eHS may play a role in the stabilization and transport of trace metals and consequently could support widespread, iron stimulated phytoplankton blooms. We set out here to address this knowledge gap and generate a comprehensive picture of the interaction between DOM composition, prokaryotic community composition, and eHS cycling. We address the following research questions:

1. How does DOM bioavailability affect humic cycling?
2. Are eHS and FDOM humic cycling controlled by the same mechanism?
3. What changes to the prokaryote community composition co-occur with eHS cycling?

Our study was conducted in the Southwest Indian Sector of the Southern Ocean because it is a region dominated by environmental gradients in DOM quality and prokaryote community

composition generated by iron supplied from sub-Antarctic islands (Obernosterer et al. 2011; Obernosterer et al. 2015). DOM quality was amended by adding DOM collected on these in-situ horizontal (highly productive surface waters downstream of sub-Antarctic islands vs HNLC surface waters) and vertical gradients (HNLC mesopelagic to HNLC deep). We incubated surface prokaryote communities with natural DOM of varying bioavailability to investigate the impact of DOM bioavailability on the cycling of eHS measured by cathodic stripping voltammetry, and coloured DOM (CDOM)/FDOM humics measured by absorbance and fluorescence spectrophotometry. Further, we identified coincident changes to the prokaryote community composition, measured using 16S rRNA sequencing.

### **4. 3. Methods**

#### **4. 3. 1. Site description**

Experiments were conducted as part of the South Indian Ocean GEOTRACES Section (SWINGS) cruise onboard the R/V Marion-Dufresne II (MD229, GS02) during 11<sup>th</sup> Jan – 8<sup>th</sup> Mar 2021 to the South West Indian part of the Southern Ocean (Figure 1). Sampling for this experiment was conducted in sub-Antarctic waters (front positions defined by Park et al. (2019) upstream of Crozet Archipelago in HNLC conditions and downstream of Crozet Archipelago inside the phytoplankton bloom associated with the island, termed the HNLC and Crozet treatments, respectively (Figure 1a).

#### **4. 3. 2. Experimental design**

Each experiment was comprised of a mix of 0.8  $\mu\text{m}$  (polycarbonate) filtered seawater (termed the prokaryote inoculum) and 0.2  $\mu\text{m}$  filtered seawater (Acropak cartridge) (termed the DOM addition) in a 25:75 ratio. Three experimental treatments were set up at the HNLC station: Surface, Mesopelagic, and Deep (Figure 1; Table S1) and one experimental treatment was set up at the Crozet station, each with three replicate incubations of 2 L. All experiments adhered to trace metal clean conditions, utilising acid-cleaned polycarbonate bottles. This experimental design aimed to prevent Fe contamination effects on prokaryote DOM cycling, given that Fe is limiting in the Southern Ocean and the known impact of Fe carbon cycling (e.g. Fourquez et al. 2020). At the interim and end time points, most

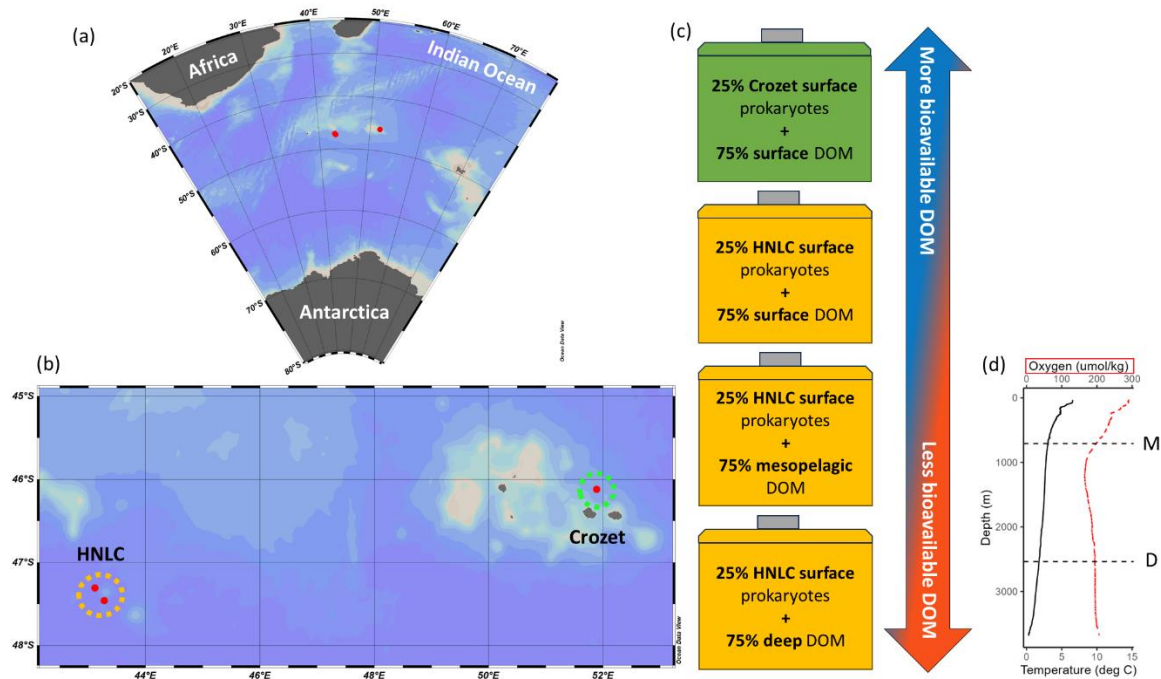


Figure 1: Sampling site and experimental design. Location at (a) basin scale within the South West Indian part of the Southern Ocean and (b) showing the position of the high nutrient low chlorophyll treatment sites upstream of Crozet Archipelago and Crozet treatment sites downstream of the islands inside the phytoplankton bloom. (c) Experimental design: different water masses and prokaryote communities were mixed within the four different treatments to generate a gradient of DOM bioavailability. (d) The water column structure at the HNLC site showing oxygen concentration (red) and temperature (black) and the depths where mesopelagic (M) and deep (D) water was collected from for the treatments.

parameters were subsampled. Otherwise, prokaryote abundance was taken at regular intervals (~1-2 days).

#### 4. 3. 3. eHS analysis

Samples for eHS concentration ([eHS]) were collected from the incubations on 'super' time points (Table S1). All sample bottles were cleaned as per the GEOTRACES cookbook (Cutter et al. 2017). Samples were filtered through 0.2  $\mu\text{m}$  syringe filter system using a peristaltic pump into 60 mL LDPE bottles prior to storage at  $-20^{\circ}\text{C}$ .

Analyses were conducted using cathodic stripping voltammetry as described in Pernet-Coudrier et al. (2013) using a  $\mu$ Autolab-III potentiostat (Ecochemie, Netherlands) controlled by NOVA software and Metrohm V663 stand controlled via Metrohm IME663. The system comprised of a hanging mercury drop working electrode, a glassy carbon auxiliary electrode, and an Ag/AgCl (3 mol L<sup>-1</sup> KCl) reference electrode. Analyses took place inside an acid cleaned glass electrochemical cell. Modifications to the method described by Pernet-Coudrier et al. (2013) include purging the sample with nitrogen gas for 600s, using a deposition time of 400s, and using the 1<sup>st</sup> derivative of the peak processed in ECD software (Omanović 2011) to quantify the humic peak. Molybdenum standards (1 ppb, BDH Spectrosol) and Suwannee River Fulvic acid (SRFA) standards (2S101H, IHSS) solutions were prepared by dilution of in Milli-Q and acidified to pH 2 using HCl TM grade (Fisher Science). Daily measurement of a reference material was used to monitor the CSV data. This reference material was Hansell lab DOC certified reference material (CRM) deep (Batch 22 Lot number 10-22). The average concentration was 22.4  $\pm$  3.23  $\mu$ g/L.

The minimum and maximum eHS Fe binding capacity (nM Fe equivalent) was calculated from minimum (0.0146 nmol Fe/  $\mu$ g SRFA, Sukekava et al. 2018) and maximum (0.032 nmol Fe/  $\mu$ g Suwannee River Humic acid, SRHA, Laglera and van den Berg 2009) reported values for humic standards using average eHS concentration of the treatment time point ( $\frac{\sum[eHS]_i}{n}$ ) (Eq.1), as in Whitby et al. (2020b).

$$\text{Eq 1. } \textit{minimum or maximum eHS Fe binding capacity} = \frac{\sum[eHS]_i}{n} \times \textit{Fe binding capacity}$$

#### 4. 3. 4. CDOM and FDOM

CDOM/FDOM samples were taken from the eHS samples in the home lab. Analyses were carried out using Cary Eclipse Fluorescence Spectrophotometer and Cary-60 UV-vis spectrophotometer (Agilent) using 1cm length cells. Two initial Crozet measurements were averaged. Data analyses were conducted in the staRdom package using R. The parameters used in this study are biological index (BIX, Fellman et al. 2010; Huguet et al. 2009), humification index (HIX, Ohno 2002), Coble peaks, slope ratio (275-295-nm slope : 350-400-nm slope, Helms et al. 2008), and specific absorbance at 254 nm (SUVA, Weishaar et al. 2003). Coble peak a, m, c are considered to be humic-like components while Coble peak b

represents tyrosine-like components and Coble peak t represents tryptophan-like components (Coble 1996; Coble 2007).

#### **4. 3. 5. DOC**

The concentration of DOC was determined in samples filtered through two combusted (450 °C, 4 h) GF/F filters. Subsamples of 10 mL (in duplicate) were transferred to pre-combusted glass ampoules and acidified with H<sub>3</sub>PO<sub>4</sub> (final pH = 2). The sealed glass ampoules were stored in the dark at room temperature until analysis. DOC concentrations were measured on a Shimadzu TOC-L analyzer as described previously (Hernandez-Magana et al. 2021). Consensus reference material (batch #04-21 DSR (700 m) consensus value [43-45] μM) provided in sealed glass ampoules (<https://hansell-lab.earth.miami.edu/consensus-reference-material/index.html>) was injected every 12 to 17 samples to insure stable operating conditions. The measured DOC concentration of this reference material was on average 44.7±2.0 μM.

#### **4. 3. 6. Prokaryote abundance**

Unfiltered seawater samples were fixed shortly after collection using glutaraldehyde (0.5 % w/v final concentration) in cryovials for >1h at 5 °C prior to flash freezing in liquid nitrogen and storage at -80 °C. In the home lab, samples were stained with SYBR Green I dye (Zubkov et al. 2006) and enumerated using a FAC Sort (Becton Dickinson) using pink beads of 0.5 μm diameter (Fluoresbrite Microparticles, polysciences) as an internal standard. Prokaryote populations were determined based on DNA content and light scatter (side scatter; SSC) properties: low nucleic acid content (LNA), high nucleic acid content with low SSC (HNA-low SSC), and HNA high SSC. A final population of LNA with double the fluorescence and SSC than LNA was denoted as LNA cells in G2 phase of their cell cycle (LNA G2) (Zubkov et al. 2006).

#### **4. 3. 7. Prokaryotic community composition**

Initial bacterial community composition samples were collected from the bacterial inoculum seawater. Seawater samples were collected from the incubations at the intermediate 'super time point' for Crozet surface only and at the end time point for all treatments. 250 mL for the Crozet Surface and 500 mL for the HNLC incubations was filtered onto a 0.2 μm polycarbonate filter using a vacuum pump prior to flash freezing in liquid nitrogen and storage at -80 °C.

Total DNA extraction was conducted on the filters utilizing the dNeasy PowerWater Kit (Qiagen), following the manufacturer's protocol with a few adjustments. Subsequently, the filters were cut into small pieces using scissors and transferred into 2mL Eppendorf tubes, where solution PW1 was added and incubated at 65°C for 10 minutes to facilitate cell lysis, as described by Liu et al. (2020b). DNA concentrations were quantified using a Quantus fluorometer (Promega) with the QuantiFluor® Double-stranded DNA (dsDNA) system. 16S rRNA gene amplicons were sequenced with Illumina MiSeq V3 2 × 300 bp chemistry and demultiplexed at the platform Biosearch Technologies (Berlin, Germany). Subsequent sequence processing was performed using the DADA2 package in R (Callahan et al. 2016) to infer amplicon sequence variants (ASVs) via the high-resolution DADA2 method. Primer sequences were trimmed, and sequences were quality-filtered based on the following parameters: DADA2 (maxN=0, maxEE=c(3,5), truncQ=2). Forward reads with a length of 240 bp and reverse reads with a length of 210 bp were retained. Error rates were estimated from the data, and sequence variant inference was performed using pooled sequences from all samples. Forward and reverse sequences were merged, and chimeras were removed. Taxonomy was assigned utilizing the SILVA database release 138 at the highest possible taxonomic level.

#### **4. 3. 8. Statistical analyses**

Microbial community composition of samples in ordination space were compared using non-metric dimensional scaling (NMDS), based on the Bray–Curtis dissimilarity matrix (Roberts 2020) using the ordinate function in the Phyloseq package (McMurdie and Holmes 2013) (4.2.1 version). The stress for the NMDS plot was inspected for less than 0.2 demonstrating satisfactory model for the data (Dexter et al. 2018). All other statistical analyses were carried out using R version 4.3.1. Spearman rank correlations were carried out using the Hmisc and rcorr package. Principle Component Analysis (PCA) was carried out using the prcomp function.

#### **4. 4. Results**

##### **4. 4. 1. Initial DOM compositions**

The experiment was designed to generate a gradient of high to low DOM bioavailability and DOC supply moving from Crozet Surface to HNLC Surface to HNLC Mesopelagic to HNLC Deep (hereafter referred to as Crozet Surface to HNLC Deep; Figure 1). From Crozet Surface

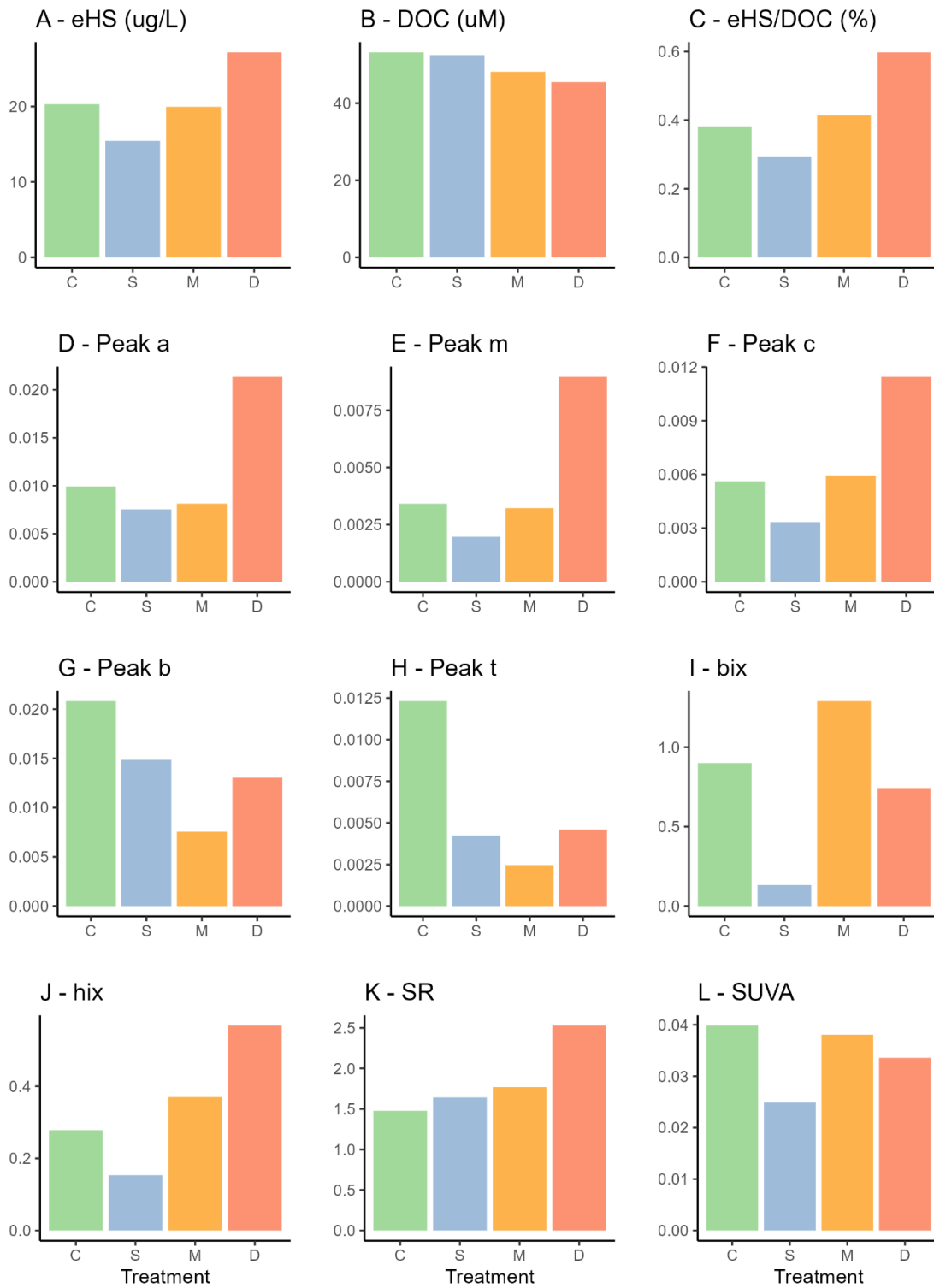


Figure 2: Comparison of initial DOM composition between incubation treatments across the treatments: Crozet Surface (C), HNLC Surface (S), HNLC Mesopelagic (M), and HNLC Deep (D).

to HNLC Deep, DOC concentration decreased and SR increased (Figure 2), indicating decreases to molecular weight (SR is inversely proportional to DOM molecular weight, Helms et al. 2008). Humics (eHS, humic Coble peaks a, m, c, and HIX) broadly followed this trend, although exhibited notable minima in Surface HNLC (Figure 2). Coble peaks (b and t), BIX, and SUVA generally decreased from Crozet Surface to HNLC Deep, but Coble peaks (b and t) exhibited minima in HNLC Mesopelagic, while BIX and SUVA exhibited minima in HNLC Surface.

#### **4. 4. 2. Prokaryote community**

##### **4. 4. 2. 1. Changes in prokaryote abundance over time**

Generally, rate of prokaryote growth was greatest in Crozet Surface, followed by HNLC Surface, and then both HNLC Mesopelagic and HNLC Deep where rate of growth was similar (Figure 3b). Prokaryote abundance in the Crozet Surface ‘crashed’ to 25 % of peak abundance between the intermediate and end time point (Figure 3b). A similar change, to a smaller degree, was observed in the HNLC Surface treatment: a minor ‘crash’ to 66 % of peak abundance occurred on day 29 (Figure 3b). Note, initial prokaryote abundance in the Surface HNLC treatment was greater than in the other HNLC treatments however, overall all treatments received a similar magnitude of prokaryote inoculum (Figure 3b).

##### **4. 4. 2. 2. Changes to the bacterial community composition**

The composition of the prokaryote community was measured using 16S rRNA genes, which by nature only describes the bacteria. Bray-Curtis similarity analyses indicated that the bacterial community composition in the initial prokaryote inoculums were more similar to each other than to the treatment end points (Figure S1). Both the Crozet and HNLC inoculums were dominated by ASV3 SAR11 Clade I (Class: Alphaproteobacteria) (Figure 3a). In the Crozet inoculum, ASV12 Flavobacteriaceae (Class: Bacteroidia) was also abundant, while many other species were present at <5% abundance. In the HNLC inoculum, all other bacteria were present at ~10 % or less abundance and included ASV12 Flavobacteriaceae, ASV92 SAR86 (Class: Gammaproteobacteria), and ASV1 Rhodobacteraceae (Class: Alphaproteobacteria). HNLC treatments were more similar to each other than to Crozet Surface time points (Figure S1). This indicates two ‘trajectories’ of changes to bacterial community composition: Crozet Surface and the HNLC incubations. Within the HNLC treatments, HNLC Mesopelagic and Deep were more similar to one another than to HNLC

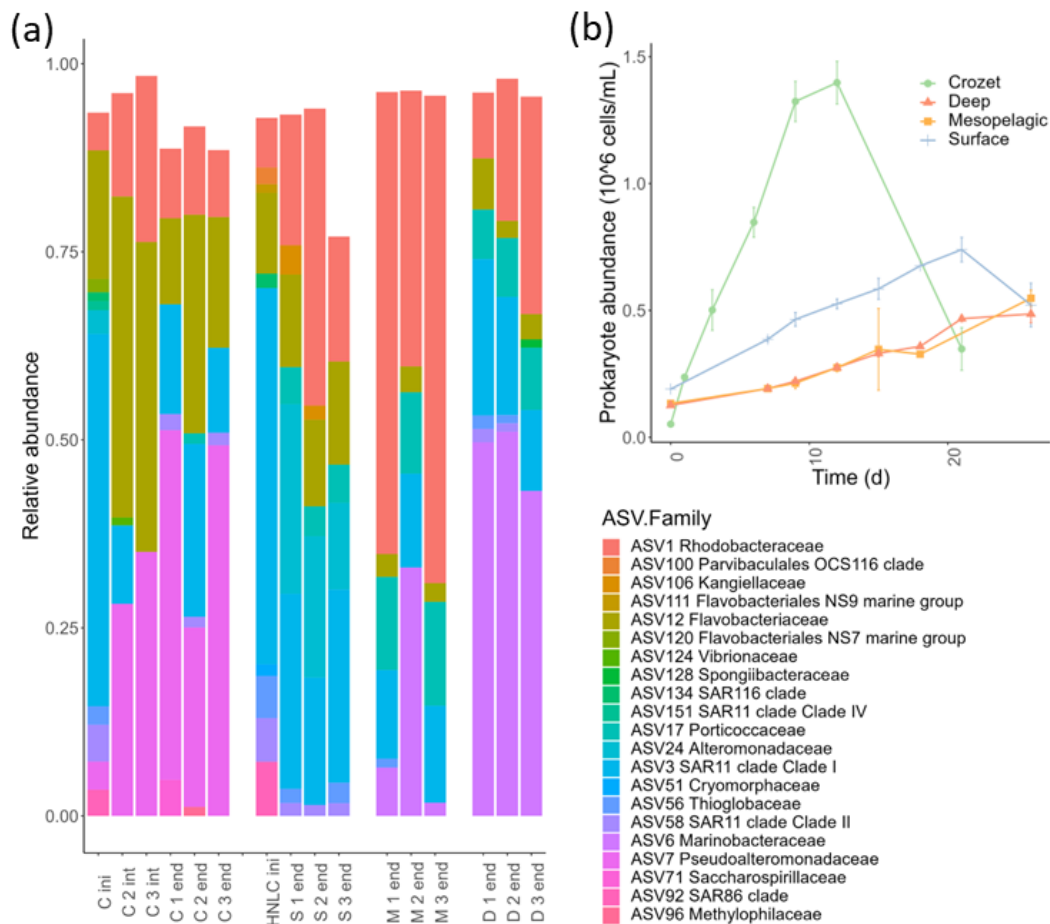


Figure 3: (a) Bacterial community composition (relative abundance, normalised to total number identified ASVs in the sample) and (b) Prokaryote abundance ( $10^6$  cells/mL) over the course of the incubations

Surface (Figure S1). Crozet Surface was dominated by ASV12 Flavobacteriaceae at the intermediate time point, followed by ASV7 Pseudoalteromonadaceae (Class: Gammaproteobacteria) (Figure 3a). By the end time point, high variability in community composition between replicates was observed. Using averages while acknowledging this high level of variability, the relative abundance of ASV7 Pseudoalteromonadaceae increased until that group was the dominant member of the community, followed by ASV12 Flavobacteriaceae (whose proportional abundance was much lower than the interim-timepoint) and ASV3 SAR11 Clade I (whose relative abundance was similar to the interim-timepoint). ASV1 Rhodobacteraceae proportional abundance was modest but was consistent between the replicates, in contrast to the other taxa.

No interim bacterial community composition data were collected for the HNLC treatments due to water budgets. HNLC Surface was dominated by ASV1 Rhodobacteraceae and ASV3 SAR11 Clade I at the end time point (Figure 3a). ASV3 SAR11 Clade I exhibited a large decrease in relative abundance and ASV1 Rhodobacteraceae exhibited a large increase in relative abundance over the course of the incubation. Notably, ASV24 Alteromonadaceae (Class: Gammaproteobacteria) was third most abundant in stark contrast to the HNLC inoculum, where it was a rare member of the community (below cut off). This was followed by ASV12 Flavobacteriaceae, which maintained consistent relative abundance throughout the incubation.

HNLC Mesopelagic was dominated by ASV1 Rhodobacteraceae at the end point (Figure 3a). ASV3 SAR11 Clade I relative abundance decreased but still remained comparatively abundant (~10%). ASV6 Marinobacteraceae (Class: Gammaproteobacteria) and ASV17 Porticoccaceae (Class: Gammaproteobacteria) increased from rare members of the HNLC inoculum to comprising ~10% of the community.

HNLC Deep was dominated by ASV6 Marinobacteraceae at the end time-point (Figure 3a). As with the other HNLC incubations, ASV3 SAR11 Clade I exhibited stark reduction in relative abundance but still remained relatively abundant at the end time point (~15%). ASV1 Rhodobacteraceae, ASV17 Porticoccaceae, and ASV128 Spongiibacteraceae (Class: Gammaproteobacteria) increased in relative abundance, while the relative abundance of ASV12 Flavobacteriaceae and other bacteria that were abundant in the HNLC inoculum decreased to <5 %.

#### **4. 4. 3. eHS and FDOM cycling**

##### **4. 4. 3. 1. DOM cycling between the treatments.**

Overall, humic and DOC cycling varied between treatments (Figure 4). eHS production and DOC removal decreased from Crozet Surface to HNLC Surface to HNLC Mesopelagic (Figure 4a-b), while humic CDOM/FDOM (HIX and humic Coble peaks (a, m, c)) production increased (Figure 4c-f). In HNLC Deep, DOC removal was minimal (Figure 4a), while net degradation of eHS and humic coble peaks (a, c), and lower production rate of HIX and humic coble peak (m) relative to other HNLC incubations were observed (Figure 4b-f). Comparing trends in humic cycling between the treatments to initial DOM conditions, change in eHS concentration was broadly positively related to DOC and molecular weight

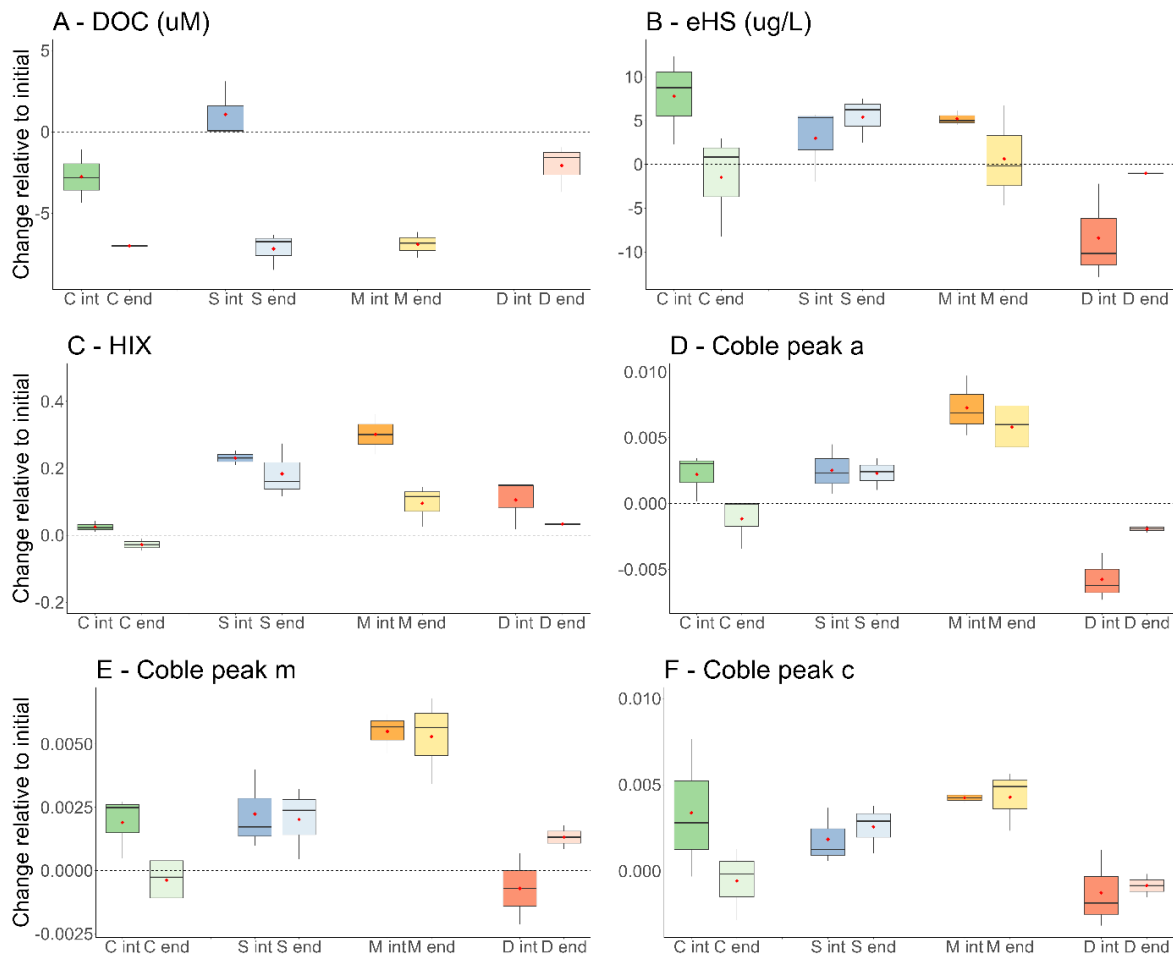


Figure 4: Changes to the humic and DOC pool (all relative to initial concentrations) at the intermediate (int) and end time points of the treatments for the Crozet Surface (C), HNLC Surface (S), HNLC Mesopelagic (M), and HNLC Deep (D).

(Figure 4b and 2b,k) and the degradation of humics (CDOM/FDOM and eHS) in HNLC Deep coincided with an initial DOM pool rich in humics (CDOM/FDOM and eHS) and poor in DOC (Figure 4b-f and 2a-b,d-f,j).

Variable DOM cycling was also observed between timepoints within treatments. In Crozet Surface, eHS and humic Coble peaks (a, m, c) increased between the initial and intermediate time points (Figure 4b-e). Between the intermediate and end time points, eHS and HIX decreased (Figure 4b-c), coincident to decrease in prokaryote abundance (Figure 3b). Over the course of this incubation, change in eHS concentration was positively correlated with change in SR (and therefore negatively correlated with DOM molecular weight, Helms et al.

2008, Spearman,  $\rho = 0.9$ ,  $p < 0.05$ ) and negatively correlated with change in Coble peak b intensity (Spearman,  $\rho = -0.8$ ,  $p < 0.05$ ).

In HNLC Surface, net production of eHS, HIX, humic Coble peaks (a, m, c) occurred between the initial and intermediate time points (Figure 4b-f). Between the intermediate and end time points, eHS and humic Coble peak c increased while HIX decreased (Figure 4b-c,f), the latter coincident to a decrease in prokaryote abundance (Figure 3b). Change in eHS concentration did not correlate to any FDOM parameters during this treatment (Spearman,  $p > 0.05$ ).

In HNLC Mesopelagic, eHS, HIX, and humic coble peaks (a, m, c) increased between the initial and intermediate time points (Figure 4b-f). Between the intermediate and end time points, HIX and eHS decreased (Figure 4b-c). Change in eHS concentration did not relate to any FDOM parameters during this treatment (Spearman,  $p > 0.05$ ).

In the HNLC Deep treatment, HIX increased while eHS and humic Coble peaks (a, c) decreased between the initial and intermediate time points (Figure 4b-d,f). Between the intermediate and end time points, net production of eHS and humic coble peaks (a, m) was observed while net removal of HIX occurred (Figure 4b-e). SUVA, a proxy for aromaticity of the DOM pool (Weishaar et al. 2003), decreased over the course of the incubation (Figure S3d). Change in eHS concentration was positively correlated to change in humic Coble peak a (Spearman,  $\rho = 0.9$ ,  $p < 0.05$ ) and Coble peak b (Spearman,  $\rho = 0.8$ ,  $p < 0.05$ ).

#### **4. 4. 3. 2. PCA**

In order to unpick which aspects of the organic matter processing were linked across the entire set of treatments, we performed a PCA on the total change in DOM composition (DOC, eHS, Coble peaks, HIX, BIX, and SR). Overall, two principal components explained a total of 64 % of the total variance in the data (Figure S2a). PC1 explained most of the separation between HNLC Deep compared to HNLC Mesopelagic and HNLC Surface, while PC2 explained most of the separation between HNLC Mesopelagic and HNLC Surface (Figure S2a). Variation between Crozet Surface and the other treatments was not explained by this analysis, however PC1 explained most of the variation between the time points. Specific clusters of organic matter were observed in the loadings (Figure S2b). eHS, HIX, SR, and

Parameter	Crozet Surface					HNLC Surface					HNLC Mesopelagic					HNLC Deep				
	eHS	HIX	a	m	c	eHS	HIX	a	m	c	eHS	HIX	a	m	c	eHS	HIX	a	m	c
Prokaryote abundance																				
HNA (low SSC)	0.8	0.8	0.9	0.8		0.8														
LNA		0.8																		
LNA G2																	0.9			
ASV3	-0.8										-0.8					0.9			0.9	
ASV6																				0.8
ASV12				0.8												0.9			0.9	
ASV56										-0.8										

Table 1: Pairwise spearman rank correlation rho between key prokaryote groups and bacterial ASVs and humic parameters in each treatment, where p<0.05.

SUVA clustered together and humic Coble peaks clustered together.

#### 4. 4. 3. 3. Links between prokaryote community and humic cycling

Prokaryote abundance did not correlate to any humic parameters in any of the incubations (Table 1). However, specific groups of the prokaryote community related to humic parameters, with stark variations between the treatments (Table 1). Humic cycling was positively linked to HNA (low SSC) prokaryote abundance in both Crozet Surface and HNLC Surface (Table 1), coinciding with more bioavailable initial DOM and greater initial DOC in these treatments (Figure 2). Humic cycling was negatively correlated to ASV12 Flavobacteriaceae and ASV3 SAR11 Clade I in both the Crozet Surface and HNLC Mesopelagic (Table 1). However, in HNLC Deep, humic cycling was linked to the prokaryote community in a different way. Here, LNA G2, ASV3 SAR11 Clade I, ASV12 Flavobacteriaceae, and ASV6 Marinobacteraceae were positively correlated to humic cycling (Table 1), coincident to lower bioavailable initial DOM and less initial DOC in these treatments (Figure 2).

#### 4. 5. Discussion

We found that prokaryote humic cycling was mediated by DOM bioavailability, and changes to the humic pool coincided with changes to the prokaryotic communities in response to the composition of the DOM. These results imply the potential for humics to impact iron cycling through changes to iron complexation and hence influence carbon cycling, both through active participation in prokaryote carbon uptake and by acting as a carbon reservoir.

#### 4. 5. 1. Role of DOM bioavailability in humic cycling and implications for Fe cycling

While DOM cycling was variable between treatments, overall, an initial pool of more bioavailable, higher molecular weight, and DOC-rich DOM stimulated eHS production (Comparing Crozet Surface to HNLC Surface to HNLC Mesopelagic; Figure 2 and 4b), consistent with FDOM humics in other incubation studies (Bouchachi et al. 2023; Xie et al. 2020). This strongly implies that prokaryote eHS production in the region is carbon limited. The impact on eHS Fe binding can be estimated by calculating the eHS Fe binding capacity envelope (Whitby et al. 2020b) (detailed in methods). Under these assumptions, we estimate that prokaryotes produced 2.5 – 5.6 pM of additional Fe binding capacity under more bioavailable carbon conditions, such as those in phytoplankton blooms. We hypothesise that this additional Fe binding capacity could produce a positive feedback loop providing Fe that sustains local phytoplankton blooms.

Conversely, CDOM/FDOM humic production was enhanced by opposite conditions to eHS. An initial pool of less bioavailable, lower molecular weight, and DOC-poor DOM stimulated FDOM humic production (Comparing HNLC Mesopelagic to HNLC Surface to Crozet Surface; Figure 2 and 4c-f). This supports that refractory DOM precursors promote humic production (Aparicio et al. 2015) but is in contrast to incubation studies performed in coastal environments (Bouchachi et al. 2023; Xie et al. 2020), likely reflecting a lower contribution of terrestrial humics here. Considering that FDOM humics linearly correlate with DFe(III) solubility (Kitayama et al. 2009; Tani et al. 2003), we infer that Fe(III) solubility increased under lower bioavailable carbon conditions such as the mesopelagic. Therefore, humic FDOM production via prokaryote DOM remineralisation could be a mechanism stabilising DFe released in the mesopelagic.

We observed differential cycling between the electroactive and CDOM/FDOM fractions of humics. eHS and FDOM humics have been reported to not correlate in the other basins (Whitby et al. 2020b) and in the (ultra)oligotrophic Pacific Ocean, eHS made a smaller contribution to humic FDOM in mesopelagic waters compared to surface or deep waters (Fourrier et al. 2022). This study suggests a similar process operates in the Southern Ocean and that divergent DOM composition could be driving these patterns. Divergent eHS and CDOM/FDOM humics cycling may be partly explained by detection of exopolymeric substances within the eHS analytical window (Hassler et al. 2011). Exopolymeric substances

exhibit different cycling of these substances compared to FDOM humics. Exopolymeric substances are rapidly degraded (Zhang et al. 2015) while FDOM humics are slowly cycled (Shimotori et al. 2009). Further, FDOM humics can be produced during prokaryote degradation of exopolymeric substances (Zhang et al. 2015), which may be contributing to 'opposite' eHS vs CDOM/FDOM humics cycling.

When the DOM pool was of the lowest bioavailability and molecular weight, poorest in DOC, and richest in humics (HNLC Deep), eHS and CDOM/FDOM humic removal was promoted (Figure 2 and 4b-f). These results suggest that under extreme carbon or energy limitation, the prokaryote community shifted towards consuming humics to satisfy carbon demand. Similar effects have been observed in a coastal incubation where consumption of FDOM humics was observed when the initial DOM pool was dominated by FDOM humics (Bouchachi et al. 2023), and in mesopelagic particulate remineralisation studies where high particulate organic carbon removal stimulated eHS removal (Whitby et al. 2020a). Considering the role of eHS and FDOM humics in Fe complexation (Laglera and van den Berg 2009; Yamashita et al. 2020), removal of eHS and CDOM/FDOM humics under low bioavailable DOM conditions reduced Fe complexation capacity by 0.13 – 0.29 pM (calculated using literature values of binding capacity). A reduction in humic Fe complexation capacity at depth was also observed in the Pacific (Fourrier et al. 2022) and might necessitate the presence of other trace metal binding ligands of unknown identity and/or stabilisation mechanisms such as colloidal phases (Bergquist et al. 2007), or a potential reduction in the local deep sea DFe inventory. This also aligns with our observations of a disparity between DFe and eHS at depth in the region (see Chapter 3). However, we also note indicators of changes in the molecular structure of the humic pool under low initial DOM bioavailability and DOC supply, including aromaticity (Figure S3d). Increases in humic aromaticity can act antagonistically with decreases in eHS concentration to influence humic Fe binding capacity (Kikuchi et al. 2017; Laglera and van den Berg 2009). Direct observations of eHS trace metal binding capacity are crucial to confirm the impact of eHS processing under different DOM conditions on eHS trace metal binding capabilities.

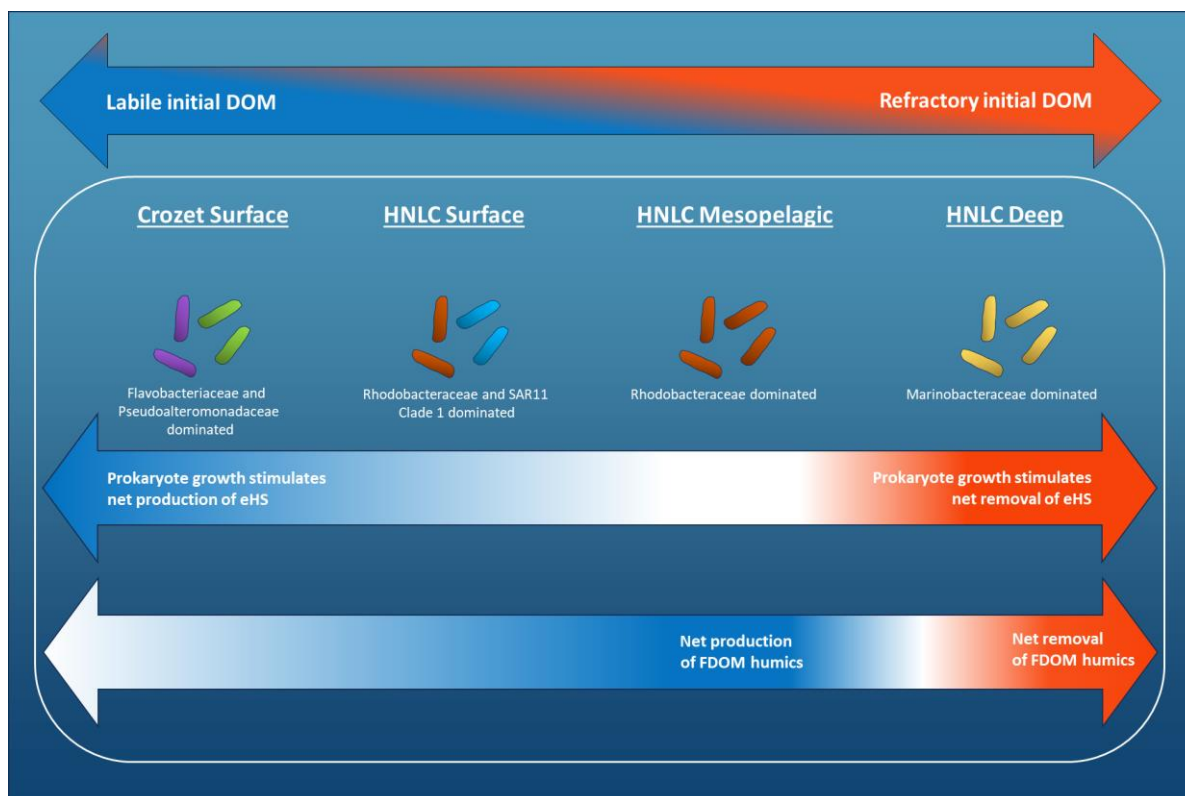


Figure 5: Schematic summarising the conceptual framework developed from results of this study. Upper arrow shows the initial DOM bioavailability in the different treatments Crozet Surface, HNLC Surface, HNLC Mesopelagic, and HNLC Deep. Resultant changes to the prokaryote community and humic pool are depicted within the white box. Blue parts of the arrow indicate production of eHS or CDOM/FDOM humics, white indicates no change in eHS or CDOM/FDOM humics, and red indicates degradation of eHS or CDOM/FDOM humics.

#### 4. 5. 2. The role of initial DOM composition in the development of prokaryotic community composition

A varying gradient of initial DOM bioavailability resulted in distinct bacterial communities, the composition of which was consistent with known characteristics of some representatives of the dominant bacterial lineages (Figure 3a). More bioavailable initial DOM (Figure 2) promoted a Flavobacteriaceae and Pseudoalteromonadaceae dominated community (Crozet Surface, Figure 3a). Some members of these lineages exhibit a copiotroph strategy associated with labile DOM partly enabled by high abundance of TonB transporters which facilitate the utilisation of a wide range of substrates (Cottrell and Kirchman 2000; Dadaglio

et al. 2018; Straza et al. 2010; Tang et al. 2012). Intermediate bioavailable initial DOM profile (Figure 2; HNLC Surface and Mesopelagic) fostered a Rhodobacteraceae and SAR11 Clade 1 dominated community (HNLC Surface), transitioning to a Rhodobacteraceae dominated community (HNLC Mesopelagic) (Figure 3a). Some members of Rhodobacteraceae can rapidly adapt to changes in DOM supply and have the capacity to utilize diverse substrates (Berkenheger and Fischer 2004; Pinhassi et al. 1999) and have also been shown to be abundant in lower bioavailability DOM-rich bathypelagic waters (Sanz-Sáez et al. 2023). The lowest bioavailability initial DOM (Figure 2; HNLC Deep) led to a Marinobacteraceae dominated community (Figure 3a). Some members of Marinobacteraceae have been shown to be more abundant in Southern Ocean 'winter water' which is richer in refractory DOM compared to other surface Southern Ocean water masses (Landa et al. 2018).

#### **4. 5. 3. Links between prokaryotic abundance and bacterial community composition with humic cycling**

Overall, humic parameters were strongly correlated to the abundance of some prokaryote groups and/or bacterial community composition (Table 1), indicating active cycling of the humic pool by the prokaryotes and underscoring the significant role of prokaryote remineralisation as a key mediator of humic biogeochemistry in the Southern Ocean (Jørgensen et al. 2011). However, the connection between humic cycling and bacterial community composition exhibited variations across treatments. Interestingly, in the HNLC Deep treatment, the abundance of low nucleic acid cells in the G2 phase of the cell cycle, indicative of active division (Zubkov et al. 2006), were implicated in HIX production (Table 1). Low nucleic acid cells are thought to be a combination of less active prokaryotes (Gasol et al. 1999) and those specialised to low supply and bioavailability of DOM (Zubkov et al. 2001), the latter explaining their activity in the lowest bioavailability DOM treatment. HIX is proxy of the humification of DOM (analogous to humic content, Ohno 2002) therefore our results suggest that actively dividing LNA cells may contribute to the production of humics. Further, correlations suggest that some members of the bacterial community play diverse roles in humic cycling according to environmental conditions (Table 1). Under high and intermediate DOM bioavailability conditions (Crozet Surface and HNLC Mesopelagic), ASV3 SAR11 was associated with degradation of humics, consistent with previous observations of the active response of members of SAR11 to humic compounds (Liu et al. 2020a). However, under the lowest bioavailable DOM conditions (HNLC Deep), ASV3 SAR11 correlated with the

production of humics in the HNLC Deep treatment. Our results suggest that changes to prokaryote community composition is part of the mechanism underpinning the response of eHS cycling to bioavailability. However, we cannot confirm that prokaryotes directly modified the humic pool because the control incubations (1 replicate where bacterial inoculum was replaced with 0.2  $\mu\text{m}$  surface water collected from the respective experiment station) were contaminated with prokaryotes and therefore no control treatment data is available.

#### **4. 5. 4. Identifying possible chemical precursors to humics**

In both Crozet Surface and HNLC Deep, humics were linked to Coble peak b (tyrosine-like, protein-like) fluorescence. Coble peak b fluorescence can indicate the presence of phenol moieties in DOM because tyrosine is a monophenol and shares fluorescence characteristic with molecular phenol (Pagano et al. 2012). Phenolic compounds serve as known precursors of humics (Stevenson 1994). Hence, we propose that the DOM responsible for Coble peak b fluorescence serves as a precursor for eHS production by prokaryotes. Notably, members of Rhodobacteraceae, a dominant taxonomic group in these treatments, possess a metabolic pathway for aerobic degradation of a wide range of aromatic phenolic compounds ( $\beta$ -ketoadipate pathway, Buchan et al. 2000). Further research should directly investigate whether phenolic DOM acts as a precursor for humics in the marine environment.

#### **4. 5. 5. The role of humics in regional carbon biogeochemistry**

Our findings suggest that under copiotroph, more bioavailable DOM conditions (such as during phytoplankton blooms), active microbial growth serves as an efficient source of eHS. This aligns with observed elevated eHS concentration in phytoplankton blooms across the SWINGS transect (see Chapter 3). Additionally, HNLC Mesopelagic treatments yielded FDOM humic production, consistent with previous observations of humic sources in the mesopelagic ocean (Fourrier et al. 2022; Kowalczyk et al. 2013; Nelson and Gauglitz 2016). The role of these humics in carbon cycling depends on the rate at which they are cycled. Our experiments identified two humic pools with distinct cycling rates. Firstly, an actively cycled semi-labile humic pool evidenced as humic removal between the mid and end time points of Crozet Surface (Figure 4b-f) and between initial and mid-point of HNLC Deep (Figure 4b,d) on a timescale of weeks, as per Hansell's (2013) definition of semi-labile. These semi-labile humics contribute to prokaryote carbon demand in this region and may explain the apparent depletion of eHS at depth in the region (see Chapter 3). Secondly, a slowly-cycled refractory

humic pool is evident in the HNLC Deep treatment (Figure 4b,d-e), suggested by net humic depletion to a certain concentration before subsequent net humic production (Aparicio et al. 2015). These humics could represent refractory DOM, serving as a carbon reservoir in the deep ocean. Future work should resolve the bioavailability of humics in the region to determine their role in Southern Ocean carbon storage.

#### **4. 6. Conclusion**

This study found strong responses in humic cycling in response to DOM composition and DOC supply, which coincided with variations in prokaryotic community composition. However, DOM composition and DOC supply had opposite impacts on eHS vs CDOM/FDOM humics. Elevated DOC supply and increased DOM bioavailability increased eHS production while reducing CDOM/FDOM humic production. We conclude that eHS cycling was constrained by carbon availability, while CDOM/FDOM humic production was limited by the scarcity of refractory chemical precursors. These findings emphasize the need to understand the biogeochemistry of these two pools separately. Production of eHS in response to carbon availability, driven by iron stimulated phytoplankton blooms in this region, suggests increases to iron complexation which has the potential to support iron-driven phytoplankton blooms. The presence of highly refractory DOM and low DOC supply promoted the removal of both electroactive and CDOM/FDOM humics, likely due to prokaryote carbon limitation. Microbial degradation of humics could reduce iron complexation capacity, which can limit deep iron reserves supplied from remineralisation. Overall, this study has unveiled an important mechanism which likely influences eHS distribution across the region. Subsequent investigations should unpick this network in order to resolve the specific role of humics in Southern Ocean carbon and trace metal biogeochemistry.

#### **4. 7. Acknowledgements**

S Felgate for CDOM/FDOM analysis advice. M Fourquez for shipboard mentorship and incubation advice. I Turnbull for help with the incubations subsampling. SWINGS trace metal team for help with collecting seawater. G Portlock and P Salaün for voltammetry guidance. We would like to thank the captain A. Eyssautier, LDA and GENAVIR officers, engineers, technicians and the crew of the R/V Marion Dufresne for their enthusiasm and their professional assistance during the SWINGS cruise. We would like to thank the chief scientists Catherine Jeandel and H el ene Planquette. We also thank Emmanuel de Saint-L eger and

Fabien Pérault (CNRS DT INSU) for their help with the preparation, deployment and maintenance of the rosette. The SWINGS project was supported by the Flotte Océanographique Française (10.17600/18001925), Agence Nationale de la Recherche (ANR 19-CE01-0012), CNRS/ INSU (Centre National de la Recherche Scientifique/Institut National des Sciences de l'Univers) through its LEFE actions, Université de Bretagne Occidentale, and IsBlue project, Interdisciplinary graduate school for the blue planet (ANR 17-EURE-0015) and co-funded by a grant from the French government under the program 'Investissements d'Avenir' embedded in France 2030. The International GEOTRACES Programme is possible in part thanks to the support from the U.S. National Science Foundation (Grant OCE-2140395) to the Scientific Committee on Oceanic Research (SCOR). C.E. was supported by Natural Environment Research Council (NERC) Independent Research Fellowship NE/M018806/1.

#### 4. 8. References

- Aparicio, F. L. and others 2015. Microbially-Mediated Fluorescent Organic Matter Transformations in the Deep Ocean. Do the Chemical Precursors Matter? *Front. Mar. Sci.* **2**.
- Bergquist, B. A., J. Wu, and E. A. Boyle. 2007. Variability in oceanic dissolved iron is dominated by the colloidal fraction. *Geochimica et Cosmochimica Acta* **71**: 2960-2974.
- Berkenheger, I., and U. Fischer. 2004. Competition for polymers among heterotrophic bacteria isolated from particles of the Equatorial Atlantic. *International Microbiology* **7**: 13-18.
- Blain, S. and others 2007. Effect of natural iron fertilization on carbon sequestration in the Southern Ocean. *Nature* **446**: 1070-1074.
- Bouchachi, N. and others 2023. Effects of Phosphorus Limitation on the Bioavailability of DOM Released by Marine Heterotrophic Prokaryotes. *Microbial Ecology* **86**: 1961-1971.
- Buchan, A., S. Collier Lauren, L. Neidle Ellen, and A. Moran Mary. 2000. Key Aromatic-Ring-Cleaving Enzyme, Protocatechuate 3,4-Dioxygenase, in the Ecologically Important *MarineRoseobacter* Lineage. *Applied and Environmental Microbiology* **66**: 4662-4672.

- Bussmann, I. 1999. Bacterial utilization of humic substances from the Arctic Ocean. *Aquatic Microbial Ecology* **19**: 37-45.
- Callahan, B. J., P. J. McMurdie, M. J. Rosen, A. W. Han, A. J. A. Johnson, and S. P. Holmes. 2016. DADA2: High-resolution sample inference from Illumina amplicon data. *Nature Methods* **13**: 581-583.
- Chen, M., and W. X. Wang. 2008. Accelerated uptake by phytoplankton of iron bound to humic acids. *Aquatic Biology* **3**: 155-166.
- Church, M. J., D. A. Hutchins, and H. W. Ducklow. 2000. Limitation of Bacterial Growth by Dissolved Organic Matter and Iron in the Southern Ocean. *Applied and Environmental Microbiology* **66**: 455-466.
- Coble, P. G. 1996. Characterization of marine and terrestrial DOM in seawater using excitation-emission matrix spectroscopy. *Marine Chemistry* **51**: 325-346.
- . 2007. Marine Optical Biogeochemistry: The Chemistry of Ocean Color. *Chemical Reviews* **107**: 402-418.
- Cottrell, M. T., and D. L. Kirchman. 2000. Natural Assemblages of Marine Proteobacteria and Members of the *Cytophaga-Flavobacter* Cluster Consuming Low- and High-Molecular-Weight Dissolved Organic Matter. *Applied and Environmental Microbiology* **66**: 1692-1697.
- Cutter, G. and others 2017. Sampling and Sample-handling Protocols for GEOTRACES Cruises. **Version 3.0**.
- Dadaglio, L., J. Dinasquet, I. Obernosterer, and F. Joux. 2018. Differential responses of bacteria to diatom-derived dissolved organic matter in the Arctic Ocean. *Aquatic Microbial Ecology* **82**: 59-72.
- Dexter, E., G. Rollwagen-Bollens, and S. M. Bollens. 2018. The trouble with stress: A flexible method for the evaluation of nonmetric multidimensional scaling. *Limnology and Oceanography: Methods* **16**: 434-443.
- Fellman, J. B., E. Hood, and R. G. M. Spencer. 2010. Fluorescence spectroscopy opens new windows into dissolved organic matter dynamics in freshwater ecosystems: A review. *Limnology and Oceanography* **55**: 2452-2462.
- Fourquez, M. and others 2020. Microbial Competition in the Subpolar Southern Ocean: An Fe–C Co-limitation Experiment. *Front. Mar. Sci.* **6**.

- Fourrier, P. and others 2022. Characterization of the vertical size distribution, composition and chemical properties of dissolved organic matter in the (ultra)oligotrophic Pacific Ocean through a multi-detection approach. *Marine Chemistry* **240**: 104068.
- Gasol, J. M., U. L. Zweifel, F. Peters, J. A. Fuhrman, and Å. Hagström. 1999. Significance of Size and Nucleic Acid Content Heterogeneity as Measured by Flow Cytometry in Natural Planktonic Bacteria. *Applied and Environmental Microbiology* **65**: 4475-4483.
- Gledhill, M., and C. M. G. van den Berg. 1994. Determination of complexation of iron(III) with natural organic complexing ligands in seawater using cathodic stripping voltammetry. *Marine Chemistry* **47**: 41-54.
- Goto, S., Y. Tada, K. Suzuki, and Y. Yamashita. 2020. Evaluation of the Production of Dissolved Organic Matter by Three Marine Bacterial Strains. *Frontiers in Microbiology* **11**.
- Hansell, D. A. 2013. Recalcitrant Dissolved Organic Carbon Fractions. *Annual Review of Marine Science* **5**: 421-445.
- Hassler, C. S., V. Schoemann, C. M. Nichols, E. C. V. Butler, and P. W. Boyd. 2011. Saccharides enhance iron bioavailability to Southern Ocean phytoplankton. *Proceedings of the National Academy of Sciences* **108**: 1076-1081.
- Heller, M. I., D. M. Gaiero, and P. L. Croot. 2013. Basin scale survey of marine humic fluorescence in the Atlantic: Relationship to iron solubility and H<sub>2</sub>O<sub>2</sub>. *Global Biogeochemical Cycles* **27**: 88-100.
- Helms, J. R., A. Stubbins, J. D. Ritchie, E. C. Minor, D. J. Kieber, and K. Mopper. 2008. Absorption spectral slopes and slope ratios as indicators of molecular weight, source, and photobleaching of chromophoric dissolved organic matter. *Limnology and Oceanography* **53**: 955-969.
- Hernandez-Magana, A. E. and others 2021. Prokaryotic diversity and activity in contrasting productivity regimes in late summer in the Kerguelen region (Southern Ocean). *Journal of Marine Systems* **221**: 103561.
- Hertkorn, N. and others 2006. Characterization of a major refractory component of marine dissolved organic matter. *Geochimica et Cosmochimica Acta* **70**: 2990-3010.
- Huguet, A., L. Vacher, S. Relexans, S. Saubusse, J. M. Froidefond, and E. Parlanti. 2009. Properties of fluorescent dissolved organic matter in the Gironde Estuary. *Organic Geochemistry* **40**: 706-719.

- Jørgensen, L., C. A. Stedmon, M. A. Granskog, and M. Middelboe. 2014. Tracing the long-term microbial production of recalcitrant fluorescent dissolved organic matter in seawater. *Geophysical Research Letters* **41**: 2481-2488.
- Jørgensen, L., C. A. Stedmon, T. Kragh, S. Markager, M. Middelboe, and M. Søndergaard. 2011. Global trends in the fluorescence characteristics and distribution of marine dissolved organic matter. *Marine Chemistry* **126**: 139-148.
- Kikuchi, T., M. Fujii, K. Terao, R. Jiwei, Y. P. Lee, and C. Yoshimura. 2017. Correlations between aromaticity of dissolved organic matter and trace metal concentrations in natural and effluent waters: A case study in the Sagami River Basin, Japan. *Science of The Total Environment* **576**: 36-45.
- Kitayama, S. and others 2009. Controls on iron distributions in the deep water column of the North Pacific Ocean: Iron(III) hydroxide solubility and marine humic-type dissolved organic matter. *Journal of Geophysical Research: Oceans* **114**.
- Kowalczyk, P., G. H. Tilstone, M. Zabłocka, R. Röttgers, and R. Thomas. 2013. Composition of dissolved organic matter along an Atlantic Meridional Transect from fluorescence spectroscopy and Parallel Factor Analysis. *Marine Chemistry* **157**: 170-184.
- Krachler, R. and others 2015. River-derived humic substances as iron chelators in seawater. *Marine Chemistry* **174**: 85-93.
- Laglera, L. M., and C. M. G. van den Berg. 2009. Evidence for geochemical control of iron by humic substances in seawater. *Limnology and Oceanography* **54**: 610-619.
- Landa, M., S. Blain, J. Harmand, S. Monchy, A. Rapaport, and I. Obernosterer. 2018. Major changes in the composition of a Southern Ocean bacterial community in response to diatom-derived dissolved organic matter. *FEMS Microbiol. Ecol.* **94**.
- Lechtenfeld, O. J., G. Kattner, R. Flerus, S. L. McCallister, P. Schmitt-Kopplin, and B. P. Koch. 2014. Molecular transformation and degradation of refractory dissolved organic matter in the Atlantic and Southern Ocean. *Geochimica et Cosmochimica Acta* **126**: 321-337.
- Lis, H., Y. Shaked, C. Kranzler, N. Keren, and F. M. M. Morel. 2015. Iron bioavailability to phytoplankton: an empirical approach. *The ISME Journal* **9**: 1003-1013.
- Liu, S. and others 2020a. Different carboxyl-rich alicyclic molecules proxy compounds select distinct bacterioplankton for oxidation of dissolved organic matter in the mesopelagic Sargasso Sea. *Limnology and Oceanography* **65**: 1532-1553.

- Liu, Y., S. Blain, O. Crispi, M. Rembauville, and I. Obernosterer. 2020b. Seasonal dynamics of prokaryotes and their associations with diatoms in the Southern Ocean as revealed by an autonomous sampler. *Environmental Microbiology* **22**: 3968-3984.
- Manna, V. and others 2020. Prokaryotic Response to Phytodetritus-Derived Organic Material in Epi- and Mesopelagic Antarctic Waters. *Frontiers in Microbiology* **11**.
- Martin, J. H. 1990. Glacial-interglacial CO<sub>2</sub> change: The Iron Hypothesis. *Paleoceanography* **5**: 1-13.
- Martin, J. H., S. E. Fitzwater, and R. M. Gordon. 1990. Iron deficiency limits phytoplankton growth in Antarctic waters. *Global Biogeochemical Cycles* **4**: 5-12.
- Martínez-Pérez, A. M., X. A. Álvarez-Salgado, J. Arístegui, and M. Nieto-Cid. 2017. Deep-ocean dissolved organic matter reactivity along the Mediterranean Sea: does size matter? *Scientific Reports* **7**: 5687.
- McMurdie, P. J., and S. Holmes. 2013. phyloseq: an R package for reproducible interactive analysis and graphics of microbiome census data. *PLoS One* **8**: e61217.
- Millero, F. J. 1998. Solubility of Fe(III) in seawater. *Earth and Planetary Science Letters* **154**: 323-329.
- Nelson, N. B., and J. M. Gauglitz. 2016. Optical Signatures of Dissolved Organic Matter Transformation in the Global Ocean. *Front. Mar. Sci.* **2**.
- Nissenbaum, A. 1979. Phosphorus in marine and non-marine humic substances. *Geochimica et Cosmochimica Acta* **43**: 1973-1978.
- Obernosterer, I., P. Catala, P. Lebaron, and N. J. West. 2011. Distinct bacterial groups contribute to carbon cycling during a naturally iron fertilized phytoplankton bloom in the Southern Ocean. *Limnology and Oceanography* **56**: 2391-2401.
- Obernosterer, I., M. Fourquez, and S. Blain. 2015. Fe and C co-limitation of heterotrophic bacteria in the naturally fertilized region off the Kerguelen Islands. *Biogeosciences* **12**: 1983-1992.
- Ohno, T. 2002. Fluorescence Inner-Filtering Correction for Determining the Humification Index of Dissolved Organic Matter. *Environmental Science & Technology* **36**: 742-746.
- Omanović, D. 2011. ElectroChemical Data Software (ECDSOFT).

- Pagano, T., A. D. Ross, J. Chiarelli, and J. E. Kenny. 2012. Multidimensional fluorescence studies of the phenolic content of dissolved organic carbon in humic substances. *Journal of Environmental Monitoring* **14**: 937-943.
- Park, Y.-H. and others 2019. Observations of the Antarctic Circumpolar Current Over the Udintsev Fracture Zone, the Narrowest Choke Point in the Southern Ocean. *Journal of Geophysical Research: Oceans* **124**: 4511-4528.
- Pernet-Coudrier, B., M. Waeles, M. Filella, F. Quentel, and R. D. Riso. 2013. Simple and simultaneous determination of glutathione, thioacetamide and refractory organic matter in natural waters by DP-CSV. *Science of The Total Environment* **463-464**: 997-1005.
- Pinhassi, J. and others 1999. Coupling between bacterioplankton species composition, population dynamics, and organic matter degradation. *Aquatic Microbial Ecology* **17**: 13-26.
- Roberts, D. W. 2020. Comparison of distance-based and model-based ordinations. *Ecology* **101**: e02908.
- Romera-Castillo, C., H. Sarmiento, X. A. Álvarez-Salgado, J. M. Gasol, and C. Marrasé. 2011. Net Production and Consumption of Fluorescent Colored Dissolved Organic Matter by Natural Bacterial Assemblages Growing on Marine Phytoplankton Exudates. *Applied and Environmental Microbiology* **77**: 7490-7498.
- Sala, M. M. and others 2020. Prokaryotic Capability to Use Organic Substrates Across the Global Tropical and Subtropical Ocean. *Frontiers in Microbiology* **11**.
- Sanz-Sáez, I. and others 2023. Top abundant deep ocean heterotrophic bacteria can be retrieved by cultivation. *ISME Communications* **3**: 92.
- Sarmiento, J. L., and J. R. Toggweiler. 1984. A new model for the role of the oceans in determining atmospheric P CO<sub>2</sub>. *Nature* **308**: 621-624.
- Shen, Y., and R. Benner. 2020. Molecular properties are a primary control on the microbial utilization of dissolved organic matter in the ocean. *Limnology and Oceanography* **65**: 1061-1071.
- Shimotori, K., Y. Omori, and T. Hama. 2009. Bacterial production of marine humic-like fluorescent dissolved organic matter and its biogeochemical importance. *Aquatic Microbial Ecology* **58**: 55-66.

- Shimotori, K., K. Watanabe, and T. Hama. 2012. Fluorescence characteristics of humic-like fluorescent dissolved organic matter produced by various taxa of marine bacteria. *Aquatic Microbial Ecology* **65**: 249-260.
- Slagter, H. A., L. M. Laglera, C. Sukekava, and L. J. A. Gerringa. 2019. Fe-Binding Organic Ligands in the Humic-Rich TransPolar Drift in the Surface Arctic Ocean Using Multiple Voltammetric Methods. *Journal of Geophysical Research: Oceans* **124**: 1491-1508.
- Stevenson, J. 1994. *Humus Chemistry: Genesis, Composition, Reactions*. John Wiley and Sons.
- Straza, T. R. A., H. W. Ducklow, A. E. Murray, and D. L. Kirchman. 2010. Abundance and single-cell activity of bacterial groups in Antarctic coastal waters. *Limnology and Oceanography* **55**: 2526-2536.
- Sukekava, C., J. Downes, H. A. Slagter, L. J. A. Gerringa, and L. M. Laglera. 2018. Determination of the contribution of humic substances to iron complexation in seawater by catalytic cathodic stripping voltammetry. *Talanta* **189**: 359-364.
- Tang, K., N. Jiao, K. Liu, Y. Zhang, and S. Li. 2012. Distribution and Functions of TonB-Dependent Transporters in Marine Bacteria and Environments: Implications for Dissolved Organic Matter Utilization. *PLOS ONE* **7**: e41204.
- Tani, H. and others 2003. Iron(III) hydroxide solubility and humic-type fluorescent organic matter in the deep water column of the Okhotsk Sea and the northwestern North Pacific Ocean. *Deep Sea Research Part I: Oceanographic Research Papers* **50**: 1063-1078.
- Watson, A. J., D. C. E. Bakker, A. J. Ridgwell, P. W. Boyd, and C. S. Law. 2000. Effect of iron supply on Southern Ocean CO<sub>2</sub> uptake and implications for glacial atmospheric CO<sub>2</sub>. *Nature* **407**: 730-733.
- Weishaar, J. L., G. R. Aiken, B. A. Bergamaschi, M. S. Fram, R. Fujii, and K. Mopper. 2003. Evaluation of Specific Ultraviolet Absorbance as an Indicator of the Chemical Composition and Reactivity of Dissolved Organic Carbon. *Environmental Science & Technology* **37**: 4702-4708.
- Whitby, H., M. Bressac, G. Sarthou, M. J. Ellwood, C. Guieu, and P. W. Boyd. 2020a. Contribution of Electroactive Humic Substances to the Iron-Binding Ligands Released During Microbial Remineralization of Sinking Particles. *Geophysical Research Letters* **47**: e2019GL086685.

- Whitby, H. and others 2020b. A call for refining the role of humic-like substances in the oceanic iron cycle. *Scientific Reports* **10**: 6144.
- Xie, R., Y. Wang, Q. Chen, W. Guo, N. Jiao, and Q. Zheng. 2020. Coupling Between Carbon and Nitrogen Metabolic Processes Mediated by Coastal Microbes in *Synechococcus*-Derived Organic Matter Addition Incubations. *Frontiers in Microbiology* **11**.
- Xu, J. and others 2022. You Exude What You Eat: How Carbon-, Nitrogen-, and Sulfur-Rich Organic Substrates Shape Microbial Community Composition and the Dissolved Organic Matter Pool. *Applied and Environmental Microbiology* **88**: e01558-01522.
- Yamashita, Y., J. Nishioka, H. Obata, and H. Ogawa. 2020. Shelf humic substances as carriers for basin-scale iron transport in the North Pacific. *Scientific Reports* **10**: 4505.
- Zhang, Z., Y. Chen, R. Wang, R. Cai, Y. Fu, and N. Jiao. 2015. The Fate of Marine Bacterial Exopolysaccharide in Natural Marine Microbial Communities. *PLOS ONE* **10**: e0142690.
- Zheng, X. and others 2022. Experimental Insight into the Enigmatic Persistence of Marine Refractory Dissolved Organic Matter. *Environmental Science & Technology* **56**: 17420-17429.
- Zigah, P. K. and others 2017. Allochthonous sources and dynamic cycling of ocean dissolved organic carbon revealed by carbon isotopes. *Geophysical Research Letters* **44**: 2407-2415.
- Zubkov, M. V., B. M. Fuchs, P. H. Burkill, and R. Amann. 2001. Comparison of Cellular and Biomass Specific Activities of Dominant Bacterioplankton Groups in Stratified Waters of the Celtic Sea. *Applied and Environmental Microbiology* **67**: 5210-5218.
- Zubkov, M. V., G. A. Tarran, and P. H. Burkill. 2006. Bacterioplankton of low and high DNA content in the suboxic waters of the Arabian Sea and the Gulf of Oman: abundance and amino acid uptake. *Aquatic Microbial Ecology* **43**: 23-32.

#### 4. 9. Supplementary materials

Location characterisation	Treatment	DOM addition collection		Prokaryote inoculum collection		'Super' time point (days)	
		Location	Depth (m)	Location	Depth (m)	Interim	End
HNLC	Surface	47.459° S, 43.276° E	~5	- 47.414°	~5	12	26
	Mesopelagic	47.307° S, 43.113° E	708	S, 43.225°			
	Deep		2537	E			
Crozet	Surface	46.12° S, 51.89° E	30	-46.12° S, 51.89° E	30	12	21

Table S1: Experimental design and subsampling time points.

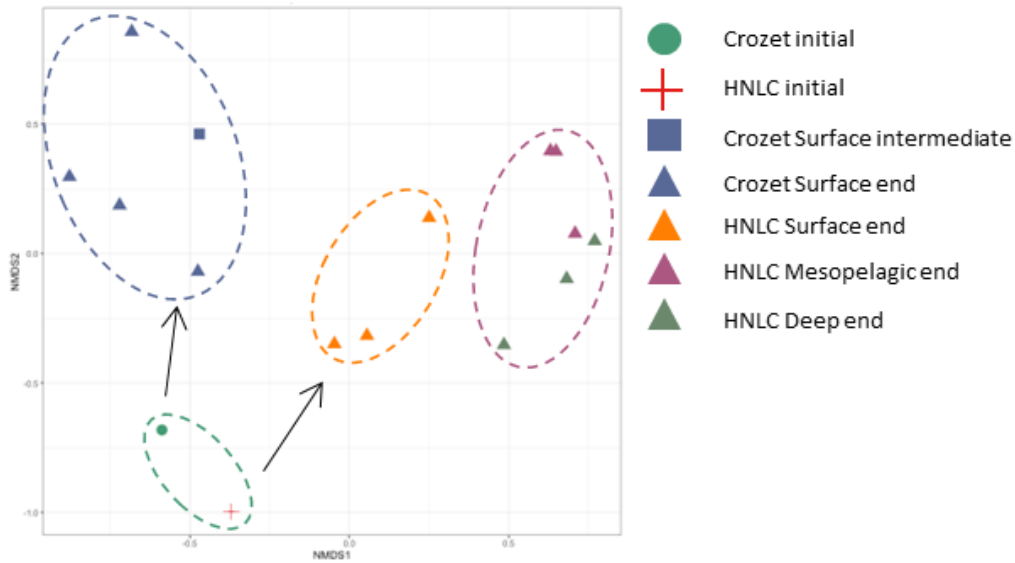


Figure S1: nMDS plot depicting the similarity of the prokaryote communities during the incubation treatments Crozet Surface (green dot), HNLC Surface (blue cross), Crozet Surface interim (blue square) and end (blue triangle), HNLC Surface end (red triangle), HNLC Mesopelagic end (pink triangle), and HNLC Deep end (green triangle) (Bray-Curtis Similarity analysis). Clusters are manually denoted. Arrows depict general 'trajectories' of the incubations from initial to interim (where collected) and end.

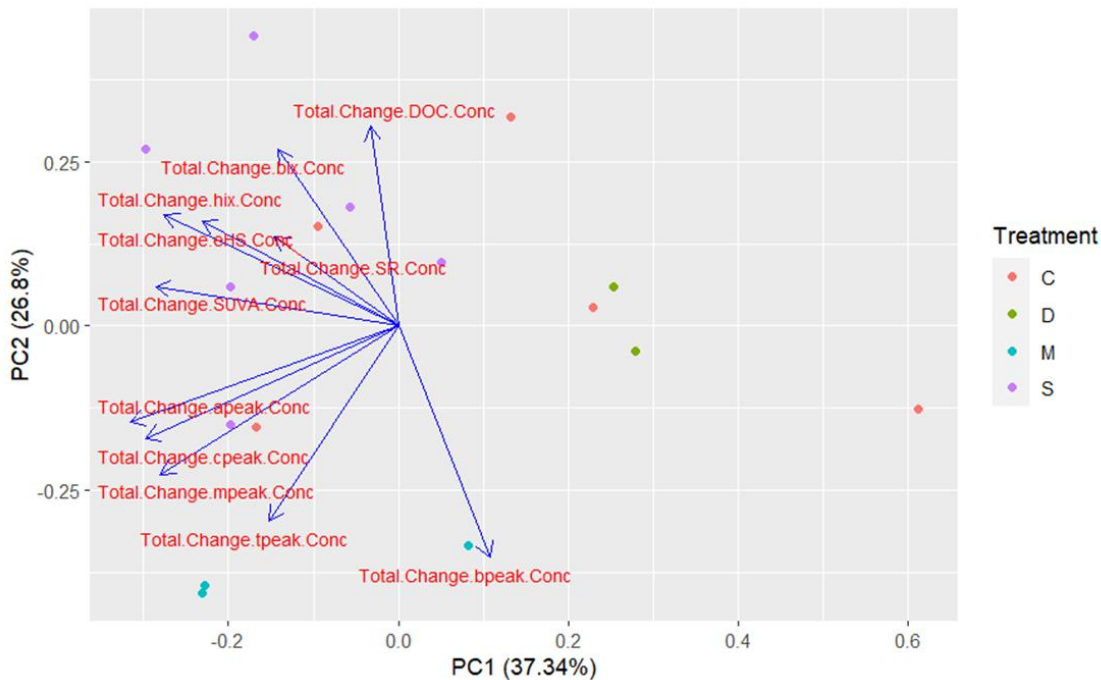
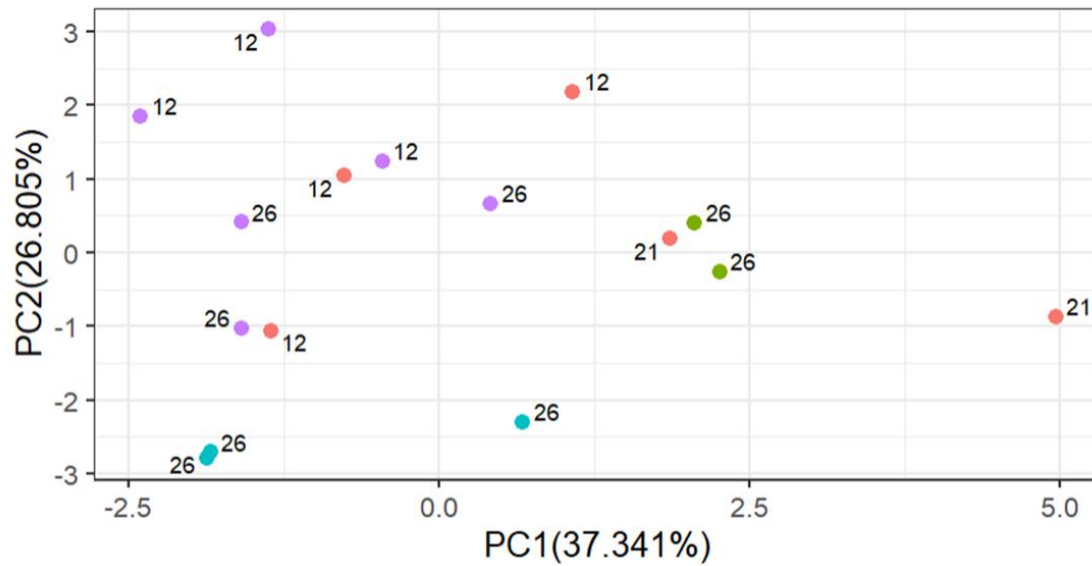


Figure S2: (a) The distribution of the treatment time points (interim and end) according to two principle components (PC1 and PC2) identified by PCA analysis. (b) PC1 and PC2 loadings plot which shows the relative orthogonal clustering of the 'change in' organic matter variables, variables which are at orthogonally clustered together are positively related to each other, variables 180° from each other are negatively related to each other, while variables 90° from each other are not related to each other. Further, the positioning of variables on the PC axes depicts the relative contribution of these variables to the variance explained by PC1 and PC2.

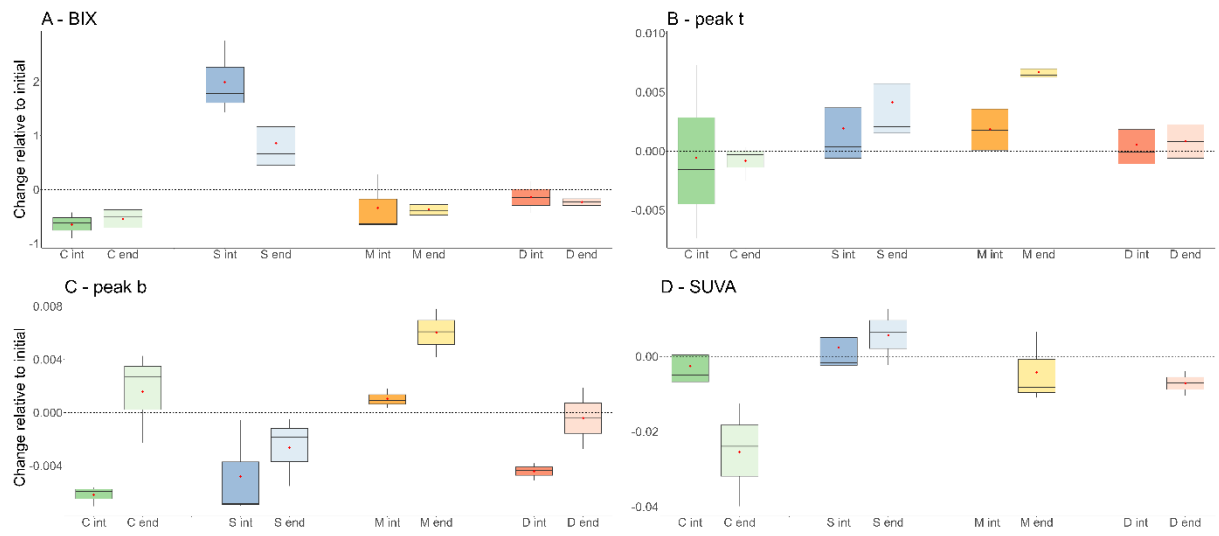


Figure S3: Changes to the DOM pool (relative to initial concentration) at the intermediate (int) and end time points of the treatments Crozet Surface (C), HNLC Surface (S), HNLC Mesopelagic (M), and HNLC Deep (D).

## Chapter 5 First evidence for net production of hydrothermal metal-binding humic substances

Millie Goddard-Dwyer<sup>1</sup>, David González-Santana<sup>2,3</sup>, Alessandro Tagliabue<sup>1</sup>, Hélène Planquette<sup>2</sup>, Erwan Roussel<sup>4</sup>, Géraldine Sarthou<sup>2</sup>, and Hannah Whitby<sup>1</sup>

1. Department of Earth, Ocean and Ecological Sciences, University of Liverpool, Liverpool, L69 3BX
2. Univ Brest, CNRS, IRD, Ifremer, LEMAR, F-29280 Plouzane, France
3. Instituto de Oceanografía y Cambio Global, IOCAG, Universidad de Las Palmas de Gran Canaria, ULPGC.
4. Centre Bretagne, Ifremer, ZI de la Pointe du Diable - CS 10070 - 29280 Plouzané.

### Author contributions:

HW performed the eHS analysis, MGD and DGS performed the modelling analysis, ER provided prokaryote abundance data, MGD performed the data analysis and wrote the manuscript, MGD, DGS, AT, HP, and HW edited the manuscript.

This chapter is prepared for submission to Geophysical research letters

### Highlights:

- First observations of eHS distribution throughout a hydrothermal plume.
- Mass balance modelling indicates a hydrothermal eHS source likely via microbial activity.
- Cu sulfide cycling appeared to exert control on eHS cycling.
- eHS have the potential to influence DFe stabilisation and transport in later stages of plume evolution.

## 5. 1. Abstract

Hydrothermal plumes are important metal sources to the deep ocean. Organic ligands such as humic substances play a role in hydrothermal metal cycling and impact transport and bioavailability. However, humic distribution and cycling during hydrothermal plume evolution remain key knowledge gaps. We quantified electroactive humic (eHS) distribution in the Trans-Atlantic Geotraverse (TAG) hydrothermal plume for the first time and established links to dissolved metals and prokaryote abundance. A mass balance model indicated hydrothermal activity was a net eHS source due to prokaryote activity and could supply 7 % of the deep ( $\geq 2000\text{m}$ ) eHS standing stock in the 500 km downstream of the vent site. Similarities between dissolved copper and eHS profiles at plume peripheries suggest that eHS were released by oxidative dissolution of Cu-sulfide particles. Although eHS did not covary with iron, it may complex a significant portion of dissolved iron 10 km from the vent. This study provides a first assessment of hydrothermal eHS production and emphasises the complex array of interactions between eHS and trace metals in hydrothermal systems.

## 5. 2. Introduction

The biogeochemical cycling of trace metals is an important control on the functioning of the Earth system. Trace metals are used as enzyme cofactors in metabolic processes (Twining and Baines 2013) and their availability has been linked with promoting or inhibiting ocean microbial activity and primary productivity, consequently controlling carbon fluxes (Azenha et al. 1995; Moore et al. 2013; Tagliabue et al. 2017). Hydrothermal vents represent an important marine source of trace metals, supplying 9 and 14 % of Fe and Cu deep ocean budgets (Sander and Koschinsky 2011) and increasing Southern Ocean carbon export by 5 – 15 % (Tagliabue et al. 2010). Although most hydrothermal Fe and Cu is rapidly lost due to aggregation and precipitation processes, a portion is stabilised for long distance transport by a variety of mechanisms including incorporation into inorganic sulfur nanoparticles, formation of colloids, and complexation by trace metal-binding organic ligands (Findlay et al. 2015; German et al. 1991; Hawkes et al. 2013; Lough et al. 2019; Roshan et al. 2020; Sander and Koschinsky 2011; Sander et al. 2007; Sarradin et al. 2009; Tagliabue et al. 2022; Yücel et al. 2011). The importance of these different stabilisation mechanisms in controlling the dispersion of trace metals in hydrothermal plumes and their long-distance transport within the ocean interior is a significant knowledge gap (Gartman and Findlay 2020).

The trace metal ligand pool is comprised of varied groups of organic molecules including siderophores, exopolymeric substances, reduced sulfur substances, and humic substances (Cotte et al. 2018; Gledhill and Buck 2012; Hassler et al. 2017; Sander et al. 2007). Of these, studies have shown that humics are an important Cu ligand and play a key role in Fe distribution in the global ocean (Laglera et al. 2019; Muller 2018; Whitby et al. 2020b; Whitby et al. 2018; Yamashita et al. 2020). Humics are an operationally defined, heterogenous group of dissolved organic matter (DOM) comprised of semi-labile organic matter such as exopolymeric substances (Hassler et al. 2011; Dulaquais et al. 2018) and recalcitrant, slowly-cycled, organic matter such as carboxylic rich alicyclic molecules (Hertkorn et al. 2006). They have the potential to play an important role in hydrothermal trace metal biogeochemistry due to their ubiquity, abundance (comprising ~50 % of the DOM pool) (Hertkorn et al. 2006; Zigah et al. 2017) and their diverse trace metal binding properties (e.g. Fe, Cu, Mn, Mo, and Hg) (Chakraborty et al. 2014; Laglera and van den Berg 2009; Oldham et al. 2017; Quentel et al. 1987; Whitby and van den Berg 2015). Humics have

the potential to impact hydrothermal trace metal cycling and dispersal via multiple mechanisms. Humics increase the solubility limit of Fe via organic complexation (Millero 1998) and can also incorporate with Fe into organic rich colloids (Batchelli et al. 2010; Guo et al. 2000), the latter of which dominates the Fe pool at hydrothermal vents (Lough et al. 2023; Tagliabue et al. 2022). Further, humics decrease Cu toxicity via organic complexation and potentially participate in Cu-sulfide aggregation processes (Sander et al. 2007; Wang et al. 2022).

Humics are actively cycled at hydrothermal vents (Sarma et al. 2018; Yang et al. 2012). However, trace metal binding humics (here measured as ‘electroactive humic substances’; eHS) have not been quantified in a hydrothermal plume to date. It is likely that eHS are actively cycled throughout the evolution of the hydrothermal plume by several processes. Firstly, by biological processes which cycle organic matter which includes vent associated biology, as organic matter produced by these communities is entrained into the plume (Bennett et al. 2011b; McCarthy et al. 2011), chemolithoautotrophic activity within the plume (Lam et al. 2004), and active microbial degradation of organic matter by chemoorganotrophs (Cathalot et al. 2021), the latter of which is known to be a source of eHS in non-hydrothermal environments (Whitby et al. 2020a). Secondly, thermal degradation is likely to degrade Cu and Fe binding eHS carbon structures and remove carboxyl groups (Hawkes et al. 2016; Hawkes et al. 2015; Rossel et al. 2017), the primary eHS Fe and Cu binding moiety (Chen et al. 2015; Lakatos et al. 1977; Town and Powell 1993). Finally, aggregation may be a significant loss term as eHS co-precipitates with metals (Duan et al. 2003; Gomez-Saez et al. 2015). These processes vary throughout the plume evolution with likely impacts on eHS distribution. For example, eHS thermal degradation and aggregation losses are likely to be highest proximal to vent site (Gomez-Saez et al. 2015; Lough et al. 2019).

The distribution and cycling of eHS within hydrothermal plumes evolution is a key knowledge gap undermining our ability to constrain hydrothermal impacts on deep ocean Fe and Cu inventories, with wider influences on global primary productivity and carbon cycling. To address this knowledge gap, we present the first observations of eHS throughout the evolution of the Trans-Atlantic Geotraverse vent (TAG) hydrothermal plume, examine the internal cycling of eHS using a mass balance model, and investigate its relationship with

dissolved Fe, dissolved Cu, and prokaryote abundance. We find evidence for a hydrothermal and/or microbial source of eHS with links to the Cu and Fe cycling at specific stages of plume evolution.

### 5. 3. Methods

#### 5. 3. 1. Study site and Sampling Strategy

Sampling occurred during HERMINE GEOTRACES GApr07 process study cruise (13<sup>th</sup> March to 28<sup>th</sup> April 2017) onboard the French Research Vessel N/O *Pourquoi Pas?* at the TAG hydrothermal site in the Central Atlantic (Figure 1a and b) using a sampling strategy described in detail in González-Santana et al. (2020). Briefly, Lowered Acoustic Doppler Current Profiler (L-ADCP) data indicated that the current was flowing in a south-southwest (SSW) direction from the vent site and suspended matter signals collected using a CTD sensor (Seabird 911plus) fitted on the trace metal-clean rosette confirmed the presence of the plume. Sampling efforts were arranged along this SSW current flow path down the axial valley; we present data from 0, 0.5, and 1 km to capture near-field plume dynamics, and at 5 and 10 km from the vent site to capture plume dynamics further afield. Sampling depths were focused within the neutrally buoyant plume, to provide a high resolution of plume dynamics.

Seawater samples were collected using a trace metal-clean polyurethane powder-coated aluminium frame rosette equipped with twenty-four 12-L, externally closing, Teflon-lined, GO-FLO bottles (General Oceanics) and attached to a Kevlar® line, following GEOTRACES guidelines. The cleaning protocols for sampling bottles and equipment also followed the

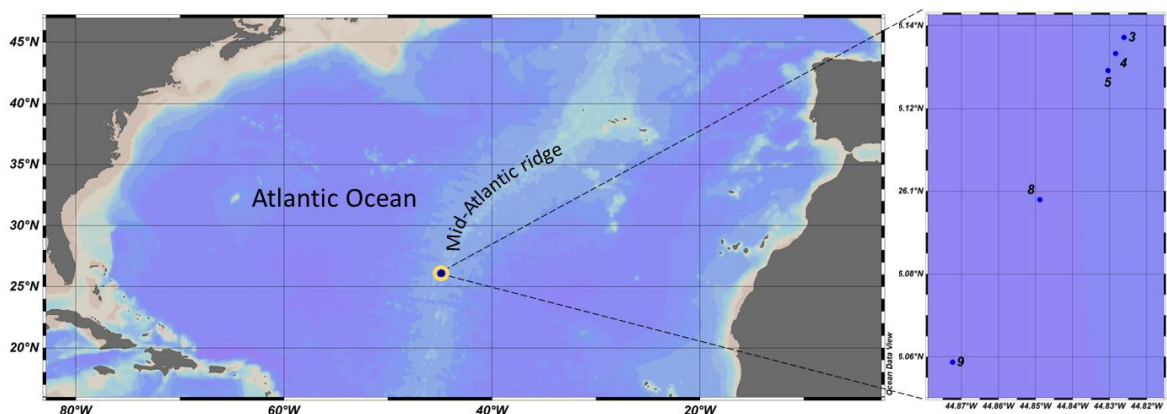


Figure 1 Location of the Trans-Atlantic Geotraverse (TAG) vent (blue dot, yellow edged) in the context of the Atlantic Ocean and Mid-Atlantic ridge with the station locations annotated.

GEOTRACES Cookbook (Cutter et al. 2017).

Upon recovery of the trace metal rosette, GO-FLO bottles were transferred to a class ISO 6 trace metal-clean sampling laboratory within a shipping container. The bottles were inverted three times to avoid settling of particles then pressurized to <8 psi with 0.2  $\mu\text{m}$  filtered  $\text{N}_2$  (Air Liquide). Samples for dissolved eHS and trace metals were collected in trace metal-clean low-density polyethylene bottles (Nalgene<sup>®</sup>) after filtration through acid-cleaned 0.45  $\mu\text{m}$  polyethersulfone filters (Supor<sup>®</sup>, 25 mm) mounted on Swinnex<sup>®</sup> filter holders, following Planquette and Sherrell (2012). Seawater samples for eHS were double bagged and stored frozen at  $-20^\circ\text{C}$  while samples for dissolved trace metals were acidified to  $\sim \text{pH } 1.7$  (2 ‰ v/v; 0.024 M) with hydrochloric acid (HCl, Ultrapure<sup>®</sup> Merck) under the class ISO 5 laminar flow hood, then double bagged and stored at ambient temperature in the dark before shore-based analysis.

### **5. 3. 2. Determination of dissolved trace metals**

Dissolved trace metals methods and dissolved Fe (DFe) data are published in González-Santana et al. (2020). Briefly, trace metal measurements were carried out within 12 months after collection on a SF-HR-ICP-MS Element XR instrument (Thermo Fisher, Bremen, Germany), at Pôle Spectrométrie Océan (IFREMER, France). The spectrometer was coupled to an ESI seaFAST-pico<sup>®</sup> introduction system and run with a method analytically similar to that of Lagerström et al. (2013).

### **5. 3. 3. Electroactive humic substances (eHS)**

There are three cathodic stripping voltammetry methods for determining eHS concentration based on their complexation with Fe, Mo, or Cu (Laglera et al. 2007; Pernet-Coudrier et al. 2013; Whitby and van den Berg 2015). The copper method was selected as these measurements do not suffer from interference from sulfides, which are abundant in the TAG plume (Konn et al. 2022; Luther and Tsamakis 1989), as the peaks appear in different places on the voltammogram. Furthermore, eHS concentrations using the copper method agree well with those obtained using the Fe method (Abualhaija et al. 2015; Whitby et al. 2020b).

The concentration of eHS was measured using cathodic stripping voltammetry of eHS with copper (Whitby and van den Berg, 2015) using  $\mu$ -Autolab III potentiostat (Ecochemie, Netherlands) connected to a 663 VA stand (Metrohm). The working electrode was a hanging

mercury drop electrode (HMDE), the reference electrode was Ag/AgCl with a 3 M KCl salt bridge and the auxiliary electrode was glassy carbon.

Samples (10 mL) were measured in a glass voltammetric cell with (N-(2-hydroxyethyl)piperazine-N'; -2-propanesulfonic acid in 1M NH<sub>4</sub>; 100 µL addition to 10 mL seawater buffered the pH to 8.05) and 30 nM added copper. Samples were purged with N<sub>2</sub> for 300 s prior to analysis. Voltammetric parameters include a deposition potential of +0.05 V, followed by a 1s jump to -0.2 V prior to scanning by differential pulse. Scans were background subtracted by subtraction of a 1 s scan and the height of the humic peak was used to quantify the eHS peak. Standard additions of International Humic Substances Society (IHSS) Suwannee River Humic Acid standard (II 2S101H) were used to quantify eHS concentrations within samples.

The concentration of eHS was converted into minimum and maximum metal-binding equivalent values for the metals where data is available. The minimum and maximum Fe binding capacity (nM) of a given eHS concentration ([eHS]; µg/L) can be calculated using minimum (0.0146 nmol Fe per µg eHS) and maximum (0.032 nmol Fe per µg eHS) eHS Fe binding capacities reported in the literature according to Equation 1 (Laglera and van den Berg 2009; Sukekava et al. 2018). The minimum and maximum Cu binding capacity (nM) of a given eHS concentration ([eHS]; µg/L) can be calculated using minimum (0.016 nmol Cu per µg eHS) and maximum (0.018 nmol Cu per µg eHS) eHS Cu binding capacities reported in the literature according to Equation 1 (Abualhaija et al. 2015; Whitby and van den Berg 2015). The envelope in this study does not include the standard deviation of the eHS measurement, however it is appreciated that the range of actual metal binding capacity of the eHS in the samples could be wider.

$$\text{Equation 1: } eHS \text{ Trace metal binding capacity} = [eHS] \times \text{trace metal binding capacity}$$

#### 5. 3. 4. Mass Balance model

The design of the model is described by González-Santana et al. (2020). Briefly, 3 boxes, with depths calculated from where the water column was exclusively within the non-buoyant plume density isopycnals ranges ( $\sigma = 27.880$  and  $27.833 \text{ kg m}^{-3}$ ), excluding at the vent site,

where the bottom of the box was set to the vent depth (3605 m). Note, pronounced density instabilities were apparent at the vent site, therefore the plume depths were calculated from predominantly within  $\sigma = 27.880$  and  $27.833 \text{ kg m}^{-3}$ . Box lengths were ascribed from the sampled stations at 0, 1, 5, and 10 km from the vent site, and width fixed to 1 m are considered. Data were included if DFe concentration of the sample exceeded background concentration (where data was available;  $0.7 \text{ nmol kg}^{-1}$  GA03w data) as in González-Santana et al. (2020).

As in Gonzalez-Santana et al. (2020), dissolved Mn (DMn) was employed as a conservative tracer to calculate the rate of plume dilution, due to the low and stable particulate Mn concentration across the plume (implying that the interaction between dissolved and particulate Mn pools were negligible at this site, Field and Sherrell 2000). Calculations assume the deep ocean is in steady state with background concentrations considered constant. The calculations also assume that samples were collected from the core axis of a single non-buoyant plume moving at constant  $1.5 \text{ cm s}^{-1}$  (based on ADCP data; Mastin 2020) in the direction of the sampling transect. Finally, we assume linear interpolation between adjacent data points accurately represents the non-buoyant plume. To calculate any excess in concentration that could not be explained by modelled dilution processes, a non-hydrothermally influenced background concentration was calculated from literature values. For DMn and DFe, background concentrations of  $0.15 \text{ nmol kg}^{-1}$  and  $0.7 \text{ nmol kg}^{-1}$  were used based on GA03w data as in (González-Santana et al. 2020). For [eHS], a background concentration of  $30.2 \pm 15.03 \text{ } \mu\text{g/L}$  was calculated from open ocean Atlantic  $\geq 2000\text{m}$  seawater data reported in the literature (Dulaquais et al. 2018; Whitby et al. 2020b). For bacterioplankton abundance,  $0.215 \times 10^5 \text{ cells/mL}$  was calculated from bathypelagic north and south Atlantic gyre data (Ruiz-González et al. 2020).

Stations at 0, 1, 5, and 10 km from the vent site were renamed Stations (n) 1 – 4, respectively. The resultant 3 boxes with ( $1 \leq |n| \leq 3$ ) have their depths calculated from the non-buoyant plume height (m,  $h_{|n-1}$  and  $h_{|n}$ ) and use lengths ( $l_{|n|}$ ; m) based on the distance between stations, and constant widths ( $w = 1 \text{ m}$ ). For each box, trace element ( $[I_{|n|}]$ ;  $\text{mol m}^{-3}$ ; Equation 2) eHS ( $[I_{|n|}]$ ;  $\text{g m}^{-3}$ ; Equation 3), and bacterial abundance ( $[I_{|n|}]$ ;  $\text{cells m}^{-3}$ ; Equation 3) average concentration was calculated.  $[I_{|n|}]$  at station  $n$  was calculated from the height of the integrated area ( $h_{|n|}$ ; m) at the top ( $NBP_{top}$ ) and base ( $NBP_{bottom}$ ) of

the non-buoyant plume, the potential density ( $\rho$ ;  $\text{kg m}^{-3}$ ; in the case of trace elements), the measured concentration ( $[i_{nh}]$ ; trace element ( $\text{nmol kg}^{-1}$ ), eHS ( $\text{g L}^{-1}$ ), and bacterial abundance ( $\text{cells L}^{-1}$ ), and the background concentration ( $[i_{bg}]$ ;  $\text{mol m}^{-3}$ ,  $\text{g m}^{-3}$ , or  $\text{cells m}^{-3}$ ). A total inventory ( $Q_{i|n|}$ ;  $\text{mol}$ ; Equation 4) was then calculated.

$$\text{Equation 2: } [I_{|n|}] = \frac{1}{h_{|n|}} \int_{NBP_{bottom}}^{NBP_{top}} \rho \cdot ([i_{nh}] - [i_{bg}]) dh_{|n|}$$

$$\text{Equation 3: } [I_{|n|}] = \frac{1}{h_{|n|}} \int_{NBP_{bottom}}^{NBP_{top}} 1000 \cdot ([i_{nh}] - [i_{bg}]) dh_{|n|}$$

$$\text{Equation 4: } Q_{i|n|} = [I_{|n|}] \cdot \frac{h_{|n-1|} + h_{|n|}}{2} \cdot l_{|n|} \cdot w$$

Flux terms were calculated in the model by Equations 8 – 10. Firstly, for each species  $i$  a horizontal hydrothermal advective flux ( $Flux_{i|n|}$ ;  $\text{mol s}^{-1}$ ) in the plume's direction of travel, both in ( $Flux_{i|n-1|}$ ) and out ( $Flux_{i|n|}$ ) of each box based on the concentration on the upstream side of the box ( $[i_{nh}]$ ;  $\text{mol m}^{-3}$ ), the horizontal velocity ( $\vec{u}$ ;  $\text{m s}^{-1}$ ), and the area of the upstream of the box ( $h_{|n-1|} \cdot w$ ;  $\text{m}^2$ ) (Equation 5). Conservative mixing of chemical species was calculated under the assumption that any change to DMn concentration was a result of dilution processes ( $Dil_{DMn|n|}$ ;  $\text{mol s}^{-1}$ ; Equation 6). Using this dilution term, the expected concentration of eHS based only on dilution processes can be calculated ( $Dil_{i|n|}$ ;  $\text{mol s}^{-1}$ ; Equation 7).

$$\text{Equation 5: } Flux_{i|n|} = [I_{|n|}] \cdot \vec{u} \cdot h_{|n-1|} \cdot w$$

$$\text{Equation 6: } Dil_{DMn|n|} = Flux_{DMn|n-1|} - Flux_{DMn|n|}$$

$$\text{Equation 7: } Dil_{i|n|} = Dil_{DMn|n|} \cdot \frac{Q_{i|n|}}{Q_{DMn|n|}}$$

Finally, a net production or removal can be derived ( $Flux_{i|n|} > 0$  and  $Flux_{i|n|} < 0$ , respectively), defined as a residual tendency term that could not be accounted for by conservative mixing alone (Equation 8). A total flux term can then be calculated that balances the system (Equation 9).

$$\text{Equation 8: } P_{i|n|} = Dil_{i|n|} - (Flux_{i|n-1|} - Flux_{i|n|})$$

$$\text{Equation 9: } \frac{d(i)}{dt_{|n|}} = \frac{1}{v_{|n|}} \cdot Dil_{i|n|} - (Flux_{i|n-1|} - Flux_{i|n|})$$

### 5. 3. 5. Statistics

All statistical tests were performed in R (version 4.3.1) stats package. Normality was assessed using Shapiro-Wilks test.

## 5. 4. Results and Discussion

### 5. 4. 1. Hydrothermal eHS cycling through the evolution of the TAG plume

The average eHS concentration [eHS] at 0, 1, 5, and 10 km from the vent within the plume was significantly greater than average non-hydrothermally influenced background Atlantic [eHS] derived from the literature (Figure 2) (Dulaquais et al. 2018; Whitby et al. 2020b)(Wilcoxon,  $p < 0.05$ ). Therefore, hydrothermal activity can be considered to be a significant source of eHS, consistent with previous observations of active humic and DOC production in hydrothermal systems (Bennett et al. 2008; Bennett et al. 2011a; Bennett et al. 2011b; Yang et al. 2012). However, there were variations in eHS behaviour throughout plume evolution (Figure 2) which will be discussed in the following sections.

Firstly, at the vent site itself, the plume was enriched in eHS relative to Atlantic deepwater (Figure 2 and 3a). Thermal degradation in the high temperature vent fluid would likely remove eHS ligand properties by decarboxylation of the eHS (Chen et al. 2015; Hawkes et al. 2016; Rossel et al. 2017; Town and Powell 1993), and therefore decrease [eHS]. Therefore, it is likely that the majority of eHS at the vent site were instead produced by vent associated communities surrounding the vents and was subsequently entrained into the plume. This is supported by our observation that average [eHS] in the water column surrounding the plume was not significantly different to average [eHS] within the plume (Figure 2) (Wilcoxon,  $p > 0.05$ ) and by previous observations for humics (Yang et al. 2017) and dissolved organic carbon (Bennett et al. 2011b; Lang et al. 2006).

Another interesting characteristic of eHS behaviour at the vent site was that it was more variable inside the plume compared to overlying waters (Figure 2; F-test,  $p < 0.05$ ) and this variability decreased with distance from the vent site (Figure 2; F-test,  $p < 0.05$ , 0 km vs. 10 km). This could result from short term variable mixing ratios and/or aggregation and co-precipitation of DOM and metals as high temperature, metal rich vent fluid mixed with surrounding organic matter rich seawater (Duan et al. 2003; Gomez-Saez et al. 2015; González-Santana et al. 2020; Lough et al. 2019). Future studies should measure eHS within

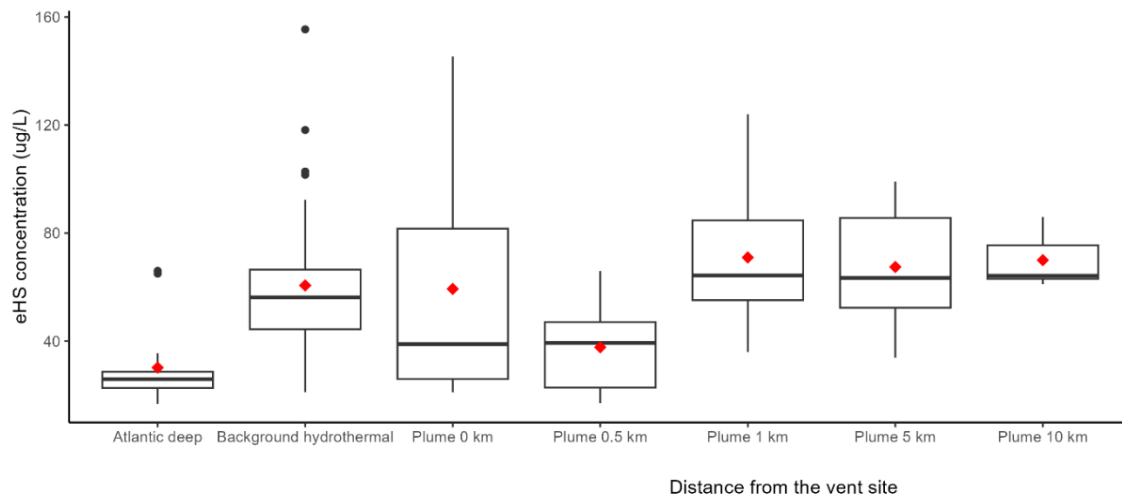


Figure 2 eHS concentration in  $\geq 2000\text{m}$  Atlantic deep water (literature values, Dulaquais et al. 2018; Whitby et al. 2020b),  $\geq 2000\text{m}$  background hydrothermal (seawater outside the plume isopycnals), and hydrothermal plume water (within the plume isopycnals) at each station with increasing distance from the vent. Solid black line = median average, red diamond = mean average, grey box = interquartile range, whiskers = minimum and maximum, filled dots = outliers.

both the dissolved and particulate phases to establish the role of aggregation in hydrothermal eHS cycling.

eHS internal cycling within the plume was assessed using a mass balance exercise to estimate the presence of any sources or sinks above simple plume dilution. Our approach has been used previously for calculating potential Fe dynamics from the same dataset (González-Santana et al. 2020). Our calculations indicate net production of eHS occurred throughout plume evolution (Figure 3a). However, as previously stated, we also find that while the average eHS concentration within the plume was significantly different to typical Atlantic deep water, it was not significantly different to the water column surrounding the plume (Figure 2). Therefore, this result supports a hydrothermal eHS source, but could not demonstrate that the eHS source was within this plume. Nonetheless, we found that eHS average concentration and production rate generally covaried with that of bacterioplankton cells within the plume (Figure 3b). This co-variance is consistent with microbial activity being a source of eHS in this plume, and agrees with high microbial chemolithoautotrophic

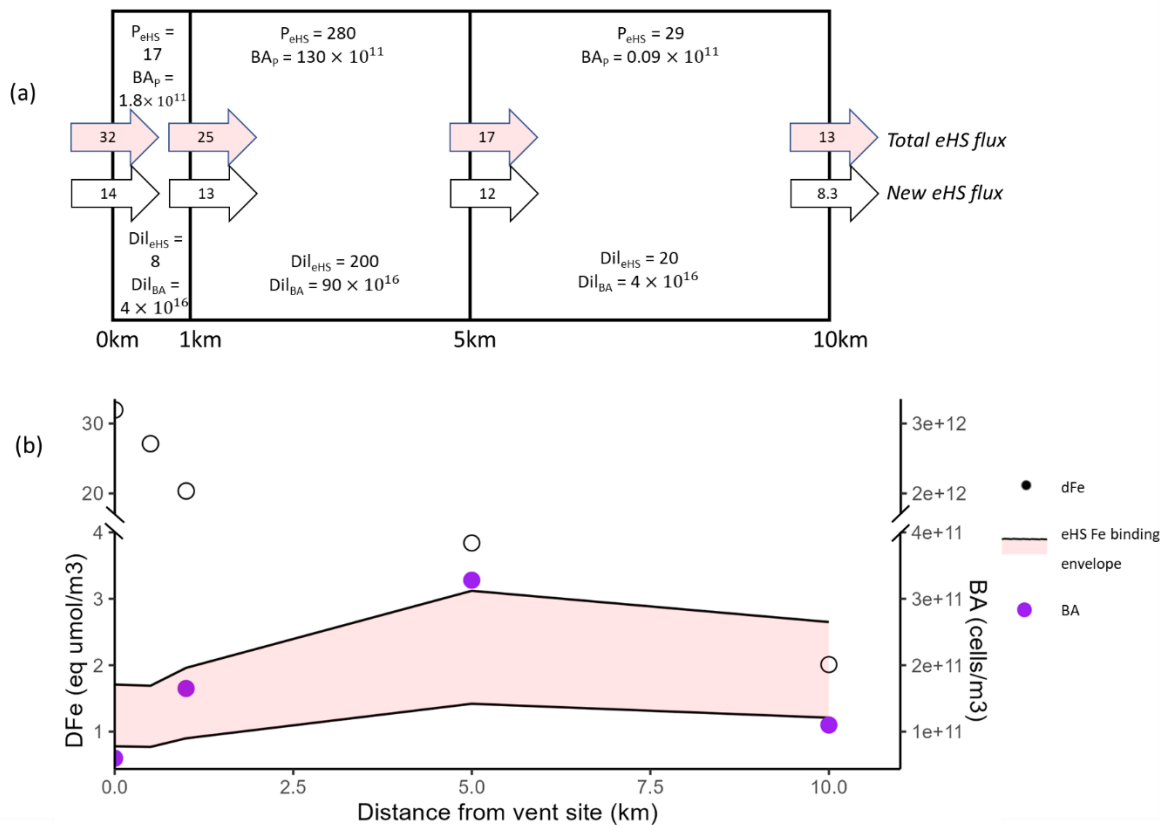


Figure 3 Modelling results for electroactive humic substances (eHS), bacterioplankton abundance (BA), and dissolved iron (DFe) throughout the TAG plume. (a) Modelled eHS fluxes and rates where arrows depict total plume eHS (pink) and ‘new’ eHS (no fill; calculated from plume eHS – background eHS) fluxes (units = kg/d),  $P_{eHS}$  and  $P_{BA}$  refers to the net eHS or BA tendency that was attributed to hydrothermal processes (units = mg/m<sup>3</sup>/d and cells/m<sup>3</sup>/d)  $Dil_{eHS}$  and  $Dil_{BA}$  refers to the estimated net eHS or prokaryote abundance (BA) tendency that was attributed to dilution processes (units = mg/m<sup>3</sup>/d and cells/m<sup>3</sup>/d). (b) Plume inventory (normalised to plume volume) of DFe (open black circle), prokaryote abundance (purple dot) and eHS expressed as minimum and maximum Fe binding capacity (black line) or eHS Fe binding envelope (pale red shaded).

abundance in other hydrothermal plumes (Lesniewski et al. 2012) and high microbial chemoorganotrophic activity previously reported in the TAG plume (Cathalot et al. 2021; Reed et al. 2015).

In later stages of plume evolution (10 km from the vent site), our calculations indicate a net flux of  $8 \text{ kg d}^{-1}$  hydrothermally produced eHS was transported further afield (Figure 3a). Under the assumption that these values are temporally consistent, the amount of eHS produced by the TAG hydrothermal plume is estimated to replenish the deep ( $\geq 2000\text{m}$ ) eHS standing stock of the study region every  $\sim 4$  months and comprise approximately 7 % of the deep ( $\geq 2000\text{m}$ ) eHS standing stock in the 500 km downstream of the vent site. Indeed, the imprint of hydrothermal activity on eHS was evident throughout deep waters across the transect where eHS was enriched in the water column surrounding the plume compared to background Atlantic deep-water concentrations (Dulaquais et al. 2018; Whitby et al. 2020b) (Wilcoxon,  $p < 0.05$ ) (Figure 2). This is consistent with previous evidence that hydrothermal plumes have important roles in marine carbon cycling (Luther III 2021; Yamashita et al. 2023; Yamashita and Tanoue 2008). Hydrothermally produced eHS may act as a carbon source for bathypelagic microbial communities or as deep ocean carbon store, dependent on the bioavailability of these eHS. Although hydrothermal humics have been shown to be recalcitrant (Rossel et al. 2015), the bioavailability of hydrothermal eHS is uncertain as the eHS pool is highly heterogenous with a range of bioavailability (Hassler et al. 2011). Future work should determine the bioavailability of these humics to establish the role of putative microbial hydrothermal eHS production in contributing to marine carbon storage.

#### **5. 4. 2. Interactions between eHS and dissolved Fe and Cu cycling**

eHS Fe binding capacity was estimated using reported values for terrestrial humic standards (see Methods). Between 0 and 1 km from the vent site eHS had the capacity to bind to 2 – 10 % of DFe present (Figure 3b and 4). This is within the range reported for bulk Fe binding ligands from other studies at TAG (4 %, Bennett et al. 2008) and other vent sites (7.5 %, Hawkes et al. 2013) at similar stages of plume evolution. Large discrepancy between DFe and eHS Fe binding capacity together with lack of correlation between [eHS] and [DFe] (Figure 3b and 4) suggests that the majority of DFe was associated with other Fe binding ligands (such as siderophores or inorganic sulfides) and/or other forms of Fe (such as colloidal oxyhydroxides and pyrite), consistent with previous observations (Gartman et al. 2014; Lough et al. 2019; Yücel et al. 2011).

Beyond 5 km from the vent site, DFe concentrations stabilised and at 10 km from the vent site DFe concentrations and calculated inventory was within the eHS Fe binding envelope

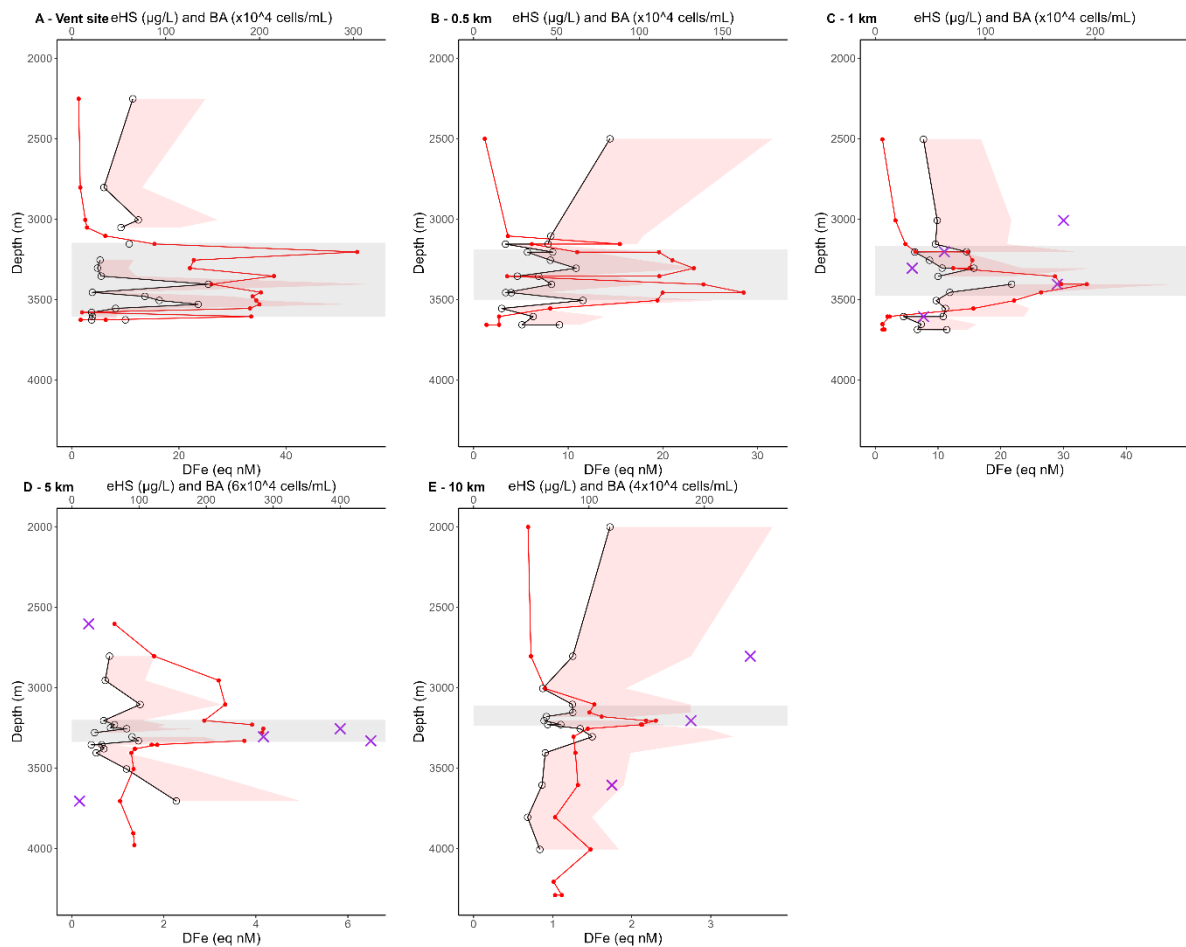


Figure 4 Profiles of electroactive humic substances (eHS) concentration (solid black line, unfilled dots;  $\mu\text{g/L}$ ), eHS Fe binding envelope (shaded pink region;  $\text{nM Fe eq}$ ), and DFe concentration (red line, filled dots;  $\text{nM Fe}$ ) at the TAG vent site and 0.5, 1, 5 and 10km away from the vent in a SSW direction. Grey shaded region indicates the depths of the plume as indicated by the plume density isopycnals. Purple crosses denote prokaryote abundance (BA).

(Figure 3b and 4). eHS have the potential to influence hydrothermal DFe dispersal here by both increasing the solubility limit of plume-derived soluble phase Fe and incorporation of Fe into organic rich colloids (Batchelli et al. 2010; Dulaquais et al. 2023; Gledhill and van den Berg 1994; Guo et al. 2000). Considering that the majority of hydrothermal DFe is present as colloids (Lough et al. 2019; Tagliabue et al. 2022), direct observations of size partitioning of eHS and better constraints on the colloidal associations between eHS and Fe within a hydrothermal plume are needed to understand the role of eHS in hydrothermal Fe binding.

We consistently observed eHS peaks on the peripheries of the plume which broadly matched peaks in DCu (Figure 5) and coincided with transitions from low to high oxygen concentration (Figure S1). This DCu behaviour has been noted by previous studies and attributed to oxidative dissolution of Cu from Cu sulfide particles which formed earlier in the plume under acidic, anoxic conditions (Sarradin et al. 2009). Humics are known to adsorb onto the surface of Cu sulfide minerals that are abundant in the TAG plume (chalcopyrite) (Findlay et al. 2015; Wang et al. 2022). Therefore, we suggest that eHS peaks on the peripheries of the plume are driven by release of eHS adsorbed onto the surface of Cu sulfides as they dissolve. Direct observations of size partitioning of eHS are required to confirm this hypothesis.

Similarities between eHS and DCu profiles at the peripheries of the plume are consistent with Sander and Koschinsky's (2011) suggestion that organic ligands stabilise DCu released by oxidative dissolution. However, DCu was almost always in excess of the estimated eHS Cu binding capacity (Figure 5), which implies other Cu chemical speciation forms were also important such as chalcopyrite (Findlay et al. 2015) and sulfide ligands (Cotte et al. 2018). This is also consistent with the high affinity of sulfides for Cu compared to that of eHS (Luther and Tsamakis 1989).

#### **5. 4. 3. Limitations**

The eHS trace metal binding envelopes used here assume that marine (and hydrothermal) eHS have trace metal binding capacity within the range of terrestrial humics. This may not be the case considering the structural differences between the terrestrial and marine humics (Harvey et al. 1983; Pocklington 1977; Stuermer and Harvey 1974) which occurs because, although some of precursors molecules and processes involved in humic production in terrestrial versus marine systems humics are thought to be shared (Hatcher et al. 1981), there are also thought to be differences (Muller 2018). Notably, lignin is a major precursor in terrestrial environments (Stevenson 1994) while biomolecules such as carotenoid pigments are thought to be major precursors in marine environments (Arakawa et al. 2017). The structure of hydrothermal humics could be more similar to marine humics than to terrestrial humics, due to lack of lignin precursors. However molecular changes during thermal alteration, such as decarboxylation (Hawkes et al. 2016), hydrolysis (Marzbali et al. 2021), and polymerisation (Zhu et al. 2021) may further change the trace metal binding capacity of

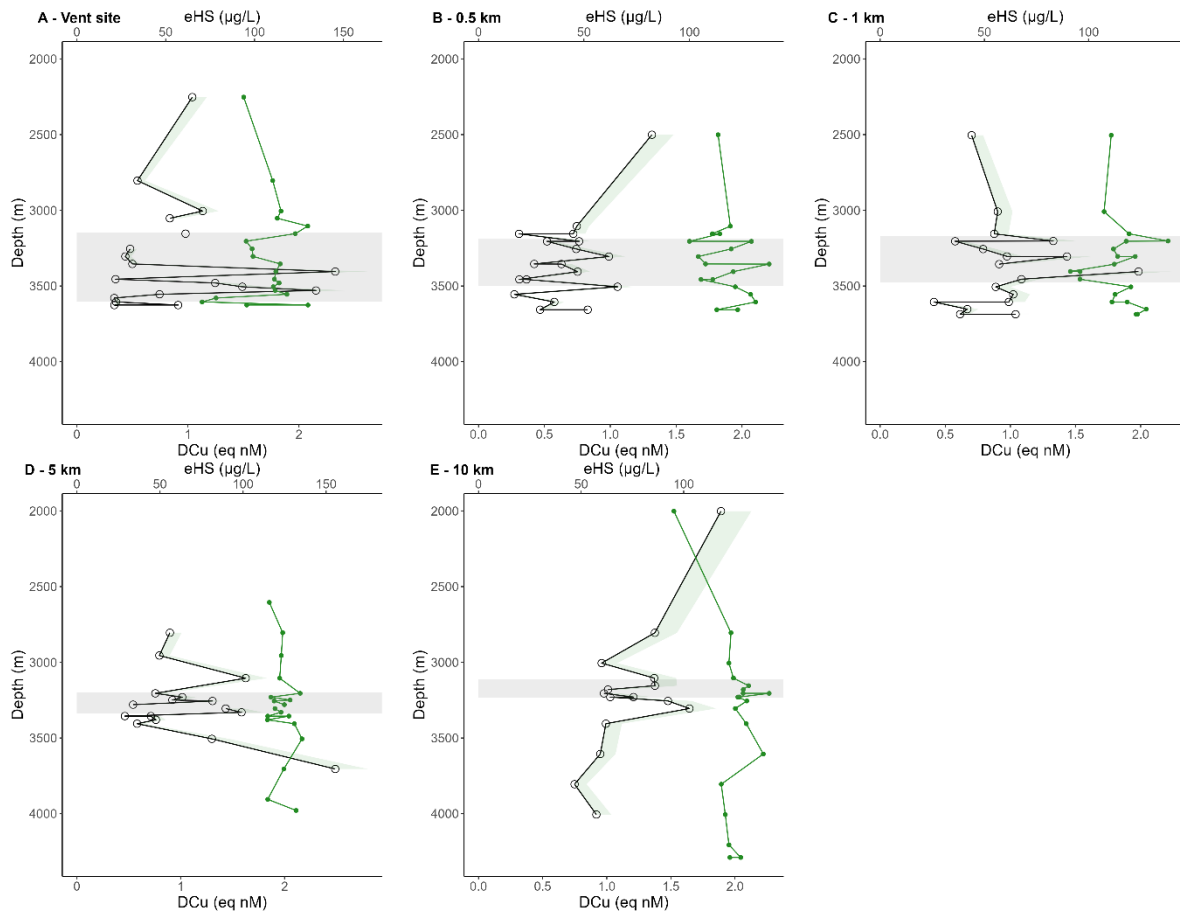


Figure 5 Profiles of electroactive humic substances (eHS) concentration (solid black line, unfilled dots;  $\mu\text{g/L}$ ), eHS Cu binding envelope (shaded green region;  $\text{nM Cu eq}$ ), and DCu concentration (red line, filled dots;  $\text{nM Fe}$ ) at the TAG vent site and 0.5, 1, 5 and 10km away from the vent in a SSW direction. Grey shaded region indicates the depths of the plume as indicated by the plume density isopycnals.

hydrothermal humics relative to that of marine humics. Cu and Fe compete for the same eHS binding sites, and eHS trace metal binding is determined to an extent by the relative concentrations and binding strengths of competing trace metals and ligands (Abualhaija et al. 2015; Kinniburgh et al. 1999; Lu and Allen 2002). However, the eHS Fe binding strength is greater than that of Cu (Laglera and van den Berg 2009; Whitby and van den Berg 2015), and eHS is likely to be outcompeted by sulfides for Cu in the sulfur rich TAG plume (*see previous section*). Nonetheless, direct observations of Fe and Cu binding capacity, arrangement, and strength of in-situ eHS is a key knowledge gap inhibiting our understanding of the role of eHS in trace metal cycling. Considering that the paucity of direct observations of eHS trace metal

binding capacity this study represents a valuable first step in resolving the understanding of eHS in the supply of trace metals to the ocean from hydrothermal vents.

## 5. 5. Conclusion

This study finds evidence of a net hydrothermal source of eHS throughout the plume evolution. Increases in eHS concentration followed increased prokaryote abundance, suggesting a role of hydrothermal microbial activity in eHS production. Data suggests Cu sulfide cycling may play a key role in controlling plume eHS cycling, however discrepancies between eHS Cu binding capacity and DCu concentration imply that eHS play a minor role in Cu stabilisation. Convergence between eHS Fe binding capacity and DFe concentration at 10 km from the vent site suggests that eHS may play a larger role in DFe stabilisation here and consequently transport DFe further afield. Size partitioning of the eHS pool and direct observation of trace metals bound to eHS remains an important knowledge gap to understand the role of eHS in plume trace metal cycling and subsequent delivery to the deep ocean.

## 5. 6. References

- Abualhija, M. M., H. Whitby, and C. M. G. van den Berg. 2015. Competition between copper and iron for humic ligands in estuarine waters. *Marine Chemistry* **172**: 46-56.
- Arakawa, N., A. J. Aluwihare, A. J. Simpson, R. Soong, B. M. Stephens, and D. Lane-Coplen. 2017. Carotenoids are the likely precursor of a significant fraction of marine dissolved organic matter. *Science Advances* **3**: e1602976.
- Azenha, M., M. T. Vasconcelos, and J. P. S. Cabral. 1995. Organic ligands reduce copper toxicity in *Pseudomonas syringae*. *Environmental Toxicology and Chemistry* **14**: 369-373.
- Batchelli, S., F. L. L. Muller, K.-C. Chang, and C.-L. Lee. 2010. Evidence for Strong but Dynamic Iron–Humic Colloidal Associations in Humic-Rich Coastal Waters. *Environmental Science & Technology* **44**: 8485-8490.
- Bennett, S. A., E. P. Achterberg, D. P. Connelly, P. J. Statham, G. R. Fones, and C. R. German. 2008. The distribution and stabilisation of dissolved Fe in deep-sea hydrothermal plumes. *Earth and Planetary Science Letters* **270**: 157-167.

- Bennett, S. A., R. L. Hansman, A. L. Sessions, K.-i. Nakamura, and K. J. Edwards. 2011a. Tracing iron-fueled microbial carbon production within the hydrothermal plume at the Loihi seamount. *Geochimica et Cosmochimica Acta* **75**: 5526-5539.
- Bennett, S. A. and others 2011b. Dissolved and particulate organic carbon in hydrothermal plumes from the East Pacific Rise, 9°50'N. *Deep Sea Research Part I: Oceanographic Research Papers* **58**: 922-931.
- Cathalot, C. and others 2021. Hydrothermal plumes as hotspots for deep-ocean heterotrophic microbial biomass production. *Nature Communications* **12**: 6861.
- Chakraborty, P., K. M. Yao, K. Chennuri, K. Vudamala, and P. V. Raghunadh Babu. 2014. Interactions of mercury with different molecular weight fractions of humic substances in aquatic systems. *Environmental Earth Sciences* **72**: 931-939.
- Chen, W., N. Habibul, X.-Y. Liu, G.-P. Sheng, and H.-Q. Yu. 2015. FTIR and Synchronous Fluorescence Heterospectral Two-Dimensional Correlation Analyses on the Binding Characteristics of Copper onto Dissolved Organic Matter. *Environmental Science & Technology* **49**: 2052-2058.
- Cotte, L. and others 2018. On the nature of dissolved copper ligands in the early buoyant plume of hydrothermal vents. *Environmental Chemistry* **15**: 58-73.
- Cutter, G. and others 2017. Sampling and Sample-handling Protocols for GEOTRACES Cruises. **Version 3.0**.
- Duan, J., N. J. D. Graham, and F. Wilson. 2003. Coagulation of humic acid by ferric chloride in saline (marine) water conditions. *Water Science and Technology* **47**: 41-48.
- Dulaquais, G. and others 2023. The role of humic-type ligands in the bioavailability and stabilization of dissolved iron in the Western Tropical South Pacific Ocean. *Front. Mar. Sci.* **10**.
- Dulaquais, G., M. Waeles, L. J. A. Gerringa, R. Middag, M. J. A. Rijkenberg, and R. Riso. 2018. The Biogeochemistry of Electroactive Humic Substances and Its Connection to Iron Chemistry in the North East Atlantic and the Western Mediterranean Sea. *Journal of Geophysical Research: Oceans* **123**: 5481-5499.
- Field, M. P., and R. M. Sherrell. 2000. Dissolved and particulate Fe in a hydrothermal plume at 9°45'N, East Pacific Rise:: Slow Fe (II) oxidation kinetics in Pacific plumes. *Geochimica et Cosmochimica Acta* **64**: 619-628.

- Findlay, A. J., A. Gartman, T. J. Shaw, and G. W. Luther. 2015. Trace metal concentration and partitioning in the first 1.5m of hydrothermal vent plumes along the Mid-Atlantic Ridge: TAG, Snakepit, and Rainbow. *Chemical Geology* **412**: 117-131.
- Gartman, A., and A. J. Findlay. 2020. Impacts of hydrothermal plume processes on oceanic metal cycles and transport. *Nature Geoscience* **13**: 396-402.
- Gartman, A., A. J. Findlay, and G. W. Luther. 2014. Nanoparticulate pyrite and other nanoparticles are a widespread component of hydrothermal vent black smoker emissions. *Chemical Geology* **366**: 32-41.
- German, C. R., A. C. Campbell, and J. M. Edmond. 1991. Hydrothermal scavenging at the Mid-Atlantic Ridge: Modification of trace element dissolved fluxes. *Earth and Planetary Science Letters* **107**: 101-114.
- Gledhill, M., and K. Buck. 2012. The Organic Complexation of Iron in the Marine Environment: A Review. *Frontiers in Microbiology* **3**.
- Gledhill, M., and C. M. G. van den Berg. 1994. Determination of complexation of iron(III) with natural organic complexing ligands in seawater using cathodic stripping voltammetry. *Marine Chemistry* **47**: 41-54.
- Gomez-Saez, G. V., T. Riedel, J. Niggemann, T. Pichler, T. Dittmar, and S. I. Bühring. 2015. Interaction between iron and dissolved organic matter in a marine shallow hydrothermal system off Dominica Island (Lesser Antilles). *Marine Chemistry* **177**: 677-686.
- González-Santana, D. and others 2020. Processes Driving Iron and Manganese Dispersal From the TAG Hydrothermal Plume (Mid-Atlantic Ridge): Results From a GEOTRACES Process Study. *Front. Mar. Sci.* **7**.
- Guo, L., P. H. Santschi, and K. W. Warnken. 2000. Trace metal composition of colloidal organic material in marine environments. *Marine Chemistry* **70**: 257-275.
- Harvey, G. R., D. A. Boran, L. A. Chesal, and J. M. Tokar. 1983. The structure of marine fulvic and humic acids. *Marine Chemistry* **12**: 119-132.
- Hassler, C. S., V. Schoemann, C. M. Nichols, E. C. V. Butler, and P. W. Boyd. 2011. Saccharides enhance iron bioavailability to Southern Ocean phytoplankton. *Proceedings of the National Academy of Sciences* **108**: 1076-1081.

- Hassler, C. S., C. M. G. van den Berg, and P. W. Boyd. 2017. Toward a Regional Classification to Provide a More Inclusive Examination of the Ocean Biogeochemistry of Iron-Binding Ligands. *Front. Mar. Sci.* **4**.
- Hatcher, P. G., G. E. Maciel, and L. W. Dennis. 1981. Aliphatic structure of humic acids; a clue to their origin. *Organic Geochemistry* **3**: 43-48.
- Hawkes, J. A., D. P. Connelly, M. Gledhill, and E. P. Achterberg. 2013. The stabilisation and transportation of dissolved iron from high temperature hydrothermal vent systems. *Earth and Planetary Science Letters* **375**: 280-290.
- Hawkes, J. A., C. T. Hansen, T. Goldhammer, W. Bach, and T. Dittmar. 2016. Molecular alteration of marine dissolved organic matter under experimental hydrothermal conditions. *Geochimica et Cosmochimica Acta* **175**: 68-85.
- Hawkes, J. A. and others 2015. Efficient removal of recalcitrant deep-ocean dissolved organic matter during hydrothermal circulation. *Nature Geoscience* **8**: 856-860.
- Hertkorn, N. and others 2006. Characterization of a major refractory component of marine dissolved organic matter. *Geochimica et Cosmochimica Acta* **70**: 2990-3010.
- Kinniburgh, D. G., W. H. van Riemsdijk, L. K. Koopal, M. Borkovec, M. F. Benedetti, and M. J. Avena. 1999. Ion binding to natural organic matter: competition, heterogeneity, stoichiometry and thermodynamic consistency. *Colloids and Surfaces A: Physicochemical and Engineering Aspects* **151**: 147-166.
- Konn, C. and others 2022. Extending the dataset of fluid geochemistry of the Menez Gwen, Lucky Strike, Rainbow, TAG and Snake Pit hydrothermal vent fields: Investigation of temporal stability and organic contribution. *Deep Sea Research Part I: Oceanographic Research Papers* **179**: 103630.
- Lagerström, M. E., M. P. Field, M. Séguret, L. Fischer, S. Hann, and R. M. Sherrell. 2013. Automated on-line flow-injection ICP-MS determination of trace metals (Mn, Fe, Co, Ni, Cu and Zn) in open ocean seawater: Application to the GEOTRACES program. *Marine Chemistry* **155**: 71-80.
- Laglera, L. M., G. Battaglia, and C. M. G. van den Berg. 2007. Determination of humic substances in natural waters by cathodic stripping voltammetry of their complexes with iron. *Analytica Chimica Acta* **599**: 58-66.
- Laglera, L. M., C. Sukekava, H. A. Slagter, J. Downes, A. Aparicio-Gonzalez, and L. J. A. Gerringa. 2019. First Quantification of the Controlling Role of Humic Substances in

- the Transport of Iron Across the Surface of the Arctic Ocean. *Environmental Science & Technology* **53**: 13136-13145.
- Laglera, L. M., and C. M. G. van den Berg. 2009. Evidence for geochemical control of iron by humic substances in seawater. *Limnology and Oceanography* **54**: 610-619.
- Lakatos, B., T. Tibai, and J. Meisel. 1977. EPR spectra of humic acids and their metal complexes. *Geoderma* **19**: 319-338.
- Lam, P., J. P. Cowen, and R. D. Jones. 2004. Autotrophic ammonia oxidation in a deep-sea hydrothermal plume. *FEMS Microbiol. Ecol.* **47**: 191-206.
- Lang, S. Q., D. A. Butterfield, M. D. Lilley, H. Paul Johnson, and J. I. Hedges. 2006. Dissolved organic carbon in ridge-axis and ridge-flank hydrothermal systems. *Geochimica et Cosmochimica Acta* **70**: 3830-3842.
- Lesniewski, R. A., S. Jain, K. Anantharaman, P. D. Schloss, and G. J. Dick. 2012. The metatranscriptome of a deep-sea hydrothermal plume is dominated by water column methanotrophs and lithotrophs. *The ISME Journal* **6**: 2257-2268.
- Lough, A. J. M. and others 2019. Soluble iron conservation and colloidal iron dynamics in a hydrothermal plume. *Chemical Geology* **511**: 225-237.
- Lough, A. J. M. and others 2023. Tracing differences in iron supply to the Mid-Atlantic Ridge valley between hydrothermal vent sites: implications for the addition of iron to the deep ocean. *Biogeosciences* **20**: 405-420.
- Lu, Y., and H. E. Allen. 2002. Characterization of copper complexation with natural dissolved organic matter (DOM)—link to acidic moieties of DOM and competition by Ca and Mg. *Water Research* **36**: 5083-5101.
- Luther, G. W., and E. Tsamakis. 1989. Concentration and form of dissolved sulfide in the oxic water column of the ocean. *Marine Chemistry* **27**: 165-177.
- Luther III, G. W. 2021. Hydrothermal Vents Are a Source of Old Refractory Organic Carbon to the Deep Ocean. *Geophysical Research Letters* **48**: e2021GL094869.
- Marzbali, M. H. and others 2021. Wet organic waste treatment via hydrothermal processing: A critical review. *Chemosphere* **279**: 130557.
- Mastin, M. 2020. Étude Tridimensionnelle du Panache Hydrothermal du site TAG : Identification des Processus D'export et de Vieillessement du Panache. . Université de Bretagne Occidentale.

- McCarthy, M. D., S. R. Beaupré, B. D. Walker, I. Voparil, T. P. Guilderson, and E. R. M. Druffel. 2011. Chemosynthetic origin of  $^{14}\text{C}$ -depleted dissolved organic matter in a ridge-flank hydrothermal system. *Nature Geoscience* **4**: 32-36.
- Millero, F. J. 1998. Solubility of Fe(III) in seawater. *Earth and Planetary Science Letters* **154**: 323-329.
- Moore, C. M. and others 2013. Processes and patterns of oceanic nutrient limitation. *Nature Geoscience* **6**: 701-710.
- Muller, F. L. L. 2018. Exploring the Potential Role of Terrestrially Derived Humic Substances in the Marine Biogeochemistry of Iron. *Frontiers in Earth Science* **6**.
- Oldham, V. E., A. Mucci, B. M. Tebo, and G. W. Luther. 2017. Soluble Mn(III)-L complexes are abundant in oxygenated waters and stabilized by humic ligands. *Geochimica et Cosmochimica Acta* **199**: 238-246.
- Pernet-Coudrier, B., M. Waeles, M. Filella, F. Quentel, and R. D. Riso. 2013. Simple and simultaneous determination of glutathione, thioacetamide and refractory organic matter in natural waters by DP-CSV. *Science of The Total Environment* **463-464**: 997-1005.
- Pocklington, R. 1977. Chemical processes and interactions involving marine organic matter. *Marine Chemistry* **5**: 477-496.
- Quentel, F., C. Madec, and J. Courtot-coupez. 1987. Determination of Humic Substances in Seawater by Electrochemistry (Mechanisms). *Analytical Letters* **20**: 47-62.
- Reed, D. C. and others 2015. Predicting the response of the deep-ocean microbiome to geochemical perturbations by hydrothermal vents. *The ISME Journal* **9**: 1857-1869.
- Roshan, S., T. DeVries, J. Wu, S. John, and T. Weber. 2020. Reversible scavenging traps hydrothermal iron in the deep ocean. *Earth and Planetary Science Letters* **542**: 116297.
- Rossel, P. E., A. Stubbins, P. F. Hach, and T. Dittmar. 2015. Bioavailability and molecular composition of dissolved organic matter from a diffuse hydrothermal system. *Marine Chemistry* **177**: 257-266.
- Rossel, P. E., A. Stubbins, T. Rebling, A. Koschinsky, J. A. Hawkes, and T. Dittmar. 2017. Thermally altered marine dissolved organic matter in hydrothermal fluids. *Organic Geochemistry* **110**: 73-86.

- Ruiz-González, C. and others 2020. Major imprint of surface plankton on deep ocean prokaryotic structure and activity. *Molecular Ecology* **29**: 1820-1838.
- Sander, S. G., and A. Koschinsky. 2011. Metal flux from hydrothermal vents increased by organic complexation. *Nature Geoscience* **4**: 145-150.
- Sander, S. G., A. Koschinsky, G. Massoth, M. Stott, and K. A. Hunter. 2007. Organic complexation of copper in deep-sea hydrothermal vent systems. *Environmental Chemistry* **4**: 81-89.
- Sarma, N. S. and others 2018. Hydrothermal Alteration Promotes Humic Acid Formation in Sediments: A Case Study of the Central Indian Ocean Basin. *Journal of Geophysical Research: Oceans* **123**: 110-130.
- Sarradin, P.-M., M. Waeles, S. Bernagout, C. Le Gall, J. Sarrazin, and R. Riso. 2009. Speciation of dissolved copper within an active hydrothermal edifice on the Lucky Strike vent field (MAR, 37°N). *Science of The Total Environment* **407**: 869-878.
- Stevenson, J. 1994. *Humus Chemistry: Genesis, Composition, Reactions*. John Wiley and Sons.
- Stuermer, D. H., and G. R. Harvey. 1974. Humic substances from seawater. *Nature* **250**: 480-481.
- Sukekava, C., J. Downes, H. A. Slagter, L. J. A. Gerringa, and L. M. Laglera. 2018. Determination of the contribution of humic substances to iron complexation in seawater by catalytic cathodic stripping voltammetry. *Talanta* **189**: 359-364.
- Tagliabue, A. and others 2010. Hydrothermal contribution to the oceanic dissolved iron inventory. *Nature Geoscience* **3**: 252-256.
- Tagliabue, A., A. R. Bowie, P. W. Boyd, K. N. Buck, K. S. Johnson, and M. A. Saito. 2017. The integral role of iron in ocean biogeochemistry. *Nature* **543**: 51-59.
- Tagliabue, A. and others 2022. Mechanisms Driving the Dispersal of Hydrothermal Iron From the Northern Mid Atlantic Ridge. *Geophysical Research Letters* **49**: e2022GL100615.
- Town, R. M., and H. K. J. Powell. 1993. Ion-selective electrode potentiometric studies on the complexation of copper(II) by solid-derived humic and fulvic acids. *Analytica Chimica Acta* **279**: 221-233.
- Twining, B. S., and S. B. Baines. 2013. The Trace Metal Composition of Marine Phytoplankton. *Annual Review of Marine Science* **5**: 191-215.

- Wang, J. and others 2022. Inhibition of humic acid on copper pollution caused by chalcopyrite biooxidation. *Science of The Total Environment* **851**: 158200.
- Whitby, H., M. Bressac, G. Sarthou, M. J. Ellwood, C. Guieu, and P. W. Boyd. 2020a. Contribution of Electroactive Humic Substances to the Iron-Binding Ligands Released During Microbial Remineralization of Sinking Particles. *Geophysical Research Letters* **47**: e2019GL086685.
- Whitby, H. and others 2020b. A call for refining the role of humic-like substances in the oceanic iron cycle. *Scientific Reports* **10**: 6144.
- Whitby, H., A. M. Posacka, M. T. Maldonado, and C. M. G. van den Berg. 2018. Copper-binding ligands in the NE Pacific. *Marine Chemistry* **204**: 36-48.
- Whitby, H., and C. M. G. van den Berg. 2015. Evidence for copper-binding humic substances in seawater. *Marine Chemistry* **173**: 282-290.
- Yamashita, Y., Y. Mori, and H. Ogawa. 2023. Hydrothermal-derived black carbon as a source of recalcitrant dissolved organic carbon in the ocean. *Science Advances* **9**: eade3807.
- Yamashita, Y., J. Nishioka, H. Obata, and H. Ogawa. 2020. Shelf humic substances as carriers for basin-scale iron transport in the North Pacific. *Scientific Reports* **10**: 4505.
- Yamashita, Y., and E. Tanoue. 2008. Production of bio-refractory fluorescent dissolved organic matter in the ocean interior. *Nature Geoscience* **1**: 579-582.
- Yang, L., H. Hong, W. Guo, C.-T. A. Chen, P.-I. Pan, and C.-C. Feng. 2012. Absorption and fluorescence of dissolved organic matter in submarine hydrothermal vents off NE Taiwan. *Marine Chemistry* **128-129**: 64-71.
- Yang, L., W.-E. Zhuang, C.-T. A. Chen, B.-J. Wang, and F.-W. Kuo. 2017. Unveiling the transformation and bioavailability of dissolved organic matter in contrasting hydrothermal vents using fluorescence EEM-PARAFAC. *Water Research* **111**: 195-203.
- Yücel, M., A. Gartman, C. S. Chan, and G. W. Luther. 2011. Hydrothermal vents as a kinetically stable source of iron-sulphide-bearing nanoparticles to the ocean. *Nature Geoscience* **4**: 367-371.
- Zhu, N., J. Gao, D. Liang, Y. Zhu, B. Li, and H. Jin. 2021. Thermal pretreatment enhances the degradation and humification of lignocellulose by stimulating thermophilic bacteria during dairy manure composting. *Bioresource Technology* **319**: 124149.

Zigah, P. K. and others 2017. Allochthonous sources and dynamic cycling of ocean dissolved organic carbon revealed by carbon isotopes. *Geophysical Research Letters* **44**: 2407-2415.

## 5. 7. Supplementary materials

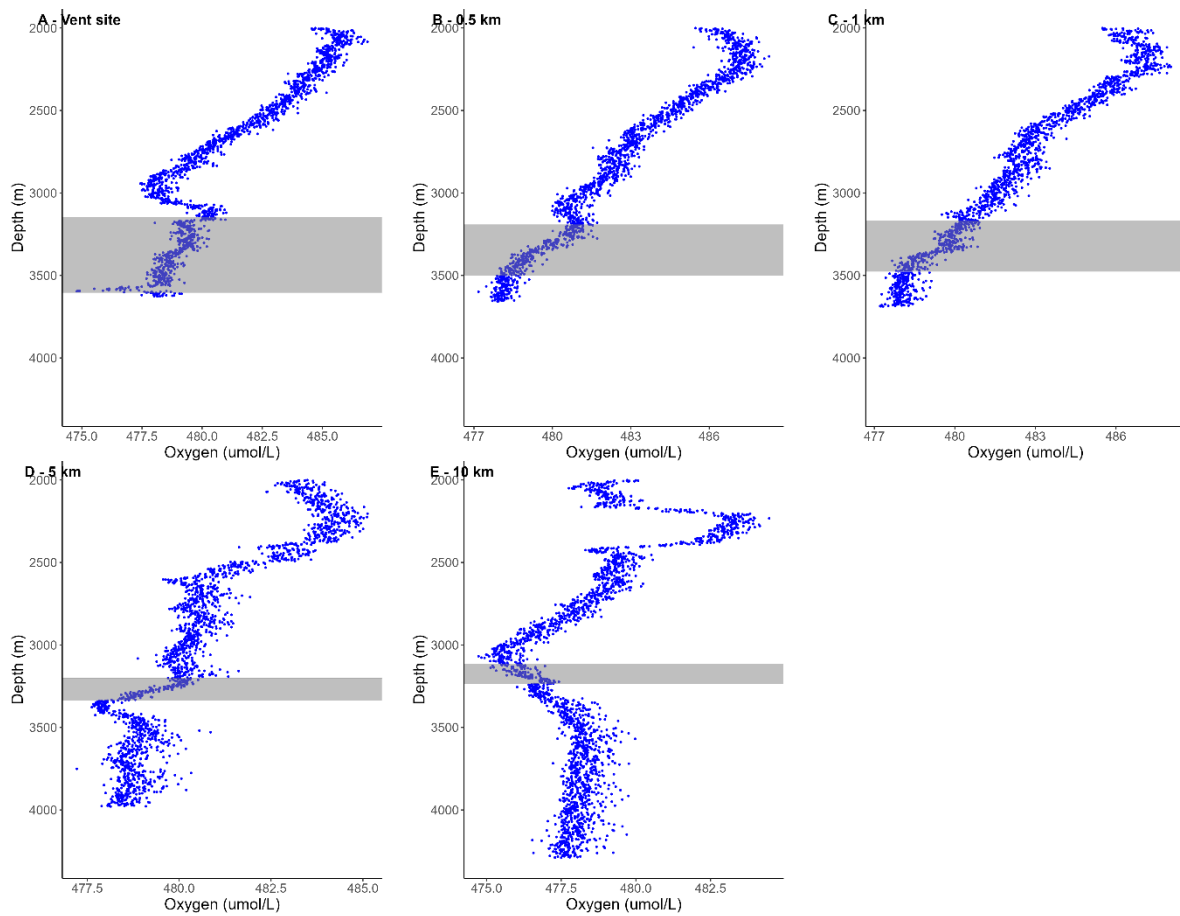


Figure S1 Oxygen concentration  $\geq 2000\text{m}$  at the TAG vent and each station moving SSW of the vent site. Grey shaded region indicates the depths of the plume as indicated by the plume density isopycnals.

## Chapter 6 Conclusions and perspectives

### 6. 1. Thesis findings

The overarching aim of this thesis was to advance our understanding of humic cycling in seawater and to consider the role of humic substances in trace metal and DOC cycling.

In Chapter 1, an overview of marine carbon and trace metal biogeochemistry and the role of ligands was presented. This included a review of existing data on the distribution of electroactive humics, processes known to be involved in humic cycling, and the known or predicted effect of these on humic ligand distribution. Chapter 2 described the principles of the two methods used to quantify the humic pool throughout the thesis: predominantly voltammetry (eHS) and, to a lesser degree, absorbance/fluorescence spectrophotometry (CDOM/FDOM humics), and the methodological considerations and limitations of each. The potential insights that can be gained from coupled voltammetric and spectrophotometric measurements were outlined, which were then implemented in Chapters 3 and 4.

Chapter 1 also identified several key knowledge gaps:

- Firstly, that there was a lack of eHS data from the Southern Ocean.
- Secondly, the drivers and controls on microbial eHS cycling were largely untested.
- Finally, the role of hydrothermal systems in eHS cycling was highly ambiguous with conflicting results from previous studies.

Addressing these knowledge gaps formed the basis of Chapters 3-5 respectively.

Chapter 3 presented the variable microbial cycling of eHS and its interaction with iron in the Southwest Indian region of the Southern Ocean. The study area selected was predominantly iron limited low productivity with diverse point sources of trace metals (in particular Kerguelen and the Heard and McDonald islands) which stimulated primary productivity and microbial activity. Resultant natural gradients in phytoplankton community composition, zooplankton grazing, and remineralisation provided a natural laboratory to untangle the biological processes involved in eHS cycling. We found that different microbial processes controlled eHS distribution under different contexts. eHS was closely linked to specific phytoplankton taxa in the phytoplankton bloom associated with Kerguelen and the Heard and McDonald islands, while at Crozet eHS was closely linked to grazing. Further,

mesopelagic microbial remineralisation was an important factor in eHS production, but only off-plateaus and in the eastward part of the transect where dissolved iron concentration was lower. The relationship between eHS and dissolved iron was equally diverse across the transect and suggested that eHS could potentially play a role in local dissolved iron supply, but less so on a regional scale.

In Chapter 4, the objective was to take a closer, mechanistic look at the role of dissolved organic matter bioavailability in mediating prokaryote cycling of electroactive and fluorescent humics in this region. For this, surface prokaryotes from two biogeochemically contrasting regions of the Southern Ocean were incubated with dissolved organic matter from surface, mesopelagic and deep waters, representing a range of dissolved organic matter (DOM) bioavailability across horizontal (productivity) and vertical gradients. We found that eHS production was promoted by increasing DOM bioavailability, while in contrast, Coloured DOM/Fluorescent DOM (CDOM/FDOM) humics production was promoted by decreasing DOM bioavailability. This suggests that prokaryote eHS production is carbon limited while CDOM/FDOM humics production is limited by the supply of refractory precursors. Both humic pools were degraded under the lowest bioavailability DOM (deep water) treatment. This implies a decrease in humic iron complexation capacity which could limit iron resupplied from remineralisation. Further, eHS and humic cycling was paired with changes to the bacterial community composition. These findings inform some results from Chapter 3. Firstly, surface prokaryotes eHS cycling could not be detected using observational data in Chapter 3. Results from Chapter 4 indicate that surface prokaryotes were involved in eHS cycling. Secondly, in Chapter 3 the role of microbial remineralisation (primarily conducted by prokaryotes), was variable across horizontal and vertical parts of the transect. Results from incubations performed in Chapter 4 reveal the important role of DOM bioavailability in mediating eHS cycling and suggest DOM bioavailability was likely a contributory factor to our observations in Chapter 3.

One finding from Chapter 3 was a putative role of a hydrothermal source in eHS production. Building on this and considering the contradictory information in the literature on humic cycling in hydrothermal systems, the role of a hydrothermal plume in eHS cycling was explicitly investigated in Chapter 5. This study provides a first assessment of eHS cycling within and surrounding a hydrothermal plume (Trans-Atlantic Geotraverse vent, Mid-Atlantic

Ridge) and determined links with the distribution of dissolved concentrations of iron and copper. A mass balance model indicated that hydrothermal activity was a net eHS source which was likely due to prokaryote activity. However, we could not directly establish that eHS production occurred inside the plume. Both eHS and dissolved copper profiles exhibited peaks at the edges of the plume coincident to transitions in oxygen which suggests that eHS were released by oxidative dissolution of copper sulfide particles here. eHS was not closely related to dissolved iron, however, similar dissolved iron concentrations compared to eHS iron binding capacity suggest that eHS have the potential to complex a significant portion of dissolved iron at 10 km from the vent. This study emphasizes the complex array of interactions between eHS and trace metals in hydrothermal systems and provides a foundation for the further work that will be required to fully establish the role of eHS in hydrothermal trace metal biogeochemistry.

## **6. 2. Future research directions**

### **6. 2. 1. Climate change related impacts on the eHS pool**

Southern Ocean phytoplankton production is expected to increase in the future (Leung et al. 2015) in response to changes in environmental drivers such as increases in iron availability, stratification, light intensity, and temperature (Henley et al. 2020). Therefore, considering the close links between phytoplankton and eHS production as revealed by Chapters 3 and 4, it is likely that overall Southern Ocean eHS concentration will also increase in response to climate change. Further, in Chapter 3, I hypothesised a positive feedback between phytoplankton eHS production and dissolved iron availability which could act to sustain phytoplankton blooms. Under this hypothesis, phytoplankton eHS production could act as a mechanism by which phytoplankton productivity exhibits non-proportional responses to future increases in Southern Ocean iron supply. This could exacerbate existing predictions and/or trends in changes in phytoplankton productivity. Future studies could address this research question by performing in-situ iron addition incubations in iron-limited regions of the Southern Ocean and quantifying resultant changes in primary production and eHS production.

Future increases in Southern Ocean primary production are also expected to be accompanied by changes in phytoplankton community composition, although studies give opposing predictions of the exact changes in species composition (Henley et al. 2020).

Chapter 3 highlighted the sensitivity of eHS to phytoplankton community composition, so it is likely that this will have a significant, but unconstrained impact on eHS. Due to the lack of knowledge on species specific eHS production, it is difficult to accurately predict the response of eHS to this driver using existing data. Culture based experiments to determine the production rate of eHS by different Southern Ocean phytoplankton species would address this knowledge gap.

Changes to Southern Ocean primary production and community composition will also influence carbon export by the biological carbon pump (Henley et al. 2020). Due to uncertain climate change related changes to phytoplankton community composition, the changes to the magnitude and strength of Southern Ocean carbon export are unresolved but likely significant (Henson et al. 2022). As such, impacts on mesopelagic microbial remineralisation, which is sustained by the supply of organic matter by the biological carbon pump, remains poorly understood. In Chapters 3 and 4, mesopelagic microbial remineralisation was identified an important source of eHS in some parts of the Southern Ocean. Climate change driven changes to the amount of eHS supplied by mesopelagic remineralisation may have a knock-on effect on mesopelagic iron stabilisation, which plays a key role in replenishing deep iron inventories. This is potentially an important mechanism which could impact future Southern Ocean iron cycling, with possible negative feedbacks on primary production and carbon storage.

Finally, future warming and increasing acidity of the Southern Ocean has direct consequences for humic trace metal binding. Increasing temperature increases reaction rates, this will likely have a positive impact on humic metal binding (Fang et al. 2015). On the other hand, ocean acidification (reduction in pH) could reduce humic metal binding via increased competition between protons and metal ions for ligand binding sites (Gledhill et al. 2015; Tufano and Raymond, 1981). Although, note that increased pH will also likely increase highly bioavailable inorganic iron concentration (Gledhill et al. 2015), so the resultant impact on dissolved iron concentration could be zero. Therefore, the direct effects of pH and temperature on humic metal binding chemistry have the potential to interact (either additively, synergistically, or antagonistically) with any predicted future changes to the size of the eHS pool , with unresolved but potentially large impacts on Southern Ocean iron cycling.

### **6. 2. 2. The role of eHS in carbon cycling**

In Chapters 3, 4, and 5, the potential for eHS to act as a carbon store and as a diagnostic of carbon storage was discussed. One significant mechanism is via the microbial carbon pump. In Chapter 5, eHS distribution implied that hydrothermal vents were hotspots of the microbial carbon pump. In Chapter 3, variation in mesopelagic eHS production by microbial remineralisation suggested that the microbial carbon pump was variable, particularly in response to phytoplankton blooms. As highlighted by a recent review (Henley et al. 2020), this is a relatively underexplored facet of Southern Ocean carbon storage, potentially due to the relatively recent advent of the microbial carbon pump paradigm (Jiao et al. 2010). However, it deserves more investigation particularly within the context of climate change impacts on the biogeochemistry of the region. Finally, in Chapter 4, observed degradation of eHS under low bioavailability DOM treatment (Deep) suggests that the role of eHS in carbon cycling (carbon store vs carbon source) can have significant implications for dissolved iron stabilisation by eHS. Understanding these mechanisms is important to understand the biogeochemical role of eHS. Future studies could address these knowledge gaps by adopting a process study and/or incubations based approach to eHS studies. These studies should aim to obtain rate-based measurements of microbial eHS cycling and develop mechanistic understanding of the interaction between eHS and carbon cycling.

### **6. 2. 3. The identity, chemical properties, and trace metal binding capacity of trace metal binding humics**

The composition of the eHS pool was investigated in this thesis by comparing electroactive and CDOM/FDOM humics. Generally, eHS was less closely related to Coble peak c than peak m which implied that electroactive properties were less closely related to the molecular characteristics traditionally associated with trace metal binding (described in more detail in Chapters 2 and 3). This is an interesting conundrum and suggests that the chemical properties responsible for eHS detection by voltammetry require further investigation. eHS molecular characteristics are unresolved but are ultimately a major driver of eHS cycling and their biogeochemical role in trace metal binding and carbon cycling. In particular, the molecular structure of humics in the Southern Ocean represents a significant knowledge gap due to lack of data. Future studies should determine the molecular structure and properties responsible for the electroactive properties of marine eHS using high resolution mass spectroscopy in tandem with voltammetry across biogeochemical regions of the ocean, in

particular the Southern Ocean. These studies would be complemented by more detailed mechanistic knowledge on the principles and conditions of voltammetric detection of eHS, which ultimately underpins the interpretation of environmental eHS data.

Calculation of the eHS trace metal binding capacity was one method used by this thesis to link eHS to dissolved iron. This method offers advantages as a simple and quick method to compare eHS and dissolved iron, and has been successfully applied in other ocean regions (Whitby et al. 2020). The assumptions and limitations of this calculation have been thoroughly discussed in this thesis. Briefly, compositional, and structural differences between marine eHS and the SRFA/HA standards reduce the confidence of the eHS trace metal binding capacity calculation. Indeed, it is possible that our observations of dissolved iron in excess of eHS iron binding capacity in some parts of the South West Indian part of the Southern Ocean (Chapter 3) are a result of higher eHS trace metal binding capacity here compared to the SRFA/HA standards. However, this is not evidenced due to lack of direct measurements of in-situ eHS trace metal binding capacity. To address this knowledge gap and increase the confidence of this calculation, one important future research direction is to directly measure eHS trace metal binding capacity (iron in particular) in eHS collected from different ocean regions and depths. These data should be made available to the community to enable accurate estimation of eHS trace metal binding capacity in other studies following a framework similar to the International Humic Substances Society. Further, if this exercise is also performed in tandem with structural characterisation (e.g. high resolution mass spectrometry) it will also give valuable insights into the links between eHS trace metal binding properties and humic structure and composition.

Previous studies have successfully linked eHS with dissolved metal concentrations to explain metal distributions (e.g. Whitby et al 2020), however it was not possible to determine a direct link between eHS and dissolved iron over the majority of the Chapter 3 transect using eHS and dissolved iron concentration alone. Part of the reason could be because dissolved iron was a strong driver for microbial eHS production and there was a complex suite of processes that controlled eHS over the transect. These results highlight a significant research question: if eHS and DFe are uncoupled, what are the implications for the biogeochemical role of eHS in trace metal binding and carbon cycling in these regions? These are emerging ideas in the field, but also seem consistent with several other recent discoveries. Firstly, that

iron organic speciation is uncoupled from iron bioavailability to phytoplankton (Fourquez et al. 2023). Secondly, that organic speciation does not control upper ocean iron dynamics (Tagliabue et al. 2023). Understanding eHS biogeochemistry through the lens of these recent developments is an important challenge for the eHS community. It may be the case that voltammetric measurements are more informative for iron biogeochemistry in particular ocean regions, data suggests this may be the Atlantic and Arctic (Laglera et al. 2019; Slagter et al. 2017; Whitby et al. 2020), while other approaches are more informative in other regions, such as FDOM in the Pacific (Kitayama et al. 2009; Tani et al. 2003) and an as yet unknown parameter in the Southern Ocean (this study). This may be underpinned by differences in the molecular structure of humics between ocean regions. Considering that the Pacific and Southern Ocean are less terrestrially influenced than the Arctic and Atlantic, this could suggest a terrestrial signature for iron binding eHS. Understanding these differences may also help us to understand the sources and sinks of humic material. Finally, unlike other studies (Mahieu et al. 2024), we did not find evidence for an electroinactive part of the humic pool (no links between FDOM humics and DFe over a subset of the transect). This could imply the presence of other, unknown ligands making up the bulk of the ligand pool. This knowledge gap could be addressed by performing bulk ligand titrations to quantify the wider ligand pool.

Measurements of eHS concentration have the advantage of being simple and quick which allows the analysis of many samples and consequentially greater data coverage over the transect. This facilitated robust comparison with microbial datasets which gave insights into the microbial processes controlling eHS. However, an improvement to this thesis would be to measure iron binding eHS directly (and the iron bound to eHS) in a subset of these samples (Sukekava et al. 2018). While this also relies on assumptions of the binding capacity of natural eHS, this would allow direct links between eHS and dissolved iron to be established. Nevertheless, the data presented in this thesis is a reasonable first step to understanding the role of eHS in iron biogeochemistry in regions of the Southern Ocean and TAG hydrothermal plumes where eHS had not be measured before.

### **6. 3. Closing remarks**

This thesis reveals the importance of microbial activity in controlling eHS distribution and broadens our knowledge on the distribution and cycling of eHS in two key areas with

significant roles in carbon and trace metal biogeochemistry: the Southern Ocean and hydrothermal vent systems. Variable microbial eHS cycling by phytoplankton, prokaryotes, and zooplankton as revealed by this study has the potential to closely interact with dissolved iron and carbon cycling. This thesis has begun addressing the research objectives set out and posed new questions, which ultimately provides a foundation for future research to further unpick this network and address the next big questions. Understanding the mechanisms underpinning eHS cycling are important to understanding the functioning of the marine organic ligand pool, which influences dissolved iron availability and consequently global carbon cycling.

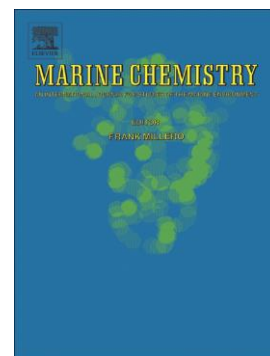
#### 6. 4. References

- Fang, K., D. Yuan, L. Zhang, L. Feng, Y. Chen, and Y. Wang. 2015. Effect of environmental factors on the complexation of iron and humic acid. *Journal of Environmental Sciences* 27: 188-196.
- Fourquez, M. and others 2023. Chasing iron bioavailability in the Southern Ocean: Insights from *Phaeocystis antarctica* and iron speciation. *Science Advances* 9: eadf9696.
- Gledhill, M., E. P. Achterberg, K. Li, K. N. Mohamed, and M. J. A. Rijkenberg. 2015. Influence of ocean acidification on the complexation of iron and copper by organic ligands in estuarine waters. *Marine Chemistry* 177: 421-433.
- Henley, S. F. and others 2020. Changing Biogeochemistry of the Southern Ocean and Its Ecosystem Implications. *Front. Mar. Sci.* 7.
- Henson, S. A., C. Laufkötter, S. Leung, S. L. C. Giering, H. I. Palevsky, and E. L. Cavan. 2022. Uncertain response of ocean biological carbon export in a changing world. *Nature Geoscience*.
- Jiao, N. and others 2010. Microbial production of recalcitrant dissolved organic matter: long-term carbon storage in the global ocean. *Nature Reviews Microbiology* 8: 593-599.
- Kitayama, S. and others 2009. Controls on iron distributions in the deep water column of the North Pacific Ocean: Iron(III) hydroxide solubility and marine humic-type dissolved organic matter. *Journal of Geophysical Research: Oceans* 114.
- Laglera, L. M., C. Sukekava, H. A. Slagter, J. Downes, A. Aparicio-Gonzalez, and L. J. A. Gerringa. 2019. First Quantification of the Controlling Role of Humic Substances in

- the Transport of Iron Across the Surface of the Arctic Ocean. *Environmental Science & Technology* **53**: 13136-13145.
- Leung, S., A. Cabré, and I. Marinov. 2015. A latitudinally banded phytoplankton response to 21st century climate change in the Southern Ocean across the CMIP5 model suite. *Biogeosciences* **12**: 5715-5734.
- Mahieu, L. and others 2024. Iron-binding by dissolved organic matter in the Western Tropical South Pacific Ocean (GEOTRACES TONGA cruise GPpr14). *Front. Mar. Sci.* **11**.
- Slagter, H. A., H. E. Reader, M. J. A. Rijkenberg, M. Rutgers van der Loeff, H. J. W. de Baar, and L. J. A. Gerringa. 2017. Organic Fe speciation in the Eurasian Basins of the Arctic Ocean and its relation to terrestrial DOM. *Marine Chemistry* **197**: 11-25.
- Sukekava, C., J. Downes, H. A. Slagter, L. J. A. Gerringa, and L. M. Laglera. 2018. Determination of the contribution of humic substances to iron complexation in seawater by catalytic cathodic stripping voltammetry. *Talanta* **189**: 359-364.
- Tagliabue, A. and others 2023. Authigenic mineral phases as a driver of the upper-ocean iron cycle. *Nature* **620**: 104-109.
- Tani, H. and others 2003. Iron(III) hydroxide solubility and humic-type fluorescent organic matter in the deep water column of the Okhotsk Sea and the northwestern North Pacific Ocean. *Deep Sea Research Part I: Oceanographic Research Papers* **50**: 1063-1078.
- Tufano, T. P., and K. N. Raymond. 1981. Coordination chemistry of microbial iron transport compounds. 21. Kinetics and mechanism of iron exchange in hydroxamate siderophore complexes. *Journal of the American Chemical Society* **103**: 6617-6624.
- Whitby, H. and others 2020. A call for refining the role of humic-like substances in the oceanic iron cycle. *Scientific Reports* **10**: 6144.

## Appendix

A hydrothermal plume on the Southwest Indian Ridge revealed by a multi-proxy approach: Impact on iron and manganese distributions (GEOTRACES GS02)



Corentin Baudet, Eva Bucciarelli, Géraldine Sarthou, Cédric Boulart, Ewan Pelleter, **Millie Goddard-Dwyer**, Hannah Whitby, Rui Zhang, Ingrid Obernosterer, David Gonzalez-Santana, Morgane Léon, Pieter van Beek, Virginie Sanial, Catherine Jeandel, Frédéric Vivier, Maria-Elena Vorrath, Wen-Hsuan Liao, Yoan Germain, Hélène Planquette

PII: S0304-4203(24)00052-5

DOI: <https://doi.org/10.1016/j.marchem.2024.104401>

Reference: MARCHE 104401

To appear in: *Marine Chemistry*

Received date: 21 April 2023

Revised date: 25 January 2024

Accepted date: 13 May 2024

Please cite this article as: C. Baudet, E. Bucciarelli, G. Sarthou, et al., A hydrothermal plume on the Southwest Indian Ridge revealed by a multi-proxy approach: Impact on iron and manganese distributions (GEOTRACES GS02), *Marine Chemistry* (2023), <https://doi.org/10.1016/j.marchem.2024.104401>

## Abstract

Iron (Fe) and manganese (Mn) are crucial micronutrients that limit oceanic primary productivity in the Southern Ocean. It has been recently suggested that hydrothermal activity may be an important source of oceanic dissolved iron, yet, this contribution is still not fully understood and only one active hydrothermal site has been reported on the Southwest Indian Ridge (SWIR), south of 40°S.

Using a multi-proxy approach, this study demonstrates the occurrence of hydrothermal venting on the SWIR in the near vicinity of the location 44°51.690 S, 36°10.460 E, which is likely to be a low or moderately high temperature fluid. Indeed, we report high values of dissolved methane to manganese ratios (up to  $11.1 \pm 1.2 \text{ mol mol}^{-1}$ ), low particulate iron (pFe) and manganese (pMn) concentrations (with maximum values of  $0.7 \text{ nmol L}^{-1}$  and  $0.06 \text{ nmol L}^{-1}$ , respectively) associated with the presence of few oxyhydroxides, as well as high Radium(Ra)  $^{223}$  and Ra  $^{224}$  activities near the seafloor. The Fe and Mn data revealed a significant enrichment at depths influenced by hydrothermal circulation on the seafloor, within the Upper Circumpolar Deep Water. Dissolved Fe (dFe) and dissolved Mn (dMn) concentrations were enriched by 3- and 7-fold, respectively, and pFe and pMn by 2- and 1.5fold, respectively, compared to a reference station located outside the SWIR. They were however lower than concentrations reported so far near high temperature vents, suggesting a weaker influence of this hydrothermal system on deep Fe and Mn reservoirs. We show that a large fraction of the dFe could be stabilized by organic complexation with humic substances (eHS, estimated 27 - 60 % of dFe). High prokaryotic abundance related to the proximity of the hydrothermal vent suggests that other Fe-complexing ligands of biological origin might also stabilize Fe in its dissolved form. Collectively, these measurements integrated within the concept of a “multi-proxy approach”, helped painting a more detailed picture of the complex interactions and processes in this region of the SWIR. Although the system is a source of both dFe and dMn to the deep ocean, the low current velocities and the bathymetry likely limit the fertilization of surface water by dFe and dMn along this section of the SWIR.